

VANESSA RODRIGUES PEGOS

**Caracterização Estrutural e Funcional do Sistema de
Captação de Fosfato da Bactéria Fitopatogênica**

Xanthomonas axonopodis pv. citri

**Structural and Functional studies of the Phosphate system
uptake from bacteria phytopathogenic *Xanthomonas*
*axonopodis pv.citri***

CAMPINAS

2015

UNIVERSIDADE ESTADUAL DE CAMPINAS
INSTITUTO DE BIOLOGIA
VANESSA RODRIGUES PEGOS

**Caracterização Estrutural e Funcional do Sistema de
Captação de Fosfato da Bactéria Fitopatogênica
Xanthomonas axonopodis pv. *citri***

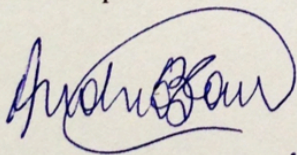
**Structural and Functional studies of the Phosphate
system uptake from bacteria phytopathogenic
Xanthomonas axonopodis pv. *citri***

Tese apresentada ao Instituto de Biologia da Universidade Estadual de Campinas como parte dos requisitos exigidos para a obtenção do título de Doutora em Genética e Biologia Molecular na área de Microorganismos.

Thesis presented to the Institute of the University of Campinas in partial fulfillment of the requirements for the degree of Doctor in Genetic and Molecular Biology, in the area of Microorganisms.

Orientador: Prof. Dra. Andrea Balan Fernandes

Este exemplar corresponde à versão final da tese defendida pela aluna Vanessa Rodrigues Pegos, e orientada pela Prof. Dra. Andrea Balan.



CAMPINAS

2015

Ficha catalográfica
Universidade Estadual de Campinas
Biblioteca do Instituto de Biologia
Mara Janaina de Oliveira - CRB 8/6972

P349c Pegos, Vanessa Rodrigues, 1987-
Caracterização estrutural e funcional do sistema de captação de fosfato da bactéria fitopatogênica *Xanthomonas axonopodis* pv. *citri* / Vanessa Rodrigues Pegos. – Campinas, SP : [s.n.], 2015.

Orientador: Andrea Balan Fernandes.
Tese (doutorado) – Universidade Estadual de Campinas, Instituto de Biologia.

1. Regulon. 2. Fosfatos. 3. Transportadores de cassetes de ligação de ATP. 4. Proteínas de ligação a fosfato. 5. *Xanthomonas axonopodis* pv. *citri*. 6. Biologia de sistemas. I. Balan, Andrea. II. Universidade Estadual de Campinas. Instituto de Biologia. III. Título.

Informações para Biblioteca Digital

Título em outro idioma: Structural and functional studies of the phosphate system uptake from bacteria phytopathogenic *Xanthomonas axonopodis* pv. *citri*

Palavras-chave em inglês:

Regulon
Phosphates
ATP-binding cassette transporters
Phosphate-binding proteins
Xanthomonas axonopodis pv. *citri*
Systems biology

Área de concentração: Genética de Microorganismos

Titulação: Doutora em Genética e Biologia Molecular

Banca examinadora:

Andrea Balan Fernandes [Orientador]
Celso Eduardo Benedetti
Cristina Pontes Vicente
Marcio Vinicius Bertacine Dias
Gabriel Padilla

Data de defesa: 03-03-2015

Programa de Pós-Graduação: Genética e Biologia Molecular

Campinas, 03 de Março de 2015.

Banca Examinadora

Prof. Dra. Andrea Balan Fernandes

Andrea Balan Fernandes

Prof. Dr. Celso Eduardo Benedetti

Celso Eduardo Benedetti

Prof. Dr. Marcio Vinicius Bertacine Dias

Marcio VB Dias

Prof. Dr. Gabriel Padilla

Gabriel Padilla

Prof. Dra. Cristina Pontes Vicente

Cristina Pontes Vicente

Prof. Dr. Roberto Nepomuceno de Souza Lima

Prof. Dra. Cristina Eliza Alvarez Martinez

Prof. Dr. Gonçalo Amarante Guimarães Pereira

Resumo

Xanthomonas axonopodis pv. *citri* (*X. citri*) é o causador do cancro cítrico em diversas espécies de citrus, sobretudo, laranjas. As epidemias de cancro cítrico tem causado severas perdas econômicas à citricultura mundial uma vez que não há estratégias de combate efetiva contra essa bactéria no campo. Diversos estudos demonstraram a importância de genes para a patogênese de *X. citri*, mas ainda não foram investigados genes envolvidos na aquisição e no metabolismo de micronutrientes tais como o fósforo. *X. citri* conserva o sistema de transporte do tipo ABC de fósforo inorgânico codificado pelo operon *pstSCAB*. Adicionalmente a bactéria possui dois outros operons *oprO/phoX* e *phoBR*, os quais codificam, respectivamente, uma porina de membrana externa e uma proteína periplasmática ligadora e o sistema dois componentes de sinalização celular, ambos integrantes do regulon de fósforo (regulon *pho*). Neste trabalho, estudamos a resposta destes operons à carência de fósforo, bem como o papel da proteína ligadora periplasmática PstS, por meio de análises proteômica, metabolômica, estruturais baseadas em cristalografia de raio-X e funcionais utilizando um mutante de *X. citri* portador de deleção no gene *pstS* (*Xac::pstS*). Os dados obtidos foram comparados entre as linhagens selvagem e mutante. Primeiramente evidenciamos que o sistema ABC de fósforo é ativado em carência do íon, incluindo um aumento de expressão de PhoX e PstS de 49 e 33 vezes, respectivamente, e que *X. citri* apresenta a maioria dos genes do regulon *pho*. PhoX e PstS são proteínas ligadoras de fósforo que partilham 70% de identidade de aminoácidos e são originadas de uma duplicação gênica. Na ausência de PstS, PhoX parece exercer a função de captação, mas não é capaz de recuperar todos os fenótipos da bactéria selvagem. Adicionalmente, ensaios de transporte de fósforo com as bactérias selvagem e mutante mostraram diferenças no transporte e que o sistema ABC permanece constitutivo na linhagem mutante. A deleção de *pstS* também culminou no retardamento do crescimento da bactéria em folhas de *C. sinensis*, mas não interferiu na adesão bacteriana e na produção da goma, estas sim, influenciadas diretamente pela concentração de fósforo no meio. Análises de metabolômica evidenciaram que a carência de fósforo induz mudanças nas rotas bioquímicas, sobretudo na linhagem mutante que utiliza da via das pentoses e do metabolismo do piruvato para a produção de ATP. Este é o primeiro trabalho que evidencia o papel do sistema ABC de transporte de fósforo nesta bactéria e que relaciona de uma forma multidisciplinar, o papel do íon e dos componentes do regulon *pho* na bactéria *X. citri*. Adicionalmente, uma vez que o sistema é bem conservado em outras espécies, os resultados obtidos servem como modelo para o gênero *Xanthomonas*.

Abstract

Xanthomonas axonopodis pv. *citri* (*X. citri*) is the cause of citrus canker in several species of citrus, especially oranges. The citrus canker epidemics have caused severe economic losses to the citrus industry worldwide since no effective combat strategies against this bacterium. Several studies have demonstrated the importance of genes related to the pathogenesis of *X. citri*, but there is no studies about mechanisms of micronutrients acquisition such as phosphate. *X. citri* has an ATP-Binding Cassete transport system for inorganic phosphate encoded by *pstSCAB* operon. In addition, the bacterium has two other operons *oprOphoX* and *phoBR*, which encode respectively, an outer membrane porin and a periplasmic binding protein and two-components system. The three operons and other related genes are members of the phosphate regulon (pho regulon). In this work we studied the response of these operons in phosphate deprivation, and the role of periplasmic-binding protein PstS through proteomics analysis, metabolomics, crystallography and functionally based on a *X. citri* mutant deleted for *pstS* gene (*Xac::pstS*). Data were compared between wild type and mutant strains. We showed that the phosphate ABC system is activated during the ion depletion, including PstS and PhoX that showed increased levels of 49 and 30 times, respectively. In addition, we showed that *X. citri* displays most of the genes of the pho regulon. PhoX and PstS are phosphate binding proteins that share 70% amino acid identity and have origin from a gene duplication. In the absence of PstS, PhoX seems to complement the uptake function, but it is not able to recover all phenotypes of the wild type bacteria. Additionally, phosphate transport assays with wild type and mutant bacteria showed differences in transport and constitutivity of the ABCsystem in the mutant strain. The deletion of *pstS* also resulted in slowing of bacteria growth in *Citrus sinensis* leaves, but did not interfere with bacterial adhesion and gum production, two phenomena directly influenced by the phosphate concentration in the medium. Metabolomic analyzes showed that phosphate deprivation induces changes in biochemical pathways, especially the mutant strain that uses the pentose and pyruvate metabolism for ATP production. This is the first work that highlights the role of the ABC system for phosphate in this bacterium and that reveals in a multidisciplinary way, the role of the ion and the pho regulon components in the phytopathogenic bacterium. Additionally, once the system is well preserved in other species, the results serve as a model for the genus *Xanthomonas*.

Sumário

1. Introdução Geral	3
1.1. <i>Xanthomonas axonopodis</i> pv. <i>citri</i> e o cancro cítrico.....	3
1.2. Desenvolvimento da Doença	5
1.3. Os fatores de Patogenicidade de <i>X. citri</i>	6
1.4. Pho Regulon: A captação de fosfato dependente dos transportadores do tipo ABC e da sinalização celular através dos sistemas dois componentes.....	9
1.5. Transportadores do tipo ABC e Sistemas de Transdução de sinal em Procariotos.....	15
1.5.1. Transportadores do tipo ABC em procariotos: captação de nutrientes, adaptação ao ambiente e patogênese bacteriana	15
1.5.2. Estrutura e Mecânica dos transportadores do tipo ABC para importação de nutrientes .	18
2. Objetivos.....	25
2.1. Análise funcional de <i>X. citri</i> e <i>X. citri</i> portador de deleção no gene <i>pstS</i> (<i>Xac::pstS</i>) em presença e carência de fósforo.....	25
2.2. Análise estrutural de proteínas do sistema Pst e dois componentes	25
3. Resultados.....	32
3.1. Artigos Publicados	32
3.2. Manuscritos.....	65
4. Discussão	161
4.1. O efeito do fosfato na fisiologia de <i>X. citri</i>	161
4.2. O efeito da deleção do gene <i>pstS</i> e do fosfato na fisiologia de <i>X. citri</i>	164
4.3. PstS, PhoX, ortólogos e análise estrutural	166
4.4. Redes de interação das linhagens selvagem e mutante: o metabolismo de <i>X. citri</i> e de <i>Xac::pstS</i>	168
5. Conclusões	171
6. Referência Bibliográfica.....	175
7. Anexo 1 - Resultados Complementares.....	184
7.1. Metodologia.....	184
7.1.1. Clonagem molecular dos genes <i>phoU</i> , <i>phoB</i> e <i>phoR</i>	184
7.1.2. Extração e Expressão das Proteínas Recombinantes	185
7.1.3. Purificação das proteínas recombinantes PhoU, PhoR e PhoB.....	186
7.1.4. Ensaios de cristalização das proteínas PhoU, PhoR e PhoB e coleta de dados de cristalização	186
7.1.5. Medidas de espalhamento de Luz e proteólise com a protease 3C.....	187

7.2. Resultados e Discussão	188
8. Anexo 2 – Material Suplementar Manuscrito III.....	194

Dedico esta tese ao meu pai Luís R. Pegos e a minha mãe Marta Regina P. Pegos. Certamente se não fosse o incentivo de vocês e a cumplicidade de abraçar meus sonhos eu não teria chegado até aqui. A realização desse meu sonho também é de vocês, pois vocês me ensinaram a sempre persistir e a sempre se dedicar e a sempre dar o meu melhor, e nem por trabalhar demais deixar de ser feliz.

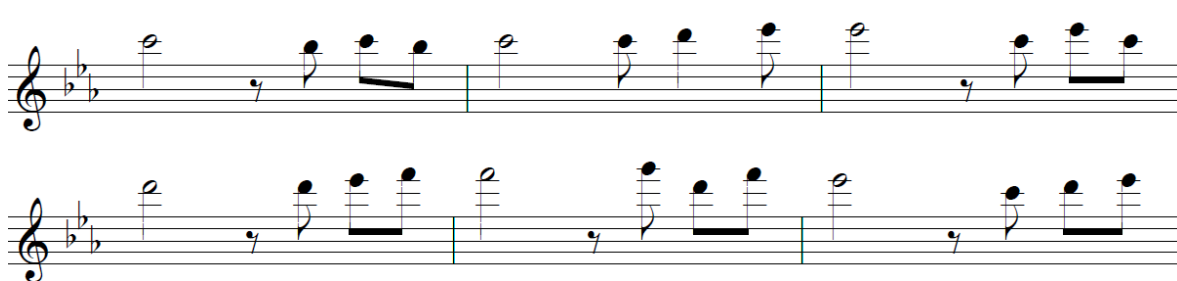
Agradecimentos

Gostaria de começar agradecendo à CAPES (Coordenação de Aperfeiçoamento de Pessoal de Nível Superior), à UNICAMP, ao Instituto de Biologia e ao Departamento de Genética e Biologia Molecular da UNICAMP, e ao LNBio (Laboratório Nacional de Biociências). Agradeço aos membros da banca de qualificação, pré-banca e banca de defesa por terem aceito o convite e a missão de contribuir com colocações construtivas de melhorias a este trabalho. Agradeço também ao professor Gonçalo Pereira por ter me aceitado como PED durante a etapa de doutoramento e a Marcela Salazar pela difusão de conhecimento. Agradeço ao Dr. Javier Medrano por ter me recebido em seu laboratório no Centro de Investaciones Biológicas (CSIC), em Madrid e me ensinado muita coisa com seu profissionalismo e empatia em me receber em pleno inverno. Agradeço ao Dr. João Alexandre Barbosa pelo incentivo em começar o mestrado e ao programa da UNICAMP Ciência e Arte nas Férias, onde vi o primeiro gel de agarose com 16 anos de idade. Agradeço a todos os colegas do LNBio: Wando, Givanil, Jackeline Zanella, Jaqueline, ao grupo do Celso, ao Américo, a Michelle, Carla, Joice e ao grupo da Adriana Paes Leme. Obrigada a todos os colaboradores deste trabalho, especialmente à Alessandra Alves, Simone Pichi, Ana Zeri e Rafael Canevarolo.

Ao grupo ABC preciso dedicar um parágrafo especial. Um grupo de pessoas que atuam como um time sempre disposto a discutir experimentos, estratégias, hipóteses científicas, partilhar atividades e ajudar o próximo nas tarefas coletivas. Os meus sinceros agradecimentos à vocês que deram essa cara ao ABC: Cris, Mel, Ana, Aline e Jéssica que me farão lembrar de como foi bom trabalhar com vocês. Também agradeço aos demais aspirantes cientistas que passaram pelo grupo e que deixaram aprendizados científicos e de desenvolvimento humano. A Balan que como líder de grupo sempre motivou a todos a se dedicar em máximo de forma mágica. Esse tipo de liderança é raro na academia e admirável na maneira como é conduzida, sendo uma das suas maiores qualidades. Obrigada Balan por demonstrar com atitudes como um bom líder é! Também gostaria de agradecer aos 7 anos que passamos juntas trabalhando nos ABCs e toda a evolução científica, e a oportunidade de tocar os sistema de fosfato no meu doutorado.

Gostaria de agradecer a todos da Metrocamp (desde a época em que fui bolsista ProMetro), aos meus professores de graduação e à Patrícia Melo por todas as oportunidades. Devo muito a este ambiente excepcional em que eu evoluí muito e aprendi a como trabalhar com pessoas, me apaixonar pelo empreendedorismo e achar uma dose de motivação cotidiana que depois de uma aula me fazia voltar eufórica para a minha bancada e realizar vários experimentos enlouquecidamente.

Por fim, agradeço a todos que diretamente ou indiretamente contribuíram para este trabalho e ao meu melhor amigo, Murilo e a minha irmã, Juju.



I've loved, I've laughed and cried
I've had my fill, my share of losing
And now as tears subside
I find it all so amusing
To think I did all that
And may I say, not in a shy way
Oh, no, no not me
I did it my way

My way – Elvis Presley

Lista de Ilustração

- Figura 1.** Eventos de desenvolvimento do cancro cítrico por *X. citri*. Disponível em: <<http://www.plantmanagementnetwork.org/pub/php/review/citruscanker/>>. Acesso em 24 de Setembro de 2014. As principais vias são a poda, tempestades, insetos e vento. 5
- Figura 2.** *Citrus sinensis* e aspectos da interação com *X. citri*. A) Colônias de *X. citri* isoladas em LB ágar com aspecto amarelo em virtude da xanthomatodina. B) *X. citri* é uma bactéria gram-negativa com coloração rosada em decorrência da fucsina na coloração de gram. C) *X. citri* saindo dos estômatos após seu rompimento, geralmente cinco dias após a invasão, imagem de microscopia eletrônica. D) Microscopia eletrônica no interior da folha mostrando a goma xantana, como principal EPS participando da matriz no qual as bactérias ficam embebidas. F) Aspecto da lesão do cancro cítrico com 20 dias após inóculo de *X. citri*. Observe que a folha se torna irregular, com pústulas e aspecto decorrente da produção da goma no interior da folha. (Adaptado de Brunnings et al, 2004). 6
- Figura 3.** Imagens de microscopia confocal a laser de varredura de *Proteus mirabilis* e mutantes de PstS e PstA. A mutação de PstS é mais severa do que a mutação de um dos componentes da proteína de membrana. É possível visualizar como o biofilme produzido por Δ pstS é formado em menor quantidade e em segregados de microcolônias, diferentemente do observado para o selvagem. Retirado de O'May et al, 2009. 12
- Figura 4.** Transdução de sinal do regulon de fosfato em *E.coli*. Modelo de captação, sinalização de Pi e regulação gênica em situações de carência nutricional. Há três eventos descritos em ordens seqüenciais: 1) a inibição de PhoR possivelmente através da PhoU ([Pi] > 4 μ M); 2) em situações de carência de fosfato, PhoR é autofosforilada na His260 ([Pi] < 4 μ M), e fosforila o fator transcricional PhoB; 3) No restabelecimento da homeostase ([Pi] > 4 μ M), PhoB é desfosforilada e PhoR é novamente inibida por PhoU. Nesse momento, a captação de fosfato através do componente do transportador ABC PstS pode ou não acontecer. Ainda é desconhecido como a proteína PstS ou o transportador inteiro, nesse caso, induzirá a ativação de PhoR para a fosforilação de PhoB através do modulador PhoU (retirado de Hsieh & Wanner, 2010; VanBogelen et al., 1996). 14
- Figura 5.** Estrutura dos transportadores ABC exportadores e importadores de procariotos. As estruturas deste complexo de proteínas foram obtidas por meio de cristalografia de raios-X. São apresentados 3 importadores e 1 exportador conforme apresentado em Hollestein et al (2007). O código PDB das estruturas é apresentado da esquerda para direita: 2HYD, 2ONK, 1L7V e 2NQ2. Adaptado de Hollestein et al 2007. 16
- Figura 6.** Distribuição dos transportadores do tipo ABC em genomas de procariotos. (A) Observa-se uma relação linear entre a quantidade de ABCs encontrados e o tamanho do genoma. Para tal busca foi levantada o número de ATPases do sistema contra o número total de genes. Roxo = archaea; Verde = eucarioto; Azul = procariotos. Retirado de Davidson et al, 2008. (B) Levantamento do número de proteínas pertencentes à família dos transportadores do tipo ABC importadores em *X. citri* e *X. campestris* baseado na anotação ou identidade de seqüência dos domínios ligadores de ATP. *X. citri* possui no total de 117 transportadores, sendo 87 importadores, 32 exportadores e 8 hipotéticos. Os transportadores de maior relevância em patogênese foram destacados pelo nosso grupo, incluindo fosfato e fosfonato (caixa preta). Comparado com outros gêneros bacterianos este número é elevado e isso pode ser resultante do habitat e processos correlacionados à colonização desta bactéria em plantas e em solo. 16
- Figura 7.** Estrutura da proteína periplasmática ligadora de fosfato PstS de *E. coli* (código PDB 1IXH). A proteína apresenta a estrutura de dois lobos, N e C-terminal, e entre eles, a fenda de ligação ao

substrato. Os resíduos em palito dentro da fenda - círculo de linha pontilhada - são os resíduos do bolsão de interação direta com o substrato. Estes resíduos garantem especificidade ao substrato através de complementariedade de cargas e acomodação do substrato em determinado espaço físico em seu interior. As interações químicas entre os resíduos de amino ácidos e os substratos geralmente ocorrem através de interações de hidrogênio com aproximadamente 2,5 Å de distância entre cada átomo. Os domínios N e C-terminal se aproximam quando a proteína interage como ligante para que o mesmo seja mantido até que toda a mecânica do transporte ocorra e os lobos N e C-terminal serão separados novamente. A estrutura de *E. coli* é mostrada em sua conformação fechada. Em laranja é possível observar o fosfato em laranja, ao centro da fenda. 19

Figura 8. Regiões da BP de interação direta com os domínios TMD do transportador do tipo ABC importador de alcano sulfonatos (A) e fosfato (B). (A) As proteínas do transportador são apresentadas em superfície e coloridas de acordo com a função: BP (superfície azul), transmembranas (superfícies amarelas) e ATPases superfícies verdes. As regiões de interação RI e RII da PB que interagem na membrana são mostradas em vermelho. Alinhamento das regiões das PBs e transmembranas são apresentados para *X. citri* e *E. coli*. (B) A distribuição de cargas dessas regiões poderão ser importantes para interação com a proteínas de membrana e liberação com o substrato. Entre as regiões RI e RII encontra-se a fenda do substrato que tem profundidade e dimensão exclusivas para acomodar o ligante, essas regiões podem ser mais ou menos hidratadas afetando a interação, afinidade e interação com proteínas de membrana através das regiões RI e RII. 20

Figura 9. Mecânica e topologia do transportador do tipo ABC importador descritos em procaríotos. A) Ilustração TMD – Domínios transmembrana localizados na membrana interna da parede celular formando o poro pelo qual o substrato será translocado. O domínio ABC – cassete ligador de ATP, também denominado como NBD (Nucleotide- Binding Domain) que liga e hidroliza o ATP durante a translocação. No espaço periplásmico temos a proteína ligadora que apresenta elevada afinidade ao substrato a ser translocado. A ilustração mostra que o transportador pode assumir dois estados conformacionais: *outward* quando aberto para o periplasma e *inward* quando aberto para o citoplasma ou estado de descanso (Retirado de Rees, et al., 2009). 21

Figura 10. Clonagem do gene *phoU* e purificação da proteína recombinante PhoU. A) Clonagem do gene *phoU* ocorreu em três etapas: amplificação do fragmento de 700 pb através do PCR, clonagem no vetor pGEM (Novagen®). A confirmação da clonagem ocorreu através da análise de restrição e o clone 1 foi utilizado para a subclonagem no vetor pET28a. A confirmação dos clones 1 e 2 do vetor pET28 foram confirmados por análise de sequenciamento e de restrição. B) Expressão do gene *phoU* em células Tuner (DE3). Após a expressão, o lisado de bactérias foi submetido a purificação de afinidade a níquel em gradiente de imidazol. A proteína PhoU foi eluída com 150 mM de Imidazol com mais de 90% de pureza. 189

Figura 11. Clonagem e purificação do domínio C-terminal *phoB* de *X. citri*. A) Clonagem através da amplificação do domínio C-terminal de 400 pb em alto rendimento. Os fragmentos foram clonados no vetor de clonagem ZeroBlunt. B) o Domínio C-terminal da proteína PhoB foi clonado no vetor de expressão pETMBP para expressão em células Tuner (DE3) com 72 kDa. 190

Figura 12. Clonagem, expressão e purificação da proteína PhoR de *X. citri*. A) Clonagem do fragmento de 1031 pares de bases referente ao gene *phoR* no vetor pGEM. O fragmento clonado no pGEM foi subclonado nos vetores de expressão pET28 e pETMBP. As amostras 1, 2, 3 e 4 foram confirmadas positivas para a clonagem do gene através do PCR de colônia e sequenciamento nos vetores pET28 e pETMBP, respectivamente. B) Expressão da proteína PhoR. Os vetores pET28phoR e pETMBPphoR foram transformados na linhagem de *E. coli* Turner (DE3) para expressão. Os géis de SDS-PAGE 12% PhoR+MBP (70 Kda) e PhoR+His tag (40 Kda) representam as seguintes amostras: PM – Marcador de peso molecular; 1 – Aliquota da

cultura bacteriana prévia adição de IPTG denominada de tempo zero de indução; 2 – Aliquota de cultura bacteriana após 4 horas de indução; 3 – Fração Solúvel após lise bacteriana; 4- Fração insolúvel após lise bacteriana. A fusão da proteína MBP na região N-terminal da proteína PhoR resultou na produção da proteína PhoR na fração solúvel, o que não foi possível sem a cauda MBP. Somente a cauda de histidina fusionada no N-terminal da proteína a proteína PhoR foi produzida nos corpúsculos de inclusão bacterianos dificultando sua recuperação. C) Purificação da proteína PhoRMBP. A eluição da proteína PhoR através de um gradiente de imidazol ocorreu na fração de 500 mM de Imidazol. A fração de 150 mM, concentraçãoo usualmente eluída grande parte das proteínas deste trabalho apresentou-se com muitos contaminantes, sugerindo adequação do volume de resina e volume de coluna utilizado para purificação em cada etapa. D) Remoção da MBP. A remoção da cauda MBP foi realizada por 18 horas utilizando a protease 3C. As amostras foram então, submetidas à filtração em gel na qual um único pico foi recuperado no volume morto da coluna. As amostras foram aplicadas no gel SDS-PAGE 12 % e revelaram que não houve a separação entre a proteína PhoR e MBP (..), assim como a ineficiência da digestão da proteína 3C (***) e a presença da protease 3C (#). Provavelmente a presença de todas essas proteínas em um mesmo pico sugerem agregação da amostra e instabilidade da proteína PhoR nas condições usadas para isolamento..... 192

Figura 13. Análise de espalhamento dinâmico de luz, DLS (Dynamic Laser Scattering). Amostras da proteína PhoRMBP não digeridas com a protease 3C na concentração de 1 mg/mL foram submetidas à análise de DLS após a exclusão molecular (gel não mostrado na figura 23). O correspondente a 85% da amostra apresentou uma polidispersividade de 17% e um raio de 5.8. A massa molecular estimada para a amostra por meio dessa medida foi de aproximadamente 206 kDa referente a um dímero em solução. 193

Lista de Abreviaturas e Siglas

<i>A. fulgidus</i>	<i>Archeoglobulus fulgidus</i>
<i>A. tumefaciens</i>	<i>Agrobacterium tumefaciens</i>
ABC	Cassete ligador de ATP
ADP	Adenosina difosfato
APEC	Avian pathogenic <i>E. coli</i>
ATP	Adenosina tri-fosfato
ATPase	Enzima que hidrolisa o ATP
<i>B. subtilis</i>	<i>Bacillus subtilis</i>
BP	Proteínas periplasmática ligadora
BP	Proteínas periplasmática ligadora
c-di-GMP	Segundo mensageiro cíclico dimérico
<i>C. sinensis</i>	<i>Citrus sinensis</i>
CA	Catalytic and ATP binding
CitrusBr	Associação Nacional dos Exportadores de Sucos Cítricos
ColRS	Sistema de sinalização bacteriano
<i>D. alkenivrans</i>	<i>Desulbacterium alkenivrans</i>
DLS	Dynamic Laser scattering
DNA	Ácido desoxiribonucleico
DSF	Cis-11-methyl-2-dodecenoid acid
DSF	<i>Cis</i> -11-methyl-2-dodecenoid acid
<i>E.coli/Eco</i>	<i>Escherichia coli</i>
EUA	Estados Unidos da América
EUA	Estados Unidos da América
FA	Fosfatase Alcalina
G/C	Guanina e Citosina
GC	Guanina e Citosina
HK	Histidina Quinase
HK	Histidina Quinase
HTH	Hélice-volta-hélice
IPTG	Isopropyl-beta-d-thiogalactopyranoside
KOD	<i>DNA polimerase</i>
LB	Luria Broth
LPS	Lipopolissacarídeo
<i>M. loti</i>	<i>Mesorhizobium loti</i>
<i>M. smegmatis</i>	<i>M. smegmatis</i>
MBP	Proteína ligadora de maltose
NDB	Domínio ligador de Nucleotídeo
OH	Hidroxila
OppA	Proteína ligadora de Oligopeptídeos
<i>P. mirabilis</i>	<i>Proteus mirabilis</i>
PAGE	Poliacrylamide gel electrophoresis
PAMP	Padrão molecular associado à patogénico

PBP	Proteína periplasmática ligadora de fosfato
PCA	<i>Análise multivariada dos componentes principais</i>
PCR	Reação em Cadeia da Polimerase
PDB	<i>Banco de proteínas com estrutura 3D elucidada</i>
pH	Potencial Hidrogenionico
Pho	Regulon de fosfato
PhoX	Proteínas periplasmática ligadora de fosfato
<i>ppGpp</i>	Guanosina pentafosfato
Pst	Sistema de transporte de Fosfato
PstS	Proteínas periplasmática ligadora de fosfato
QS	Sensor de quórum
RMN	Ressonancia Magnética Nuclear
RNA	Ácido ribonucleico
RR	Proteína regulatória
RR	Proteína regulatória de resposta
<i>S. aureus</i>	<i>Staphylococcus aureus</i>
<i>T. maritima</i>	<i>Thermotoga maritima</i>
TAQ	DNA polimerase
TCS	Two-component system/ Sistemas dois componentes
TMD	Domínio Transmembrana
X-gal	5-bromo-4-chloro-3-indolyl-beta-D-galacto-pyranoside
<i>X. citri</i>	<i>Xanthomonas axonopodis pv. citri</i>
<i>X. citri</i>	<i>Xanthomonas axonopodis pv. citri</i>
<i>Y. Pestis</i>	<i>Yersinia pestis</i>

Introdução

A introdução do presente trabalho será baseada na revisão de literatura para aprofundamento dos resultados apresentados na sessão 3.

1. Introdução Geral

1.1. *Xanthomonas axonopodis* pv. *citri* e o cancro cítrico

Xanthomonas axonopodis pv. *citri* (*X. citri*) é uma bactéria Gram-negativa que pertence à divisão gama das proteobactérias. Agente etiológico do cancro cítrico, doença bacteriana que ataca espécies de citros, sobretudo, laranjas. O histórico da origem desta bactéria é antigo, reportado no século XIX na China e Índia. Atualmente o gênero *Xanthomonas* sp. compreende 27 espécies, sendo laranjeiras somente um dos 400 possíveis hospedeiros vegetais e com considerável relevância econômica para o Brasil. Após os anos 20 no século XIX foram registrados os primeiros relatos do aparecimento da bactéria em continente americano causando o cancro, mas há alguns relatos a respeito da introdução do mesmo pelos colonizadores portugueses (Ryan et al 2011).

Embora atualmente já tenham sido relatadas pelos citricultores e comunidade científica outras pragas e doenças que acometem laranjeiras, e que podem impactar economicamente em um curto prazo, de forma ainda mais grave que o cancro cítrico, nenhuma solução para o combate ou a erradicação de *X. citri* foi proposta. Na literatura e na citricultura de uma forma geral, há relatos de várias epidemias de *X. citri* nos laranjais ao redor do mundo ao longo do último século. Em território brasileiro, no estado de São Paulo, a epidemia de 1996 (Graham et al., 2004) motivou alguns pesquisadores brasileiros a realizarem o sequenciamento do genoma desta bactéria, logo após a finalização da montagem do genoma da *Xyllela fastidiosa*, outro fitopatógeno relevante. As informações oriundas da genômica foram fundamentais para a realização do presente trabalho e todos os outros, que como aspirante à cientista, estive envolvida (da Silva, et al., 2002).

Ao redor do mundo, anualmente são gastos milhões de dólares em estratégias de prevenção do cancro cítrico tais como programas de erradicação, controle de doenças e até mesmo legislações severas com elevada rastreabilidade na laranja para exportação. No entanto, inevitavelmente, as infestações de cancro cítrico são difíceis de serem evitadas e essa tem sido uma das principais razões para a disseminação da bactéria (Stall et al, 1983; Das, 2003). Atualmente, uma das formas de controle no campo ainda é a extensa utilização de bactericidas à base de cobre. O desenvolvimento de

estratégias de controle que possam gerar inclusive patentes, tem sido estimulado pela enorme quantidade de dados produzidos nos artigos científicos que visam a caracterização da fisiologia bacteriana, mecanismos de infecção e patogênese e desenvolvimento da doença. Alguns exemplos: produção de árvores resistentes ao cancro cítrico (Patente Numero: PCT/US2012/021043); composição e processo para redução do cancro cítrico (Patente Numero: PCT/US2002/020159); combinação ácida – reação única para uso de produtos agrícolas (Patente Numero: US8216972 B1); composição e método para o controle de bactérias fitopatogênicas usando fosfito de cobre (Patente Numero: US8795736 B2).

Diferentemente da classificação tradicional bacteriana baseadas em taxonomia clássica, as bactérias desse gênero são classificadas de acordo com o *patovar*. Na prática, isso implica em uma classificação das espécies considerando a especificidade do hospedeiro ou tecido, o que permite a distinção das espécies em 27 patovares, os quais talvez não fossem evidentes se utilizássemos as bases tradicionais (Brunnings et al, 2003).

X. citri é uma bactéria fitopatogênica com temperatura ótima de crescimento entre 25°C e 30°C, com um flagelo polar, de forma bacilar, aeróbica e que apresenta colônias facilmente identificadas a olho nu em razão de um pigmento amarelo denominado de xantomatodina, cuja função é proteger a bactéria de danos fotobiológicos (Buttner et al., 2010). O nome *Xanthomonas* é derivado do grego por conta do aspecto amarelado e característico que este pigmento confere à bactéria, *xantho* significa amarelo (figura 2A).

As provas de identificação clássicas baseadas nos testes bioquímicos revelam que *X. citri* é positiva para hidrólise de açúcar, hidrólise de caseína, catalase positiva, produtora de tirosinase e negativa para redução de nitrato (Das et al., 2003). Os dados oriundos do sequenciamento do genoma desta bactéria revelam um elevado conteúdo de GC, 60% do genoma, com 4313 genes codantes para proteínas, 87 elementos de inserção (IS) e dois plasmídeos extras. Os plasmídeos pXAC33 e pXAC64 são exclusivos da *X. citri* e são codantes para 42 e 73 proteínas, respectivamente (da Silva et al., 2002). Não obstante, as espécies de *Xanthomonas* sp. possuem regiões do DNA e proteínas com alta homologia entre si, mesmo infectando hospedeiros distintos e/ou locais diferentes, como é o caso da *X. citri* e da *Xanthomonas campestris* pv. *campestris* (*X. campestris*) (Buttner et al., 2010).

Causadora do cancrose do tipo A (origem asiática), que é a forma mais severa de cancroses em virtude da área de lesão que é mais extensa e pronunciada, a infecção por *X. citri* leva à quarentena da região e, pode ser transmitida entre diversas plantas através do fluxo de pessoas, materiais de trabalho contaminados e tempestades, não existindo um vetor de transmissão propriamente dito (figura 1). Além

disso, tornados e ventos podem dispersar a bactéria para mais longe facilitando a penetração desta através dos estômatos ou por feridas realizadas pelos insetos.

1.2. Desenvolvimento da Doença

Folhas novas, galhos, caules e frutos são mais susceptíveis à infecção por *X. citri* do que estruturas e tecido mais antigos que são mais resistentes. Ainda não foram encontradas evidências de que também estaria presente em sementes. A infecção é favorecida em regiões mais tropicais em épocas de temperatura mais quentes próximas à temperatura ótima de crescimento do microrganismo e temperaturas mais amenas reduzem a população bacteriana. Geralmente, *X. citri* sobrevive na superfície das folhas de forma epifítica e no solo seu número é bem reduzido, sobrevivendo apenas quando está associada aos restos das plantas e raízes. A goma xantana, polissacarídeo de alta complexidade produzido por *X. citri* e demais bactérias do gênero *Xanthomonas* sp., protege as bactérias nessas situações extremas quanto a clima como também pode favorecer sua dispersão através de chuvas, ventos ou trânsito humanos e de maquinários (Graham, et al, 2004)

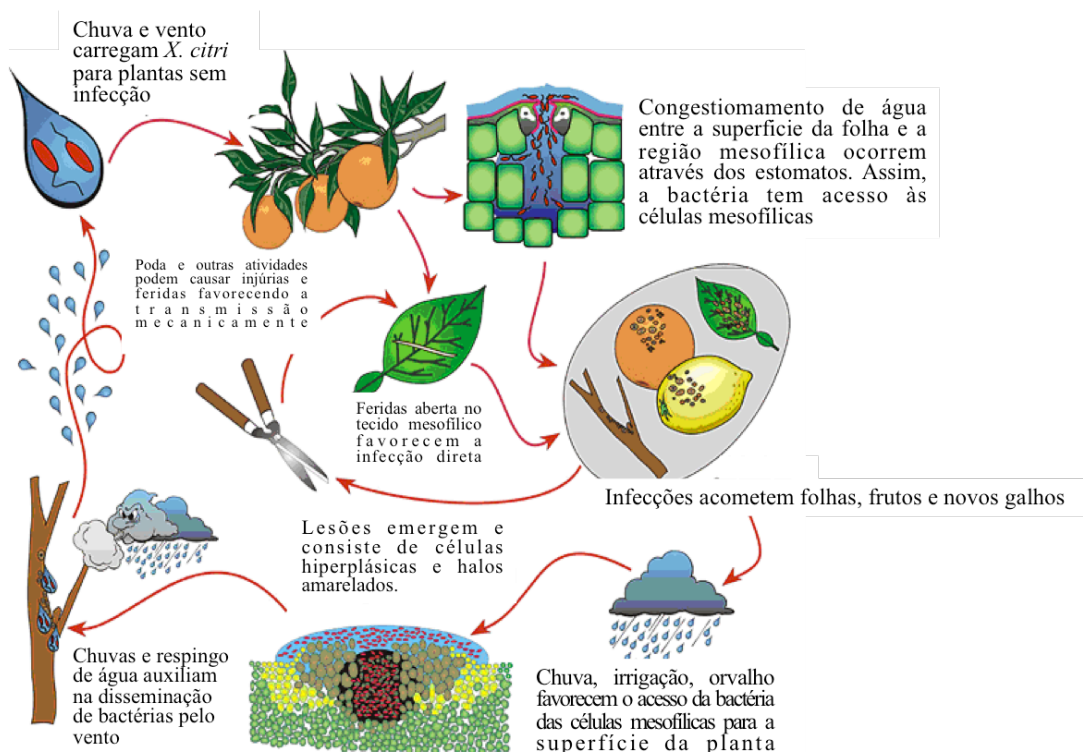


Figura 1. Eventos de desenvolvimento do cancro cítrico por *X. citri*. Disponível em: <<http://www.plantmanagementnetwork.org/pub/php/review/citruscanker/>>. Acesso em 24 de Setembro de 2014. As principais vias são a poda, tempestades, insetos e vento.

Após a infiltração no tecido vegetal através dos estômatos, *X. citri* migra para células mesofilicas e inicia sua proliferação originando sintomas que serão dependentes da quantidade de células bacterianas. As lesões podem apresentar clorose que são os halos amarelos circundados por pústulas e à medida que aumentam de tamanho, tornam-se salientes e parecem estar embebidas em água - *water-soaking lesion* - (figura 2F). As pústulas, inicialmente amarelas, tornam-se amarronzadas em decorrência da resposta de hipersensibilidade da planta, que leva à morte do tecido ou necrose. Interessantemente, as rupturas da epiderme e dos estômatos colocam a bactéria em contato com o meio ambiente favorecendo a dispersão da mesma como um importante veículo de inóculo para outras plantas (figura 2C) (Graham et al, 2004). Em estágio avançado ocorre a perda da folhas e de frutos, de forma imatura, bem como sua deformação, prejudicando economicamente o mercado de suco concentrado e processado.



Figura 2. *Citrus sinensis* e aspectos da interação com *X. citri*. A) Colônias de *X. citri* isoladas em LB ágar com aspecto amarelo em virtude da xanthomatodina. B) *X. citri* é uma bactéria gram-negativa com coloração rosada em decorrência da fucsina na coloração de gram. C) *X. citri* saindo dos estômatos após seu rompimento, geralmente cinco dias após a invasão, imagem de microscopia eletrônica. D) Microscopia eletrônica no interior da folha mostrando a goma xantana, como principal EPS participando da matriz no qual as bactérias ficam embebidas. F) Aspecto da lesão do cancro cítrico com 20 dias após inóculo de *X. citri*. Observe que a folha se torna irregular, com pústulas e aspecto decorrente da produção da goma no interior da folha. (Adaptado de Brunnings et al, 2004).

1.3. Os fatores de Patogenicidade de *X. citri*

Algumas proteínas produzidas por *X. citri* diretamente relacionadas à patogenicidade foram identificadas em diversos trabalhos oriundos da genômica (da Silva et al, 2002), de microarranjos (Monge et al, 2005), proteômica (Zimaro et al, 2013), bioinformática e biologia molecular (Mhedbi

Hajri et al, 2011) e high-throughput screening de mutantes (Yan, et al, 2012). Essas proteínas podem representar a ativação de importantes vias de motilidade celular, adesão, sinalização celular, biofilme, sensor de quórum, sistemas de secreção, importação de nutrientes, produção de goma, secreção de enzimas degradativas e antígenos de superfície. Algumas bactérias deste gênero, como *X. campestris*, também são empregadas na indústria de alimentos para a produção da goma xantana como espessante em diversos segmentos como molhos e cremes a base de queijo, por exemplo. A goma é um polissacarídeo de alto peso molecular consistindo de duas unidades de glicose, duas de manose e uma de ácido glucorônico. É sintetizada pelo óperon *gum* e consiste em um dos principais fatores de patogenicidade, uma vez que secretada para o meio extracelular propicia a adesão da bactéria na folha ou no tecido a ser colonizado, ajuda na retenção de água caracterizando o fenótipo da infecção. Adicionalmente, retém nutrientes e é a principal matriz do biofilme como estratégia de colonização, protege a bactéria de agentes agressivos, e favorece a dispersão da bactéria no meio ambiente (figura 2D).

A mutação deletional em alguns dos genes do óperon *gum*, dentre eles o gene *gumB*, reduz brutalmente a sintomatologia do cancro cítrico em folhas de *Citrus limon* (Yan et al, 2012). Além disso, alguns mutantes de genes do operon *gum* também apresentaram dificuldades para sobreviver ao estresse oxidativo durante a fase estacionária (Rigano et al, 2007; Vojnov et al, 1998). Enzimas como a catalase (KatE) e superóxido dismutase (SodC ou SodM) são ativadas como mecanismos de proteção das bactérias em seu ambiente intracelular em resposta à reação de hipersensibilidade da planta durante à infecção e fatores transcricionais.

Via de regra, as proteínas mais citadas nos trabalhos estão presentes na membrana externa com a função ou de proteínas de adesão fimbriais e adesinas não fimbriais tais como a YapH e FhaB. Essas proteínas são elementares para a adesão da bactéria nos estágios iniciais da infecção do tecido vegetal e desenvolvimento do biofilme e têm sido muito alvos de estudos nos últimos 5 anos por diversos grupos de pesquisa (Yan et al, 2012; Chung et al, 2007; Silva et al, 2011). Gottig e colaboradores (2009) mostraram por meio de deleção a importância do gene *fhaB* na adesão e formação de biofilme em superfícies bióticas e abióticas. Curiosamente, como consequência, *X. citri* passou a apresentar uma motilidade aumentada e aumentou também a produção de EPS (goma xantana). Tal comportamento celular seria uma adaptação para que interações com o hospedeiro e construção dos estágios iniciais do biofilme sejam mantidos. Como forma de regulação da ativação deste gene, foi encontrado em seu promotor região do PiP box, um elemento regulatório no qual parece ser induzido pela planta.

Proteínas de membranas são importantes no auxílio da infecção, algumas vezes compostas de várias subunidades ou de complexos de proteínas. Entre estas encontramos os sistemas de secreção e

sistemas dois componentes (*Two Component System*) os quais estão relacionados ao envio de substâncias ou sinais químicos através de vias de sinalização para monitoramento do ambiente. Receptores de membrana também têm sido descritos como relevantes na infecção uma vez que favorecem mecanismos de adaptação e podem garantir a especificidade das espécies em relação ao seu patovar (Mhebdi Hajri et al, 2011). TonB, um receptor clássico de membrana foi extensivamente identificado nos estudos de proteômica realizados no presente trabalho (capítulo 3, sessões 3.1 e 3.2) em condições de estresse.

Adicionalmente, *X. citri* possui 114 genes anotados para o sistema de dois componentes, sendo dois bem descritos em fitopatógenos e em *X. citri*: HprG e ColR/S. O sistema ColR/S está envolvido na regulação negativa da enzima catalase, produção de LPS (lipopolissacarídeo), formação de biofilme, atividade ou síntese da PthA e estresse ambiental (Yan, et al, 2011). Ainda, *X. citri* apresenta uma gama de mecanismos para o transporte de proteínas efetoras que podem modular a atividade celular e molecular da célula hospedeira. Geralmente proteínas efetoras como AvrBs3, PthA, XopD são translocadas através dos sistemas de secreção do tipo III (Cernadas et al, 2009; Rayan et al, 2011). Este sistema é um dos mais importantes para a patogenicidade, pois proteínas efetoras acessam o núcleo da célula hospedeira e modulam a expressão de alguns genes essenciais para o desenvolvimento de fenótipos característicos do cancro cítrico (Gürlebeck et al, 2006). Os sistemas de secreção tipo III formam extensos poros que funcionam como apêndices para conectar *X. citri* com a membrana da células vegetais e são resultante da transcrição dos óperons *hrp* e *hrx* que recebem este nome por desencadear uma resposta de hipersensibilidade (HR). A HR consiste da resposta inata da planta levando a região atingida à morte celular através do ataque de espécies radiculares de oxigênio (EROS). A deleção de genes do óperon *hrp* interferiu na expressão de diversos sistemas dois componentes – aumentando o reduzindo a expressão destes - em *X. citri* como também de proteínas regulatórias do Pho regulon tais como PhoU (Guo et al, 2011).

O sistema de secreção do tipo II secreta enzimas degradativas como celulases, proteases e outras no intuito de quebrar a parede celular vegetal. O sistema de secreção to tipo II é formado na membrana externa e interna da bactéria e não faz contato direto com à célula do hospedeiro, diferentemente do que ocorre nos sistemas de secreção do tipo III e IV. *X. citri* possui 11 genes codantes para o sistema de secreção do tipo II que são parte do óperon *xps*, que quando foram alvos de intervenções genéticas afetaram a virulência da bactéria (Buttner et al, 2010).

Adicionalmente, outros sistemas podem atuar como secundários na virulência e patogenicidade da *X. citri*. Podemos destacar os sistemas de transporte do tipo ABC (do inglês ATP-Binding Cassete) que funcionam como bombas de captação de macronutrientes variados e que indiretamente afetam a

produção de fatores de virulência como a goma, por exemplo (da silva et al, 2002; Rojas et al, 2013; Araújo et al, 2013). É interessante ressaltar que o genoma de *X. citri* dedica 4% do seu genoma a estes sistemas de transporte, que são altamente especializados, utilizam ATP e estão relacionados à nutrição em situações de carência nutricional. O estudo de bactérias mutantes com transportadores do tipo ABC, deletados por exclusão alélica, evidenciaram que a bactéria pode apresentar deformidade estrutural, dificuldade de agregação, dificuldade de crescimento e influência no desenvolvimento do cancro. Esses dados ainda sob análise, mostram a patogenicidade dependente de sistemas essenciais de nutrição (Sampaio, 2015).

1.4. Pho Regulon: A captação de fosfato dependente dos transportadores do tipo ABC e da sinalização celular através dos sistemas dois componentes

O fosfato é um importante nutriente para qualquer sistema vivo pois é encontrado sob a forma de energia, no DNA, membrana, transdução de sinal e tantos outros processos no ambiente celular. A disponibilidade de fosfato no ambiente e sua ciclagem nas mais variadas formas, seja livre, ou complexada com metais, ou ainda mineralizadas em rochas que são encontradas no ambiente, ocorre devido ao ciclo biogeoquímico do fósforo. Diferentes formas de fontes de fósforo estão disponíveis em sistemas vivos tais como o ortofosfato (fosfato inorgânico) ou fosfonatos e glicose-6-fosfato, quando incorporado com matéria orgânica (Gupta et al, 2014; Wanner 1996). Embora as fontes de fósforos sejam diversas, a quantidade de fosfato orgânico (PO_4) livre disponíveis no solo pode variar de 200 à 6000 $\mu g\ g^{-1}$ dependendo do tipo de solo e pH. Logo, a quantidade de fosfato disponível em solo além de ser baixa na forma livre, também pode estar complexada a outros íons metálicos como ferro e arsênio; mineralizada sob a forma de apatita, insolúvel quando complexada ao cálcio (Gupta et al, 2014).

A células bacterianas dispõem de diversos sistemas para evitar carências nutricionais como também estímulos físicos e químicos na tentativa de eliminar os riscos da seleção natural. Alguns destes sistemas quando mutados ou removidos de determinado organismo revelam a resposta biológica efetora que podem estar envolvidos. Neste contexto, bactérias em geral, possuem sistemas especializados e sofisticados de captação de fosfato e de fontes alternativas de fósforo para resistir aos estresses ambientais. Evolutivamente, estes organismos desenvolveram sistemas especializados de captação e transporte como transportadores ABC e sensoriais como os sistemas dois componentes. No caso do fosfato em *E. coli*, tais sistemas pertencem ao bem conhecido e estudado regulon Pho, o qual compreende no mínimo 31 genes regulados pelo íon (Hsieh et al, 2010). É importante ressaltar, que

além do regulon de fosfato, a bactéria quando em situação de não carência nutricional ou elevada disponibilidade utiliza de um sistema menos específico para importação denominado de sistema Pit (Phosphate- inorganic-transportation) ao invés do regulon de fosfato. O sistema Pit não utiliza da hidrólise de ATP, mas de uma força próton-motriz para internalização do macronutriente, não é ativado sob condições de carência de nutricional como os membros do regulon de fosfato e sua ativação não responde à oscilação da concentração de fosfato no ambiente intra e extracelular (Wanner et al., 1996).

Alternativamente, os genes do regulon Pho codificam sistemas de elevada afinidade ao fosfato e outras fontes de fósforo para internalização - metabolismo em situações de carência -, sistemas dois componentes para sensoriamento de fosfato no meio extracelular, e enzimas para hidrólise de componentes fosfatados ou fosforilados. Mediante ao papel biológico do fosfato no ambiente intracelular tais como, íon, agente tamponante, agente sinalizador ou um integrante estrutural de macromoléculas biológicas, é notório que uma gama de diferentes sistemas biológicos atuam sinergicamente para manter sua concentração constante. Atualmente, o regulon Pho tem sido alvo de estudo de *E. coli* (Hsieh et al, 2010), *M. smegmatis* (Gebhard et al, 2009), *Siborhizobium meliloti* (Yuan, et al, 1993), *Bacteroides fragilis* (Wakimoto et al, 2013), *Proteus mirabilis* (O' May et al, 2009), *X. citri* (Pegos et al., 2014a; 2014b), entre outros. Recentemente organismos marinhos tais como *Trichodesmium* ssp. têm sido estudados em virtude das características do seu habitat oligotrófico e revelaram a presença de duplicações gênicas de diversas enzimas e sistemas de alta afinidade para captação de fosfato (Orchard, et al, 2009).

A forma preferencial para recrutar fontes de fósforo é a captação de P_i (ortofosfato) em virtude de seu estado de oxidação e sua fácil metabolização. Uma das formas para reduzir este problema em ambientes com restrição à esse macronutriente, é a captação mediada por transportadores ABC (*Phosphate Specific Transport*, Pst) os quais apresentam uma proteína periplasmática com elevada afinidade ao substrato que dispara alterações conformacionais necessárias na permease e ATPase para que exista um transporte com gasto de ATP. Tradicionalmente ativo em condições de inanição ou em ambientes de reduzida disponibilidade de fosfato, em *E. coli*, o operon *pstSCAB* codifica uma proteína periplasmática ligadora de fosfato, PstS, um homodímero de duas ATPases (PstB) e um heterodímero de duas permeases, PstA e PstC. Além do sistema de transporte ser ativo contra um gradiente de concentração, os transportadores de fosfato são altamente específicos sendo a cinética de Michaelis Menten para captação do PstSCAB de *S. meliloti* de 0,2 μ M e a velocidade máxima (V_{max}) de 70 nmol/min/mg caracterizando este sistema de alta velocidade (Yuan et al, 2006). Essas velocidades são maiores do que as registradas para o sistema Pit. A proteína periplasmática ligadora de fosfato recebe o nome de PstS (do inglês, *Phosphate Specific Transport*) ou eventualmente de PBP (*Periplasmic*

Phosphate Binding-protein). A conservação deste sistema é indispensável para o crescimento celular, a tal ponto que bactérias que sobrevivem em ambientes oligotróficos apresentam duas cópias do gene da *pstS*. A afinidade da PstS de *E. coli* foi caracterizada ainda na década de 1990 por Wang e colaboradores (1997) e revelou um K_d de 0,31 μ M quando em pH 8,5.

O estudo com mutantes deletionais do operon *pstCAB* em *E. coli* O78 que frequentemente acomete aves, revelou que a ausência deste sistema não só reduz drasticamente a viabilidade celular, quanto dificulta a capacidade de aglutinação requerendo mais unidades formadoras de colônias por mililitro (UFC/mL) do que a bactéria selvagem. Além disso, foram reportados dados com a redução da produção da fimbria tipo 1 à medida que o regulon Pho era ativado (Bertrand et al, 2010).

Em *Proteus mirabilis* HI4320 o sistema Pst foi estudado através de espectrometria de massas, mutantes e ensaios de biofilme (O' May, et al, 2009). Neste organismo a presença da proteína PstS é fundamental para a manutenção da viabilidade celular em relação à selvagem. Imagens obtidas através de microscopia confocal à laser de varredura comparando o biofilme entre as cepas selvagem, Δ pstS e Δ pstA foram realizadas (figura 3) indicando que não apenas a contagem de células viáveis de PstS são reduzidas como também a capacidade de formar biofilme maduro. Acredita-se que o fato do regulon Pho ser expresso constitutivamente nesses mutantes justifique a dificuldade na formação de biofilme, neste caso, por reprimir também o sensor de quórum e a síntese de pequenas moléculas reguladoras deste processo (O'May et al, 2009; Crépin et al, 2006). Neste caso a deleção de *pstS* afeta os mecanismos de transporte como também de regulação do sistema Pst. Muitas vezes os sistemas de importação de fosfato inorgânico não estão unicamente relacionados à importação deste macronutriente, mas também com uma regulação ainda não totalmente compreendida. Neste cenário, a deleção de um componente periplasmático leva à expressão constitutiva da fosfatase alcalina (FA), assim como a produção constitutiva do sistema Pst (Wanner, 1996).

Crépin e colaboradores (2008) estudaram o transcriptoma de um mutante deletional de *pstS* da APEC (**A**vian **P**atogenic **E***Escherichia coli*) e identificaram mais de 470 proteínas diferencialmente expressas. Dentre os genes que são regulados positivamente encontramos aqueles envolvidos na defesa de espécies reativas de oxigênio tais como SodM e catalase, proteínas que aumentam o tempo de meia vida de RpoS, diretamente ligada ao estresse, superregulação de transportadores do tipo ABC importadores de oligopeptídeos (OppA), FA, PhoB, proteínas de resistência ácida, metabolismo energético, entre outros. A hipótese é que a bactéria se prepare para evitar ataques de espécies reativas de oxigênio produzindo SodM e catalase; transcreva genes de resposta ácida para protegê-la durante o crescimento na fase exponencial e logarítmica; e utilize do sistema OppA para importação de aminoácidos que além de servir como fonte de nitrogênio, carbono e ATP, poderiam proteger as células

de outros estresses. Ainda, como em alguns organismos, a deleção de *pstS* implicou na redução das fímbrias do tipo I e na dificuldade de aglutinação, sendo o papel desta fímbria necessário para adesão e colonização no tecido hospedeiro e uma das relações estabelecidas entre um transportador de íons específico e a relação com a formação do biofilme.

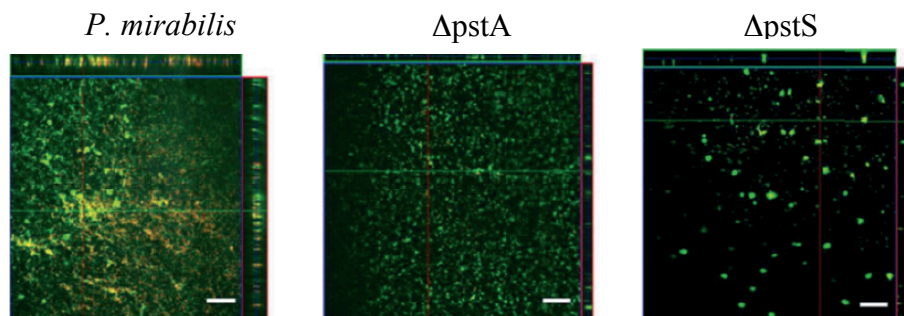


Figura 3. Imagens de microscopia confocal a laser de varredura de *Proteus mirabilis* e mutantes de PstS e PstA. A mutação de PstS é mais severa do que a mutação de um dos componentes da proteína de membrana. É possível visualizar como o biofilme produzido por Δ pstS é formado em menor quantidade e em segregados de microcolônias, diferentemente do observado para o selvagem. Retirado de O'May et al, 2009.

Além do transporte de fosfato e fontes alternativas de fósforo, diversos estudos também apontam a participação de uma fosfatase alcalina encontrada no espaço periplásmico de bactérias gram-negativas. Essa enzima é estudada desde 1960 e se tornou um marcador de ativação clássico do regulon Pho, produzida rapidamente quando a bactéria encontra situações de depleção de fosfato. Geralmente é um dímero ativo em pH alcalino (pH 8,5 – 9,5) e tem zinco como seu cofator (Torriani, 1990; Levinthal et al, 1962). A enzima FA é regulada por PhoB na carência de fosfato sendo sua síntese e atividade completamente reprimidas quando concentrações satisfatórias de fosfato estão presentes. Após a entrada de monoésteres no espaço periplasmático, a FA promove a clivagem e liberação do fosfato para que este seja capturado por proteínas periplasmáticas PstS. A atividade da enzima FA na carência de fosfato é correlacionada com a ativação de componentes do regulon Pho (Orchad et al, 2009; Yuan et al, 2006; Wend et al, 2009; Torriani et al, 1960). Assim, diversos trabalhos utilizam a atividade dessa enzima como medida contundente para atestar a ativação do regulon de fosfato em situações de carência nutricional induzidas em laboratório (Wanner et al, 1993).

Embora o Transportador do tipo ABC seja responsável pelo transporte, o sensoriamento quanto à abundância de fosfato no ambiente extracelular e os fenômenos de transdução de sinal que controlam a resposta celular ocorrem através do sistema dois componentes (TCS- Two Component System). O monitoramento do ambiente extracelular e o disparo de respostas adaptativas não é exclusivo do sistema de fosfato, sistemas dois componentes específicos são relatados para estresse osmótico,

quimiotaxia, resistência à drogas, quórum sensing e diversos outros processos (Kaserer et al, 2010). As proteínas PhoR-PhoB são membros do regulon de fosfato e integram o TCS que é responsável pelas mudanças moleculares e celulares visando a adaptação celular mediante a carência de fosfato (Hiesh, et al., 2010).

PhoR é a histidina quinase (HK) e PhoB é a proteína reguladora de resposta (RR), que juntamente com o sigma 70 modula a atividade da RNA polimerase (holoenzima) (Makino et al, 1993). Após a ativação de PhoB através da fosforilação de PhoR em um ácido aspártico, a proteína PhoB, através do domínio c-terminal interage com o DNA em regiões promotoras ou intergênicas que possuam a sequência consenso denominada de Pho-Box (CTGTCATATATCTGTCAT) (van Bogelen et al, 1996) (figura 4). Novas regiões têm sido identificadas sugerindo que outros fatores sigma também podem contribuir com o início da transcrição de genes regulados diretamente pela carência de fosfato. Curiosamente, nem sempre o PhoB será encontrado próximas as regiões -35 e -10 do promotor, algumas regiões do DNA esse sítio pode estar até 1000 pares de base distante do nucleotídeo na posição +1 a ser transcrito (Yuan et al, 2006; Yoshida et al, 2012).

Acredita-se que o regulon Pho e a modulação de sua ativação não ocorra somente em decorrência das baixas disponibilidades de fosfato e estímulos para síntese de transportadores de alta afinidade, mas que também PhoB conecte outros sistemas de resposta centrais fazendo parte de uma rede biológica ainda maior. Especula-se que a forma como o Pho regulon ative respostas secundárias frente à depleção de fosfato, como resposta ácida e estresse oxidativo, poderia ocorrer tanto a partir da ativação de PhoB através de outras HK, que não somente PhoR, como também da conservação e distribuição de *phobox* em outras regiões do DNA (Wanner et al, 1996; Crépin et al 2008). Experimentos realizados por Yoshida e colaboradores (2012) baseados em ensaios com gene repórter e mutantes duplos de PhoRB, revelaram que a regulação exercida pelo sistema PhoRB parece ser do tipo “on” e “off”. Em alguns organismos PhoB pode induzir respostas patogênicas secundárias em decorrência da necessidade de fosfato, como também pode estar envolvida na sobrevivência destes organismos (Wakimoto et al, 2013).

A mecânica de ativação do regulon de fosfato que resulta em todos esses efeitos celulares e moleculares discutidos até aqui é representada na figura 4 através da transdução de sinal desencadeada pelo sistema PhoRB e a importação de fosfato pelo sistema Pst. Em decorrência da queda da concentração de fosfato no meio extracelular em valores menores que 4 μ M, PhoR utiliza a hidrólise de uma molécula de ATP para auto-fosforilar um resíduo de histidina encontrado na porção citosólica. Após fosforilada, a proteína transfere este fosfato para um ácido aspártico da proteína PhoB que será ativada para controlar a expressão de genes diretamente ligados ao metabolismo de fosfato através da

interação com DNA nas regiões consenso *phobox* (Hsieh et al, 2010), incluindo genes do sistema Pst que ativa a importação de fosfato e a atividade da enzima FA no periplasma.

Após o restabelecimento da homeostase e com a disponibilidade de fosfato maior que 4 μM no ambiente extracelular, PhoB é desfosforilada e PhoR apresenta-se inativa formando possivelmente um complexo repressor com o sistema Pst, PhoU (proteína sem função definida), localizada na membrana plasmática. Por conseguinte, o sistema Pst não realiza o transporte de fosfato pois a saturação foi atingida e pode ser o responsável pelo estado inativo de PhoR.

Estudos funcionais revelam que é necessário que o sistema Pst esteja completo e que PhoU esteja presente para desativar PhoR. PhoU, parece participar do processo entre o sistema ABC e o dois componentes como um regulador negativo, de forma a sincronizar a captação de fosfato com os estágios de ativação de PhoR (Gardner et al, 2014). Embora esteja associada à proteínas que estão ancoradas na membrana, PhoU carece de características de proteínas de membrana.

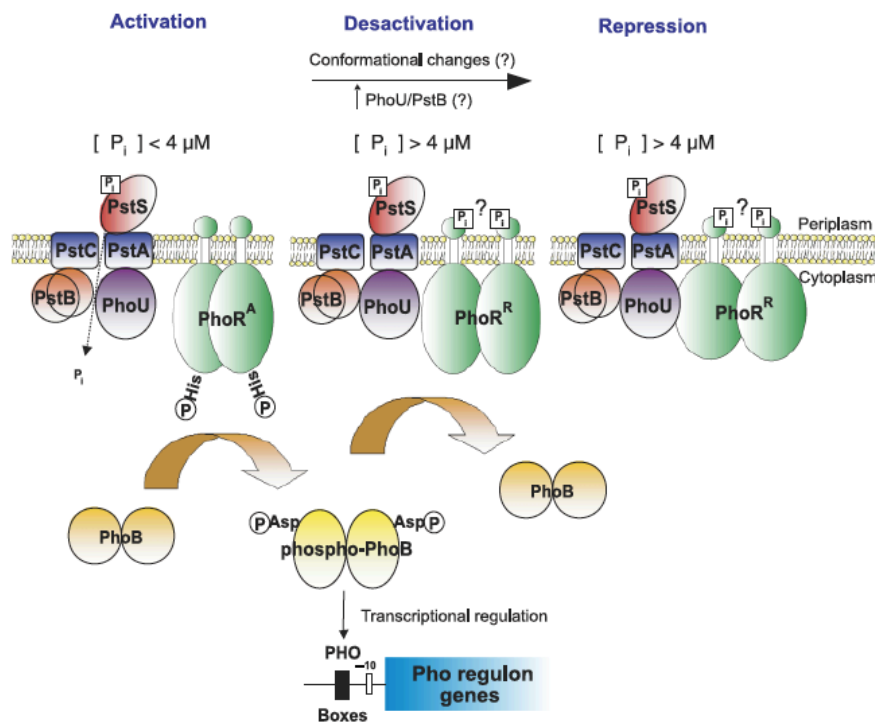


Figura 4. Transdução de sinal do regulon de fosfato em *E. coli*. Modelo de captação, sinalização de P_i e regulação gênica em situações de carência nutricional. Há três eventos descritos em ordens sequenciais: 1) a inibição de PhoR possivelmente através da PhoU ($[P_i] > 4 \mu\text{M}$); 2) em situações de carência de fosfato, PhoR é autofosforilada na His260 ($[P_i] < 4 \mu\text{M}$), e fosforila o fator transcritor PhoB; 3) No restabelecimento da homeostase ($[P_i] > 4 \mu\text{M}$), PhoB é desfosforilada e PhoR é novamente inibida por PhoU. Nesse momento, a captação de fosfato através do componente do transportador ABC PstS pode ou não acontecer. Ainda é desconhecido como a proteína PstS ou o transportador inteiro, nesse caso, induzirá a ativação de PhoR para a fosforilação de PhoB através do modulador PhoU (retirado de Hsieh & Wanner, 2010; VanBogelen et al., 1996).

Apesar dos avanços, o mecanismo de como ocorre a comunicação do sistema entre a captação do fosfato, através de um transportador ABC e a sinalização através de PhoRB não foram completamente esclarecidos. Uma das questões também em aberto é se o limiar de ativação para outros gêneros bacterianos é também próximo à 4 μM . *E. coli* é um dos organismos que mais se estudou este sistema, a disponibilidade de fosfato nos diversos ambientes não é investigado ao ponto de determinar as situações de ativação para outros gêneros bacterianos. As estruturas das proteínas PstS, FA e PhoB, análises baseadas em mutantes, proteômica e transcriptômica são algumas das abordagens usadas para a compreensão do sistema Pho e que demonstram que todos os componentes são essenciais para o regulon de fosfato. A deleção de quaisquer proteínas dos sistema pode causar diversas alterações quanto a ativação do mesmo. Por esse motivo, há muito tempo o regulon de fosfato é alvo de investigação científica. Assim, encerramos este tópico trazendo o desafio proposto na conclusão do trabalho de Torriane e colaboradores que desde a década de 90 permanece em aberto:

“Nós sabemos que a repressão do regulon Pho não é dependente do transporte de fosfato através do sistema Pst. Contudo, nós também sabemos que a repressão do Pho é combinada através de PhoR e PstS” (Torriani et al, 1990).

1.5. Transportadores do tipo ABC e Sistemas de Transdução de sinal em Procariotos

1.5.1. Transportadores do tipo ABC em procariotos: captação de nutrientes, adaptação ao ambiente e patogênese bacteriana

A manutenção da homeostase no ambiente intracelular é mediada através do intercâmbio de substâncias entre o ambiente intracelular e extracelular. O transporte de substâncias através da membrana plasmática deverá ocorrer por meio da seleção do tamanho do soluto, carga, concentração e necessidade ou relevância do mesmo no ambiente celular. Neste contexto, os transportadores do tipo ABC, encontrados em todos os organismos, são responsáveis pela importação e exportação de substâncias (figura 5) e que podem captar uma diversidade de substratos tais como íons, peptídeos, aminoácidos, vitaminas, poliaminas, sideroforos, entre outros (Davidson et al, 2008).

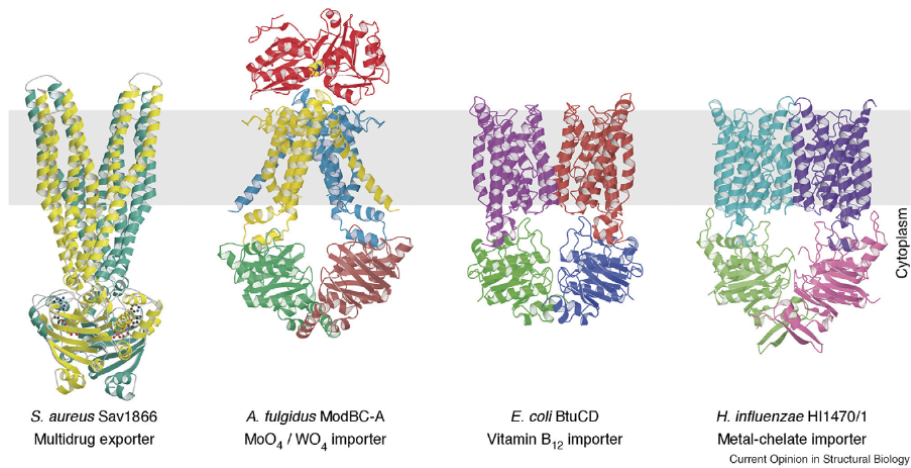


Figura 5. Estrutura dos transportadores ABC exportadores e importadores de procaríotos. As estruturas deste complexo de proteínas foram obtidas por meio de cristalografia de raios-X. São apresentados 3 importadores e 1 exportador conforme apresentado em Hollestein et al (2007). O código PDB das estruturas é apresentado da esquerda para direita: 2HYD, 2ONK, 1L7V e 2NQ2. Adaptado de Hollestein et al 2007.

A estrutura dos sistemas importadores é bem descrita na literatura com base nos sistemas de captação de maltose (Oldham et al, 2008) e molibdato de *Arqueoglobus fulgidus* (*A. fulgidus*), (Hollenstein et al, 2007a; 2007b) (figura 6). A quantidade de transportadores ABC em bactéria está linearmente relacionada ao tamanho do genoma, segundo Davidson e colaboradores (2008) (figura 6A) e também ao estilo de vida bacteriano.

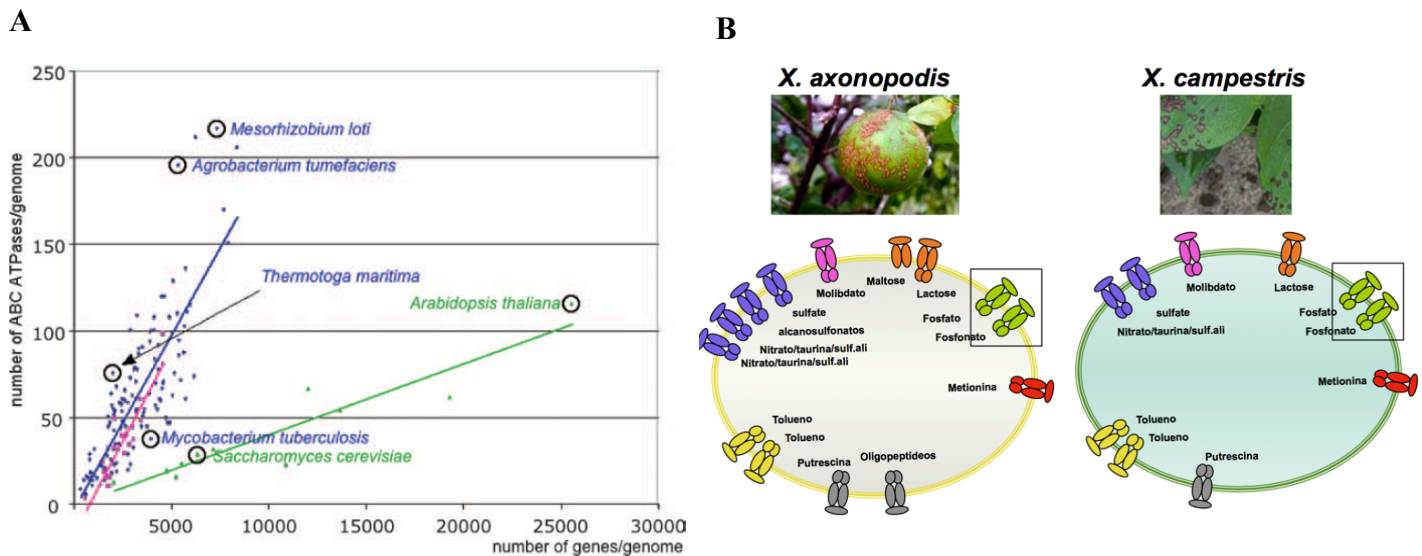


Figura 6. Distribuição dos transportadores do tipo ABC em genomas de procaríotos. (A) Observa-se uma relação linear entre a quantidade de ABCs encontrados e o tamanho do genoma. Para tal busca foi levantada o número de ATPases do sistema contra o número total de genes. Roxo = archaea; Verde = eucarioto; Azul = procaríotos. Retirado de Davidson et al, 2008. (B) Levantamento do número de proteínas pertencentes à família dos transportadores do tipo ABC importadores em *X. citri* e *X. campestris* baseado na anotação ou identidade de sequência dos domínios ligadores de ATP. *X. citri* possui no total de 117 transportadores, sendo 87 importadores, 32 exportadores e 8 hipotéticos. Os transportadores de maior relevância em patogênese foram destacados pelo nosso grupo, incluindo fosfato e fosfonato (caixa preta). Comparado com outros gêneros bacterianos este número é elevado e isso pode ser resultante do habitat e processos correlacionados à colonização desta bactéria em plantas e em solo.

Bactérias que são patógenos intracelulares, como por exemplo *Mycobacterium tuberculosis* (MT), que se concentra nos granulomas durante a intensa reação inflamatória, apresentam uma quantidade relativamente pequena de genes anotados para os transportadores do tipo ABC em seu genoma o que é justificado pela abundante oferta de nutrientes nestas condições. Comparado com outros gêneros bacterianos, *X. citri* apresenta um elevado número destes sistemas o que pode ser um importante fator para garantir o processo de colonização e multiplicação. A figura 6B mostra alguns transportadores do tipo importador identificados em *X. citri* e *X. campestris* destacando que os transportadores ABC são relevantes para as bactérias do gênero *Xanthomonas* sp e que colonizam regiões distintas do hospedeiro.

Há uma gama de transportadores responsáveis por internalizar alguns macronutrientes essenciais que apresentam correlação direta com a virulência tais como ferro, manganês, cobre ou zinco. Esses íons metálicos apresentam transportadores especializados para sua incorporação em virtude de sua restrita biodisponibilidade. Além disso, é uma estratégia de combate do próprio hospedeiro a não garantir abundantes concentrações livres dos mesmos por uma questão de proteção à colonização de micróbios e também de toxicidade celular por estes compostos. Muitos destes elementos são fundamentais para modulação de atividades enzimáticas e biológicas, estima-se que 30% das proteínas presentes na célula podem requerer algum tipo de interação com metal, sejam essas enzimas, centros de ferro-enxofre envolvidas gradiente de prótons H^+ ou proteínas com sítios alostéricos (Lewis et al, 2012). No caso do fosfato, ele é um componente majoritário participando de vias de sinalização celular, energia, DNA, membrana, equilíbrio de fluídos biológicos, entre outros. É natural que microrganismos sejam preparados para perceber alterações ambientais rapidamente, modificar o padrão de expressão gênica e captar moléculas importantes. Além disso, quando se faz referência à disponibilidade de íons metálicos e de fontes de enxofre e fósforo há que considerar que a disponibilidade também envolve os estados de oxidação destes elementos, como por exemplo o ferro que em bactérias é importado em seu estado reduzido (Fe^{3+}) por sideróforos. Alguns elementos como fontes de fósforo nunca estão livres no solo, mas complexados com moléculas orgânicas, como por exemplo, fosfonatos (Wanner et al, 1990). O papel biológico dos transportadores ABC é, portanto, através de sua elevada afinidade, e gasto de ATP, prover macronutrientes com baixa disponibilidade no ambiente em que a bactéria está. A importação de fosfato em microrganismos gram-negativos pode ser realizada através do sistema ABC Pst em situações de carência e de um sistema de baixa afinidade denominado PitA em condições de não carência (Gebhard et al, 2009).

1.5.2. Estrutura e Mecânica dos transportadores do tipo ABC para importação de nutrientes

De uma forma geral, os transportadores do tipo ABC possuem quatro domínios: dois domínios transmembrana (TMD – Transmembrane domains) que formarão o poro de passagem, e dois domínios citoplasmáticos (domínio ligador de nucleotídeo, NBD- Nucleotide Binding Domain) que são responsáveis pela interação e hidrólise do ATP. Adicionalmente, transportadores do tipo importadores, possuem um componente externo, a proteína ligadora periplasmática, que confere especificidade e afinidade aos sistemas (Rees et al, 2009) (figura 6Ae B). A interação desta proteína com a proteína de membrana induz mudanças conformacionais nas permeases que ativarão as ATPases (Oldham et al., 2008; Holleinstein et al., 20011). Na figura 5, são apresentados os transportadores ABC do tipo exportador de drogas de *Staphylococcus aureus* e os transportadores do tipo importadores de molibdato de *A. fulgidus* e vitamina B12 (Hollenstein et al, 2007). A comparação estrutural mostra que existem diferenças significativas, especialmente na organização e formação de proteínas de membrana.

Os domínios NBD são os mais conservados do sistema e apresentam além dos motivos de ligação ao ATP, dois motivos característicos de transportadores ABC, Walker A (GXXGXXGKS-T) e Walker B (XXXXD). Ainda são identificados a sequência assinatura LSGGQ e dois resíduos formadores do sítio Q-loop (glutamina) e H-loop (histidina) (Davidson et al, 2008). A organização genômica dos transportadores ABC em procariotos geralmente ocorre na forma de óperon, no qual todos os genes estão sob o controle do mesmo promotor.

Os domínios transmembrana, por sua vez, são os menos conservados. Localizados na membrana plasmática, suas hélices podem variar e alterar o tamanho e volume de cada canal (Lewis et al, 2012). Petronilli e colaboradores (1991) evidenciaram que os domínios transmembrana possuem baixa afinidade pelo substrato, somente para manter o reconhecimento do mesmo e permitir sua translocação. Recentemente, Oldham e colaboradores (2013) mostraram que no transportador de maltose de *E. coli*, somente uma das permeases (MalF) é importante para o transporte do açúcar.

Em transportadores do tipo ABC o componente periplasmático, denominado neste texto de BP (proteína periplasmática ligadora; binding protein), é o componente responsável pela interação com o substrato a ser translocado e responsável pela alta afinidade. Em bactérias gram-negativas, a BP é encontrada livre no periplasma, mas em gram-positivas, cujo espaço periplásmico é limitado, esta proteína permanece ancorada à membrana. Usualmente, são proteínas monoméricas com massa molecular de 25 kDa a 50 kDa, que possuem apenas um sítio para ligação do substrato localizado na fenda formada entre os dois domínios: o N- e o C-terminal. Geralmente são proteínas específicas para seu substrato, pois a fenda de ligação a ele tem carga e profundidade adequada. Entre as fendas estão os

lobos que compreendem os domínios N e C-terminal. Esses lobos são constituídos de hélices alfa e folha beta sendo a estrutura secundária desta molécula do tipo alfa-beta (figura 7).

As periplasmáticas são classificadas em grupos, e recentemente, a classificação em grupos foi realizada com base nos atributos estruturais dessas proteínas tais como alças de ligação dos domínios. As periplasmáticas classificadas como tipo I apresentam hélices alfa entre os domínios e são representadas pelas proteínas ligadoras de ferro, metal quelado, zinco e manganês; as do tipo II apresentam loops pequenos conectando hélices e fitas entre os domínios e são representadas pelas proteínas ligadoras de açúcar e também auto-indutores; e as do tipo III acomodam grandes substratos como espermidina, e podem apresentar extensas regiões extras entre os domínios para acomodá-los; e, finalmente, as do tipo IV que apresentam entre os domínios loops e que se ligam à oxianions tetraédricos tais como fosfato e molibdato (Berntsson et al, 2010).

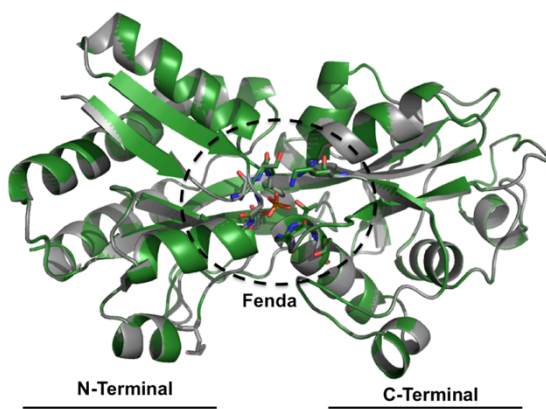


Figura 7. Estrutura da proteína periplasmática ligadora de fosfato PstS de *E. coli* (código PDB 1IXH). A proteína apresenta a estrutura de dois lobos, N e C-terminal, e entre eles, a fenda de ligação ao substrato. Os resíduos em palito dentro da fenda - círculo de linha pontilhada - são os resíduos do bolsão de interação direta com o substrato. Estes resíduos garantem especificidade ao substrato através de complementariedade de cargas e acomodação do substrato em determinado espaço físico em seu interior. As interações químicas entre os resíduos de aminoácidos e os substratos geralmente ocorrem através de interações de hidrogênio com aproximadamente 2,5 Å de distância entre cada átomo. Os domínios N e C-terminal se aproximam quando a proteína interage como ligante para que o mesmo seja mantido até que toda a mecânica do transporte ocorra e os lobos N e C-terminal serão separados novamente. A estrutura de *E. coli* é mostrada em sua conformação fechada. Em laranja é possível observar o fosfato em laranja, ao centro da fenda.

O bolsão de interação com o ligante, apresenta características eletrostáticas e volume coerente com os respectivos ligantes e podem ser extremamente conservados, como em proteínas ligadoras de íons (Santacruz et al, 2013). Além disso, divergem entre si dependendo da classe de moléculas que interagem, por exemplo, há divergências entre os bolsões das proteínas ligadoras de açúcar, de aminoácidos e entre diversos oxianions para que essas proteínas possam ser específicas para cada substrato (Medrano et al, 2014). Adicionalmente, ao interagirem com os seus ligantes, estas proteínas sofrem mudanças conformacionais decorrentes da aproximação dos domínios e fechamento do bolsão com o substrato capturado em sua fenda. Neste estado, tais proteínas interagem com os segmentos das

permeases, por meio de duas regiões, uma de cada domínio, aqui denominadas RI e RII, respectivamente para o domínio I ou (N-terminal) e II (C-terminal). Um exemplo destas regiões e interação é apresentado na figura 8.

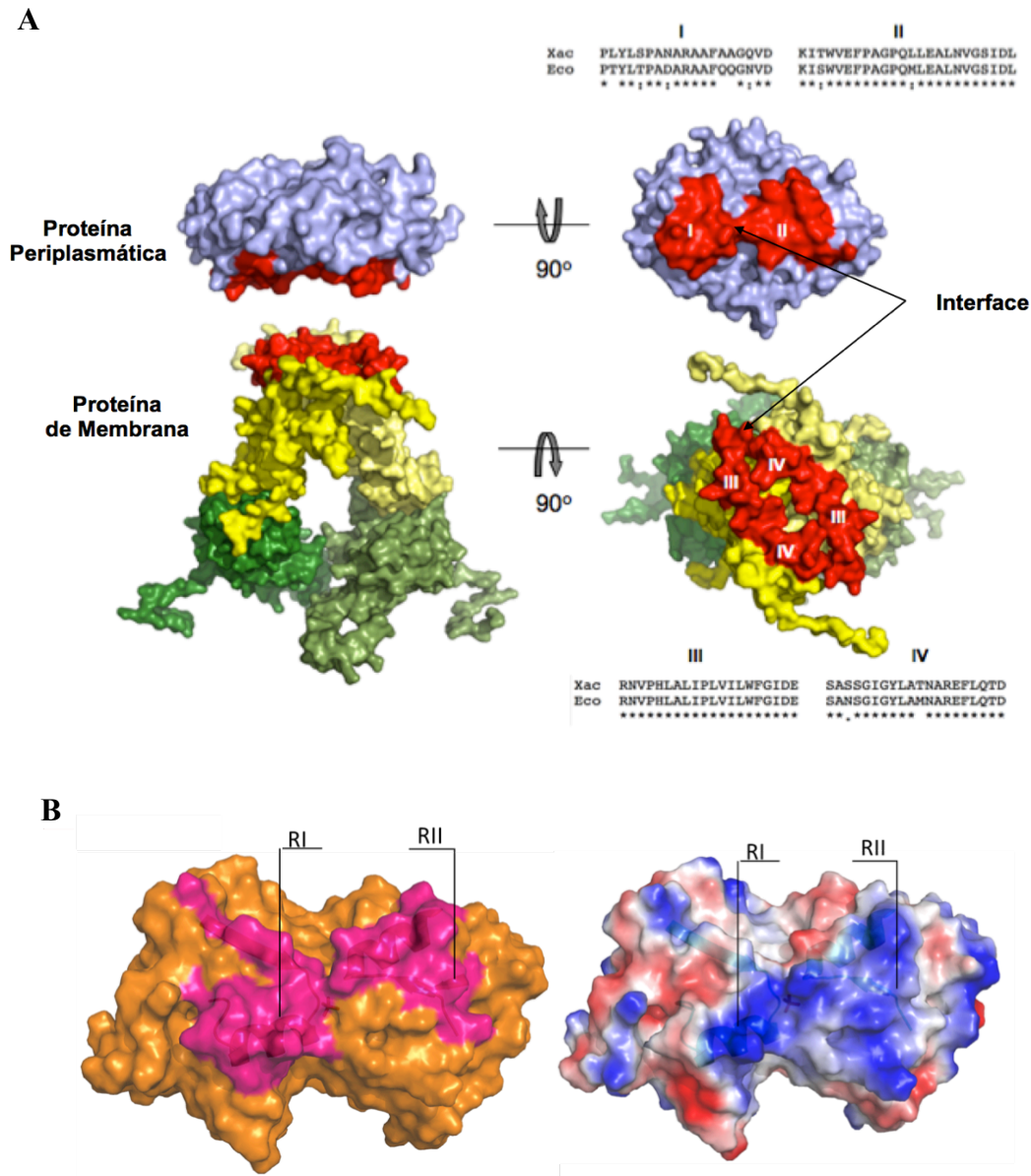


Figura 8. Regiões da BP de interação direta com os domínios TMD do transportador do tipo ABC importador de alceno sulfonatos (A) e fosfato (B). (A) As proteínas do transportador são apresentadas em superfície e coloridas de acordo com a função: BP (superfície azul), transmembranas (superfícies amarelas) e ATPases superfícies verdes. As regiões de interação RI e RII da PB que interagem na membrana são mostradas em vermelho. Alinhamento das regiões das PBs e transmembranas são apresentados para *X. citri* e *E. coli*. (B) A distribuição de cargas dessas regiões poderão ser importantes para interação com a proteínas de membrana e liberação com o substrato. Entre as regiões RI e RII encontra-se a fenda do substrato que tem profundidade e dimensão exclusivas para acomodar o ligante, essas regiões podem ser mais ou menos hidratadas afetando a interação, afinidade e interação com proteínas de membrana através das regiões RI e RII.

A atividade dessas proteínas é dependente das alterações estruturais nos estados aberto e fechado, ou seja quando os domínios N e C-terminal estão separados e quando estão unidos,

respectivamente. Santacruz e colaboradores (2013) identificaram a conservação de duas hélices formadoras de um dipolo para sustentação do molibdato na proteína ModA de *X. citri*, as quais são altamente conservadas nos transportadores de íons. As análises de dinâmica molecular sugerem que um dos domínios sofre maior mudança conformacional no fechamento, induzindo a liberação do ligante no poro (Davidson., et al, 2008).

Finalmente, baseado na estrutura do transportador de maltose, um modelo de funcionamento é proposto no qual a proteína ligadora periplasmática interage com o substrato e o leva à membrana, onde mudanças conformacionais na permease vão ativar a aproximação das ATPases, permitindo a ligação dos nucleotídeos e quebra de uma molécula de ATP. A energia desta quebra é suficiente para promover as alterações conformacionais que abrirão as permeases para recepção do substrato. Ao interagir no poro, os substratos induzem novas mudanças conformacionais que sinalizam para a quebra da segunda molécula de ATP, a qual posiciona as ATPases novamente afastadas e abre o canal (figura 9).

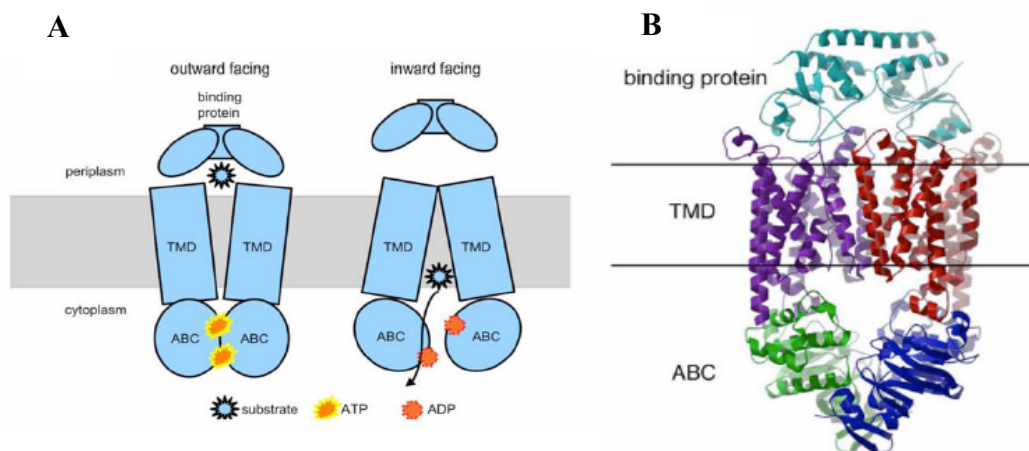


Figura 9. Mecânica e topologia do transportador do tipo ABC importador descritos em procaríotos. A) Ilustração TMD – Domínios transmembrana localizados na membrana interna da parede celular formando o poro pelo qual o substrato será translocado. O domínio ABC – cassete ligador de ATP, também denominado como NBD (Nucleotide-Binding Domain) que liga e hidroliza o ATP durante a translocação. No espaço periplásmico temos a proteína ligadora que apresenta elevada afinidade ao substrato a ser translocado. A ilustração mostra que o transportador pode assumir dois estados conformacionais: *outward* quando aberto para o periplasma e *inward* quando aberto para o citoplasma ou estado de descanso (Retirado de Rees, et al., 2009).

Por fim, objetivou-se descrever e caracterizar de forma mais ampla possível o regulon de fosfato de *X. citri*. Para tal objetivo diversas ferramentas foram utilizadas, como por exemplo, espectrometria de massas para averiguar a abundância das proteínas e consequentemente a ativação do do sistema Pst na carência de fosfato. Pioneiramente, foi empregada a técnica de metabolômica para bactérias, iniciativa em que resultou na publicação em um artigo de métodos mediante as dificuldades enfrentadas durante a etapa de padronização. A extração dos metabólitos da fase polar contribuiu para

identificação e quantificação de metabólitos das principais vias do metabolismo bacteriano. Além disso, a análise de metabolômica neste contexto, permitiu explorar o impacto do fosfato no metabolismo bacteriano em conjunto com os dados de proteômica. Esses dois dados, ao final resultarão em mapas de interação para identificar diretamente quais dos processos moleculares sofrem diretamente com a carência de fosfato, mapas esses que também são conhecidos como interatoma ou redes de interação. Todos esses dados foram obtidos em paralelo aos dados de cristalografia de raios-X, no qual o objetivo concentrava-se em elucidar a estrutura 3D das proteínas do regulon de fosfato. Essa gama de ferramentas avançadas do ponto de vista tecnológico permitiram explorar o sistema de regulon de fosfato em *X. citri* em dois grandes caminhos: o da biologia estrutural para compreensão das estruturas 3D bem como peculiaridades do transporte de fosfato em *X. citri*; e a caracterização funcional, para o estudo das relações do fosfato na fisiologia, patogenicidade e metabolismo bacteriano.

Objetivos

O regulon Pho é um sistema bem caracterizado em diversas bactérias que apresentam os mais variados habitats e hospedeiros e tem sido relacionado à uma série de processos fisiológicos incluindo patogênese e virulência. No entanto, não existiam dados sobre este sistema em fitopatógenos, tanto em nível estrutural como funcional. Neste sentido, esta tese tem como objetivo principal a caracterização dos sistemas Pst e sistema dois componentes de *X. citri*.

2. Objetivos

Dividimos os objetivos do trabalho em duas abordagens: funcional e estrutural conforme apresentadas a seguir:

2.1. Análise funcional de *X. citri* e *X. citri* portador de deleção no gene *pstS* (*Xac::pstS*) em presença e carência de fósforo

- Influência da deleção de *pstS* e da carência de fosfato no crescimento *in vitro* e *in vivo*, na formação de goma, formação de biofilme e desenvolvimento do cancro cítrico;
- Análise proteômica de extratos de culturas de *X. citri* e *Xac::pstS* crescidas em presença e privação de fósforo: caracterização do sistema Pst e dois componentes;
- Análise do papel da PstS na produção de metabólitos por *X. citri* e *Xac::pstS* crescidas em presença e privação de fósforo no meio de cultura.

2.2. Análise estrutural de proteínas do sistema Pst e dois componentes

- Expressão, purificação e análises de cristalografia das proteínas:
 - PhoX do sistema Pst de *X. citri*
 - PhoU, PhoR e PhoB do sistema dois componentes de *X. citri*
- Resolução das estruturas tridimensionais das proteínas de interesse;
- Comparação estrutural das proteínas periplasmáticas PstS e PhoX de *X. citri* utilizando diferentes abordagens como bioinformática, modelagem molecular e filogenia.

Resultados

A sessão de resultados da presente tese será composta por artigos já publicados no item 3.1 e manuscritos para submissão no item 3.2 que contemplam a descrição do sistema de captação de fosfato em *X. citri* utilizando as abordagens de proteômica por espectrometria de massas, metabolômica por RMN, ensaios funcionais, interatoma e cristalografia de proteínas.

Os dados apresentados nesta sessão foram desenvolvidos no período de 2011 – 2014 no *Laboratório Nacional de Biociências* (LNBio) em Campinas sob orientação da Dra. Andrea Balan, e em colaboração com os seguintes pesquisadores: Dr. Francisco Javier Medrano no *Centro de Investigaciones Biológicas* (CSIC) em Madrid, Dra. Rita Café e Dr. Beny Spira do Depto. de Microbiologia da *Universidade de São Paulo* (USP), Dr. Rodrigo Santos do Depto. de Genética da USP, Dra. Ana Zeri no *Laboratório Nacional de Biociências* (LNBio), Dra. Gabriela Meirelles do LNBio, MsC Rafael R. Canevarolo na *Universidade Estadual de Campinas* (UNICAMP), Dra. Alessandra Souza e Dra. Simone Pichhi do *Centro de Citricultura Sylvio Moreira*.

O artigo intitulado “Phosphate regulated proteins of *Xanthomonas citri* subsp. *citri*: A proteomic approach”, publicado no “Journal of Proteomics”, descreve os membros do regulon Pho em *X. citri* a partir de análises de bioinformática baseadas em homologia de sequências, organização genética e espectrometria de massas. Essencialmente, *X. citri* foi cultivada em meio A, o qual tem sido descrito como padrão para caracterização da ativação da enzima fosfatase alcalina (Levinthal et al, 1962) e meio A suplementado com fosfato (A+Pi). Foi analisado as diferenças em termos da abundância de cada proteína, incluindo principalmente as proteínas já descritas como pertencentes ao regulon Pho e proteínas relacionadas. Como resultado, o estudo relata a identificação de 272 proteínas por espectrometria de massas utilizando gel 1D de poliacrilamida preparado com SDS, que foram inclusas em 19 categorias. Por meio desta análise foi possível identificar proteínas que sofreram regulação direta ou indireta em decorrência da concentração de fosfato. Os dados de proteômica revelam que *X. citri* apresenta ativação do sistema Pst em carência de fosfato e regulação aumentada para membros do regulon Pho, incluindo a fosfatase alcalina. Adicionalmente, evidenciamos alguns componentes de transportadores do tipo ABC envolvidos com o transporte de íons.

O segundo artigo apresentado é intitulado “Xanthan gum removal for 1H-NMR analysis of the intracellular metabolome of the bactéria *Xanthomonas axonopodis* pv. *citri* 306”. Este trabalho foi desenvolvido a partir da necessidade de obtermos um protocolo para a realização de ensaios de metabolômica com *X. citri*. Vimos, nas primeiras análises, que seria impossível realizarmos os ensaios e obtermos os metabólitos *X. citri* recuperados através da fase polar devido à presença da goma xantana. Neste sentido, desenvolvemos um protocolo específico para extração dos metabólitos

intracelulares à base de metanol/clorofórmio e ultracentrifugação, que se mostrou bastante eficiente. Além disso, otimizamos a quantidade de célula (pelete seco) a ser trabalhada para estabelecer um intervalo de confiança quanto a identificação e quantificação dos metabólitos. Este protocolo foi importante para a realização dos ensaios que compõem o manuscrito número 3. A goma xantana nesta etapa inviabilizaria a obtenção, identificação e quantificação de cada uma das pequenas moléculas que compõe o metabolismo. Em virtude do tempo dispendido para a padronização do método compreender aproximadamente 1,5 ano de trabalho, o artigo foi incluído como resultados da presente tese para que todas as nuances metodológicas fossem exploradas.

O terceiro artigo intitulado “Crystallization and preliminary X-ray diffraction analysis of the phosphate binding protein PhoX from *Xanthomonas citri*” refere-se à expressão, purificação e cristalização da proteína PhoX de *X. citri*, descrita como proteína ligadora de fosfato. A proteína PhoX foi expressa em cepas de *E.coli* BL21 (DE3) e purificada com gradiente de imizadol (IMAC) e exclusão molecular. Amostras com elevado grau de pureza originaram cristais pertencentes ao grupo espacial P2₁ que difrataram a 3Å de resolução.

Por fim, serão apresentados três manuscritos em preparação e em fase de submissão. O manuscrito intitulado “Two phosphate-binding proteins from the phytopathogen *X. citri*: phylogeny and structural studies”, realizado em colaboração com o Dr. Rodrigo Santos (Depto. de Genética, USP) e Dr. Javier Medrano (CSIC-Espanha), teve como foco explicar a presença de duas proteínas periplasmáticas ligadoras de fosfato em *X. citri*, PhoX e PstS, e apresentar dados comparativos em relação à estrutura, como sítio de interação com o íon e regiões de interação com as permeases. Os resultados mostram que essas proteínas possuem identidade de aminoácidos de 70%, incluindo conservação do sítio de ligação ao fosfato. Além disso, são oriundas de uma duplicação gênica, provavelmente em decorrência de transferência horizontal de genes, a partir de um ancestral de *Desulfatibacterium alkenivrans* (delta-proteobacteria). Deste ancestral também foram originadas as proteínas ligadoras de fosfato em *Xylella fastidiosa*, *E. coli*, *Y. pestis*, entre outras. Ainda, neste mesmo manuscrito descrevemos a estrutura cristalográfica da proteína PhoX destacando a presença de uma longa fita beta que conecta os domínios, diferente do que é evidenciado nas demais proteínas ligadoras de fosfato, implicando em menor flexibilidade estrutural. A estrutura 3D da proteína PstS foi modelada com base na estrutura de PhoX e comparada. Mesmo com 70% dos resíduos de aminoácidos idênticos incluindo o sítio de interação com o fosfato, o potencial eletrostático de superfície dessas moléculas mostraram-se divergentes. A implicação biológica desta divergência estaria relacionada à afinidade e velocidade de transporte do íon, bem como com a interação das proteínas com as permeases na membrana.

O segundo manuscrito intitulado “Low phosphate availability stimulates xanthan gum and biofilm production in *X. citri*” contempla os ensaios funcionais realizados com a linhagem selvagem e mutante para estabelecimento do papel da PstS no crescimento da bactéria em meios de cultivo e em folhas de *Citrus sinensis* (laranja doce), na produção de biofilme, produção de goma e captação de fosfato. Os dados mostram que a deleção do gene *pstS* não resulta em alteração do fenótipo do cancro e tampouco nos dados de biofilme, o que sugere que a PhoX poderia estar exercendo a função da PstS, corroborando os dados anteriores de duplicação e similaridade de função. Por outro lado, a carência de fosfato é um fator importante para a produção de goma xantana e favorecimento da formação de biofilme em superfície abióticas, sugerindo que o íon, como em outras bactérias, está relacionado à respostas adaptativas secundárias. Finalmente, os ensaios de captação de fosfato mostram que durante a carência nutricional PhoX realiza a captação de fosfato, mas PstS estaria envolvida na regulação molecular do operon *pst*, função não compensada por PhoX.

O terceiro e último manuscrito tem como objetivo apresentar de forma sistêmica, o papel da PstS e do fosfato a partir dos dados de proteoma e de metabolômica obtidos com a linhagem selvagem *X. citri* e mutante. As alterações no proteoma evidenciadas nas linhagens evidenciaram a constitutividade do regulon Pho e efeito compensatório de PhoX, conforme verificado no manuscrito anterior. Adicionalmente, a deleção do gene *pstS* leva à regulação positiva de proteínas envolvidas na adesão bacteriana, sistemas de secreção, enzimas degradativas, e proteínas envolvidas no sensor de quórum, enfatizando a participação do gene *pstS* na regulação durante a carência de fosfato. Com relação aos dados de metabolômica, o total de 57 metabólitos foram identificados e quantificados considerando ambas linhagens. Os dados oriundo do proteoma e metaboloma foram empregados em mapas de interação para entendimento do resposta do fosfato bem como da mutação nos principais processos biológicos. Dentre todos os manuscritos apresentados, este ainda está em preparação, sobretudo quando considera-se a análise integrada dos dados de proteômica e metabólica a fim de construir redes de interação.

3. Resultados

3.1. Artigos Publicados

Artigo 1

Xanthan Gum Removal for ¹H-NMR Analysis of the Intracellular Metabolome of the Bacteria *Xanthomonas axonopodis* pv. *citri* 306

Vanessa R. Pegos, Rafael Canevarolo, Aline P. Sampaio, Andrea Balan and Ana C. M. Zeri.

(doi:10.3390/metabo4020218)

Xanthan Gum Removal for ¹H-NMR Analysis of the Intracellular Metabolome of the Bacteria *Xanthomonas axonopodis* pv. *citri* 306

Vanessa R. Pegos^{1,†}, Rafael R. Canevarolo^{1,2,†}, Aline P. Sampaio¹, Andrea Balan¹ and Ana C. M. Zeri^{1,*}

¹ Brazilian Biosciences National Laboratory, Rua Giuseppe Máximo Scolfaro, 10.000-Polo II de Alta Tecnologia, Caixa Postal 6192, CEP 13083-970, Campinas/SP, Brazil; E-Mails: vanessa.pegos@lnbio.cnpem.br (V.R.P.); aline.sampaio@lnbio.cnpem.br (A.P.S.); andrea.balan@lnbio.cnpem.br (A.B.); ana.zeri@lnbio.cnpem.br (A.C.M.Z.)

² Molecular Biology Laboratory, Boldrini Children Hospital, Rua Dr. Gabriel Porto, 1270 Cidade Universitária, CEP 13083-210, Campinas/SP, Brazil

† These authors contributed equally to this work.

* Author to whom correspondence should be addressed; E-Mail: ana.zeri@lnbio.cnpem.br; Tel.: +55-19-3512-1119; Fax: +55-19-3512-1006.

Received: 31 October 2013; in revised form: 5 March 2014 / Accepted: 11 April 2014
/ Published: 22 April 2014

Abstract: *Xanthomonas* is a genus of phytopathogenic bacteria, which produces a slimy, polysaccharide matrix known as xanthan gum, which involves, protects and helps the bacteria during host colonization. Although broadly used as a stabilizer and thickener in the cosmetic and food industries, xanthan gum can be a troubling artifact in molecular investigations due to its rheological properties. In particular, a cross-reaction between reference compounds and the xanthan gum could compromise metabolic quantification by NMR spectroscopy. Aiming at an efficient gum extraction protocol, for a ¹H-NMR-based metabolic profiling study of *Xanthomonas*, we tested four different interventions on the broadly used methanol-chloroform extraction protocol for the intracellular metabolic

contents observation. Lower limits for bacterial pellet volumes for extraction were also probed, and a strategy is illustrated with an initial analysis of *X. citri*'s metabolism by $^1\text{H-NMR}$ spectroscopy.

Keywords: *Xanthomonas*; xanthan gum removal; $^1\text{H-NMR}$; cell extraction protocol; metabolomics of bacteria; metabolomics of microorganisms

Abbreviations

D_2O = deuterium oxide; FID = free induction decay; $^1\text{H-NMR}$ = proton nuclear magnetic resonance; HR-MAS-NMR = high resolution solid-state NMR; LB = Luria Bertani Broth medium; MAS = magic angle spinning; M/C = methanol/chloroform; OD = optical density; RF = radio frequency; TBS = tris-buffered saline; TSP = 3-(Trimethylsilyl)propanoic acid; *X. citri* = *Xanthomonas axonopodis* pv. *citri* 306.

1. Introduction

Xanthomonas is a genus of Gram-negative, yellow-pigmented bacteria which resides at the base of the Gammaproteobacteria and comprises 27 species. Collectively, the genus cause serious diseases in ~400 plant hosts, including a wide variety of economically important crops, such as rice, citrus, banana, cabbage, tomato, pepper and beans [1]. One of its species, *Xanthomonas axonopodis* pv. *citri* (*X. citri*), parasitizes lime, lemon and orange trees' leaves, stems and fruits, provoking defoliation, blemished fruit, premature fruit drop, die-back of twigs and general debilitation of the tree, thus inflicting considerable economic impact on the citriculture in many subtropical to tropical regions of the world [2]. The genus *Xanthomonas* secretes a peculiar water-soluble, heteropolyssacharidic extracellular matrix named xanthan gum, believed to help the microorganism against diverse environmental constraints during its process of host infestation such as biofilm formation. Mutations in genes related to xanthan gum biosynthesis considerably reduce *Xanthomonas* virulence and, thus, citrus canker symptoms [3]. Due to its rheological properties such as high viscosity and pseudoelasticity, xanthan gum has been widely employed in industry, from a thickening agent of salad dressings and a sausage emulsifier, to a versatile stabilizer of cosmetic products and even some usages in oil drilling and in building products to optimize material properties [4]. Even though it is a desired product in the industry, xanthan gum presence can be a real challenge for some analyses.

A search for studies regarding microorganisms' metabolomics reveals a crescent but still small number of reports [5–11], with just a few of them exploiting sample preparation methods [12,13]. Surprisingly, we could find no references regarding adjustments in methodology and protocols directed to the improvement of NMR-based investigations of bacterial metabolome. Although Sana *et al.* [14] studied the differential metabolic response of susceptible or resistant rice plants after a *X.*

oryzae infection, to our knowledge no metabolomic studies have dealt specifically with the metabolome of any of the *Xanthomonas*' species.

The main reason that impelled our efforts in this study rose after an exploratory $^1\text{H-NMR}$ analysis of the intracellular metabolic content of *X. citri*, extracted by the methanol-chloroform (M/C) than method [15] without any specific adaptations. Prior the analysis in the NMR spectrometer, the sample's viscosity and turbidity already called our attention, indicating that molecules other metabolites remained in the sample. The NMR spectra acquisition was hampered by the difficulty in setup, specifically with the shimming procedure; furthermore, the signal for the internal reference of concentration (3-(Trimethylsilyl)propanoic acid, TSP) exhibited a considerable reduction in amplitude, suggesting that a cross reaction might be happening between TSP molecules and the interfering substance. We hypothesized that the interfering materials in question were the polysaccharidic constituents of the xanthan gum, once proteins, lipids and genetic material were depleted during the M/C extraction step. The objective of this study was to investigate the effectiveness of four methodological interventions for xanthan gum removal during sample preparation for a NMR spectroscopy analysis of the metabolic content of *X. citri*. Interventions to the intracellular metabolome extraction protocol were added prior to or after the cell lysis step (performed by sonication in a M/C solution). *In vitro* production of bacteria can be really challenging under abnormal culture conditions (for example, under intentional physicochemical constraints or nutrition restriction), so we turned our attention towards finding out the minimal volume of a pellet of bacteria needed for a robust $^1\text{H-NMR}$ analysis of the *X. citri* metabolome, expecting that this might be useful to help researchers save their efforts and resources basing their experiments on an optimized protocol.

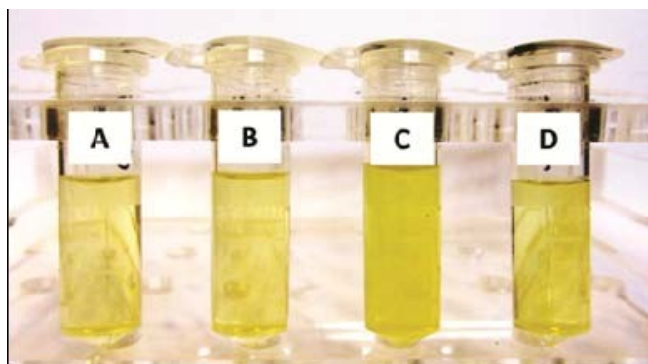
2. Results and Discussion

During a $^1\text{H-NMR}$ exploratory study of the intracellular metabolic content of the phytopathogen *Xanthomonas axonopodis* pv. *citri*, we found some difficulty in setting up the experiments. Notably, the peak of the internal reference of concentration was specially altered and reduced in size, suggesting that a chemical interference was occurring. The distortion observed in the sample would make any attempts of metabolite identification and/or quantification in the $^1\text{H-NMR}$ spectrum questionable especially when employing the targeted profiling approach [16]. We attributed this interference to the presence of the polysaccharide constituents of the xanthan gum. The first part of this section describes our efforts to eliminate it, with results for the four methodological interventions tested, and a suggestion of which of them seems to be the most suitable method for the xanthan gum removal. The second part is an extension of the first: once defined a method for gum depletion, decreasing volumes of cells were subjected to the chosen protocol, as a way of defining the trustable threshold of the technique.

2.1. Selection of the Best Intervention Procedure for Xanthan Gum Removal

As no references for the xanthan gum removal in metabolomic studies could be found, we planned four different intervention methods on the basic M/C intracellular content extraction procedure of the *X. citri* metabolome studies. These interventions consisted on the insertion of (i) 3 or (ii) 5 cell washing cycles with a TBS buffer before the cell lysis (by sonication in a M/C solution); (iii) conventional centrifugation at 3.1×10^3 g or (iv) ultracentrifugation at 8.0×10^4 g step after cell disruption. At the final phase of all tested protocols, cell lysates were centrifuged (in different velocities, depending on the protocol) and the supernatant was collected for solvent drying.

Figure 1. illustrates the variation in color and opacity seen in the supernatants obtained from the four different protocols. The method based on conventional centrifugation was not capable of removing xanthan gum components (Figure 1C), as suggested by the opacity of the sample. Conversely, more cycles of washing and ultracentrifugation clearly produced better results. **Figure 1.** Differences observed in the cellular supernatants of *X. citri* after treatment with four protocols for metabolic extraction. (A) three washing cycles; (B) five washing cycles; (C) conventional centrifugation; and (D) ultracentrifugation. The opaque, dark yellow supernatant in c indicates that xanthan gum components



1.1.1. Cell-Washing Protocols Lead to a Marked Decrease in Overall Intracellular Metabolites' Retrieval, but One in Particular Followed the Opposite Trend remained in the sample.

The conventional centrifugation sample spectrum allowed a linewidth resolution of around 1.80 Hz for the internal reference of concentration (TSP) after shimming, whereas other sharp singlet peaks along the spectrum exhibited linewidth values around 0.80 Hz (Figure 2b). This finding confirmed the suspicion that gum vestiges remained in the sample, given its turbid aspect (Figure 1) As expected, spectra from pellets washed 3 or 5 cycles before lysis showed a reduced intensity for the majority of the peaks compared to those from the ultracentrifuged sample. This characteristic was even more pronounced in the 5-washing-cycles sample, suggesting a correlation between cell washes and loss of the metabolic content (Figure 2c). Following the opposite tendency, signals of

astonishing intensity appeared in the 5-washing-cycles sample, with decreasing intensities for the 3-washings and the ultracentrifugation sample (Figure 2d). These peaks were identified as belonging to trehalose—a disaccharide implicated in anhydrobiosis (the ability of plants, animals and microorganisms to withstand prolonged periods of desiccation). Table 1 brings the list of the metabolites found in each of the spectra with their respective concentrations. Spectra analysis and metabolite concentrations indicated that cell-washing protocols indeed eliminated most of the extracellular xanthan gum components; however, at the cost of losing a considerable portion of the internal metabolites possibly due to cell loss and/or the disruption of its membrane. In addition, large amounts of trehalose found in these samples indicated that bacteria suffered considerable hydric stress during the washing process; even though they were performed with isotonic buffer. Ultracentrifugation presented two major advantages, compared to the cell-washing protocol: (1) it required a minimum of extra intervention, with no addition of solvents or other chemical compounds; (2) the ultracentrifugation step occurred after cell lysis, thus avoiding disturbances in the always responsive intracellular metabolic content of a living cell. We believe this technique could be extended to other types of organisms, aiming the removal of other matrixes and gums with varied chemical composition; however, we recommend other authors to perform pilot studies on their systems. In combination, all these results indicated that the insertion of an ultracentrifugation step proved to be the most appropriated protocol improvement for the xanthan gum removal for $^1\text{H-NMR}$ -based metabolomic experiments.

Figure 2. (A) Spectra overview of ultracentrifugation protocol; (B) TSP signal across samples. Detail for the distorted and broadened peak for the “conventional centrifugation” sample, possibly due to its reaction with xanthan gum constituents vestiges; (C) Differential metabolite concentrations across samples. The overall reduced peak intensities in washed samples could be an indicative of metabolic loss and/or cell lysis; (D) The intense peaks of trehalose (shaded in yellow under arrows) found in the washed samples. (Black = ultracentrifugation; red = three washing cycles; blue = five washing cycles; green = conventional centrifugation).

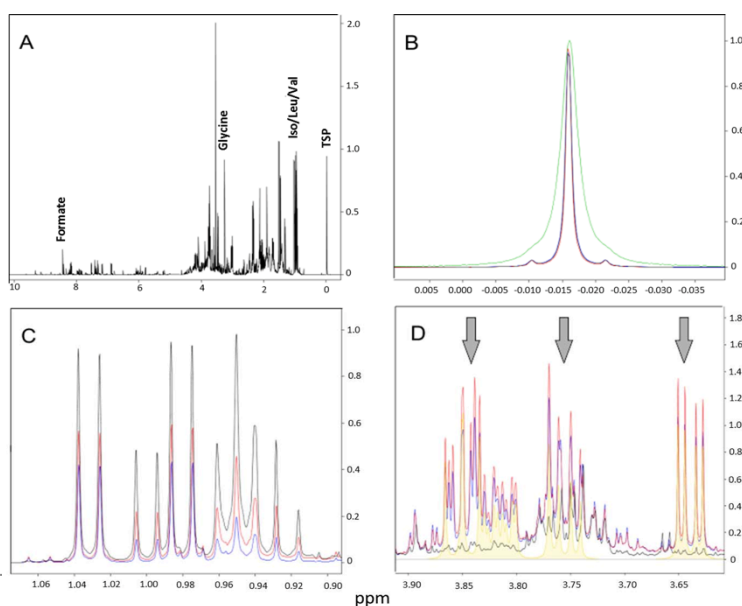


Table 1. Metabolites concentrations (μM) identified in the different protocols. The “conventional centrifugation” sample is missing due to impairments in its TSP signal (concentration reference), making any quantification attempt invalid. In bold, the highest value found for every metabolite. Once a protocol presented the highest value for a metabolite, it scored 1 point; at the end of the table, the sum of scores indicated that ultracentrifugation is the method with the best results.

Metabolites	Ultracentrifugation	3 washing cycles	5 washing cycles
2-Aminoadipate	1,659.9	1,638.5	1,608.5
2-Methylglutarate	21.6	57.7	44.3
3-Hydroxybutyrate	186.2	992.4	515.5
3-Hydroxyisovalerate	12.3	9.0	5.4
4-Aminohippurate	48.1	20.9	24.7
AMP	24.2	36.9	29.6
ATP	42.7	54.9	56.9
Acetate	1,044.2	941.1	842.0
Adenine	39.2	35.6	33.1
Adenosine	129.1	305.2	282.9
Alanine	2,817.5	3,519.6	1,996.2
Asparagine	171.6	260.3	153.1
Aspartate	805.9	1,175.2	997.6
Beta-Alanine	497.8	358.2	313.6
Betaine	741.9	885.4	789.0
Cytidine	199.1	247.0	183.6
Dimethylamine	15.4	21.0	22.4
Dimethylformamide	2.2	6.9	N.Q.
dTTP	105.6	64.7	63.0
Formate	1,118.5	1,201.3	1,387.3
Fumarate	70.0	11.3	17.6
GTP	51.7	96.2	119.9
Glucose	902.2	4,351.7	3,225.6
Glutamate	9,596.4	9,021.5	6,871.9
Glutamine	2,134.1	1,336.5	1,277.5
Glycerol	283.6	408.9	N.Q.
Glycine	4,289.0	2,848.7	2,511.9
Guanosine	128.2	97.8	66.4
Hypoxanthine	718.7	339.8	287.4
Inosine	200.0	108.7	92.2
Isoleucine	1,851.1	841.9	365.1
Isovalerate	61.6	37.0	11.0
Lactate	159.8	154.5	125.4
Leucine	3,041.4	1,492.0	564.5
Lysine	2,699.0	1386.3	1,019.9
Methionine	878.7	539.0	282.3
Methylhistidine	68.8	11.1	0
NAD+	498.2	476.7	484.3
NADP+	60.3	60.7	66.4
Niacinamide	84.2	43.1	28.0
Phenylalanine	1,218.1	376.4	76.4
Proline	1,453.1	1,693.5	1,139.6
Pyroglutamate	612.1	451.2	154.5
Succinate	89.0	897.2	864.3
Threonine	1,204.5	1,286.8	663.5
Thymidine	29.2	23.9	19.5

Table 1. Cont.

Metabolites	Ultracentrifugation	3 washing cycles	5 washing cycles
Trehalose	306.6	9,496.0	11,356.6
Trimethylamine	13.0	12.0	14.0
Tryptophan	297.6	149.1	77.9
Tyrosine	782.2	496.1	353.6
UDP-Acetylglucosamine	80.2	63.7	50.6
UDP-galactose	66.2	54.8	36.8
UDP-glucose	114.0	75.7	69.3
UDP-glucuronate	25.8	21.0	20.0
Uracil	673.0	203.1	233.3
Uridine	224.5	147.0	108.3
Urocanate	0	4.0	0
Valine	3,673.5	2,361.9	1,628.9
Xanthosine	4.9	6.5	7.8
SCORE	35	17	7

N.Q.: non quantifiable.

2.1.2. Decrease in Overall Metabolites' Concentration in Cell-Washing Protocols is Due to Cell Loss

After comparing the quality of the spectra of the *X. citri* cellular supernatants obtained from four protocol interventions, as well as the values of metabolite concentrations, it was possible to conclude that the “ultracentrifugation” method seemed to be the most appropriate intervention in the M/C extraction protocol for gum removal in *Xanthomonas*. However, the lower metabolite's concentrations found in both 3- and 5-washed samples compared to the ultracentrifuged one raised the question of whether such reduction would be due to cell loss or simply to bacterial metabolic released during the washing process.

To answer this question, we plated *Xanthomonas* previously submitted to the same washing protocol for gum removal, with aliquots washed for 3 or 5 cycles in TBS 1×. Along eight serial dilutions, colonies were counted for unwashed (control), 3- and 5-times washed bacteria aliquots. The results are shown in Table 2. Considering 1:10 the factor of dilution across the series and the fact that the unwashed aliquot had to be diluted two more times (thus, 100× in absolute scale) than the washed ones for their colonies numbers to reach a countable scale, these experiments indicate that the washing process for xanthan gum removal might be harmful to bacteria, causing cell loss by extrication or death.

Table 2. Colony counting on a 1:10 scale serial dilution for 3-, 5-times-washed and unwashed (control) aliquots of *X. citri*. Noteworthy is that the control aliquot had to be diluted two more times than the washed samples for their colonies enter a countable scale, suggesting that bacteria-washing process causes cell loss. ID = indeterminable due to high number of colonies.

Dilution	Unwashed	3 washing cycles	5 washing cycles
1:10 ³	ID	ID	ID
1:10 ⁴	ID	800/816	656/680
1:10 ⁵	ID	146/190	126/156
1:10 ⁶	664/672	17/24	30/46
1:10 ⁷	480/696	0/1	6/6

2.2. Lower Amounts of Cells for Metabolomic Studies by ¹H-NMR

Sample size and availability has always been one of the major problems in biological experiments. High costs, waiting time and specimen rarity—or any combination of them—are commonly the principal reasons why big sampling groups are not always ready at the researcher hands. To circumvent this issue and aiming at a thorough study of *X. citri* by metabolic profiling, we searched for the lower limits of *X. citri* cells pellet size for metabolomic studies using ¹H-NMR spectroscopy, using a 5 mm triple resonance cold probe on a 600 MHz machine (Agilent, Inc., Santa Clara, CA, USA). Four volumes of samples were tested: 500 µL, 250 µL, 125 µL and 62.5 µL.

Differences between pellets began already at the sample preparation stage. The reduced volume of cells in the 62.5 µL vial produced a thin, fragile interphasic proteic ring, between the polar and apolar phases, which did not resist the high pressures of ultracentrifugation. Whereas no occurrences happened with the 125 µL or bigger samples, the interphasic proteic ring that separates the supernatant, methanolic phase, from the apolar, chloroformic phase of the 62.5 µL pellet samples, cracked during ultracentrifugation (data not shown). It is plausible to assume that this crack led, at least to some extent, to the mixture of phases during the supernatant collection step, thus interfering with the internal reference integrity (as observed by the great difficulty in shimming the sample) and compromising metabolites' quantification (data not shown). Table 3 brings the metabolite's concentrations found in the three available pellet volumes.

Table 3. Concentration of metabolites (µM) identified in the 500 µL, 250 µL and 125 µL pellets submitted to ultracentrifugation prior to the analysis. (Mean ± SD, *n* = 3 for each group).

Metabolites	Pellet volumes		
	500 µL	250 µL	125 µL
2-Amino adipate	653.9 ± 12.6	305.9 ± 33.2	148.6 ± 13.1
2-Methylglutarate	55.9 ± 2.5	21.9 ± 7.5	7.0 ± 0.2
3-Hydroxybutyrate	235.5 ± 22.7	115.2 ± 12.9	52.4 ± 4.4
3-Hydroxyisovalerate	116.8 ± 18.2	73.3 ± 5.9	30.4 ± 5.0
4-Aminohippurate	84.6 ± 4.9	30.2 ± 9.1	11.9 ± 1.2
AMP	1.9 ± 0.4	7.1 ± 4.3	12.7 ± 4.0
ATP	75.3 ± 3.5	32.1 ± 5.7	17.5 ± 3.3
Acetate	914.3 ± 173.7	470.7 ± 116.8	213.8 ± 26.7
Adenine	124.7 ± 8.5	58.0 ± 13.3	29.4 ± 4.4
Adenosine	268.6 ± 49.5	121.8 ± 20.8	49.6 ± 5.1

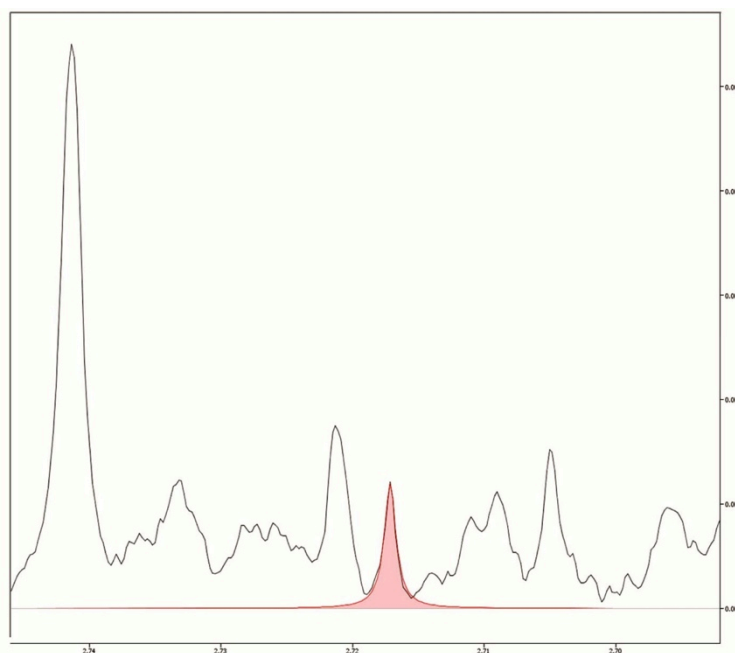
Metabolites **2014**, *4*

Alanine	4,475.6 ± 226.7	1,999.3 ± 383.6	1,042.9 ± 89.6
Asparagine	188.2 ± 7	90.3 ± 22.6	51.2 ± 8.1
Aspartate	1,579.5 ± 145.9	738.3 ± 100.8	368.0 ± 34.6
Beta-Alanine	288.3 ± 30.4	166.3 ± 16.1	79.3 ± 4.6
Betaine	842.9 ± 31.0	377.6 ± 52.3	188.7 ± 12.4
Cytidine	196.8 ± 19.7	54.4 ± 18.3	25.8 ± 2.1
Dimethylamine	3.2 ± 0.8	2.3 ± 0.2	1.0 ± 0.1
Dimethylformamide	26.1 ± 4.5	11.5 ± 2.2	4.4 ± 1.4
dTTP	145.5 ± 2.5	77.3 ± 8.6	41.0 ± 3.8
Formate	1,517.6 ± 250.1	801.4 ± 130.0	478.1 ± 40.3
Fumarate	9.4 ± 1.8	4.2 ± 0.7	2.2 ± 0.2
GTP	53.6 ± 2.9	21.9 ± 7.9	12.4 ± 2.9
Glucose	740.3 ± 51.6	279.8 ± 63.2	149.0 ± 18.4
Glutamate	12,186.7 ± 401.5	5,571.3 ± 595.8	2,725.4 ± 244.0
Glutamine	2,820.6 ± 15.9	1,411.0 ± 218.3	694.5 ± 58.8
Glycerol	781.2 ± 41.5	332.6 ± 34.2	210.9 ± 46.5
Glycine	5,078.8 ± 401.2	2,324.3 ± 371.9	1,162.5 ± 97.6
Guanosine	132.7 ± 14	55.2 ± 16.1	26.6 ± 2.4
Hypoxanthine	877.9 ± 18.8	376.6 ± 69.3	167.1 ± 15.4
Inosine	161.6 ± 35.2	33.3 ± 8.4	19.6 ± 3.2
Isoleucine	2,668.0 ± 105.8	1,259.1 ± 182.3	654.6 ± 63.3
Isovalerate	255.3 ± 27.2	121.5 ± 13.6	45.2 ± 3.0
Lactate	279 ± 38.7	123.3 ± 18.6	66.7 ± 12.1
Leucine	4,479.2 ± 107.7	2,059.9 ± 343.0	1,084.8 ± 104.2
Lysine	3,142.5 ± 250.2	1,630.0 ± 138.5	898.5 ± 43.6
Methionine	1,243.4 ± 56.3	614.5 ± 80.6	335.8 ± 21.4
Methylhistidine	127.2 ± 8.9	50.0 ± 7.0	23.6 ± 1.5
NAD+	499.1 ± 33.1	234.8 ± 25.1	110.4 ± 10.3
NADP+	40.6 ± 3.2	15.7 ± 5.8	9.5 ± 0.4
Niacinamide	170.5 ± 16.4	78.9 ± 7.5	33.8 ± 4.2
Nicotinate	73.6 ± 6.2	32 ± 3.8	14.8 ± 1.0
Nicotinic acid adenine dinucleotide	18.3 ± 2.5	8.7 ± 1.3	4.9 ± 1.6
Phenylalanine	2,213.1 ± 39.9	1,062.5 ± 123.9	544.5 ± 33.0
Proline	2,132.1 ± 145	843.2 ± 192.5	453.3 ± 57.4
Pyroglutamate	1,360.7 ± 109.1	629.0 ± 88.0	285.6 ± 28.2
Succinate	423.9 ± 36	147.4 ± 37.2	71.0 ± 9.8
Threonine	2,494.9 ± 149.1	1,120.0 ± 150.2	564.9 ± 44.7
Thymidine	35.4 ± 1.4	9.2 ± 4.3	3.9 ± 0.2
Trehalose	313.8 ± 39.4	182.3 ± 27.1	73.1 ± 5.5
Trimethylamine	9.9 ± 0.9	7.6 ± 0.9	6.4 ± 0.9
Tryptophan	432.3 ± 30.4	244.2 ± 44.4	140.0 ± 14.8
Tyrosine	1,266.3 ± 48.1	626.3 ± 80.2	311.1 ± 26.8
UDP-Acetylglucosamine	66.7 ± 4.2	28.6 ± 4.2	18.1 ± 0.6

UDP-galactose	68.3 ± 2	32.1 ± 6.3	16.9 ± 1.1
UDP-glucose	147.8 ± 7	78.8 ± 10.8	43.1 ± 3.1
UDP-glucuronate	22.0 ± 0	9.4 ± 1.0	5.8 ± 1.3
Uracil	1,013.9 ± 101.6	438.5 ± 57.4	199.4 ± 14.0
Uridine	198.4 ± 15	61.7 ± 17.0	22.6 ± 0.5
Urocanate	16.0 ± 2.1	9.1 ± 1.6	3.5 ± 0.4
Valine	4,583.7 ± 167.1	2,167.1 ± 296.2	1,106.0 ± 84.9
Xanthosine	19.5 ± 0.5	8.5 ± 1.2	4.2 ± 0.2

These results suggest that pellets as small as 125 μ L could be used in a ^1H -NMR-based metabolomic investigation without losses in metabolic detection, in a similar NMR setup. Considering our metabolite detection limit, based on the Chenomx peak identification protocol, we found no metabolite that reached undetectable levels as the pellet volumes decreased, suggesting that pellets with 125 μ L could be as informative as pellets four times bigger (Figure 3). Indeed, we believe that even smaller pellets could still be successfully employed in metabolomics studies if centrifuge tubes with reduced diameters were used, thus yielding thicker inter-phase protein rings and ensuring sample's integrity during the ultracentrifugation process. Our research group is starting to explore low speed/low volume Magic Angle Spinning (MAS) in high-resolution solid-state NMR (HR-MAS-NMR) methods, which may enable studies with small pellet and lower volume samples obtained from extraction procedures.

Figure 3. Detail of the 125 μ L pellet spectrum. In red, the fitting of the dimethylamine peak, whose concentration was the lowest among all the metabolites detected. As occurred to all compounds, its marked, well-defined peak provided a high signal:noise ratio and, therefore, a reliable quantification.



3. Experimental Section

3.1. Bacterial Strains and Cell Culture Growth Conditions

Cultures of *Xanthomonas axonopodis* pv. *citri* 306 were prepared by inoculating a single colony in 500 mL of Luria Bertani Broth medium (LB), containing tryptone (10 g), yeast extract (5 g) and NaCl (10 g) per liter of water [17]. Bacteria were left to grow overnight at 200 rpm shaking and 30 °C and harvested at 1.0×10^4 g for 15 min. Cell proliferation until stationary phase was monitored by OD₆₀₀, when pellets proceeded for metabolites recovery.

3.2. Metabolic Extraction Procedures

The here named “M/C protocol without specific adaptations” for metabolic recovery was adapted from Le Belle *et al.* [15]. A major adaptation was an increase in the solvent volumes due to the large volume of cell pellets studied. This extraction method consisted in adding to the pellets methanol and chloroform (4 °C) in a ratio of 2:1 (v/v, 2.5 mL/bacteria pellet). The cell pellet-solvent mixtures, immersed in iced water, were sonicated for 3 minutes with a 10 s interval between each minute. Chloroform and distilled water (4 °C) were then added to the samples in a ratio of 1:1 (2.5 mL/bacteria pellet). After a brief vortexing to form an emulsion, the samples were centrifuged at 3.116×10^3 g for 20 min at 4 °C. The upper phase (methanol, water and polar metabolites) was collected and totally dried in a vacuum concentrator (Speedvac) at low speed and without heating. For xanthan gum removal, the tested adaptations here called “3- and 5-washing-cycles” consisted of washing the bacteria pellets in 10 mL of TBS 1× buffer, with subsequent cell recovery at 1.152×10^4 g for 10 min between each wash. This step occurred before the metabolic extraction procedure detailed above. The “conventional centrifugation” and “ultracentrifugation” procedures were very similar to the “M/C protocol without specific adaptations”, with the exception that samples were centrifuged at 1.555×10^4 g and 8.0×10^4 g, respectively. In both cases, time and temperature of centrifugation were kept the same as the original protocol.

3.3. Colony Formation Units

Successive 10-fold serial dilutions were done with bacterial pellets submitted to none, 3 and 5 washing cycles for colony forming units monitoring. Pellets were diluted in TBS 1× until $1:10^{-7}$ and plated on 90 × 15 mm polystyrene dishes containing 25 mL of LB medium supplemented with ampicillin (100 mg/mL). Serial dilutions were done twice from each pellet. The bacterial colonies were counted after 48 h of incubation at 28 °C.

3.4. Sample Preparation for NMR Analysis

After drying the samples in a vacuum concentrator (Speedvac), the remaining solid phase was rehydrated in 600 μ L of deuterium oxide (D_2O , 99.9%; Cambridge Isotope Laboratories Inc., Tewksbury, MA, USA), containing phosphate buffer (0.1 M, pH 7.4) and 0.5 mM of TSP (3-(Trimethylsilyl)propanoic acid; Sigma-Aldrich) for internal reference. Samples were added to a 5 mm NMR tube for immediate acquisition.

3.5. NMR Data Acquisition and Metabolite Identification

1H -NMR spectra of samples were acquired using a Agilent Inova NMR spectrometer (Agilent Technologies Inc., Santa Clara, CA, USA) equipped with a 5 mm triple resonance cold probe and operating at a 1H resonance frequency of 600 MHz and constant temperature of 298 K (25 °C). A total of 128 free induction decays (FIDs) were collected with 32 K data points over a spectral width of

16 ppm. A 1.5 s relaxation delay was incorporated between FIDs, during which a continual water pre-saturation radio frequency (RF) field was applied. Spectral phase and baseline corrections, as well as the identification and quantification of the metabolites present in the samples, were performed using the Chenomx NMR Suite 7.6 software (Chenomx Inc., Edmonton, AB, Canada).

4. Conclusions

An appropriate pre-treatment step is essential for an efficient removal of the xanthan gum from *Xanthomonas*' pellets prior to NMR spectroscopy experiments. The ultracentrifugation intervention presented the best results in terms of both spectra quality and potential for metabolite quantification. Conventional cell-washing protocols exhibited an overall decrease in metabolite's concentrations due to cell extrication or death along the washing cycles. In addition to its ease of implementation, a minimal extra manipulation after cell lysis—thus avoiding disturbances in the metabolic milieu of the living system—can be pointed as an advantage of the ultracentrifugation intervention for the xanthan gum removal. We don't claim to have exhausted all the alternatives to solve this issue, but to start answering questions we faced during answering our own research questions, which may be of interest to others, and as an exercise in collaboration and creativity in the solving of new problems.

Acknowledgments

The authors acknowledge the Brazilian Biosciences National Laboratory (LNBio), at the Brazilian Center for Research in Energy and Materials—CNPEM, Campinas, Brazil, for their support with the use of the NMR spectrometers and vacuum ultracentrifuge, at the open NMR and the Viral Vector facilities. We also acknowledge the Coordination for the Improvement of Higher Education

Personnel (CAPES) and the São Paulo State Research Foundation (FAPESP) for the students fellowship support.

Author Contributions

Aline P. Sampaio performed the experiments on bacterial growth. Vanessa R. Pegos performed colony counting. Rafael R. Canevarolo acquired and analyzed NMR spectra. Vanessa R. Pegos and Rafael R. Canevarolo tested the different protocols and their optimization for metabolite extraction, prepared the figures and wrote the manuscript. Andrea Balan and Ana C. M. Zeri supervised the research and corrected the manuscript.

Conflicts of Interest

The authors declare no conflict of interest.

References

1. Ryan, R.P.; Vorholter, F.J.; Potnis, N.; Jones, J.B.; van Sluys, M.A.; Bogdanove, A.J.; Dow, J.M. Pathogenomics of xanthomonas: Understanding bacterium-plant interactions. *Nat. Rev. Microbiol.* **2011**, *9*, 344–355.
2. Graham, J.H.; Gottwald, T.R.; Cubero, J.; Achor, D.S. Xanthomonas axonopodis pv. Citri: Factors affecting successful eradication of citrus canker. *Mol. Plant Pathol.* **2004**, *5*, 1–15.
3. Yan, Q.; Wang, N. High-throughput screening and analysis of genes of xanthomonas citri subsp. citri involved in citrus canker symptom development. *Mol. Plant-Microbe Interact.* **2012**, *25*, 69–84.
4. Savvides, A.L.; Katsifas, E.A.; Hatzinikolaou, D.G.; Karagouni, A.D. Xanthan production by xanthomonas campestris using whey permeate medium. *World J. Microbiol. Biotechnol.* **2012**, *28*, 2759–2764.
5. Koek, M.M.; Muilwijk, B.; van der Werf, M.J.; Hankemeier, T. Microbial metabolomics with gas chromatography/mass spectrometry. *Anal. Chem.* **2006**, *78*, 1272–1281.
6. Liebeke, M.; Dorries, K.; Meyer, H.; Lalk, M. Metabolome analysis of gram-positive bacteria such as staphylococcus aureus by gc-ms and lc-ms. *Methods Mol. Biol.* **2012**, *815*, 377–398.
7. Martinez, P.; Galvez, S.; Ohtsuka, N.; Budinich, M.; Cortes, M.P.; Serpell, C.; Nakahigashi, K.; Hirayama, A.; Tomita, M.; Soga, T.; *et al.* Metabolomic study of chilean biomining bacteria acidithiobacillus ferrooxidans strain wenelen and acidithiobacillus thiooxidans strain licanantay. *Metabolomics* **2013**, *9*, 247–257.
8. Tang, J. Microbial metabolomics. *Curr. Genomics* **2011**, *12*, 391–403.

9. Tremaroli, V.; Workentine, M.L.; Weljie, A.M.; Vogel, H.J.; Ceri, H.; Viti, C.; Tatti, E.; Zhang, P.; Hynes, A.P.; Turner, R.J.; *et al.* Metabolomic investigation of the bacterial response to a metal challenge. *Appl. Environ. Microbiol.* **2009**, *75*, 719–728.
10. Van der Werf, M.J.; Overkamp, K.M.; Muilwijk, B.; Coulier, L.; Hankemeier, T. Microbial metabolomics: Toward a platform with full metabolome coverage. *Anal. Biochem.* **2007**, *370*, 17–25.
11. Wang, Q.Z.; Wu, C.Y.; Chen, T.; Chen, X.; Zhao, X.M. Integrating metabolomics into a systems biology framework to exploit metabolic complexity: Strategies and applications in microorganisms. *Appl. Microbiol. Biotechnol.* **2006**, *70*, 151–161.
12. Maharjan, R.P.; Ferenci, T. Global metabolite analysis: The influence of extraction methodology on metabolome profiles of escherichia coli. *Anal. Biochem.* **2003**, *313*, 145–154.
13. Bolten, C.J.; Kiefer, P.; Letisse, F.; Portais, J.C.; Wittmann, C. Sampling for metabolome analysis of microorganisms. *Anal. Chem.* **2007**, *79*, 3843–3849.
14. Sana, T.R.; Fischer, S.; Wohlgemuth, G.; Katrekar, A.; Jung, K.H.; Ronald, P.C.; Fiehn, O. Metabolomic and transcriptomic analysis of the rice response to the bacterial blight pathogen *Xanthomonas oryzae* pv. *Oryzae*. *Metabolomics* **2010**, *6*, 451–465.
15. Le Belle, J.E.; Harris, N.G.; Williams, S.R.; Bhakoo, K.K. A comparison of cell and tissue extraction techniques using high-resolution 1h-nmr spectroscopy. *NMR Biomed.* **2002**, *15*, 37–44.
16. Weljie, A.M.; Newton, J.; Mercier, P.; Carlson, E.; Slupsky, C.M. Targeted profiling: quantitative analysis of 1h nmr metabolomics data. *Anal. Chem.* **2006**, *78*, 4430–4442.
17. Miller, J.H. *A Short Course in Bacterial Genetics: A Laboratory Manual and Handbook for Escherichia Coli and Related Bacteria*; Cold Spring Harbor Laboratory Press: Plainview, NY, USA, 1992.

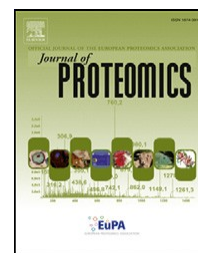
© 2014 by the authors; licensee MDPI, Basel, Switzerland. This article is an open access article distributed under the terms and conditions of the Creative Commons Attribution license (<http://creativecommons.org/licenses/by/3.0/>)

Artigo 2

Phosphate Regulated Proteins of *Xanthomonas citri* subsp. *citri*: A proteomic approach

Vanessa R. Pegos, Jessica Faria Nascimento, Tiago José Paschoal Sobreira, Bianca Alves,
Adriana Paes-Leme, Andrea Balan.

(doi: 10.1016/j.jprot.2014.05.005)



Phosphate regulated proteins of *Xanthomonas citri* subsp. *citri*: A proteomic approach



Vanessa Rodrigues Pegos^{a,b}, Jéssica Faria Nascimento^a, Tiago José Paschoal Sobreira^a, Bianca Alves Pauletti^a, Adriana Paes-Leme^a, Andrea Balan^{a,c,*}

^aLaboratório Nacional de Biociências — LNBio, Centro de Pesquisas em Energia e Materiais — CNPEM, Campinas, SP, Brazil

^bUniversidade Estadual de Campinas — UNICAMP, Instituto de Biologia, Campinas, SP, Brazil

^cUniversidade de São Paulo — USP, Instituto de Ciências Biomédicas II, Departamento de Microbiologia, - São Paulo - SP, Brazil

ARTICLE INFO

Article history:

Received 17 February 2014

Accepted 12 May 2014

Available online 17 May 2014

Keywords:

ABC transporter

Phosphate regulon

Pst system

Xanthomonas citri subsp. *citri*

ABSTRACT

Xanthomonas citri subsp. *citri* (*X. citri*) is the causative agent of the citrus canker, a disease that affects several citrus plants in Brazil and across the world. Although many studies have demonstrated the importance of genes for infection and pathogenesis in this bacterium, there are no data related to phosphate uptake and assimilation pathways. To identify the proteins that are involved in the phosphate response, we performed a proteomic analysis of *X. citri* extracts after growth in three culture media with different phosphate concentrations. Using mass spectrometry and bioinformatics analysis, we showed that *X. citri* conserved orthologous genes from Pho regulon in *Escherichia coli*, including the two-component system PhoR/PhoB, ATP binding cassette (ABC transporter) Pst for phosphate uptake, and the alkaline phosphatase PhoA. Analysis performed under phosphate starvation provided evidence of the relevance of the Pst system for phosphate uptake, as well as both periplasmic binding proteins, PhoX and PstS, which were formed in high abundance. The results from this study are the first evidence of the Pho regulon activation in *X. citri* and bring new insights for studies related to the bacterial metabolism and physiology.

Biological significance

Using proteomics and bioinformatics analysis we showed for the first time that the phytopathogenic bacterium *X. citri* conserves a set of proteins that belong to the Pho regulon, which are induced during phosphate starvation. The most relevant in terms of conservation and up-regulation were the periplasmic-binding proteins PstS and PhoX from the ABC transporter PstSBAC for phosphate, the two-component system composed by PhoR/PhoB and the alkaline phosphatase PhoA.

© 2014 Elsevier B.V. All rights reserved.

1. Introduction

Phosphate (Pi) is an essential element for microorganisms because it is involved in energy metabolism and signal transduction, virulence, pathogenicity, adherence and infec-

tion [1–3]. In depletion of P_i *Escherichia coli* activates adaptive, pathogenic [4] and survival [5] responses, which involve the up and down regulation of many genes, nearly 10% of the genome [6,7]. Many genes that are regulated during the adaptive response are members of the Pho (phosphate)

* Corresponding author.

E-mail address: abalan@usp.br (A. Balan).

<http://dx.doi.org/10.1016/j.jprot.2014.05.005>

1874-3919/© 2014 Elsevier B.V. All rights reserved.

regulon [7] defined by the involvement of a two-component regulatory system that comprises the PhoR and PhoB proteins [2]. PhoR encodes a histidine kinase, and PhoB encodes a response regulator that responds when the extracellular phosphate concentration falls below 4 μ M. Activation or repression mediated by PhoB involves its phosphorylation and binding to the Pho-dependent promoter regions known as Pho-boxes [2]. One of these systems is the phosphate starvation system (Pst), a specific ATP-binding cassette transporter (ABC transporter) that is responsible for Pi uptake, signal transduction and transport with high affinity [2,7]. Mutations on genes of the Pst system lead to the constitutive expression of the Pho regulon evidencing the function of this transporter also as a regulator [8]. Although many genes have been identified as Pi-regulated in *E. coli* only 31 genes were shown to be directly controlled by the PhoR/PhoB proteins, which include mostly genes involved with uptake and assimilation of other sources of phosphate, the genes of the Pst system and others [8]. Compared to iron and other relevant ions that absence or starvation can stimulate pathogenic processes, phosphate is also important for survival and proliferation by virtue of its relevance for the constitution of nucleic acids and phosphorylation. A number of reports have shown the relationship between pho genes and virulence [2], adhesion [9], biofilm formation [10], toxin production [11] and stress response [3,2]. However, despite the importance of this ion and its relationship with pathogenesis, there is scant information in the literature regarding if protein expression is controlled by phosphate starvation and the expression of the Pho regulon proteins in the phytopathogenic bacterium *Xanthomonas citri*. *X. citri* is the causative agent of the citrus canker, a disease that affects citrus plants and the economy of many countries, including Brazil, which is one of the largest exporters of orange fruit and juice [12].

In this work, we analysed the proteome of *X. citri* after growing it in culture media with different phosphate concentrations in order to identify the putative Pho regulon members and to compare the proteins expressed during the adaptive responses. Using bioinformatics to support our results, we demonstrated that a set of proteins is regulated by phosphate, which includes a two-component system, the PstSCAB transporter and PhoA, an alkaline phosphatase that is up regulated when the Pho regulon is activated [7]. The proteomic and associated bioinformatics analyses indicate that the majority of the Pho regulon genes in *X. citri* are conserved and reveal, for the first time, the importance of the ABC transporter PstSCAB for phosphate assimilation in *X. citri*.

2. Material and methods

2.1. Search for Pho regulon orthologues in *X. citri* genome

The *X. citri* used in this work was *Xanthomonas axonopodis* pv. *citri* strain 306 [13]. Amino acid sequences of the *E. coli* Pho regulon proteins described by Hsieh and Wanner [8] were obtained from KEGG2 server (Bioinformatics Center Institute for Chemical Research Kyoto University, www.genome.jp) and used to perform a basic local alignment search BlastP ([\[blast.ncbi.nlm.nih.gov\]\(http://blast.ncbi.nlm.nih.gov\)\) against the *Xanthomonas axonopodis* pv. *citri* \(taxid:346\) database using non-redundant protein sequence \(nr\) as parameter for search. All the additional parameters were defined as a default of the programme. The list of all proteins and their KEGG entry are shown in Table S1 \(Supplementary information\). The amino acid sequence alignments were carried out using ClustalW \(\[www.ebi.ac.uk/clustalw/\]\(http://www.ebi.ac.uk/clustalw/\)\) and cut-off value of 60% on query coverage. To identify the promoter regions of the *X. citri* Pho regulon genes, we submitted a sequence of 100 nucleotides upstream of the start codon of isolated genes or from the first gene belonging to an operon, to the bacterial promoter prediction programme BPROM from the SoftBerry server \(<http://linux1.softberry.com>\). The identified promoter sequences were compared to the Pho-boxes as described by VanBogelen et al. \[6\].](http://</p>
</div>
<div data-bbox=)

2.2. Bacterial strains, culture conditions and protein preparation

Cultivation was performed in LB as a rich medium, A medium [14] (Tris 120 mM, NaCl 80 mM, KCl 20 mM, Na₂Cl 20 mM, Na₂SO₄ 3 mM, MgCl₂ 1 mM, ZnCl₂ 51 μ M, bacto peptona 0.5%, Glucose 0.5%; CaCl₂ 0.2 mM) and A medium supplemented with 10 mM phosphate (NaH₂PO₄) (A + Pi medium). The cultures of *X. citri* were prepared by inoculating a single colony in 5 mL LB and allowing growth overnight at 30 °C and 200 r.p.m. Afterward, to define the time necessary for reaching the stationary phase, approximately 1.2×10^4 cell/mL were washed, and transferred to 3 distinct flasks containing fresh A, A + Pi and LB media, incubated at 30 °C during a period of 80 h for A and A + Pi and 25 hs for LB. Replicate samples were collected at 25 h. and 48 h. from LB and A/A + Pi, respectively. The cells were centrifuged at 5000 \times g for 15 min and the pellets were suspended in 1 mL of 10 mM Tris–NaCl, pH 8.0, and 5 mM EDTA, followed by sonication times of 2 min (5 cycles of 15 s. on and 15 s. off). The lysates were centrifuged at 20,000 \times g for 30 min at 4 °C, and the supernatants were quantified using Bradford method [15].

2.3. SDS-PAGE electrophoresis and in gel-trypsin digestion

Samples containing 100 μ g protein per were applied on 12% SDS-PAGE gels. After running at 150 V for 1 h, the gels were stained with comassie blue and destained with 45% (v/v) ethanol and 10% (v/v) acetic acid. Nine bands were excised from the gels and used for trypsin digestion, as previously described in Paes-Leme et al. [16].

2.4. Activity of alkaline phosphatase

To identify the activation of Pho regulon in the experimental conditions, the activity of the alkaline phosphatase PhoA was measured in A and A + Pi media according Tse and collaborators [17].

2.5. Mass spectrometry MS/MS and data analysis

The peptide mixture was separated by a column C18 (100 μ M \times 100 mm) Rp-nano UPLC (nanoAcquity, Waters

Corp. Milford, MA, U.S.A.) coupled with a Q-ToF Ultima API mass spectrometer (Waters Corp. Milford, MA, U.S.A.) with a nano electrospray source at a flow rate of 0.6 nL/min. The gradient was 2–90% acetonitrile in 0.1% formic acid over 45 min for the digested proteins. The nano electrospray voltage was set to 3.5 kV, the cone voltage was 30 V, and the source temperature was 100 °C. The instrument was operated in the ‘top three’ mode, in which one MS spectrum is acquired, followed by MS/MS of the top three most intense peaks. Technical triplicates spectra were acquired using MassLynx v.4.1 software, and the raw data files were converted to a peak list format (mgf) by the Mascot Distiller v.2.3.2.0, 2009 software (Matrix Science Ltd., Boston, MA, U.S.A.) and searched against a *Xanthomonas axonopodis* pv. *citri* str. 306 database (taxonomy ID: 190486; 9,747 sequences; 3,345,870 residues, release date April, 2002) using Mascot [18] engine v.2.3.01 (Matrix Science Ltd., Boston, MA, U.S.A.), with carbamidomethylation as a fixed modification, oxidation of methionine as a variable modification, one trypsin missed cleavage and a tolerance of 0.1 Da for the precursor and fragment ions. For protein quantity measurement, the Mascot output files were analysed in Scaffold Q+ (version 3.6, Proteome Software Inc., Portland, OR, USA). Scaffold was used to calculate the normalised spectral counts and to validate peptide and protein identifications [19], considering the scoring parameters (95% of peptide confidence level identification, 99% peptide probability and at least 2 unique peptides) to obtain a false discovery rate (FDR) of less than 1% for proteins and peptides. All mass spectrometric raw files associated with this study are available for downloading via FTP from the PeptideAtlas data repository by accessing the following link: <http://www.peptideatlas.org/PASS/PASS00348>. The original full data are shown in Table S2 (Supplementary information).

2.6. Statistical analysis

Scaffold uses Bayesian statistics to estimate the peptide and protein probabilities according Keller et al. [20] and Nesvizhskii et al. [19], respectively. Protein Prophet uses both algorithms as part of the Trans Proteome Pipeline distributed by the Institute for Systems Biology (<http://www.systemsbio.org>). Scaffold determines the distributions of the Mascot scores, which depends on database size and the specific characteristics of the samples, and translates them into probabilities for correct identification. The value reported as the spectral count for each protein was calculated as the average of all samples in the same treatment (two and three independent experiments were performed for A and A + Pi media analyses). All the assigned spectra for each protein were used for spectral counting. Prior to statistical analysis, protein spectral counts were normalised using the Scaffold software by calculating and averaging the number of identified spectra in each sample and then multiplying the number of spectra assigned to each protein by the ratio of the average spectral count and the number of total spectra in that sample. The ratio of the normalised spectral counts for each identified protein between each culture condition was computed using a t-test, and p-values < 0.05 were considered significant (Tables S2 and S3, Supplementary information).

3. Results

3.1. Orthologues of Pho regulon present in *X. citri* subsp. *citri*

Although the phosphate levels in the environment affect the expression of many genes, at least 36 genes were characterised in *E. coli* with altered expression levels due to limited phosphate availability (Pho regulon genes) [2,7,8]. Using the sequences of the corresponding proteins and the BlastP tool, we examined the *X. citri* database to identify orthologues of these 36 proteins. The results revealed that *X. citri* conserved at least 22 putative orthologues from the 36

Pho regulon genes previously characterised in *E. coli* [8], as shown in Table S1 (Supplementary information). Most of them are positioned in a conserved genome organisation under control of promoters that also conserve the pho-boxes region (Fig. 1). Remarkably, we identified the two-component system genes *phoR* and *phoB* and the ABC transporter genes *pstSCAB* (sequence identity values greater than 40%) (Supplementary information, Table S1). Similarly to *E. coli*, *pst* genes are organised in an operon that also contains the *phoU* gene, which function was described as negative regulator of PhoR/ PhoB two-component system (Fig. 1A). The *pst* operon is under control of a promoter that conserves the pho-box region as described by VanBogelen et al. [6] (Fig. 1B). Close to this operon, there are two additional genes that encode another periplasmic-binding protein PhoX, and the polyphosphate-selective porin O, *OprO*. These two genes are under control of one promoter sequence located upstream of the *oprO* gene (Fig. 1A and B). *OprO* porin has no homology with any protein from *E. coli*, including PhoE, but revealed high amino acid sequence identity when compared to orthologues from *Xanthomonas* species (67% to 100%) and the *Pseudomonas aeruginosa* P47 polyphosphate-selective porin *OprP* (31%), which three-dimensional structure was solved by Moraes and collaborators [21] (PDB Code 2O4V). The genes *phoB* and *phoR* also are organised at the *X. citri* genome in an operon that includes the genes *ppk* and *ppx* encoding a polyphosphate kinase and an exopolyphosphatase, respectively (Fig. 1A). The *Ppx* and *Ppk* proteins of *X. citri* share 40% and 34% amino acid sequence identity, respectively, with the *E. coli* orthologues (Supplementary information, Table S1) and the genetic organisation is similar to that described in *Klebsiella aerogenes* and *Streptomyces lividans* [22,23]. The *X. citri* alkaline phosphatase PhoA shared 32% of sequence identity with the *E. coli* orthologue and it is isolated in the genome, but also presents the pho-box in its promoter region. The Blastp using the *E. coli* glycerol-3-phosphate transporter genes identified genes involved with sugar uptake organised in one operon that includes an orthologue of *lacI* (Fig. 1A). With exception of *X. citri* *ugpC* gene that shared 54% of sequence identity with its *E. coli* orthologue and that is located in a complete different position at the genome (Fig. 1A), the three other genes (*lacG*, *malE* and *lacF*) did not show high sequence similarity (Supplementary information, Table S1). *LacG* and *LacF* are described as sugar ABC transporter permeases and *MalE* is the sugar-binding protein. None promoter was identified upstream of the *ugpC* gene (Fig. 1B). Absences were identified for genes encoding the carbon-phosphoryl lyase complex

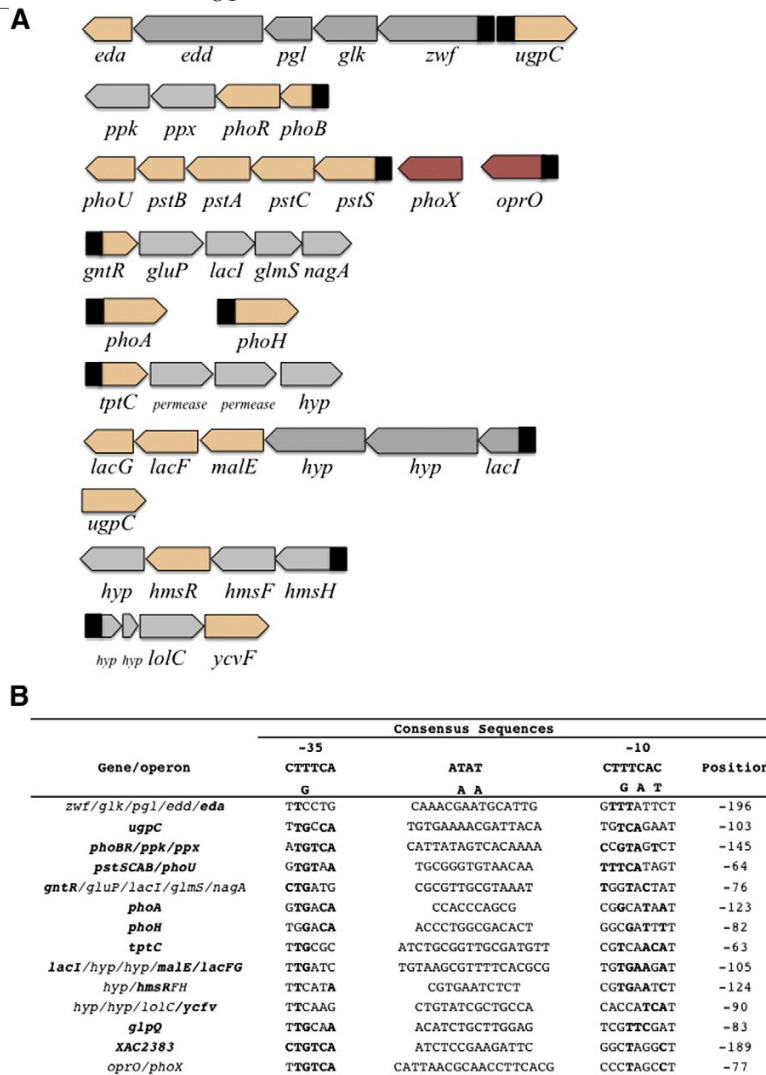


Fig. 1 – Genetic organisation of the Pho regulon genes in *Xanthomonas citri* subsp. *citri*. (A) Gene orthologues of Pho regulon as described by Hsieh and Wanner [8] identified in *X. citri* and their location in the genome. Genes are represented by arrows the same way as found in the *X. citri* genome. Genes as described in Table S1 (Supplementary information) that shared amino acid sequence identity with their orthologues in *E. coli* and those that are only present in *X. citri* were coloured in salmon and red, respectively. Grey arrows show the genes that belong to the same operon. The promoter sequences of each gene or operon are shown as black boxes. (B) Promoter sequences identified for each gene/operon and their comparison with the pho-box consensus sequences as described by VanBogelen et al. [6]. Bold genes represent the orthologues identified in *X. citri*.

Conserved pho-box nucleotides are also evidenced in bold.

components (phnPOM/JIHG genes) (Supplementary information, Table S1). Lastly, similarly to what is shown in *E. coli*, *X. citri* conserves the systems for transport and signalling transduction mediated by Pi. In *X. citri*, OprO is the most pertinent porin for transport of phosphate from the environment to the periplasm. Low concentrations of phosphate would activate the PhoR and PhoB and the transport of phosphate into the cytoplasm would be performed by the highly conserved Pst system. A representation of the

membrane organisation of these components in *X. citri* is shown in Fig. 2.

3.2. Total proteins identified in *X. citri* and functional classification

The mass spectrometry analysis of *X. citri* cell extract from cultures grown under different conditions (Fig. 3A) revealed a total of 272 proteins, 196 of which had known functions

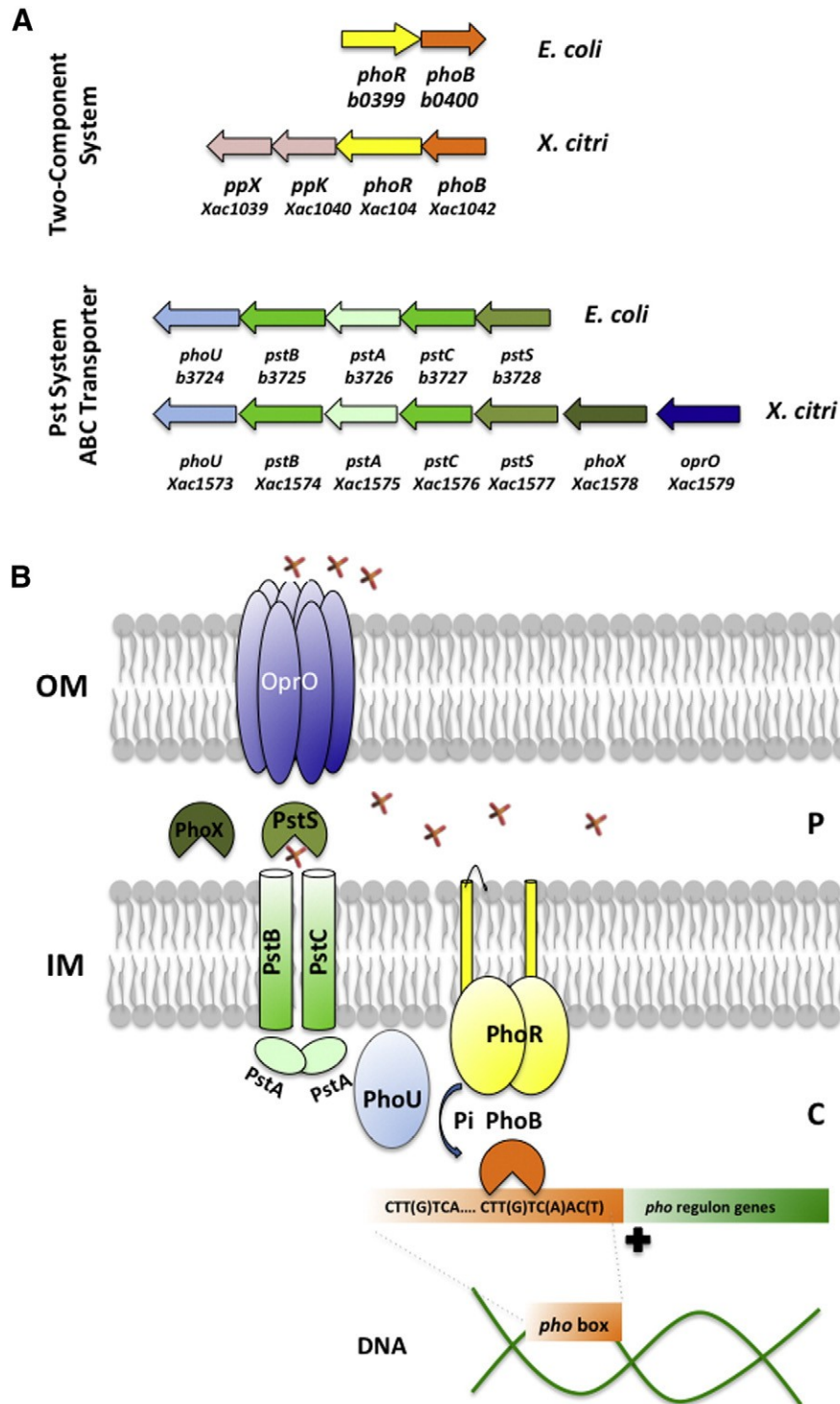


Fig. 2 – The *Xanthomonas citri* subsp. *citri* Pho regulon. (A) Comparison between the two-component *phoR*–*phoB* and phosphate uptake *pst* operons of *E. coli* and *X. citri*. The function of the genes showed is introduced in the Table S1 (Supplementary information). (B) Structural scheme of the Pho regulon orthologues found in *Xanthomonas citri* subsp. *citri* that is involved in transport and signalling mediated by phosphate. Proteins are shown in cartoon, inorganic phosphate is shown in sticks and the inner membrane is shown in grey. The external phosphate crosses the outer membrane (OM) through the OprO porin. In the periplasm (P), the specific ligand-binding proteins PstS and PhoX are responsible for the transport of the ion to the permeases PstB and PstC, which similarly to PhoR, are located in the inner membrane (IM). PhoB and PhoU are located in the cytoplasm and act respectively, in the Pst system and *pho*-box regions of Pho regulon genes.

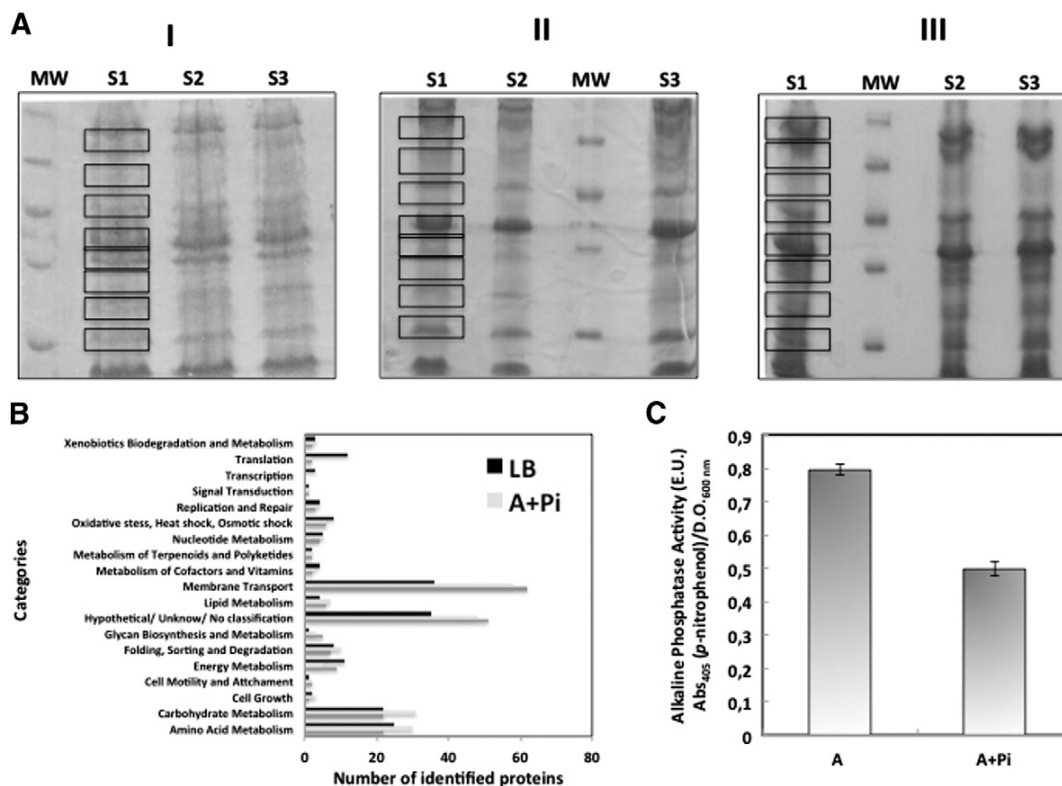


Fig. 3 – Functional classification of the *X. citri* proteins identified in the proteomics analysis and phosphatase alkaline activity. (A) SDS-PAGE 12% of samples from (I) LB medium, (II) A minimal medium and (III) A + Pi minimal medium, collected in the described times. S1, S2 and S3: three different samples, MW: molecular weight. Nine bands were excised on each gel as shown by squared lines and submitted extraction and tryptic digestion protocol. All samples analysed in the experiments contained 100 μ g of protein per well. (B) Number of proteins identified upon growth of *X. citri* in LB, A + Pi medium and A medium. The proteins were classified in 19 categories. (C) Activity of alkaline phosphatase measured from *X. citri* cells grown in A and A + Pi media. Samples were obtained from 1 ml of cultures after cell permeabilization with chloroform and 0.1% SDS according Tse et al. [17], and incubation with p-nitrophenylphosphate solution. Enzymatic units (E.U.) were calculated using values of p-nitrophenol measured by absorbance at 405 nm related to the optical density ($O.D_{600nm}$).

(Supplementary information, Table S4). The proteins were classified in 19 categories from which amino acid and carbohydrate metabolism, membrane transport and hypothetical proteins represent the majority (Fig. 3B). When the cells were cultivated in phosphate starvation a significant increase of transport related proteins, glycan biosynthesis, metabolism, or hypothetical functions was observed. On the other hand, the number of proteins belonging to translation and transcription was decreased. Patently, outer membrane proteins composed a large group in the proteomics data from the three different media (Supplementary information, Table S5). TonB-dependent receptors represented a significant number of the proteins related to Vitamin B₁₂ (6 from 19) and iron-uptake (13 from 19) transporters. In *Xanthomonas* genus, TonB-dependent receptors are also involved in sugar transport [24]. Iron-uptake proteins also included bacterioferritin, ferric enterobactin receptors and ferripyoverdine receptors. Other proteins were outer lipoproteins and membrane-associated proteins (Supplementary information, Table S5). Indeed,

depletion of phosphate led to a significant increase of iron-uptake proteins as observed for A and A + Pi media when compared to LB. Membrane components of ABC transporters were not identified but the periplasmic-binding proteins from alkane sulphonates, sulphate, nitrate/taurine, molybdate and phosphate transporters were found (Supplementary information, Table S6). Sbp, the sulphate-binding protein (*XAC1017*) from the putative sulphate transporter, was identified under all the conditions suggesting its importance for bacterium growth. Experiments performed in our laboratory have shown that Sbp is also expressed during in vivo infection in *Citrus sinensis* leaves (unpublished data). Interestingly, in addition to Sbp two other periplasmic-binding proteins involved with sulphur assimilation were identified when *X. citri* was grown in A + Pi medium. Nit/Tau (*XAC0829*) and SsuA1 (*XAC0849*) represent the periplasmic-component that binds with high affinity aliphatic sulphonates and alkane sulphonates, respectively. In *E. coli*, both belong to the *cys regulon* [25] and are regulated by the same proteins CysB/Cbl. Both

transport systems are induced for high affinity transport of sulphonates when sulphate is absent [25].

3.3. Effect of phosphate in the activation of Pho regulon proteins in *X. citri*

The effect of phosphate starvation on *X. citri* was analysed based on the results obtained in A and A + Pi media, applying the t-test [19]. Proteins were considered up or down regulated by phosphate when expression levels were increased more than 1.5-fold or decreased more than 0.67-fold according to Crabbé and collaborators [26] (Supplementary information, Tables S2 and S3). The analysis of the down regulated subproteome revealed 15 proteins that were involved in the metabolism of carbohydrates, amino acids, outer membrane proteins and enzymes from replication and nucleotide synthesis (Table 1). Conversely, 17 proteins were up regulated, highlighting the importance of the alkaline phosphatase (PhoA), which is a Pho member that is used as a marker fo

Table 1 – List of up and down regulated proteins in response to phosphate starvation in *Xanthomonas citri* subsp. *citri* ($p < 0.05$). The complete table with normalised spectral counts is presented in the supplementary information Table S3.

KEGG ID	Protein	Gene name	Fold change
<i>Down regulated</i>			
XAC3352	Glyceraldehyde-3-phosphate dehydrogenase	gapA	0.17
XAC0743	Serine hydroxymethyltransferase	glyA	0.55
XAC3847	N-acyl-L-amino acid amidohydrolase	amA	0.23
XAC4009	Arginase	argI	0.42
XAC3309	Aminopeptidase	–	0.31
XAC3225	Transglycosylase	mltB	0.25
XAC0120	T1D	t1D	0.53
XAC3341	Cysteine synthase	cysK	0.39
XAC2959	Ligase	purM	0.38
XAC1435	Iron receptor	fhuA	0.31
XAC0291	Oar protein	–	0.05
XAC3613	TonB-receptor dependent	cirA	0.06
XAC0823	Outer hemin	phuR	0.16
XAC2772	Outer membrane porin	–	0.47
XAC0030	Cellulase	egl	0.56
<i>Up regulated</i>			
XAC2151	YapH adhesin	yapH	6.4
XAC2386	Superoxidase dismutase	sodM	2.48
XAC2783	Thioredoxin	trx	2.2
XAC1204	Alanyl dipeptidyl peptidase	–	2.0
XAC3388	Type II citrate synthase	gltA	3.3
XAC2620	VirB9	virB9	3.1
XAC2619	VirB10	virB10	3.9
XAC3534	General secretion pathway protein D	xpsD	4.4
XAC3158	TonB-dependent receptor	fhuA	6.0
XAC3334	TonB-dependent receptor	fecA	7.6
XAC2780	Lipoprotein	–	2.5
XAC3472	Polyphosphate-selective porin O ^a	oprO	3.6
XAC0009	Biopolymer transport ExbB protein	exbB	2.1
XAC2759	Alkaline phosphatase ^a	phoA	19.8
XAC1577	ABC transporter phosphate-binding protein ^a	pstS	33.5
XAC1578	Phosphate-binding protein ^a	phoX	49.1
XAC3358	Molybdate-binding protein	modA	12.4

Pho regulon activation [2,8] (Table 1). These data were corroborated by the assays of alkaline phosphatase activity that evidenced a higher activity measured in A medium when compared to A + Pi medium (Fig. 3C). Other relevant Pho regulon proteins that were up regulated include the polyphosphate-selective porin (OprO) and the two periplasmic-binding proteins, PhoX and PstS (Table 1). Periplasmic-binding proteins are essential components of ABC transporters that capture phosphate under starvation conditions with high affinity [27]. These results show the formation of the phosphate ABC transporter and the importance of the PstS for *X. citri* in phosphate starvation conditions. PstS is well established to serve as a phosphate-binding protein in other bacteria [8], and in *X. citri* its role is supported by the high sequence identity with *E. coli* orthologue (56%) and structural comparison of the ligand-binding site that contains conserved residues for phosphate binding (unpublished results). However, differently of *E. coli*, *X. citri* has another protein identified as phosphate-binding protein, PhoX (XAC1578), which function is still unclear, and its abundance in subproteome results is even higher than that of PstS (fold change of 49.17 vs. 33.50) (Table 1 and Table S3, Supplementary information). Phosphate starvation also up regulated SodM (2.48-fold) and Trx (2.2-fold) from the oxidative stress category, VirB9 and VirB 10 from the type IV secretion system (3.1- and 3.9-fold, respectively), XpsD from the type II

secretion system (4.4 fold) and TonB-dependent receptors (6.00- and 7.62-fold) (Table 1 and Table S3, Supplementary information). Similarly to what is observed in other bacteria [2], phosphate starvation in *X. citri* induces the activation of proteins as an adaptive response.

3.4. Identification of proteins of *X. citri*, which orthologues from other bacteria have been related to pathogenesis and virulence

Phosphate starvation and pathogenesis are closely related. Altered induction of the Pho regulon genes significantly reduced the capsular antigen at the cell surface and resistance to the bactericidal effect of the avian pathogenic *E. coli* O78 strain [2,3], decreased the resistance to cationic antimicrobial peptides and the production of polysaccharides in the membrane [28] and the production of type I fimbriae [29]. In *X. citri*, however, the relationship between phosphate starvation, activation of Pho regulon proteins and pathogenesis has not been directly evidenced. With this proposal and based on the literature, we identified a dataset of proteins that previously were described to affect direct or indirectly the bacterial pathogenesis and virulence, specially in *Xanthomonas* genus and related species. Although the analysis points to specific proteins, some with significant differences in the expression levels, it is important to detach that the induction of genes involved in pathogenesis might not be specific only for a phosphate response but also for a general starvation response, which may be induced by other essential elements.

A total of 36 proteins were classified in categories related to the bacterial secretion system, attachment, heat shock, osmotic and oxidative stress, xanthan gum synthesis and tolerance to toluene (Table 2). From the list of proteins that were identified but not affected by the phosphate concentrations we detach TolC, GumB and YapH. TolC, a protein

Table 2 – Identification of the 1D gel separated *X. citri* proteins that were previously related to the pathogenesis or have orthologues from other *Xanthomonas* involved on pathogenesis and virulence. Proteins in *italic* and underlined were exclusively identified in the A + Pi and A media, respectively. Proteins up and down regulated are evidenced with one or two asterisks, respectively. (–) protein not identified in the samples; (X) protein identified in the samples. Two and three independent experiments were performed for A and A + Pi media analyses.

KEGG ID	Protein name	Function	A Medium	A + Pi Medium	Reference
Bacterial secretion system					
XAC0221	SecB	Preprotein translocase subunit SecB	X	X	[36]
XAC2619	VirB10*	VirB10	X	–	[34]
XAC2620	VirB9*	VirB9	X	–	[6,34]
XAC3463	TolC	TolC	X	X	[17,29]
XAC3534	XpsD*	General secretion pathway protein D	X	X	[8]
Biopolymer transport					
XAC0009	ExbB	Biopolymer transport ExbB protein	X	X	[37]
Heat shock, osmotic and oxidative stress					
XAC0209	YojM	Superoxide dismutase-like protein	X	X	[38]
XAC0210	SodC2	Superoxide dismutase	X	–	[12,35,38]
XAC0493	Bfr	Bacterioferritin	–	X	[39]
XAC0609	–	Zinc protease	X	X	[40]
XAC0723	DsbA	Disulphide oxidoreductase	X	X	[41]
XAC1211	KatE	Catalase	X	X	[12,15]
XAC1321	MucD	Periplasmic protease	X	X	[42]
XAC1456	Dpc	Peptidyl-dipeptidase	X	X	[43]
XAC2386	SodM*	Superoxidase dismutase	X	X	[9,35]
XAC2783	Trx*	Thioredoxin	X	X	[44]
Fimbrial — tipo IV					
XAC2017	PilF	Type IV pilus assembly protein pilF	X	X	[11]
XAC2665	PilY1	Type IV pilus assembly protein	–	X	[11]
Xanthan gum synthesis					
XAC2585	GumB	GumB protein	X	X	[5,30,31]
Toluene					
XAC4342	YrbC	Toluene tolerance protein	X	X	[45]
TolB					
XAC3142	TolB	Translocation protein TolB;	X	X	[46]
Folding and sort degradation					
XAC0023	Ctp	Carboxyl-terminal protease	X	X	[47]
XAC0541	GroES	Co-chaperonin GroES	X	X	[48]
XAC0542	GroEL	Chaperonina 60 kDa	X	X	[48]
XAC0669	Prc	Tail-specific protease	–	X	[49]
XAC0723	DsbA	Disulphide oxidoreductase	X	X	[50]
XAC0865	SurA	Peptidyl-prolyl cis-trans isomerase	X	X	[5]
XAC1078	ClpP	ATP-dependent Clp protease proteolytic subunit	X	X	[51]
XAC1085	PpiD	Peptidyl-prolyl cis-trans isomerase	X	X	[5,30]
XAC1550	FkpA	FKBP-type peptidyl-prolyl cis-trans isomerase	X	X	[5]
XAC3550	DsbC	Disulphide isomerase	–	X	[52]
XAC3980	HtrA	Protease DO	X	–	[53]
XAC4008	EcnA	Entericidin A	–	X	[54]
XAC0029	Egl	Cellulase	–	X	[33]
XAC0030	Egl**	Cellulase	X	X	[33]
Adhesin					
XAC2151	YapH*	YapH adhesin	X	X	[32,33]

localised to the outer membrane of *X. citri* was previously described to be involved with *Xyllela fastidiosa* pathogenicity [30], another phytopathogenic bacteria. Similar results were obtained for important proteases that are related to mesophilic cell invasion and for GumB, the first protein from the xanthan gum metabolic pathway [31]. Indeed, the non-fimbrial adhesion protein YapH identified in A and A + Pi media and up regulated (6.4 fold), was previously

shown to be up regulated in *Xanthomonas* species during biofilm formation [32,33]. Interestingly, from the list of proteins found in both media, the proteins XpsD, SodM, Trx and YapH were up regulated (Table 2, one asterisk) while Egl (XAC0030) was down regulated (Table 2, two asterisks).

The four proteins VirB9, VirB10, SodC2 and HtrA were identified only in phosphate starvation conditions (A medium) (Table 2, underlined). From these, VirB9 and VirB10 were up

regulated (Table 2, one asterisk). VirB9 and VirB10 are members of the type IV secretion system, previously related to pathogenesis in several microbes, since they mediate the horizontal genetic transfer and translocation of effector proteins [34]. Other proteins that were identified only in the A medium was a protease and the superoxide dismutase SodC (Table 2, underlined). SodC belongs to the class of pathogen-associated molecular patterns (PAMP) induced by plant defence, and it is conserved in most bacteria with a similar function [35]. From the six proteins exclusively identified in the A + Pi medium, most of them are involved in degradation or folding processes (Table 2, italicised), such as the peptidyl-prolyl cis-trans isomerase (PpiD) required for folding of outer membrane proteins and biofilm formation in *X. fastidiosa* [30]. The cellulase Egl encoded by the gene XAC0030 was down regulated in A + Pi (Table 2, two asterisks).

4. Discussion

The Pho regulon has been largely described in *E. coli* as well as the relationship between Pho regulon genes and virulence and pathogenesis [1,2], but there are no available data reporting the phosphate regulation in phytopathogenic bacteria from *Xanthomonas* genus, including *X. citri*. In this work, we performed a simple, rapid and inexpensive method to characterise the *X. citri* proteome based on 1D SDS-PAGE gel fractionation. A total of 272 proteins were identified and classified in 19 categories. The results provided the first evidence of the presence and activation of Pho regulon genes in *X. citri*, induced by phosphate. Furthermore, the evidences that *X. citri* conserves the two-component PhoR/PhoB system and the Pst system, both activated under phosphate starvation conditions, strongly suggest that these systems belong to a part of a conserved mechanism for the regulation and capture of this ion. The bioinformatics analysis showed the presence and conservation of pho-box [6] regions in almost all putative genes from Pho regulon in *X. citri*, including *phoA* and *pst* operon suggesting a conservative means of regulation involving PhoB.

These data associated to the proteome results from cells grown in A medium showing that PhoA (the Pho regulon marker) and PstS were significantly up regulated, are the final evidences that both proteins belong to a Pho regulon present in *X. citri* and that the Pst system is functional and activated in phosphate starvation conditions. Also relevant was the up regulation of the periplasmic-binding protein PhoX and the porin OprO, which genes are located close to *pst* operon in *X. citri* but under control of a different promoter that conserves the pho-box sequence. This fact could explain the differences in the expression levels of PhoX and PstS. PhoX is only present in *X. citri* and conserves the residues for phosphate binding, but it has a completely different electrostatic potential when compared to the periplasmic-binding protein PstS. Its role during phosphate starvation is not clear, but its importance was clearly evidenced by its level of up regulation and has been studied by our group using *X. citri* mutants. The *phoRB* operon has two genes coding for kinases that are involved in inorganic polyphosphate (polyP) intracellular metabolism [7]. Differently, in *E. coli*, the corresponding genes are

dispersed within the genome and they were not identified as a member of the Pho regulon. Not only the absence of an alternative system for the capture of phosphonate (Phn system), but also the presence of putative glycerol-3-phosphate enzymes and proteins related to the transport of sugars that form an ABC transporter is intriguing once *X. citri* can live in the soils where phosphonates are highly abundant.

The comparative analyses of the proteome from cultures grown in LB, A and A + Pi media evidenced a decrease in translation and transcription processes in defined media, and an increase in the abundance of the proteins that are involved in transport, metabolism, and stress suggesting an adaptive/survival response to phosphate deprivation, which among many changes occurred in the cell, involves the modification of their cell surface components [2]. Remarkably, the induction of the expression of substrate-binding proteins involved with different transport systems of high affinity that are induced in depletion of nutrients [27] reinforces the idea that *X. citri*, similar to what is described for *E. coli*, induces an adaptive response mediated by the low level of bioavailability of phosphate. Genes involved with metal ion stress response were super expressed in *E. coli* *phoB* mutant strain grown in Pi limitation suggesting that PhoB plays an additional control in metal ion metabolism or stress response [8]. Moreover, regarding the transport category, the results showed the presence of the periplasmic components of ABC transporters for molybdate, sulphonate, alkane sulphonate, nitrate and phosphate. These results indicate a relationship between ABC transporters and starvation in *X. citri*. Another important protein essential for *X. citri* pathogenesis identified in phosphate starvation conditions is GumB, the first enzyme of the xanthan gum synthesis pathway [31]. The majority of phytopathogenic bacteria produce some kind of extracellular polysaccharide (EPS) that contributes to the pathogenicity [55]. Xanthan gum production by *X. citri* is directly involved with quorum sensing [31], induction of sensibility in the host plant and virulence [56], and mutants of gum genes which losses their ability of adhesion and biofilm formation [57].

5. Conclusions

Altogether, our data showed the first set of evidences of the presence of Pho regulon genes in *X. citri*, the bacterium responsible for the citrus canker disease. Firstly, we showed that *X. citri* conserves the phosphate ABC transporter PstSCAB and the two-component system PhoR/PhoB and that both systems are highly induced during phosphate starvation. The presence and induction of the alkaline phosphatase PhoA also corroborates the Pho regulon activation. On the other hand, although we did not identify a large number of proteins, the proteomics dataset shows significant differences in the expression of membrane proteins, ABC transporters and proteins related to the pathogenesis, mostly related to the biofilm formation and xanthan gum synthesis.

Since bacteria from *Xanthomonas* genus are phylogenetically closely related and share more than 80% of their genomes, the data obtained in this work can be used for further comparisons and better understanding of the physiology of these important bacteria.

Supplementary data to this article can be found online at <http://dx.doi.org/10.1016/j.jprot.2014.05.005>.

Conflict of interest

The authors declare no conflict interest.

Acknowledgements

This work was supported by the Coordenação de Aperfeiçoamento Pessoal de Nível Superior — CAPES, Laboratório Nacional de Biociências, LNBio, Campinas, Brazil.

REFERENCES

- [1] Crépin S, Chekabab SM, Bihan GL, Bertrand N, Dozois CM, Harel J. The Pho regulon and the pathogenesis of *Escherichia coli*. *Vet Microbiol* 2011;153:82–8.
- [2] Lamarche MG, Wanner BL, Crépin S, Harel J. The phosphate regulon and bacterial virulence: a regulatory network connecting phosphate homeostasis and pathogenesis. *FEMS Microbiol Rev* 2008;32:461–73.
- [3] Crépin S, Lamarche MG, Garneau P, Séguin J, Proulx J, Dozois CM, Harel J. Genome-wide transcriptional response of an avian pathogenic *Escherichia coli* (APEC) pst mutant. *BMC Genomics* 2008;9:1–17.
- [4] Sinai A. Hyper-invasive mutants define a novel Pho-regulated invasion pathway in *Escherichia coli*. *Mol Microbiol* 1993;10:1125–37.
- [5] Spence J, Cegielska A, Georgopolus C. Role of *Escherichia coli* heat shock proteins Dnak and HtpG (C62.5) in response to nutritional deprivation. *J Bacteriol* 1990;12:7157–66.
- [6] VanBogelen RA, Olson ER, Wanner BL, Neidhardt FC. Global analysis of proteins synthesized during phosphorus restriction in *Escherichia coli*. *J Bacteriol* 1996;178:4344–6.
- [7] Wanner B. Phosphorus assimilation and control of the phosphate regulon. *Escherichia coli and Salmonella typhimurium cellular and molecular biology*, 51. New York: ASM Press; 1996 47–54.
- [8] Hsieh YJ, Wanner BL. Global regulation by the seven-component Pi signalling system. *Curr Opin Microbiol* 2010;13:198–203.
- [9] Ferreira GM, Spira B. The pst operon of enteropathogenic *Escherichia coli* enhances bacterial adherence to epithelial cells. *Microbiology* 2008;154:2025–36.
- [10] O'May GA, Jacobsen SM, Longwell M, Stoodley P, Mobley HLT, Shirliff ME. The high affinity phosphate transporter Pst in *Proteus mirabilis* HI4320 and its importance in biofilm formation. *Microbiology* 2009;155:1523–35.
- [11] Yoshida Y, Sugiyama S, Oyamada T, Yokoyama K, Makino K. Identification and characterization of novel phosphate regulon genes, *ecs0540-ecs0544*, in *Escherichia coli* O157:H7. *Mol Genet Genomics* 2010;284:197–205.
- [12] Neves MF, Trombin VG, Milan P, Lopes FF, Cressoni F, Kalaki R. O retrato da citricultura brasileira. *Citrus BR: Citrus Br*; 2010.
- [13] da Silva AC, Ferro JA, Reinach FC, Farah CS, Furlan LR, Quaggio RB, et al. Comparison of the genomes of two *Xanthomonas* pathogens with differing host specificities. *Nature* 2002;417:459–63.
- [14] Levinthal C, Signer ER, Fetherolf K. Reactivation and hybridization of reduced alkaline phosphatase. *Biochemistry* 1962;48:1230–7.
- [15] Bradford MM. A rapid and sensitive method for the quantitation of microgram quantities of protein utilizing the principle of protein-dye binding. *Anal Biochem* 1976;72:248–54.
- [16] Paes-Leme AF, Sherman NE, Smalley DM, Sizukusa LO, Oliveira AK, Menezes MC, et al. Hemorrhagic activity of HF3, a snake venom metalloproteinase: Insights from the proteomic analysis of mouse skin and blood plasma. *J Proteome Res* 2012;11:279–91.
- [17] Tse YM, Yu M, Tsang JSH. Topological analysis of a haloacid permease of *Burkholderia* sp. Bacterium with a PhoA-LacZ reporter. *BMC Microbiol* 2009;9:1–12.
- [18] Perkins DN, Pappin DJ, Creasy DM, Cottrell JS. Probability-based protein identification by searching sequence database using mass spectrometry data. *Biochemistry* 1999;20:3551–67.
- [19] Nesvizhskii AI, Keller A, Kolker E, Aebersold R. A statistical model for identifying proteins by tandem mass spectrometry. *Anal Chem* 2003;75:4646–58.
- [20] Keller A, Nesvizhskii AI, Kolker E, Aebersold R. Empirical statistical model to estimate the accuracy of peptide identifications made by MS/MS and database search. *Anal Chem* 2002;20:5383–92.
- [21] Moraes TF, Bains M, Hancock RE, Strynadka NC. An arginine ladder in OprP mediates phosphate-specific transfer across the outer membrane. *Nat Struct Mol Biol* 2007;1:85–7.
- [22] Kato J, Yamamoto T, Yamada K, Ohtake H. Genetic improvement of *Escherichia coli* for enhanced biological removal of phosphate from wastewater. *Appl Environ Microbiol* 1993;59:3744–9.
- [23] Ghorbel S, Smirnov A, Chouayekh BS, Esnault C, Kromanec J, Virolle MJ. Regulation of *ppk* Expression and in vivo function of Ppk in *Streptomyces lividans* TK24. *J Bacteriol* 2006;17:6269–76.
- [24] Blanvillain S, Meyer D, Boulanger A, Lautier M, Guynet C, Denance N, et al. Plant carbohydrate scavenging through tonB-dependent receptors: a feature shared by phytopathogenic and aquatic bacteria. *PLoS One* 2007;2:e224.
- [25] van der Ploeg JR, Eichhorn E. Sulfonate-sulfur metabolism and its regulation in *Escherichia coli*. *Arch Microbiol* 2001;176:1–8.
- [26] Crabbé A, Leroy B, Wattiez R, Aerstsens A, Leys N, Cornelis P, et al. Differential proteomics and physiology of *Pseudomonas putida* KT2440 under filament-inducing conditions. *BMC Microbiol* 2012;12:282–90.
- [27] Davidson AL, Dassa E, Orelle C, Chen J. Structure, function, and evolution of bacterial ATP-binding cassette systems. *Microbiol Mol Biol Rev* 2008;72:317–64.
- [28] Daigle F, Fairbrother JM, Harel J. Identification of a mutation in the pst-phoU operon that reduces pathogenicity of an *Escherichia coli* strain causing septicemia in Pigs. *Inf Immun* 1995;63:4924–7.
- [29] Lamarche MG, Harel J. Membrane homeostasis requires intact pst in extraintestinal pathogenic in *Escherichia coli*. *Curr Microbiol* 2010;60:356–9.
- [30] Silva MS, De Souza AA, Takita MA, Labate CA, Machado MA. Analysis of the biofilm proteome of *Xylella fastidiosa*. *Proteome Sci* 2011;9:1–10.
- [31] Vojnov AA, Zorreguieta A, Dow JM, Daniels MJ, Dankert MA. Evidence for a role for the gumB and gumC gene products in the formation of xanthan from its pentasaccharide repeating unit by *Xanthomonas campestris*. *Microbiology* 1998;144:1487–93.

- [32] Zimaro T, Thomas L, Marondedze C, Garavaglia BS, Gehring C, Ottado J, et al. Insights into *Xanthomonas axonopodis* pv. *citri* biofilm through proteomics. *BMC Microbiol* 2013;13:1–14.
- [33] Monge AG, Astua JF, Bacocina G, Roncoletta J, Carvalho SA, Machado MA. Expression profiling of virulence and pathogenicity genes of *Xanthomonas axonopodis* pv. *citri*. *J Bacteriol* 2005;187:1201–5.
- [34] Kane KA, Dorman CJ. VirB-mediated positive feedback control of the virulence gene regulatory cascade of *Shigella flexneri*. *J Bacteriol* 2012;194:5264–73.
- [35] Watt SA, Tellström V, Patschkowski T, Niehaus K. Identification of the bacterial superoxide dismutase (SodM) as plant-inducible elicitor of an oxidative burst reaction in tobacco cell suspension cultures. *J Biotechnol* 2006;126:78–86.
- [36] Lee VT, Schneewind O. Protein secretion and the pathogenesis of bacterial infections. *Genes Dev* 2001;15:1725–52.
- [37] Moeck GS, Coulton JW. TonB-dependent iron acquisition: mechanism of siderophores-mediated active transport. *Mol Microbiol* 1998;28:675–81.
- [38] Fee JA. Regulation of *sod* genes in *Escherichia coli*: relevance to superoxide dismutase function. *Mol Microbiol* 1991;5:2599–610.
- [39] Reddy PV, Puri VR, Khera A, Tyagi AK. Iron storage proteins are essential for the survival and pathogenesis of *Mycobacterium tuberculosis* in THP-1 Macrophages and the Guinea Pig model of infection. *J Bacteriol* 2012;194:567–75.
- [40] Cafardi V, Biagini M, Martinelli M, Leuzzi R, Rubino JT, Cantini F, et al. Identification of a novel zinc metalloprotease through a global analysis of *Clostridium difficile* extracellular proteins. *PLoS ONE* 2013;8:1–14.
- [41] Collet JF, Bardwell JCA. Oxidative protein folding in bacteria. *Mol Microbiol* 2002;44:1–8.
- [42] Wood LF, Ohman DE. Independent regulation of MucD, and Htra-like protease in *Pseudomonas aeruginosa*, and the role of its proteolytic motif in alginate gene regulation. *J Bacteriol* 2006;188:3134–7.
- [43] Harty DWS, Hunter N. Carboxypeptidase activity common to viridans group streptococci cleaves angiotensin I to angiotensin II: an activity homologous to angiotensin-converting enzyme (ACE). *Microbiology* 2011;157:2143–51.
- [44] Zeller T, Klug G. Thioredoxins in bacteria: function in oxidative stress response and regulation of thioredoxin genes. *Naturwissenschaften* 2006;93:259–66.
- [45] Choi JH, Yoo JS, Jeong YK, Joo WH. Involvement of antioxidant defense system in solvent tolerance of *Pseudomonas putida* BCNU 106. *J Basic Microbiol* 2013;53:1–6.
- [46] Rigal A, Bouveret E, Lloubes R, Lazdunski C, Benedetti H. The TolB protein interacts with the porins in *Escherichia coli*. *J Bacteriol* 1997;179:7274–9.
- [47] Bandara AB, Sriranganathan N, Schurig GG, Boyle SM. Carboxyl-terminal protease regulates *Brucella suis* morphology in culture and persistence in macrophages and mice. *J Bacteriol* 2005;187:5767–75.
- [48] Lemos JA, Luzardo Y, Burne RA. Physiologic effects of forced down-regulation of *dnaK* and *groEL* expression in *Streptococcus mutans*. *J Bacteriol* 2007;189:1582–8.
- [49] Wang CY, Wang SW, Huang WC, Kim KS, Chang NS, Wang YH, et al. Prc contributes to *Escherichia coli* evasion of classical complement mediated serum killing. *Infect Immun* 2012;80:3399–409.
- [50] Mavrodi OV, Mavrodi DV, Park AA, Weller DM, Thomashow LS. The role of *dsbA* in colonization of the wheat rhizosphere by *Pseudomonas fluorescens* Q8r1-96. *Microbiology* 2006;152:863–72.
- [51] Frees D, Gerth U, Ingmer H. Clp chaperones and proteases are central in stress survival, virulence and antibiotic resistance of *Staphylococcus aureus*. *Int J Med Microbiol* 2014;304:142–9.
- [52] Hiniker A, Collet JF, Bardwell JCA. Copper stress causes an in vivo requirement for the *Escherichia coli* disulfide isomerase DsbC. *J Biol Chem* 2005;280:33785–91.
- [53] Chitlaru T, Zaide G, Ehrlich S, Inbar I, Cohen O, Shafferman A. HtrA is a major virulence determinant of *Bacillus anthracis*. *Mol Microbiol* 2011;81:1542–59.
- [54] Bishop RE, Leski BK, Hodges RS, Kay CM, Weiner JH. The entericidin locus of *Escherichia coli* and its implications for programmed bacterial cell death. *J Mol Biol* 1998;280:583–96.
- [55] Denny TP. Involvement of bacterial polysaccharide in plant pathogenesis. *Annu Rev Phytopathol* 1995;33:173–97.
- [56] Yun MH, Torres PS, El Oirdi M, Rigano LA, Gonzalez-Lamothe R, Marano MR, et al. Xanthan induces plant susceptibility by suppressing callose deposition. *Plant Physiol* 2006;141:178–87.
- [57] Rigano LA, Siciliano F, Enrique R, Sendín L, Filippone P, Torres PS, et al. Biofilm formation, epiphytic fitness, and canker development in *Xanthomonas axonopodis* pv. *citri*. *Mol Plant Microbe Interact* 2007;10:1222–30.

Artigo 3

Crystallization and preliminary X-ray diffraction analysis of the phosphate-binding protein PhoX from *Xanthomonas citri*

Vanessa R. Pegos, Francisco Javier Medrano and Andrea Balan.

(doi:10.1107/S2053230X14021840)

Crystallization and preliminary X-ray diffraction analysis of the phosphate-binding protein PhoX from *Xanthomonas citri*

Vanessa R. Pegos,^a
Francisco Javier Medrano^b and
Andrea Balan^{a,c,*}

^aLaboratório Nacional de Biociências (LNBio), Centro de Pesquisa em Energia e Materiais (CNPem), 13083-970 Campinas-SP, Brazil, ^bCentro de Investigaciones Biológicas, Madrid, Spain, and ^cDepartamento de Microbiologia, Instituto de Ciências Biomédicas II, Universidade de São Paulo, Av. Prof. Lineu Prestes 1374, Cidade Universitária, 05508-900 São Paulo-SP, Brazil

Correspondence e-mail: abalan@usp.br

Received 21 June 2014
Accepted 3 October 2014

Xanthomonas axonopodis pv. *citri* (*X. citri*) is an important bacterium that causes citrus canker disease in plants in Brazil and around the world, leading to significant economic losses. Determination of the physiology and mechanisms of pathogenesis of this bacterium is an important step in the development of strategies for its containment. Phosphate is an essential ion in all microorganisms owing its importance during the synthesis of macromolecules and in gene and protein regulation. Interestingly, *X. citri* has been identified to present two periplasmic binding proteins that have not been further characterized: PstS, from an ATP-binding cassette for high-affinity uptake and transport of phosphate, and PhoX, which is encoded by an operon that also contains a putative porin for the transport of phosphate. Here, the expression, purification and crystallization of the phosphate-binding protein PhoX and X-ray data collection at 3.0 Å resolution are described. Biochemical, biophysical and structural data for this protein will be helpful in the elucidation of its function in phosphate uptake and the physiology of the bacterium.

1. Introduction

Periplasmic binding proteins from ATP-binding cassette transporters (ABC transporters) are essential components owing to their role in substrate uptake and delivery to the transporter. They consist of two domains connected by a hinge that form a cleft for substrate binding (Davidson et al., 2008). More than 100 structures of periplasmic binding proteins have been solved in different conformations, essentially demonstrating the changes that occur after ligand binding (Berntsson et al., 2010) and the essential residues for substrate binding and transport. In bacteria, the PstSABC system is the ABC transporter specific for inorganic phosphate (P_i), which contains the PstS protein as a model high-affinity phosphate-binding protein. At present, 18 structures of phosphate-binding proteins are available in the Protein Data Bank, including 12 structures of PstS from *Escherichia coli*, including the wild type and mutants (Wang et al., 1994, 1997; Yao et al., 1996; Hirshberg et al., 1998; Ledvina et al., 1998), structures of the orthologues from *Yersinia pestis* (Tanabe et al., 2007), *Streptococcus pneumoniae* (PDB entry 4ex1; Center for Structural Genomics of Infectious Diseases, unpublished work), *Borrelia burgdorferi* (Brautigam et al., 2014) and *Clostridium perfringens* (PDB entry 4gd5; Center for Structural Genomics of Infectious Diseases, unpublished work), and the structures of PstS-1 and PstS-3 from *Mycobacterium tuberculosis* (Vyas et al., 2003; Ferraris et al., 2014). The structures showed similarities, including the two domains forming the cleft for the phosphate, conservation in the ligand-binding pocket and the importance of residues for high-affinity binding. The expression of *pst* genes is regulated by low phosphorus levels through the activation of the Pho regulon proteins (Van-Bogelen et al., 1996), which induces an adaptive response into the cell (Lamarche et al., 2008). Indirectly, the upregulation and down-regulation of many genes mediated by phosphate levels has been



© 2014 International Union of Crystallography
All rights reserved

Table 1Orthologues of *X. citri* PhoX with solved structures deposited in the Protein Data Bank and sequence comparison.

Protein name	Organism	Sequence identity (%)	Query coverage (%)	E-value	PDB code and reference
Phosphate-binding protein PstS	<i>Yersinia pestis</i>	57	88	2.00×10^{-122}	2z22 (Tanabe <i>et al.</i> , 2007)
Phosphate-binding protein	<i>Escherichia coli</i>	51	88	4.00×10^{-121}	2abh (Yao <i>et al.</i> , 1996)
Phosphate-binding protein	<i>Escherichia coli</i>	56	88	4.00×10^{-121}	1ixh (Wang <i>et al.</i> , 1997)
Periplasmic binding protein	<i>Streptococcus pneumoniae</i> Canada	55	25	2.00×10^{-7}	4exl (Center for Structural Genomics of Infectious Diseases, unpublished work)
Phosphate receptor PstS-1	<i>Mycobacterium tuberculosis</i>	32	91	6.00×10^{-38}	1pc3 (Vyas <i>et al.</i> , 2003)
Phosphate-binding protein PstS-3	<i>Mycobacterium tuberculosis</i>	31	91	7.00×10^{-35}	4lvq (Ferraris <i>et al.</i> , 2014)
Phosphate-binding protein	<i>Clostridium perfringens</i>	27	59	4.00×10^{-7}	4gd5 (Center for Structural Genomics of Infectious Diseases, unpublished work)
Phosphate-binding protein PstS	<i>Borrelia burgdorferi</i>	21	75	2.10×10^{-2}	4n13 (Brautigam <i>et al.</i> , 2014)

Table 2Crystallization screening and refinement conditions for *X. citri* PhoX in the absence and presence of phosphate.

The best crystals obtained after refinement are shown in Fig. 1.

Sample	Protein concentration (mg ml ⁻¹)	Screening	Refinement	Crystals	Resolution after refinement (Å)
PhoX + sodium phosphate	10	25% PEG 3350, 200 mM sodium iodide, 100 mM bis-tris pH 5.5	20% PEG 3350, 200 mM sodium iodide	Fig. 1(a)	3.0
PhoX	8	20% PEG 3350, 200 mM sodium iodide	17% PEG 3350, 200 mM sodium iodide	Fig. 1(b)	5.0
PhoX	10	20% PEG 3350, 200 mM sodium iodide	17% PEG 3350, 250 mM sodium iodide	Fig. 1(c)	6.0
PhoX + sodium phosphate	15	20% PEG 3350, 200 mM sodium iodide	17% PEG 3350, 250 mM sodium iodide	Fig. 1(d)	2.9
PhoX + sodium phosphate	15	17% PEG 3350, 250 mM sodium iodide	15% PEG 3350, 250 mM sodium iodide	Fig. 1(e)	3.0

Curiously, in *Xanthomonas axonopodis* pv. *citri* (*X. citri*), the causative agent of citrus canker disease (Brunings & Gabriel, 2003), we identified the presence of two genes encoding phosphate-binding proteins, pstS (XAC1577) and phoX (XAC1578), which belong to the pstSCABU and oprOphoX operons, respectively (Pegos *et al.*, 2014). Sequence analysis of the proteins revealed a sequence identity of 65%. A sequence identity of greater than 50% was observed when the sequence of PhoX was compared with those of the PstS orthologues from *E. coli*, *Y. pestis* and *S. pneumoniae* (Table 1). PhoX also conserved the residues forming the putative active site found in these proteins. In previous studies, we have demonstrated that phoX is found in a large number of *Xanthomonas* strains and is identified in many species of proteobacteria. Recently, based on a proteomics analysis we have shown that the expression of PstS and PhoX is upregulated during depletion of phosphate, indicating that both proteins play an important function in bacterial growth (Pegos *et al.*, 2014).

In order to obtain structural information for the PhoX protein from *X. citri*, the recombinant mature protein fused to an N-terminal His₆-tag sequence was expressed in *E. coli* Tuner (DE3) cells with an apparent molecular weight of 33 kDa and was purified using immobilized metal-affinity chromatography. The purified protein was crystallized in different conditions in the presence and absence of phosphate. The crystal structure of *X. citri* PhoX will be an important achievement for the study of phosphate uptake and regulation in the

2. Materials and methods

2.1. Cloning, expression and purification of PhoX protein

The PhoX-encoding gene was amplified from *X. axonopodis* pv. *citri* genomic DNA (gi:21242328) using the following oligonucleotides: F_PhoX_NdeI, 5' -CATATGGCCGACGTCACCGGTG-3' and R_PhoX_XhoI, 5' -CTCGAGTTAGTGCGGCAGATTCTGGC-3'. The amplified fragment of 951 bp consisted of the sequence encoding the mature protein without 24 amino acids from the N-terminus flanked by the restriction enzymes NdeI and XhoI at the beginning and end of the gene, respectively, and was cloned into the pET-28a vector. Recombinant *X. citri* PhoX protein fused at the N-terminal end to a His₆-thrombin cleavage site tag was obtained after expression tests in *E. coli* Tuner (DE3) strain transformed with a pET-28 derivative carrying the phoX gene (pET_phoX). Induction of expression occurred when the cells reached an optical density at 600 nm of 0.5 after the addition of 0.1 mM IPTG for 4 h at 30 °C. Cell extracts were obtained as previously reported for the alkanesulfonate-binding protein SsuA (Araújo *et al.*, 2013) and the protein was purified by immobilized nickel-affinity chromatography with 150 mM imidazole in the purification buffer (10 mM Tris-NaCl pH 8.0, 500 mM NaCl). The purified fractions were concentrated and

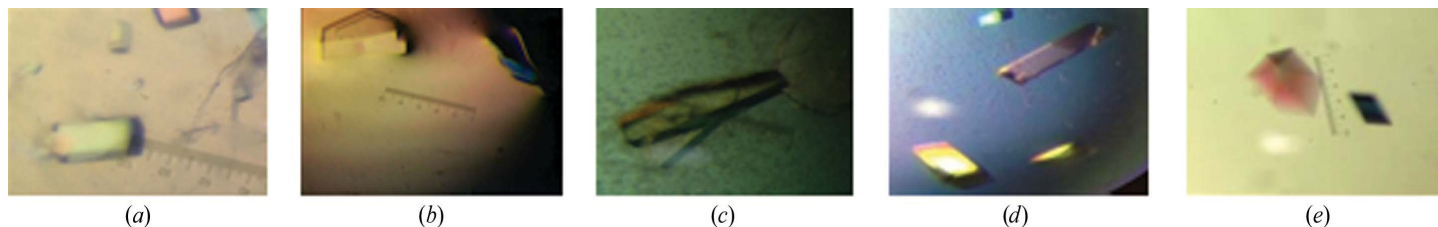
Figure 1 Crystals of *X. citri* PhoX obtained in the absence and presence of phosphate (see Table 2 for details).

Table 3

Data-collection and processing statistics.

Values in parentheses are for the highest resolution shell.

Diffraction source (Å)	1.459	W01B-MX2, LNLS Wavelength
Temperature (K)	110	
Detector		MAR Mosaic 225 CCD Crystal-to-
detector distance (mm)	120	
Rotation range per image (°)	0.5	
Total rotation range (°)	164.5	
Exposure time per image (s)	30	
Space group	P2 ₁	
a, b, c (Å)	81.56, 115.60, 133.30	
α, β, γ (°)	90.00, 90.33, 90.00	
Mosaicity (°)	0.45	
Resolution range (Å)	87.36–3.00 (3.11–3.00)	
Total No. of reflections	131283 (12689)	No. of
unique reflections	46810 (4633)	Completeness (%)
94.3 (95.5) Multiplicity		2.8 (2.7)
hI/ (I)j	8.4 (2.5)	
R _{meas}	0.145 (0.554)	Overall B factor
from Wilson plot (Å ²)	39.95	

dialyzed against 10 mM Tris–HCl pH 8.0 and kept at 20 °C at a final concentration of 10 mg ml⁻¹.

2.2. Protein crystallization

Samples of recombinant *X. citri* PhoX were submitted to crystallization trials at the automatized crystallization facility at the Brazilian National Laboratory of Biosciences (LNBio; CNPEM, Campinas, SP, Brazil) using the hanging-drop vapour-diffusion method, mixing equal volumes (1:1 ml) of protein and reservoir solution and incubating at 290 K. Initial screening with protein at 10 mg ml⁻¹ was performed using commercial crystallization screening kits from Hampton Research and Jena Biosciences. Conditions that showed crystalline structures or needles were refined, varying the pH, precipitant concentration and protein concentration to yield suitable crystals. A list of all of the conditions that allowed crystal growth and refinement is shown in Table 2 and crystals are shown in Fig. 1.

2.3. Data collection and processing

PhoX crystals were mounted in nylon loops and flash-cooled in mother liquor using liquid nitrogen; the high PEG concentration was sufficient to provide cryoprotection. The PhoX data set was collected

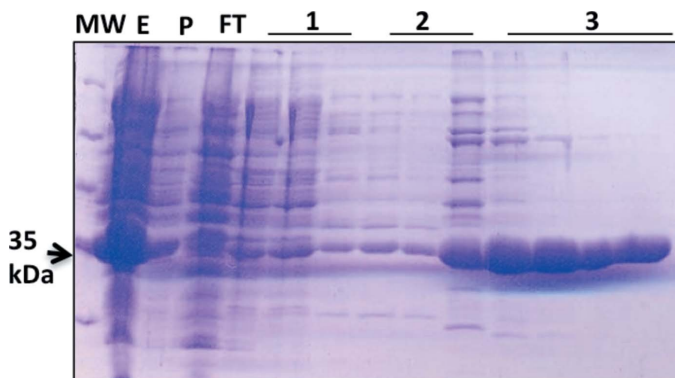


Figure 2

Expression and purification of *X. citri* PhoX. PhoX was expressed from *E. coli* Tuner (DE3) cells after IPTG induction and was purified by immobilized metal-affinity chromatography using nickel columns. Lane MW, molecular-weight markers; lane E, cell extract; lane P, cell pellet; lane FT, flowthrough of the immobilized nickel-affinity chromatography; lane 1, eluted samples from washing with 5 mM imidazole; lanes 2 and 3, eluted samples using 50 and 150 mM imidazole, respectively.

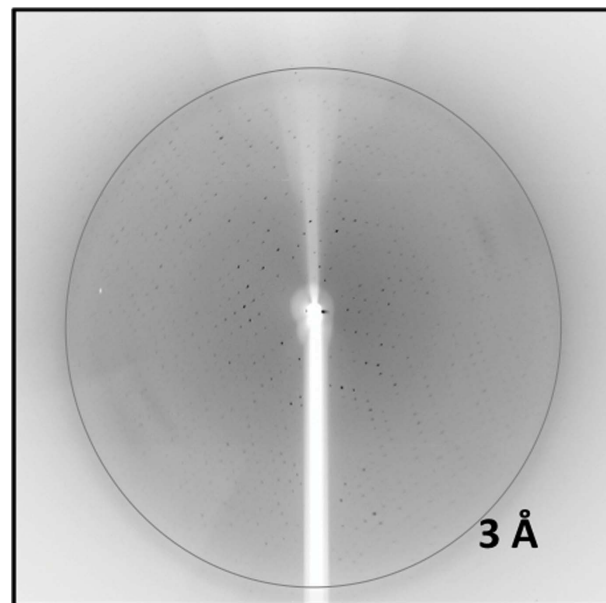
on the W01B-MX2 protein crystallography beamline at Laboratório Nacional de Luz Síncrotron (LNLS), Brazil using a wavelength of 1.459 Å and a MAR Mosaic 225 CCD detector. Diffraction data were indexed and integrated using XDS (Kabsch, 2010) and merged and scaled using AIMLESS (Evans, 2011) from the CCP4 package (Winn et al., 2011). Molecular replacement was performed with PHENIX (Adams et al., 2010) using PstS from *E. coli* K12 (PDB entry 2abh; Yao et al., 1996), which shares 51% amino-acid identity with PhoX, as a model. The phosphate, water molecules, H atoms and atoms with zero occupancy were removed from the 2abh structure to provide a better search model. Data-collection statistics are shown in Table 3.

3. Results and discussion

PhoX was produced from *E. coli* cells in a soluble form and purified in a single step of purification using immobilized metal-affinity



(a)



(b)

Figure 3

Crystal and diffraction pattern of *X. citri* PhoX. (a) Crystal of PhoX obtained in 20% PEG 3350, 200 mM sodium iodide and sodium phosphate with protein at 10 mg ml⁻¹. (b) Diffraction pattern of the crystal to 3.0 Å resolution (circle).

chromatography (Fig. 2). The purified protein was submitted to crystallization trials in the absence and presence of phosphate, resulting in needles and very small crystals that were less than 15 μm in the longest dimension. Most of the crystals were grown in PEG 3350 and sodium iodide. Refinement of these conditions improved the size and shape of the crystals, especially reducing the percentage of PEG 3350 and increasing the concentration of sodium iodide (Table 2). The presence of phosphate also increased the hardness of the crystals, suggesting a possible rearrangement of the structure upon ligand binding. The best diffraction pattern was obtained from a crystal grown in 200 mM sodium iodide, 20% PEG 3350 (Fig. 3). This crystal diffracted to a maximum resolution of 3.0 \AA and the data were processed using XDS (Kabsch, 2010). The crystals showed the symmetry and systematic absences of the primitive monoclinic space group $P2_1$. All data-collection statistics are shown in Table 3.

The range of possibilities for the Matthews coefficient (Matthews, 1968) of between 1.83 and 3.30 $\text{\AA}^3 \text{Da}^{-1}$ indicated the presence of between nine and five protein molecules in the asymmetric unit, respectively. After molecular replacement and analysis of the data, the best number of molecules in the asymmetric unit with no packing clashes was eight, for which the Matthews coefficient was calculated to be 2.01 $\text{\AA}^3 \text{Da}^{-1}$ and the solvent content to be 40.3%. The molecular-replacement procedure was performed using the E. coli phosphate-binding protein structure modified by CHAINSAW (Stein, 2008) as a search model (Yao et al., 1996; PDB entry 2abh) in Phaser (McCoy et al., 2007). The initial maps produced are encouragingly good, clearly showing electron density for the phosphate. The model is being rebuilt and refined.

This work was supported by CAPES (Coordenação de Aperfeiçoamento de Pessoal de Nível Superior) and the Laboratório Nacional de Biosciências (LNBio) at the Centro Nacional de Pesquisa em Energia e Materiais (CNPEM), Campinas, São Paulo, Brazil. We kindly thank Ronan Keegan and Andrey Lebedev (CCP4) for support and help with the data processing.

References

- Adams, P. D. et al. (2010). *Acta Cryst.* D66, 213–221.
- Berntsson, R. P.-A., Smits, S. H. J., Schmitt, L., Slotboom, D. J. & Poolman, B. (2010). *FEBS Lett.* 584, 2606–2617.
- Brautigam, C. A., Ouyang, Z., Deka, R. K. & Norgard, M. V. (2014). *Protein Sci.* 23, 200–212.
- Brunings, A. M. & Gabriel, D. W. (2003). *Mol. Plant Pathol.* 4, 141–157.
- Crépin, S., Chekabab, S. M., Le Bihan, G., Bertrand, N., Dozois, C. M. & Harel, J. (2011). *Vet. Microbiol.* 153, 82–88.
- Davidson, A. L., Dassa, E., Orelle, C. & Chen, J. (2008). *Microbiol. Mol. Biol. Rev.* 72, 317–364.
- Evans, P. R. (2011). *Acta Cryst.* D67, 282–292.
- Ferraris, D. M., Spallek, R., Oehlmann, W., Singh, M. & Rizzi, M. (2014). *Proteins*, 82, 2268–2274.
- Hirschberg, M., Henrick, K., Haire, L. L., Vasisht, N., Brune, M., Corrie, J. E. T. & Webb, M. R. (1998). *Biochemistry*, 37, 10381–10385.
- Kabsch, W. (2010). *Acta Cryst.* D66, 125–132.
- Lamarche, M. G., Wanner, B. L., Crépin, S. & Harel, J. (2008). *FEMS Microbiol. Rev.* 32, 461–473.
- Ledvina, P. S., Tsai, A.-L., Wang, Z., Koehl, E. & Quioco, F. A. (1998). *Protein Sci.* 7, 2550–2559.
- Matthews, B. W. (1968). *J. Mol. Biol.* 33, 491–497.
- McCoy, A. J., Grosse-Kunstleve, R. W., Adams, P. D., Winn, M. D., Storoni, L. C. & Read, R. J. (2007). *J. Appl. Cryst.* 40, 658–674.
- Pegos, V. R., Nascimento, J. F., Sobreira, T. J. P., Pauletti, B. A., Paes-Leme, A. & Balan, A. (2014). *J. Proteomics*, 108, 78–88.
- Stein, N. (2008). *J. Appl. Cryst.* 41, 641–643.
- Tanabe, M., Mirza, O., Bertrand, T., Atkins, H. S., Titball, R. W., Iwata, S., Brown, K. A. & Byrne, B. (2007). *Acta Cryst.* D63, 1185–1193.
- Tófoli de Araújo, F., Bolanos-Garcia, V. M., Pereira, C. T., Sanches, M., Oshiro, E. E., Ferreira, R. C. C., Chigardze, D. Y., Barbosa, J. A. G., de Souza Ferreira, L. C., Benedetti, C. E., Blundell, T. L. & Balan, A. (2013). *PLoS One*, 8, e80083.
- VanBogelen, R. A., Olson, E. R., Wanner, B. L. & Neidhardt, F. C. (1996). *J. Bacteriol.* 178, 4344–4366.
- Vyas, N. K., Vyas, M. N. & Quioco, F. A. (2003). *Structure*, 11, 765–774.
- Wang, Z., Choudhary, A., Ledvina, P. S. & Quioco, F. A. (1994). *J. Biol. Chem.* 269, 25091–25094.
- Wang, Z., Luecke, H., Yao, N. & Quioco, F. A. (1997). *Nature Struct. Biol.* 4, 519–522.
- Winn, M. D. et al. (2011). *Acta Cryst.* D67, 235–242.
- Yao, N., Ledvina, P. S., Choudhary, A. & Quioco, F. A. (1996). *Biochemistry*,

3.2. Manuscritos

Manuscrito I

The Two phosphate-binding proteins from the phytopathogen *Xanthomonas axonopodis* pv. *citri*: phylogeny and structural studies

Vanessa Rodrigues Pegos, Rodrigo M.L. Santos, Francisco Javier Medrano, Andrea Balan

**The two phosphate-binding proteins from the phytopathogen *Xanthomonas axonopodis* pv. *citri*:
phylogeny and structural studies**

Vanessa Rodrigues Pegos^{1,2}; Rodrigo M. L. Santos³; Francisco Javier Medrano⁴; Andrea Balan^{3*}.

¹Universidade Estadual de Campinas – UNICAMP, Instituto de Biologia (IB), Campinas, São Paulo, Brazil.

²Centro Nacional de Energia e Materiais (CNPEM), Laboratório Nacional de Biociências (LNBio), Campinas, São Paulo, Brazil.

³Universidade de São Paulo (USP), Instituto de Ciências Biomédicas II (ICBII), São Paulo, São Paulo, Brazil.

⁴Centro de Investigaciones Biológicas (CSIC), Madrid , Spain.

* Corresponding author

E-mail: abalan@usp.br (AB)

Abstract

The ATP-Binding Cassete (ABC) transporter is a high-affinity system involved in the uptake of several micronutrients, including phosphate ion. In *Escherichia coli*, the ABC transporter for phosphate is encoded by the *pstSABC* operon, which belongs to the Pho regulon. PstS is the periplasmic component responsible for affinity and specificity of the system and has been also related to a regulatory function during depletion of phosphate. Differently from what is observed in *E. coli*, the phytopathogenic bacterium *Xanthomonas axonopodis* pv. *citri* (*X. citri*) has two genes, *phoX* and *pstS*, that putatively encode for periplasmic phosphate binding proteins that share 60% of amino acid residues. In order to understand the origin of these proteins and to get functional and structural comparison between them we used phylogenetic analysis, crystallography and molecular modeling. The phylogenetic tree built with orthologues from different evolutionary classes revealed that PstS and PhoX are originated from a gene duplication and horizontal transfer from a common ancestral from *Desulfatibacterium alkenivorans*. To compare structures, we firstly solved the three-dimensional structure of PhoX and use it for building of the structural model of PstS. Structure and model were superimposed and showed high conservation of the residues involved with the phosphate binding, which also were highly identical to the ligand-binding sites from orthologues of *E. coli* and *Y. pestis*. However, despite these similarities there are significant differences in the electrostatic potential of the regions involved with the interactions in the membrane components, possibly suggesting differences in the transport. Finally, thermal denaturation analysis of both proteins in absence and presence of phosphate revealed that PhoX is more resistant to denaturation than PstS, what could be explained by the presence of a higher level of β -sheet structures.

Introduction

Phosphorus is an essential nutrient for any living organism due its presence in nucleic acids, plasmatic membrane, enzymes, and other elementary functions for the cell. Due this biological relevance, the bacteria developed a different specialized system for uptake phosphorus source known as PitA as a low affinity transporter and Phosphate Starvation System (Pst) as an ATP-Binding Cassete (ABC transporter). Pst system belongs to the well-characterized Pho regulon comprising at least 32 identified genes that are involved in adaptive response under phosphate starvation (Wanner et al., 1996; Monds, et al, 2006; Gebhard et al, 2006) and that has been related to oxidative stress, cell surface modification, activation of virulence, adaptive on environment, adhesion and pathogenesis (Crépin et al, 2011). Structurally, the Pst system consists of two transmembrane proteins, two associated cytoplasmic ATPases and a periplasmic protein, which is responsible for the affinity and specificity of the system. In *E. coli*, the periplasmic binding protein is PstS, an alpha/beta protein consisting of two domains connected by a hinge that allows the movement for ligand binding. The cleft between both domains forms the ligand-binding site that is highly conserved in orthologues of different species and where the phosphate ion is bound. In ABC transporters, besides uptake and transport of the substrates, periplasmic components have important role in the signaling and induction of conformational changes that occurs in the transmembrane and cytoplasmic domains (Chen et al, 2001). In addition to the phosphate uptake function, PstS from *E. coli* has a supposed role in DNA damage process due the up-regulation observed (Khil et al, 2002).

In a previous work, we characterized the putative Pho regulon proteins from the plant pathogenic bacterium *X. citri*, the causative agent of citrus canker disease, and showed the presence of two putative phosphate-binding proteins, PstS (XAC1577) and PhoX (XAC1578) that share 60% of amino acid sequence identity. Proteomic studies based on mass spectroscopy approaches revealed that under phosphate limitations PhoX and PstS are highly induced with fold change values of 43,5 and

39,1 respectively, indicating that both proteins have active role in the Pst system. Moreover, we showed that *pstS* and *phoX* genes are under control of different promoters what might explain the differences in the expression levels (Pegos et al, 2014). However, the specific function of each protein is still not clear. To understand the origin and to get functional information, we performed phylogenetic analysis of PstS and PhoX orthologues from distinct classes and carried out structural analysis using bioinformatics, molecular modeling, crystallography and spectroscopic methods. PstS and PhoX are originated from a gene duplication and horizontal transfer from a common ancestral that conserve all residues for the phosphate interaction but showed slight differences in the thermal resistance after binding and electrostatic potential of the regions that interact with the membranes that might affect the transport and protein/protein interaction mechanism.

Methods

Plasmid construction, protein expression and purification

Amplification and cloning of *phoX* gene was performed according Pegos et al. (2014b). The *pstS* gene encoding the mature PstS protein without the first N-terminal 20 amino acids was amplified by PCR using the following primers (Forward: 5'-CATATGGCGTGCTCGCCCGCAAG-3' and Reverse 5'-CTCGAGTTACTTGAACTCGCTGCCCC-3'), which, respectively, contain *NdeI* and *XhoI* restriction enzyme sites (underlined). The PCR reaction was carried out in a final volume of 50 μ L following the HiFi *Taq* DNA polymerase protocol (Invitrogen) and analyzed using 0.8% agarose gel electrophoresis. The fragment of 1032 nucleotides was cloned into pGEM T-Easy vector (Promega, USA) and subcloned into pET28a(+) expression vector (Novagen, USA) to originate the pET28a_ *pstS* plasmid. The cloning was confirmed by DNA sequencing and the plasmid used for transformation of *E.coli* Turner (DE3) competent cells. Protocols for PstS expression and purification were exactly the same

previously described for PhoX by Pegos and collaborators (2014). Both proteins were concentrated up to 30 mg/mL using centrifugal filters 10 MWCO (Amicon Millipore, USA).

Spectroscopy analysis

Circular dichroism measurements of PhoX and PstS in presence and absence of phosphate were carried out in a Jasco J-810 spectropolarimeter (Jasco) equipped with a Peltier type temperature controller. Spectra were obtained in 1 mm path length quartz cell using 2 μM of protein concentration (0,13 mg/mL and 0,15 mg/mL for PhoX and PstS, respectively) diluted in 10 mM Tris-Cl buffer at pH 8.0 in absence and presence of 30 μM $\text{NaH}_2\text{P}_i\text{O}_4$. The far-UV CD was performed from 260 nm until 190 nm with 35 consecutive scans and the average spectra was corrected subtracting the buffer and ligand contribution. The observed ellipticities were converted into mean residues ellipticities $[\theta]$ based on a mean residue molecular mass according the extinction coefficients of PstS ($64.400 \text{ M}^{-1} \text{ cm}^{-1}$) and PhoX ($61.880 \text{ M}^{-1} \text{ cm}^{-1}$). The secondary structure was estimated using Dichroweb package (Wittmore, 2004). In addition, the thermal unfolding experiments were measured at 222 nm increasing the temperature from 20°C to 95°C and the midpoint of the curve was considered the unfolding transitions.

Determination of the three-dimensional structure of the PhoX and molecular modeling of PstS

The purified PhoX was previously submitted to crystallization trials and obtained from crystals originated in 20% PEG 3350 and 200 mM sodium iodine diffracted at 3.0 Å resolution and showed crystallographic symmetry of the P2_1 spatial group (Pegos et al., 2014b). After processing using XDS package (Kabsch, 2010), the data were merged and scaled with Aimless (Evans, 2011) and Free-R

flag column was added using Uniqueify (CCP4i). The Matthews coefficient was calculated 2.25 with 45% of solvent content, most likely indicating that were 8 protein copies of PhoX in the asymmetric unit (Pegos et al., 2014b). The structural coordinates of the *E. coli* phosphate-binding protein PstS (Yao et al., 1996; PDB code 2ABH) that shares 60% of amino acid sequence identity with *X. citri* PhoX was prepared with Chainsaw (Stein, 2008) and used as a search model in Phaser program (McCoy, et al, 2007). Buccaneer software (Cowtan, 2006) was used for automated model building of protein and a twinned refinement was carried out using REFMAC (Murshudov, et al, 1996) up to a final Rfree/Rfactor of 0.18/0.24. The atomic coordinates and their structure have been deposited in the PDB under 4WTT accession code.

To perform comparisons between PhoX and PstS, a structure model of PstS was built based on the structural coordinates of *X. citri* PhoX (PDB 4WTT), which shares 70% of amino acid sequence identity with PstS. Once we had obtained the three-dimensional structure of PhoX and that *X. citri* PstS showed high amino acid sequence conservation when compared with orthologues of different microorganisms, including the PstS of *E. coli* (Yao et al., 1996; PDB code 2ABH) and *Yersinia Pestis* (Tanabe et al., 2007; PDB code 2Z22), the confidence in the three-dimensional model of PstS was very high. Twenty models were built using Modeller (Sali et al, 1993) and the best one was chosen based on the free energy and quality stereochemical parameters. The structural superposition of the proteins was performed in COOT (Emsley, et al, 2010) using the secondary structure matching tool (Krissinel et al, 2004). Figures and analyses of proteins were prepared using Pymol program (The Pymol Molecular Graphics System, version 1.5.0.4, Schrödinger, LLC).

Phylogenetic and evolutionary relationships of *X. citri* PstS and PhoX

To analyze the phylogenetic and evolutionary relationship of *X. citri* PstS and PhoX in proteobacteria, including alpha, beta, gamma and delta- branches, a list of different microorganisms was chosen based on the presence of PstS, PhoX or both proteins (accession numbers and species are described in Table S1, supplementary material). Firstly, we searched for microorganisms and orthologues using the String server (Snel et al., 2000) and then we performed a psi-BlastP of *X. citri* PstS and PhoX amino acid sequences against the genome of the reference organism. The choices were confirmed and sequences were included when they showed at least 20% of amino acid sequence identity over a minimum of 50% of query coverage and the gene annotation or function related with phosphate binding. Amino acid sequences were previously analysed using SEAL software (Pireddu et al, 2011) and manually aligned based on the secondary structure and then refined by Muscle (Edgar, 2004). Phylogenetic reconstructions were built with MEGA 6 software (Tamura et al., 2011) using distance and statistical reconstructions methods. For the statistical method we used a LG+G model of amino acid substitution pointed by Mr. Modeltest (Nylander, 2004) as most appropriate. In both analyses, the support indices obtained by 5000 bootstrap replicates. As outgroup member we chose *Thermanaerovibrio acidaminovorans*, a representant of the Synergistetes group.

Results

ABC transporter and Two-component Systems are highly conserved in proteobacteria and PhoX and PstS represent gene duplication in *X. citri*

X. citri PhoX and PstS amino acid sequences were used to search orthologues in different bacteria from proteobacteria branch using Blastp and cutoff of 30% of identity and at least 50% of query-coverage for criteria of choice. The presence and conservation of PhoX and PstS orthologues

was identified in distinct members of the proteobacteria branch, including microorganisms that live in a variety of habitats as gastrointestinal and respiratory tracts, human mucose, ocean and marine sediments, water, citrus, soil and roots (Table 1). We first observed that there is no consensus for the nomenclature PstS, PhoX or PBP and that the three terms correspond to phosphate-binding protein. Second, Table 1 reveals that members of α - and β -proteobacteria only presented one phosphate-binding protein, with exception of *Thiobacillus denitrificans* that showed two orthologues that compared to *X. citri* PstS and PhoX, shared around 50% of amino acid sequence identity. Similarly, in Δ -proteobacteria, only *Desulfatibacterium alkenivorans* has two orthologues, which share 24% and 23% with *X. citri* PstS and PhoX, respectively. On the other hand, the presence of two or more orthologues of the phosphate-binding protein is found in γ -proteobacteria, which represented members are exclusively pathogens, detaching the importance of phosphate in these organisms and the low availability of the ion in their environments (Shen, et al, 2011;Gupta, 2014). Moreover, in these branches, orthologues shared amino acid sequence identity from 24% up to 93%. The higher values are evidenced when compared orthologues from the closely related species *X. citri*, *X. campestris*, *Xyllela fastidiosa* and *Stenotrophomonas maltophilia*. Otherwise, despite the differences regarding the presence of additional phosphate-binding proteins, all the microorganisms studied showed all the ABC transporter components for phosphate uptake as well as the two-component system PhoR and PhoB (Table S1). All sequences on table S1 that had at least amino acid sequence identity and query coverage established on material and methods section were select to perform phylogeny studies based on protein sequences *X. citri* PhoX and PstS. After the amino acid sequence alignment, the neighbor-joining tree was built evidencing the phylogenetic relationship and origin of PstS and PhoX proteins (Figure 1).

Table 1. Sequence identity and occurrence of phosphate-binding proteins in proteobacteria compared to PstS and PhoX. Proteins were firstly identified in String server and then the sequences used for BLASTp X *X. citri* database. The protein identification shows the 3 letter code of the microorganism, KEGG number and the function associated to the putative protein.

Microorganism	PstS			PhoX			Environment
	Protein Identification	Amino acid Sequence Identity	E-value	Protein Identification	Amino acid Sequence Identity	E-value	
α-proteobacteria							
<i>Paracoccus denitrificans</i>	-	-	-	pde_PDEN4330_PBP	26%	0,05	Soil
<i>Sphingopyxis alaskensis</i>	sal_SALA0826_PBP	25%	4,00E-06	-	-	-	Marine sediments
<i>Sphingomonas wittichii</i>	swi_Swit_1104_PBP	53%	1,00E-99	swi_Swit_1104_PBP	55%	5,00E-117	Water, root and soil
<i>Phenylobacterium zucineum</i>	pzu_PHZC2494_PstS	-	-	pzu_PHZC2494_PstS	-	-	Soil and water
β-proteobacteria							
<i>Thiobacillus denitrificans</i>	tbd_TBD1136_PBP	48%	3,00E-94	tbd_TBD1136_PBP	50%	1,00E-96	Soil and Marine sediments
	tbd_TBD1420_PBP	50%	1E-97	tbd_TBD1420_PBP	49%	7E-96	
<i>Nitrospira multiformis</i>	nmu_NMULA0486_PBP	20%	4,00E-07	-	-	-	Soil
<i>Nitrosomonas europaea</i>	neu_NE0531_PBP	25%	1,00E-06	-	-	-	Soil
γ-proteobacteria							

<i>Xanthomonas axonopodis</i> pv. <i>citri</i>	xac_XAC1577_PstS	100%	0,00E+00	xac_XAC1578_Phox	100%	0,00E+00	Soil and citrus
<i>Escherichia coli</i>	eco_b3728_PstS	49%	3,00E-99	eco_b3728_PstS	55%	7,00E-117	Gastrointestinal
<i>Yersinia Pestis</i>	ype_YPO4117_PstS ype_YPO3203_PstS	50% 23%	3,00E-101 0.68	ype_YPO4117_PstS ype_YPO3203_PstS	56% -	2,00E-118 -	Gastrointestinal
<i>Pseudomonas aeruginosa</i> PAO1	pae_PA5369_PstS	24%	6,00E-04	-	-	-	Soil and citrus
<i>Xanthomonas campestris</i> 33913	xcc_XCC1527_PstS	94%	0,00E+00	xcc_XCC1528_Phox	93%	0,00E+00	Soil and citrus
<i>Shewanella oneidensis</i> MRI	son_SO4292_PstS	23%	1,00E-4	son_SO4292_PstS	25%	7,00E-07	Ocean
<i>Haemophilus influenzae</i>	hin_HI1383m_PstS	57%	1,00E-130	hin_HI1383m_PstS	55%	2,00E-119	Respiratory tract
<i>Xylella fastidiosa</i>	xfa_XF2141_PBP	77%	0,00E+00	xfa_XF2141_PBP	68%	9,00E-152	Citrus
<i>Stenotrophomonas maltophilia</i>	sml_Smlt1552_PBP	80%	0,00E+00	sml_Smlt1554_PstS	80%	8,00E-118	Human mucose
<i>Vibrio Cholerae</i> N16961	vch_VCA0070_PBP	28%	6,00E-05	vch_VCA0070_PBP	24%	8,00E-05	Diverse ecosystems
<i>Photobacterium profundum</i>	ppr_PBPRB0883_PBP ppr_PBPRA1394_PBP	- 28%	- 2,00E-04	ppr_PBPRB0883_PBP ppr_PBPRA1394_PBP	26% -	4,00E-05 -	Marine sediments
<i>Kangiella Koreensis</i>	-	-	-	kko_KKO2087_PBP	24%	7,00E-05	Ocean
<i>Listeria monocytogenes</i>	Lmo_lmo2499_PBP	30%	3,00E-15	Lmo_lmo2499_PBP	29%	7,00E-13	Gastrointestinal
<i>Nitrosococcus oceani</i>	noc_NOC0584_PBP	25%	8,00E-05	noc_NOC0584_PBP	28%	2,00E-09	Ocean

Δ-proteobacteria

<i>Anaeromyxobacter dehalogenans</i>	ade_ADEH4006_PBP	29%	4,00E-06	ade_ADEH4006_PBP	26%	9,00E-04	Soil and marine sediments
<i>Sorangium cellulosum</i>	scl_SCE2946_PstS	48%	2,00E-85	scl_SCE2946_PstS	45%	3,00E-82	Soil and animal faeces
<i>Desulfatibacterium alkenivorans</i>	dal_Dalk1427_PBP	24%	2,00E-06	dal_Dalk1427_PBP	23%	3,00E-06	Marine sediments
<i>Sulfurospirillum deleyianum</i>	sde_SDEL1859_PBP	27%	1,00E-03	sde_SDEL1859_PBP	26%	3,60E+00	Water
<i>Syntrophus aciditrophicus</i>	sat_SYN02226_PBP	27%	1,00E-07	sat_SYN02226_PBP	26%	0,001	sewage treatment plant
<i>Lawsonia intracellularis</i>	lip_LI1028_PBP	32%	2,00E-15	lip_LI1028_PBP	29%	3,00E-09	Animal small intestine
<i>Nautilia profundicola</i>	Nam_NAMH0308	40%	1,00E-66	Nam_NAMH0308	41%	7,00-75	Deep Sea
<i>Sulfurovum sp.</i>	sun_SUN2272_PstS	41%	2,00E-06	sun_SUN2272_PstS	42%	4,00E-72	Marine sediments
Synergistetes							
<i>Thermanaerovibrio acidaminovorans</i>	tai_Taci0095_PBP	27%	8,00E-02	tai_Taci0095_PBP	24%	6,00E+00	Sugar refinery reactor

Table S1. Occurrence of proteins belonging to the putative phosphate ABC transporter (Pst system) and the two-component system in proteobacteria. The protein identification was based on the sequence homology after BlastP of the *X. citri* proteins against the sequence data bank. The functional protein association networks String (Franceschini et al, 2013) was used to support the presence, identity and relationship among the proteins.

Organism	Org code	Two component System		ABC Transport					Regulator	Porin
		PhoB	PhoR	PstS	PhoX or PstS2	PstA	PstC	PstB	PhoU	OprO
a-proteobacteria										
<i>Paracoccus denitrificans</i>	pde	PDEN4325	PDEN3938	PDEN4330	-	PDEN4328	PDEN4329	PDEN4327	PDEN4326	-
<i>Novosphingobium aromaticivorans</i>	nar	SARO2282	SARO2275	SARO2276	-	SARO2277	SARO2278	SARO2279	SARO2280	-
<i>Sphingopyxis alaskensis</i>	saI	SALA0821	SALA0822	SALA0826	-	SALA0824	SALA0825	SALA0823	SALA0822	-
<i>Sphingomonas wittichii</i>	swi	SWIT3577	SWIT1099 SWIT3575	SWIT1104	SWIT1104	SWIT1102	SWIT1103	SWIT1101	SWIT3576	-
<i>Phenylobacterium zucineum</i>	pzu	PHZ507	PHZ0501 PHZ0502	PHZ2494	-	PHZ0504	PHZ0503	PHZ0503	PHZ505	PHZ1100 PHZ3312

b-proteobacteria

<i>Thiobacillus denitrificans</i>	tbd	TBD0216	TBD0217	TBD1420 TBD1136	TBD1420 TBD1136	TDB1138	TDB1137	TDB1136	TBD0025	-
<i>Nitrosospira multiformis</i>	nmu	NMUIA2231	NMUIA2232	NMUIA0486	NMUIA0897	NMUIA1086	NMUIA1087	NMUIA1088	NMULA0435	NMULA0898
<i>Nitrosomonas europaea</i>	neu	NE2131	NE1288	NE0531	-	NE0999	NE1000	NE1001	NE1744	-

g-proteobacteria

<i>Xanthomonas axonopodis</i> pv. <i>citri</i>	xac	XAC1042	XAC1041	XAC1577	XAC1578	XAC1575	XAC1576	XAC1574	XAC1573	XAC3484
<i>Escherichia coli</i> K-12 <i>MG1655</i>	eco	B0399	B0400	B3728	B3728	B3726	B3727	B3725	B3724	-
<i>Yersinia pestis</i>	ype	YPO3205	YPO3204	YPO3203 YPO4117	YPO3203 YPO4117	YPO4115	YPO4116	YPO4114	YPO4113	-
<i>Pseudomonas aeruginosa</i> <i>PAO1</i>	pae	PA5360	PA5361	PA5369 PA0688	-	PA5367	PA5368	PA5366	PA5365	-
<i>Xanthomonas campestris</i> <i>33913</i>	xcc	XCC0963	XCC0962	XCC1527	XCC1528	XCC1525	XCC1526	XCC1524	XCC1523	XCC1529
<i>Azotobacter vinelandii</i>	avn	AVIN_48520	AVIN_48530	AVIN_48600 AVIN_28890	-	AVIN_48580	AVIN_48590	AVIN_48570	AVIN_48560	-
<i>Shewanella oneidensis</i> MR1	son	SO_1558	SO_1559	SO_4292 SO_1560	-	SO_4291	SO_4290	SO_4289	-	SO_1557
<i>Haemophilus influenzae</i>	hin	HI1379	HI1380	HI1383	-	HI1381	HI1382	HI1380	-	-
<i>Xylella fastidiosa</i>	xfa	XF2593	XF2592	XF2141	-	XF2142	XF2143	XF2144	XF2145	-

<i>Stenotrophomonas maltophilia</i>	sml	SMLT0978	SMLT0977	SMLT1552	SMLT1554	SMLT1550	SMLT1551	SMLT1549	SMLT1548	SMLT1555
<i>Vibrio Cholerae N16961</i>	vch	VC0719	VC0720	VC07121 VC0070	-	VC0724	VC0725	VC0726	VC0727	-
<i>Photobacterium profundum</i>	ppr	PBPRA0721	PBPRA0722	PBPRA0723 PBPRA0775 PBPRA 0883 PBPRA1394	-	PBPRA0728 PBPRA1392	PBPRA0729 PBPRA1393	PBPRA1391 PBPRA0730	PBPRA0731	-
<i>Kangiella Koreensis</i>	kko	KKOR2094	KKO2093	-	KKO2087	KKOR2098	KKO2097	KKOR2096	KKOR2095	KKOR2099
<i>Nitrosococcus oceani</i>	noc	NOC2400	NOC2401	NOC2399 NOC0584	NOC0584	NOC0580 NOC2398	NOC0582 NOC2397	NOC0581 NOC2396	NOC2395	-

D-proteobacteria

<i>Anaeromyxobacter dehalogenans</i>	ade	ADEH4009	ADEH4008	ADEH4006	-	ADEH4005	ADEH4004	ADEH4003	ADEH4002	-
<i>Sorangium cellulosum</i>	scl	SCE2948 SCE5073	SCE2947 SCE3423 SCE7574	SCE2946	-	SCE2944	SCE2945	SCE2943	SCE2942	-
<i>Desulfatibacillum alkenivorans</i>	dal	DALK1425	DALK1426	DALK1427 DALK2845	-	DALK1428	DALK1429	DALK1430	DALK1431	-
<i>Sulfurospirillum deleyianum</i>	sdl	-	-	SDEL1859	-	ADEI1858	SDEL1857	SDEL1856	268680491	-
<i>Sulfurovum sp.</i>	sun	SUN2268	SUN2267	SUN2272	SUN2272	SUN2270	SUN2271	SUN2269	SUN2273	-

Mollicutes

<i>Mycoplasma genitalium</i>	mge	-	-	MG412	-	MG411	-	MG410	MG409	-
------------------------------	-----	---	---	-------	---	-------	---	-------	-------	---

Synergistetes

<i>Thermanaerovibrio acidaminovorans</i>	tai	TACI0090	TACI0089	TACI0095	-	TACI0093	TACI0094	TACI0092	TACI0091	-
--	-----	----------	----------	----------	---	----------	----------	----------	----------	---

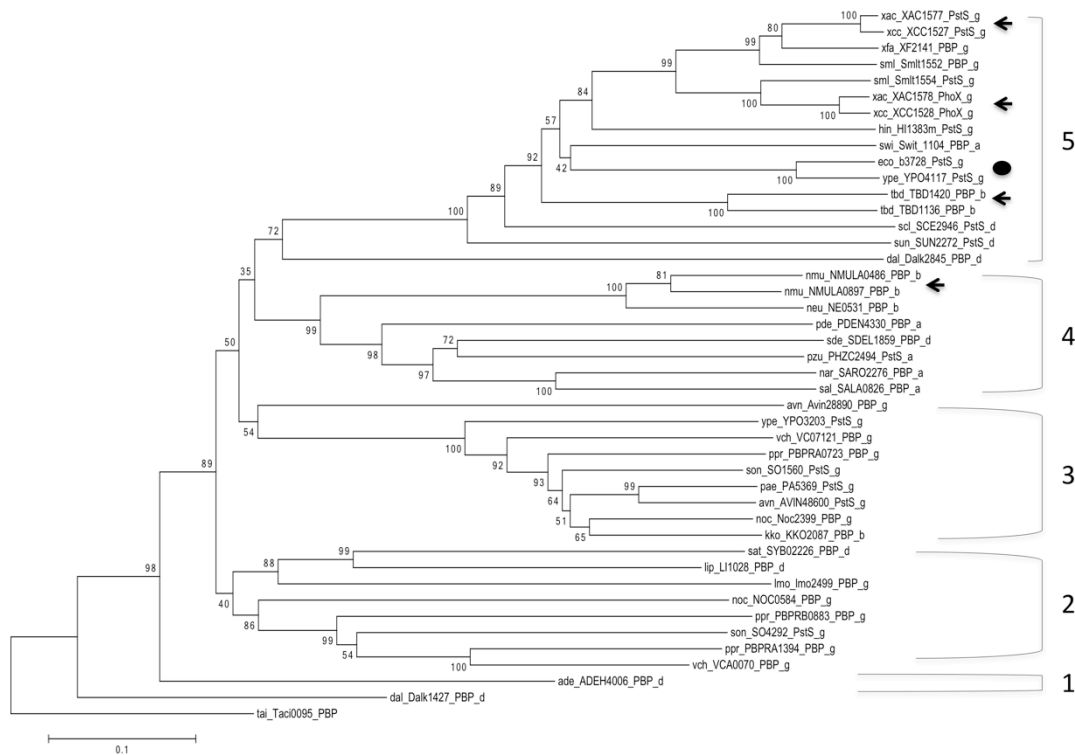


Figure 1. Phylogenetic relationship among orthologues of PstS and PhoX. Five groups classify the distinct orthologues from proteobacteria. All the organisms used in this tree as well as their reference codes are described in Table 1. The tree was generated using MEGA 6.0 software and the neighbor-joining algorithm according MM section. The numbers at the nodes indicate the bootstrap percentages of 1.000 replicates. Arrows and black circle indicate gene duplication and horizontal gene transfer, respectively.

The oldest ancestral of the phosphate-binding proteins is the orthologue from *Desulfatibacterium alkenivorans*, a δ -proteobacteria that presented two copies of PstS, Dalk1427 and Dalk2845. Dalk1427 originated all the groups including the orthologue from the γ -proteobacteria *Anaeromyxobacter dehalogenans*, AdeH4006 (group 1). Four other monophyletic groups were defined with uncertain relationship between each other: groups 2 and 3 that include orthologues of γ -proteobacteria, group 4 with orthologues of α -, β - and δ -proteobacteria and group 5 that includes the Dalk2845 paralogous. In this group we detect 4 duplications of the phosphate-binding proteins supported by bootstrap values on the tree (Figure 1, pointed by arrows): Xac1577 and Xac1578 (PstS and PhoX), Xcc1527 and Xcc1528 and TBD1420 and TBD1146. Another duplication, NMULA0486 and NMULA0897, is present in the group 4. Moreover, PstS proteins from *E. coli* (b3728) and *Yersinia pestis* (YPO4117) probably were acquired by horizontal gene transfer (Figure 1, black dot).

PhoX and PstS were expressed as soluble and stable proteins

The recombinant expression and purification of PhoX was performed as previously published (Pegos et al., 2014). Similarly, the recombinant PstS was expressed as His₆-tag N-terminal fusion in *E. coli* Tuner (DE3) and purified by a single step of immobilized metal affinity chromatography in a 5 mL HiTrap column (Amersham, USA, Pittsburg). Samples of PstS eluted on 50 mM and 150 mM of imidazole (Figure 2A, lanes 4 and 5, respectively) as a first purification step showed high purity level and were submitted to size exclusion chromatography to eliminate contaminants and aggregates which was eluted on 44 mL around 200 mAU (Figure 2B). Two peaks of PstS were obtained on 65 mL and 76 mL of elution volume indicating that the protein even had two different peaks had monomeric conformation in solution. Both peaks were concentrated separately in centrifugal filters 10 MWCO (AMICON Millipore, Massachusetts) to the final concentration of 30 mg/mL and the peak two did not showed contaminants on SDS PAGE 12% (Figure 2B).

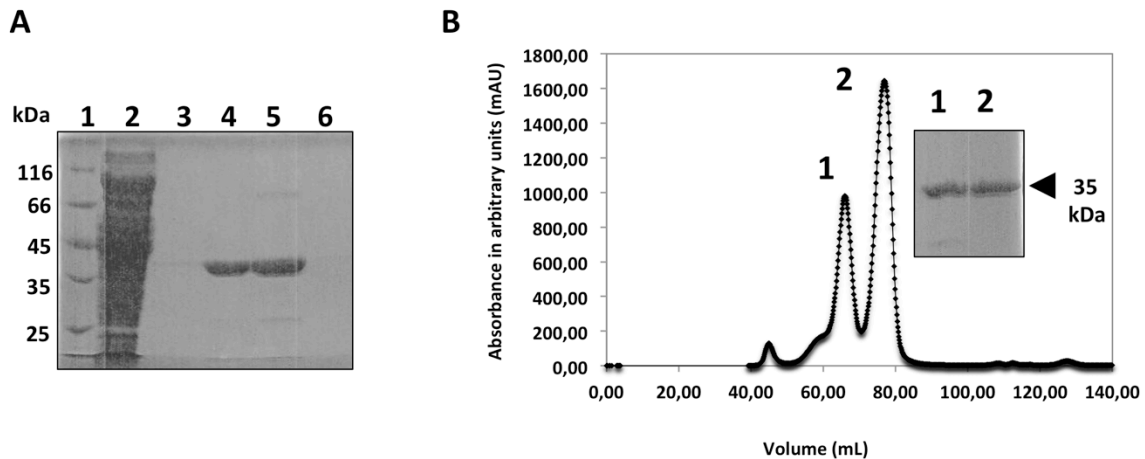


Figure 2. Purification of *X. citri* phosphate-binding protein PstS. (A) Immobilized metal affinity chromatography of PstS using Nickel column. Lane 1: molecular marker; lane 2: Flowthrough; lane 3: wash step with Tris-Cl 20 mM pH 8.0; Imidazole; lane 4: elution fraction with 50 mM imidazole; lane 5: elution fraction with 100 mM imidazole; lane 6: 500 mM imidazole. (B) Size-exclusion chromatography in column Hi Load 16/60 200 superdex (GE Healthcare Life Science). The elution was performed using 10 mM of Tris-Cl pH 8.0. Two peaks were obtained representing the aggregates and monomeric states, respectively, of the proteins. The inset gel is showing the Coomassie staining gel of the purified samples in each peak. Peak 2 was used for further experiments.

Three-dimensional structure of *X. citri* PhoX shows the periplasmic-binding protein folding and the phosphate inside the ligand-binding pocket

The crystal structure of *X. citri* PhoX was solved in the closed-ligand conformation at 3.0 Å resolution with eight molecules organized in the asymmetric unit and revealed a typical periplasmic binding protein with two domains (I and II, Figure 3A, blue and cyan, respectively), each one consisting of a β -sheet (Figure 3A, yellow) surrounded by α -helices. Domain I is formed by three segments consisting of residues 26 to 100, 252 to 265 and 277 to 340, and domain II is formed by the continuous residues 101 to 251. All the eight molecules were in the same closed conformation with a phosphate completely enclosed inside the ligand-binding pocket between both domains (Figure 3B). Interestingly, the hinge between both domains is formed by a β -strand (β 2) of 16 residues long (93 to 108) that probably limits the PhoX flexibility in comparison with other phosphate-binding proteins. That characteristic includes PhoX in the type II of substrate-binding proteins, according Fukami-Kobayashi and collaborators (1999).

The superposition of PhoX structure and the model of *X. citri* PstS showed the conservation of the residues for phosphate interaction and positioning inside the pocket (Figure 3C). The ion in *X. citri* PhoX is coordinated by 11 hydrogen bonds between the oxigens from phosphate and lateral chains from residues Ser34, Ser62, Asp80, Arg159, Gly164, Thr165 and Asn201. In the *E. coli* PstS an aspartate is responsible to recognize the phosphate proton and discriminate among other tetrahedral ionized oxyanions (Wang et al, 1997; Luecke et al 1990). The calculated distances of the hydrogen bonds on *X. citri* PhoX showed two shortened hydrogen bonds performed by Ser62 (1.9 Å) and Arg159 that stabilizes O1 and O2 from phosphate, with 2.3 Å and 2.0 Å, respectively (Table S2). The distance and interactions are similar to the previously

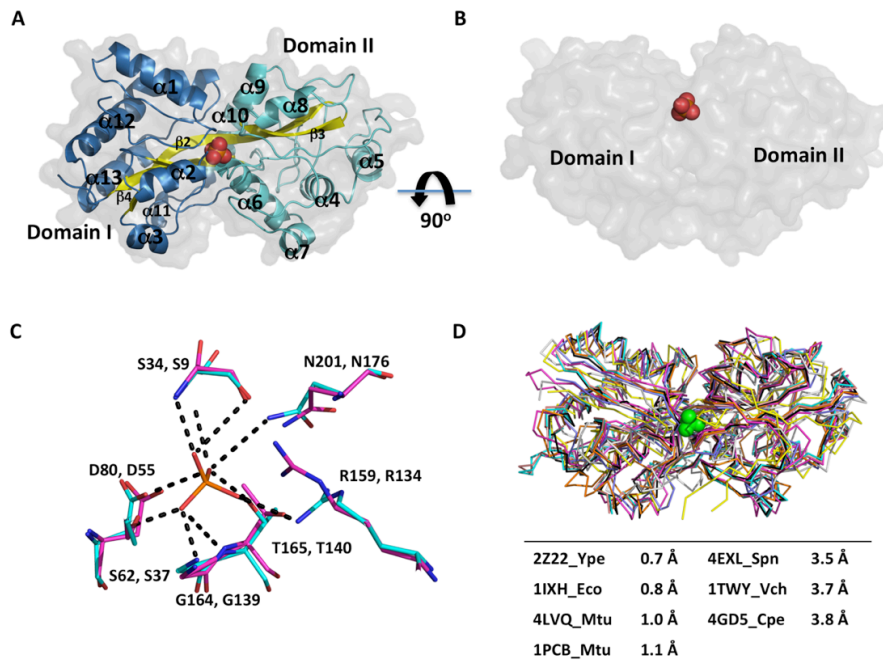


Figure 3. Crystal structure of the phosphate-binding protein PhoX from *X. citri*. (A) Cartoon representation of the three-dimensional structure of PhoX evidencing the the α/β folding and the surface (transparent gray). α -helices and loops from domain I and II are shown in blue and cyan, respectively. The β -sheet is colored in yellow. All the secondary structures are nominated. A phosphate ion between the domains is shown as red spheres. (B) Side-view of PhoX in surface with the ion (red spheres) inside the ligand-binding pocket. The phosphate is buried inside the pocket between both domains. (C) Structural superposition of the crystal structure of PhoX and model of PstS evidencing a detailed view of the residues that interact with the phosphate in PhoX (cyan stick). All residues are conserved in PstS (magenta stick) and localized in a similar position. (D) Structural superposition of *X. citri* PhoX (PDB code 4WTT, black) with the following structures of orthologues *Y. pestis* PstS (PDB code 2Z22, cyan), *E. coli* PstS (PDB code 1IXH, yellow), *M. tuberculosis* PstS1 (PDB code 4LVQ, magenta), *M. tuberculosis* PstS3 (PDB code 1PCB, blue), *Streptococcus pneumoniae* PstS1 (PDB code 4EXL, green), *Vibrio cholerae* PBP (PDB code 1TWY, salmon) and *Clostridium perfringens* PBP (PDB code 4GD5, light gray). Proteins are shown in ribbon and the phosphate ion from *E. coli* structure in red spheres. R.m.s.d. values for the structural superposition of PhoX and each protein is shown in angstroms in the Table inset.

described for PstS from *E. coli* by Luecke and coworkers (1990), but in *X. citri* PhoX the short interaction directly with phosphate is performed by an arginine (Arg159) and not by an aspartate. That distinctions related to the length of hydrogen bonds implicate in different affinities and discrimination of the protein to binding and recognize other oxyanions.

PstS and PhoX from *X. citri* show high sequence identity and structural similarity in the region that interacts with the membrane components

A comparison between PhoX and PstS proteins from *X. citri* was performed in order to get information regarding their structural differences and similarities that could explain the presence of two related proteins in the same microorganism. In a previous work, we showed that *phoX* gene does not belong to the putative operon that includes *pstSABC* genes encoding the ATP-Binding Cassete transporter for phosphate uptake. In addition, we showed that PstS and PhoX are up regulated in different levels under phosphate starvation, suggesting that the mechanisms of induction and control of expression of these proteins are variable (Pegos et al., 2014). Since the two proteins showed conservation of all residues involved the ligand-binding site and ligand interactions (Figure 2D), we looked at the interface of these proteins that should interact with the membrane components PstC and PstA. The amino acid sequence alignment of the residues located in the interface regions of the periplasmic-binding proteins and permeases, respectively (Figure 4A), denominated RI and RII for domains I and II, show that the regions are highly conserved in PhoX and PstS proteins and also when compared their location on PhoX and PstS structure, (Figure 4B and C). Despite PhoX and PstS shared 70% of all amino acid residues including the binding site and RI and RII, the electrostatic potential of RI, RII and residues around the binding site are slight difference from each other. The potential electrostatic between domains where phosphate is located is more positive on that PhoX structure and PstS model (Figure 4D and Figure 4E, box). The charges of surfaces amino acids of RI and RII and the residues around the

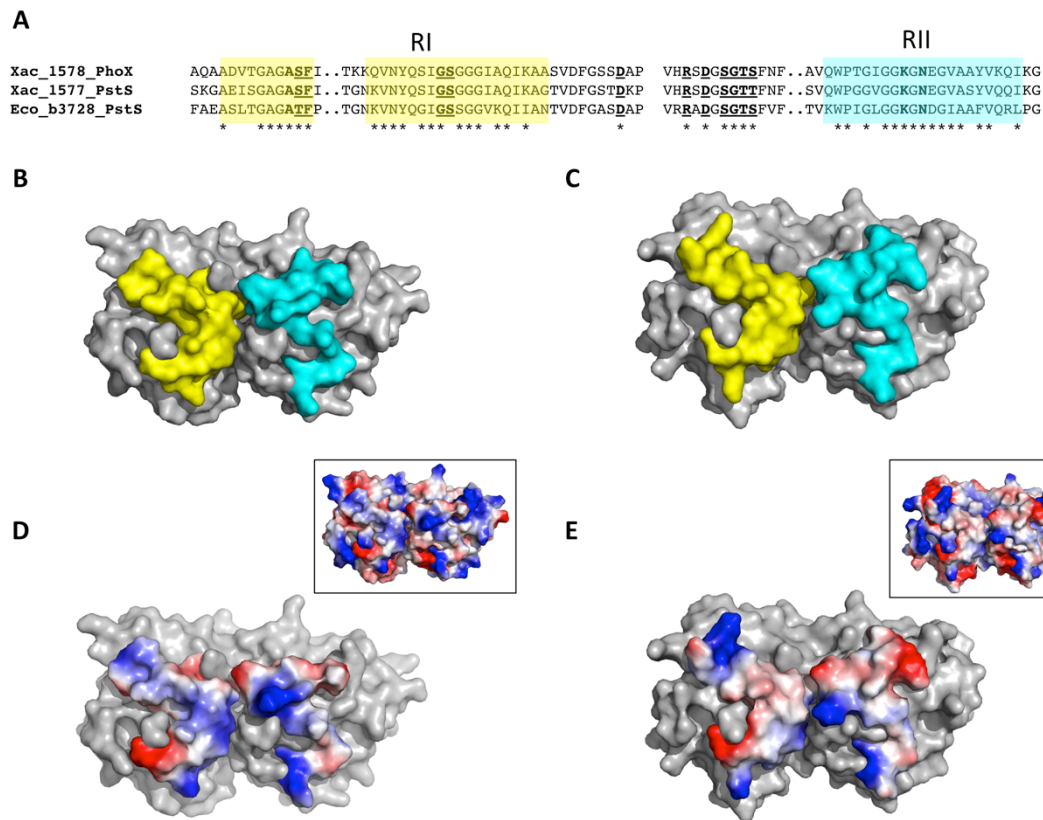


Figure 4. Comparison of the interface regions from PhoX and PstS that putatively interact with the permeases. (A) Amino acid sequence alignment of RI and RII from PhoX, PstS and *E. coli* PstS evidencing the high level of conservation (asterisks). The localization of the RI (yellow) and RII (cyan) close to the entrance of the ligand-binding pocket of PhoX (B) and PstS (C) is shown in surface. Charge distribution of RI and RII of PhoX (D) and PstS (E) proteins. The inset figures show the total charge distribution from the pocket entrance view.

binding site could suggest different speed of phosphate transportation (kinetic transportation). The RI of PhoX 3D structure showed more positive and more neutral regions (blue and white, respectively) when compared with RI of PstS model including the region near the binding site (Figure 4 D and E). Moreover the high conservative amino acid residues of RI and RII regions, both periplasmic component PhoX and PstS are supposed interact with the same permease heterodimer PstA and PstC.

Phosphate interaction between *X. citri* PhoX and PstS proteins induces the increasing of the thermal stability

The secondary structure and folding of PhoX and PstS in absence and presence of phosphate was compared using circular dichroism (CD) analyses. The far-UV scans were recorded separately for both proteins before and after sodium phosphate incubation and revealed a similar profile consisting of a maximum peak at 195 nm and two relative minimum peaks at 208 and 222 nm, which corroborates α/β fold (Figure 5A and B), as expected from the three-dimensional structure of PhoX and model of PstS. However, differences slight proteins showed in the secondary structure content as evidenced by the CD signals (Figure 5A and B). According to the CD data that shows the protein in solution, the α -helix content of *X. citri*

PstS is higher than that presented for PhoX and in the opposite way, PhoX has a higher content of β -sheet. Compared to the orthologues with three-dimensional structure solved, we also observed some differences as decreasing in the secondary structure content of the *X. citri* proteins, which can reflect the methods used for analysis. In fact, CD analysis involves proteins in solution and with the tags that are not counted in the structure analysis. Moreover, it is possible that in solution these proteins acquire more flexible structures.

Although there are no significant differences evidenced in absence or presence of phosphate, the slight changes in the minimum 222 nm peak when the proteins are incubated with phosphate might evidence

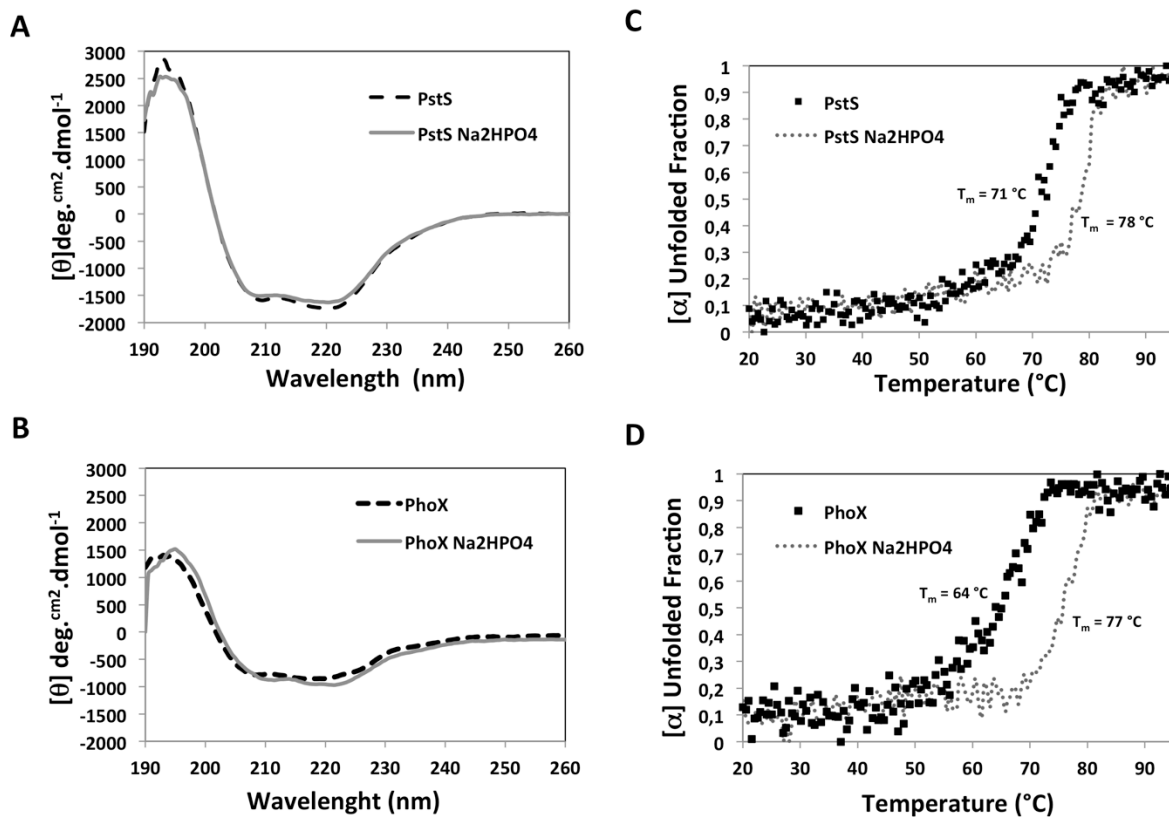


Figure 5. Spectroscopic analysis of *X. citri* PstS and PhoX in presence and absence of phosphate.

Secondary structure prediction of PstS (A) and PhoX (B) was measured by circular dichroism after 20 accumulations. Traced line: PstS and PhoX in absence of phosphate; Black line: PstS and PhoX in absence of phosphate. Gray line: PhoX and PstS incubated with 30 μ M of phosphate. The thermal stability of the proteins in absence (black dots) and presence (gray dots) of phosphate was measured at 222 nm for PstS (C) and PhoX (D). The temperature of melting (T_m) was calculated and it is shown for both conditions. Three biological independent samples were analysed.

small structural changes due the ligand interaction and closing of the domains. As previously described, it was expected that the of a 16 residues long β strand connecting the domains would infer a limit in the opening movement. On the other hand, despite the lack of structural changes, the melting temperature (T_m) of

PhoX and PstS proteins was highly increased 13 °C and 7 °C, respectively presence of sodium phosphate (Figure 5C and D), strongly suggesting its interaction with the proteins. In fact, at least the data obtained for PhoX are in accordance with its structure that evidenced the phosphate coordination through 11 hydrogen bonds (Figure 3C). Moreover, since PstS shows a very similar ligand-binding pocket, the melting temperatures are also in agreement. In addition, PstS and PhoX showed irreversible denaturation.

Discussion

Phosphate is an elementary macronutrient for bacteria growth, which is not freely abundant. To overcome the depletion of phosphate prokaryotic developed specialized systems for uptake of phosphate, which the most studied and characterized is the ABC transporter Pst, an ATP-dependent system of high affinity. Despite the knowledge of these transporters in bacteria, there is a lack of information regarding this system in *Xanthomonas* genus. In this work we focused on the characterization of the two phosphate-binding proteins from *X. citri*, PhoX and PstS that share 70% of amino acid sequence identity. Proteomics analysis of *X. citri* cell extracts after growth under phosphate starvation showed that PhoX and PstS had different expression levels suggesting a distinct up regulation of these proteins. Moreover, *phoX* and *pstS* genes are supposedly regulated by different operons (Pegos et al, 2014).

Based on phylogenetic analysis of orthologues of PhoX and PstS belonging to different species of Proteobacteria, we identified that both proteins had origin from the gene duplication occurred in the *D. alkenivorans* orthologue and then again on the *Xanthomonas* sp group, since two copies of these genes were found in *X. citri* and *X. campestris*. *X. citri* and *X. campestris* are not the only organisms that showed more than one copy of the putative phosphate binding proteins, but *Protobacterium* sp., *Thiobacillus denitrificans* and *Yersinia pestis*, showed 2 up to 4 copies in their sequencing genome, which could be directly related to

the availability of phosphate in the environment that these bacteria survive. The acquisitions of these genes in bacteria that share similar environment detach the relevance of horizontal gene transfer events. It is important to point out that many other paralogous sequences might have been continually created, replaced or lost during the evolution of this system. This seems to be the case in the absence of support for a close relationship between Gamma 1 and Gamma 2 Groups. In evolution, the presence of two periplasmic-binding proteins would increase the chances of uptake and the velocity of the transport giving to them higher competitive skills (Gupta et al, 2014). Indeed, we observed that the presence of the periplasmic component(s) and its cognate ABC transporter is accompanied in all the samples by the presence of the two-component system formed by PhoR and PhoB. In fact, this is in accordance with the evidences found in Firmicutes that show a clear coevolutionary relationship between ABC permeases and histidine kinases from two component systems (Dintner et al, 2011).

PhoX three-dimensional structure is quite similar to the orthologues, particularly from the *E. coli* and *Y. pestis*, that belong to the same phylogenetic branch. The direct comparison with *X. citri* PstS evidencing the high conservation level of the residues from ligand-binding site and also regions for interaction with the membrane components (RI and RII) support the hypothesis of gene duplication. Moreover, since RI and RII were also quite similar in both proteins, these results suggest that they use the same transporter Pst as expected. Following the comparison, we evidenced that PhoX is slight more resistant (5°C) than PstS after thermal denaturation in presence of phosphate. Although both proteins conserve the residues that interact directly with phosphate and showed similar volume of the ligand pocket, we noticed differences in the electrostatic potential of the entrance of the pocket and cavity that might affect the binding and dissociation parameters and consequently, the velocity of transport. In PhoX this region is more positive than in PstS. Indeed, changes in the melting temperature could be related to the small differences in the secondary structure content estimated for PhoX and PstS, which showed that PhoX presented higher content of beta-sheet and a long beta strand joining both domains.

Finally, this work shows the first structure of an ABC transporter component involved with phosphate uptake from a phytopathogenic bacterium that could be used as a model in the *Xanthomonas* genus, since they share high amino acid sequence identity. We also showed that the two phosphate-binding proteins clearly share functions but might be different affinities for phosphate and transport.

Acknowledgments

We acknowledge the Coordenação de Aperfeiçoamento de Pessoal de Nível Superior (CAPES).

References

- Chen J, Sharma S, Quijcho FA, Davidson AI (2001). Trapping the transition state of an ATP-binding cassette transporter? Evidence for a concerted mechanism of maltose transport. PNAS 98:1525-1530.
- Cowtan K (2006). The Buccaneer software for automated model building .1. Tracing protein chains. Acta Cryst. D 62:1002-1011.
- Crépin S, Chekabab SM, Bihan GL, Bertrand N, Dozois CM, Harel J (2011). The Pho regulon and the pathogenesis of *Escherichia coli*. Veterinary Microbiology 153: 82-88.
- Dintner S, Starón A, Berchtold E, Petri T, Mascher T, Gebhard S. (2011). Coevolution of ABC transporters and Two-component regulatory systems as resistance modules against antimicrobial peptides in *Firmicutes* bacteria. Journal Bacteriology 153:3851-3862.
- Edelhoch H (1967). Spectroscopy determination of tryptofan and tyrosine in proteins. Biochemistry 6: 1948-1954.
- Edgar, RC (2004). MUSCLE: multiple sequence alignment with high accuracy and high throughput. Nucleic Acids Res 32:1792-1797s.
- Emsley P, Lohkamp B, Scott W, Cowtan K (2010). Features and Development of Coot. Acta Cryst D 66: 486-501
- Evans PR (2011). An introduction to data reduction: space-group determination, scaling and intensity statistics. Acta Cryst D 67: 282-292.
- Fukami-Kobayashi K, Tateno Y, Nishikawa K. (1999). Domain dislocation: a change of core structure in periplasmic binding proteins in their evolutionary history. J Mol Biol 286:279-90.
- Gebhard S, Tran SL, Cook MG (2006). The Phn system of *Mycobacterium smegmatis*: a second high-affinity ABC-transporter for phosphate. Microbiology 152: 3453-3465.
- Gupta DK, Chatterjee S, Datta S, Veer V, Walther C (2014). Role of phosphate fertilizers in heavy metal uptake and detoxification of toxic metals. Chemosphere.
- Kabsch W (2010a). XDS. Acta Cryst D 66:125-132
- Khil P, Camerini-Otero D. (2002). Over 1000 genes are involved in the DNA damage response of *Escherichia coli*. Molecular Microbiology, 44:89-105.
- Krissinel E, Henrick K (2004). Secondary-structure matching (SSM), a new tool for fast protein structure alignment in three dimensions. Acta Crystallogr D 60: 2256-2268.
- Luecke H, Quijcho FA (1990). High specificity of a phosphate transport protein determined by hydrogen bonds. Nature 347: 402-406.

- McCoy AJ, Grosse-Kunstleve RW, Adams PD, Winn MD, Storoni LC, Read R J (2007). Phaser crystallographic software. *J. Appl. Cryst* **40**: 658-674.
- Monds RD, Newell PD, Schwartzman JA, O'Toole G (2006). Conservation of the Pho regulon in *Pseudomonas fluorescens* Pf0-1. *Applied and Environmental Microbiology* **72**:1910-1924.
- Murshudov G, Vagin A, Dodson E (1996). REFMAC5 for the refinement of macromolecular crystal structure. *Acta Cryst. D* **67**:355-367.
- Nylander, JAA (2004). MrModeltest v2. Program distributed by the author. Evolutionary Biology Centre, Uppsala University.
- Pegos VR, Nascimento JF, Sobreira TJP, Pauletti BA, Paes-Leme A, Balan A (2014). Phosphate regulated proteins in *Xanthomonas subsp.citri*: A proteomic approach. *Journal of proteomics* **108**: 78-88.
- Pegos VR, Medrano FJ, Balan A (2014). Crystallization and preliminary X-ray diffraction analysis of the phosphate-binding protein PhoX from *Xanthomonas citri*. *Acta Crystallographica Section F* **70**: 1604-1607.
- Pireddu L, Leo Simone, Zanetti G. (2011). SEAL: a distributed short read mapping and duplicate removal tool. *Bioinformatics*, **27**:2159-2160.
- Sali A, Blundell TL (1993). Comparative protein modelling by satisfaction of spatial restraints. *J. Mol. Biol* **234**: 779-815.
- Schrödinger LLC. The pymol molecular graphics system. Version 1.5.0.4.
- Shen J, Yuan L, Zhang J, Li H, Bai Z, Chen X, Zhang W, Zang F (2011). Phosphorus Dynamics: From Soil to Plant. *Plant Physiology* **156**: 997-1005.
- Snel B, Lehmann G, Bork P, Huynen M A (2000). String: a web-server to retrieve and display the repeatedly occurring neighbourhood of a gene. *Nucleic Acids Res* **28**: 3442-4.
- Stein N (2008). CHAINSAW: a program for mutating pdb files used as templates in molecular replacement. *J. Appl. Cryst* **41**:641 – 643.
- Tamura K, Peterson D, Peterson N, Stecher G, Nei M, and Kumar S (2011). MEGA5: Molecular Evolutionary Genetics Analysis using Maximum Likelihood, Evolutionary Distance, and Maximum Parsimony Methods. *Molecular biology and Evolution* **28**: 2731-2739.
- Tanabe M, Mirza O, Bertrand T, Atkins HS, Titball RW, Iwata S, Brown KA, Byrne B (2007). Structures of OppA and PstS from *Yersinia pestis* indicate variability of interaction with transmembrane domains. *Acta Crystallographica D* **63**:1185-1193.
- Vyas NK, Vyas MN, Quijcho FA (2003). Crystal structure of *M.tuberculosis* ABC phosphate transport receptor: Specificity and Charge compensation Dominated by Ion-dipole Interactions. *Structure* **11**: 765-774.
- Wang, Z, Luecke H, Yao N, Quijcho FA (1997). A low energy short hydrogen bond in very-high resolution structures protein receptor-phosphate complexes. *Nature* **4**:519-522.
- Wanner BL (1993). Gene regulation by phosphate in enteric bacteria. *Journal of cellular biochemistry* **51**: 47-54.
- Wittmore L, Wallace BA (2004). Dichroweb: an online server for protein secondary structure analyses from circular dichroism spectroscopic data. *Nucleic acid Research* **32**: 668-673.
- Yao N, Ledvina PS, Choudhary A, Quijcho FA. (1996). Modulation of a salt link does not affect binding of phosphate to its specific active transport receptor. *Biochemistry*, **35**:2079-85.

Manuscrito II

Low phosphate availability stimulates xanthan gum and biofilm production in *X. citri*

(In preparation)

Vanessa Rodrigues Pegos, Rita Café, Simone Picchi, Alessandra Alves de Souza, Luiz Almeida, Beny Spira, Andrea Balan .

Low phosphate availability stimulates xanthan gum and biofilm production in *Xanthomonas axonopodis* pv. *citri*

Vanessa Rodrigues Pegos^{1,2}; Simone Picchi³; Alessandra Alves de Souza³; Rita Café Ferreira⁴; Luiz Almeida⁴; Beny Spira⁴; Andrea Balan^{4*}.

1- Laboratório Nacional de Biociências (LNBio), Centro de Pesquisas em Energia e Materiais (CNPEM), Campinas, São Paulo, Brazil.

2- Universidade Estadual de Campinas (UNICAMP) Instituto de Biologia (IB), Campinas, São Paulo, Brazil.

3- Centro de Citricultura Sylvio Moreira, Cordeiropolis, São Paulo, Brazil.

4- Universidade de São Paulo (USP), Instituto de Ciências Biomédicas II, Departamento de Microbiologia, São Paulo, São Paulo, Brazil.

*Correspondent Author: abalan@usp.br

Address for correspondence:

Laboratório de Biologia Estrutural Aplicada (LBEA), Departamento de Microbiologia, Instituto de Ciências Biomédicas II, Universidade de São Paulo, São Paulo, SP, Brazil. Avenida Professor Lineu Prestes, 1374 Sala 154; CEP 05508-000, Tel: +55 11 3091-7544

Key-words: Phosphate-binding protein, PstS, PhoX, phosphate regulon, Pst system, *Xanthomonas citri*.

ABSTRACT

X. citri is a phytopathogen that causes the citrus canker on citrus species. Due the silent disease evolution no combat or prevention has been available causing a worldwide economic loss. The aims of this work are investigate the biofilm formation, xanthan production under phosphate starvation and citrus canker development with a defective bacterium no able to uptake phosphate. To do that a *pstS* deletion mutant of *X. citri* was constructed. Considering the deletion effects, the *pstS* gene belong to ABC transporter system know as phosphate specific transport that is activated under phosphate starvation. The *pstS* mutant strain was able to grow under low phosphate availability *in vitro* but showed a difficulty to grow inside of the *C. sinensis* leaves increasing the *lag* phase on *in vivo* grow curve during the disease evolution. Furthermore, *pstS* absence also retarded the ability to attach *in vivo* surfaces when compared with wild type on 24 hours. Despite the lack of *psts* the radioactive experiments reveals that mutant strain was able to uptake phosphate under phosphate starvation showing the same behavior of wild type strain. Under high phosphate availability and no phosphate starvation the mutant strain showed a constitutive activation of pho regulon. Also, *X. citri* has an extra copy of PstS know as PhoX suggesting a compensatory function to uptake phosphate under starvation and PstS is responsible to uptake phosphate and also be involved with phosphate metabolism regulation, a role that PhoX does not. Considering the phosphate response, low phosphate availability stimulates secondary responses such as stress stimulating to xanthan gum and biofilm formation. Due to extra copy of PstS, the low phosphate availability increases the xanthan production and attachment on polypropylene surface and no differences were notice between wild type and mutant strains.

1. Introduction

Xanthomonas axonopodis pv. *citri* (*X. citri*) is the causative agent of citrus canker. The bacterium is found in tropical and subtropical areas causing enormous economic losses that conducted to genomic studies from Brazilian Institutes (Da silva et al, 2002). The disease develops when the bacterium access the mesophyll cells through stomata or lesions and starts colonization and growth. The phenotype is well characterized with appearing of water-soaked lesions, chlorosis, loss of leaves and fruits (Gudesblat et al, 2009). The operon *gum* encoding 12 enzymes is responsible to produce an extracellular polysaccharide known as xanthan gum. Despite innumerous biotechnological applications of xanthan gum in the industries, its biological importance is to participate as an essential constituent of the extracellular biofilm matrix (EPS) and biofilm formation. Biofilm formation helps the bacterium adhesion on surfaces, cellular communication, water retaining and protection. Mutations in *gum* genes lead a reduction of the citrus canker symptoms and drastically reduce the virulence (Yan, et al 2012; Rigano et al 2011). In a previous study, we showed that similar to what happens in other species (Wanner et al, 1993; Gebhard et al, 2006; Yuan et al, 2006), Phosphate is an essential element to induce changes in the protein profile of *X. citri*, including many those associated with pathogenesis and infection, as well as the ones belonging to the phosphate regulon (Pho regulon) (Pegos et al., 2104). The phosphate availability is elementary to cell growth, production of macromolecules, metabolism and energy production. As an important member of Pho regulon, the phosphate specific ATP-Binding Cassete transporter (ABC transporter Pst) encodes a high affinity system for uptake and transport of inorganic phosphate. In *X. citri*, the Pst system is constituted by a periplasmic-binding protein (PstS), a heterodimer of transmembrane domains (PstB and PstC), and a homodimer of the ATPases (PstA). In addition to the PstS, *X. citri* has another periplasmic-binding protein capable to bind phosphate and that share more than 60% of amino acid sequence identity and structural features with many phosphate-binding proteins (Pegos et al., in prep). Proteomics analysis revealed that both periplasmic-binding proteins had the expression level highly induced during depletion of phosphate evidencing the regulation of the system by this element.

Studies with PstS from *E. coli* have shown its relevance besides the transport. PstS was related to the biofilm formation, adherence and also had regulatory function in this bacterium. In this sense, in order to understand the role of PstS in the physiology and pathogenesis of *X. citri*, we built a *X. citri* mutated strain deleted for *pstS* gene (*Xac::pstS*) and analysed its behavior during *in vitro* and *in vivo* growth, through a set of parameters that are important for the transport and canker development. All data were collected having phosphate as a key element.

2. Methods

Bacterial strains and culture conditions

Wild type *Xanthomonas axonopodis* pv. *citri* 306 (da Silva et al, 2002) and its mutant *Xac::pstS* were kept on -80°C until the cultivation. For assays, cells were grown in Luria Bertani (LB) medium during 24 hours, 200 rpm, 28°C with appropriated antibiotic to selection. After this period, the cells were gently harvested by centrifugation on 6000 g and washed with water sterile to remove excess of LB media, resuspended in 1 mL of water and used for measuring of the absorbance at 600 nm. Aliquots corresponding to 10⁶ cel/mL were inoculated in media A (Levinthal et al, 1962) and A+P₁ (supplemented with 10 mM of Na₂HP₁O₄ is A+P₁).

Construction of *X. citri::pstS* mutant and strain for complementation *X. citri::pstSc*

X. citri deleted strain (*Xac::pstS*) was built according Oshiro and collaborators (2006) through a suicide vector pNPpstS containing a antibiotic cassette resistant Kan/Spec.

The complementation strain was built as previously described by Araújo et al (2013) using pKX33 vector (Baldini, et al 1999). Firstly, a fragment of 750 pb upstream of the XAC1579 gene encoding the promoter region of *X. citri pst* operon was amplified by PCR using the forward 5'

GGTACCGGGAGATTCTCTAGGCAACG 3' and reverse 5' GGATCCAGATGCCTTGCGACCTGAGAAA 3' oligonucleotides. Similarly, a fragment of 1092 pb encoding *pstS* gene (XAC1577) including the signal peptide was amplified using the forward and reverse oligonucleotides: 5' GGATCCATGAAATTTGCAGTCGG 3' and 5' GAGCTCTTACTTGAAGCTCGCTG 3', respectively. Both fragments were then cloned separately into pGEM T-Easy vector. The construction of pKX33-*ppstS* was obtained after the subcloning of the promoter and *pstS* sequences in the restrictions sites *KpnI* and *BamHI* and *BamHI* and *SallI*, respectively. *E. coli* DH5 α cells were used for transformation of the ligation mixture and positive clones were confirmed by colony PCR using specific primers. Electrocompetent cells of *Xac::pstS* strain were transformed with pKX33-*ppstS* according Oshiro and collaborators (2006) to originate the *Xac::pstSc* strain. Positive colonies were obtained after 48 hours.

***In vitro* growth curve**

In order to analyze the growth rates among *X. citri*, *X. citri::pstS* and *X. citri::pstSc* strains in 100 mL of A and A+Pi, approximately a 10⁶ UFC/mL (OD_{600nm} = 0,04) previously washed as mentioned before, were inoculated in each media supplemented with ampicillin (50 mg/mL) spectinomycin (75 mg/mL) and kanamycin (100mg/mL) antibiotics for selection. The samples were maintained at 30°C, 200 rpm for 72 hours. Samples of 1 mL were collect from the cultures at times of 0 h (just after inoculum), 24 h and 72 h. Each sample was diluted by serial dilution in sterile water and plated on LB agar. The plates were kept 28 °C during 48 hours and the CFU/mL were counted. Availability of phosphate trace in A medium was provided by peptone in the formulation (Levinthal et al, 1962).

***In vivo* growth curves**

To test the growth of *X. citri* wild type, mutant and complemented strains in *Citrus sinensis* leaves (sweet orange) we adapted the protocol of Yan and collaborators (2012). Firstly, the bacteria were grown in LB medium during 24 hours until the O.D._{600 nm} = 1.2 at 28°C and then centrifuged at 6000 g, washed and diluted on sterile water until O.D._{600 nm} = 0,05, which represents 10⁶ CFU/mL. The samples were infiltrated using a needleless syringe in three distinct areas of the same *C. sinensis* leaf, in triplicates and the development was followed by 14 days. To recovery of the cells from the leaves, 1 cm² from each area was excised each 48 hours. The leaves samples were macerated in 1 mL of sterile water and diluted by serial dilution with gentle vortexing. Each dilution was plated into LB agars with appropriated antibiotic for selection of wild type, mutant and complementary strain. The plates were kept at 28°C and after 48 hours the CFU/mL were counted.

Analysis of biofilm formation in abiotic an biotic surfaces and production of xanthan gum

In order to analyze the adhesion of *X. citri* wild type and *Xac:pstS* in abiotic surface (polypropylene), the strains were growth on A, A+P_i and LB media and the experiments performed according Guo and collaborators (2012). The biofilm formation in biotic surfaces was analyzed in *C. sinensis* leaves using a detach leaf from the tree. A cell suspension containing 10⁴ cel/mL was drop-off on the abaxial surface and maintained for 24 and 48 hours, when the areas were gently washed with water and stained with violet crystal 2%. Each leaf was photographed and at least 3 leaves were assayed for each measurement time.

The production of xanthan gum was performed according Vojnov and collaborators (1998) by precipitation using 2% of KCl and ethanol PA. The produced gum by each strain was recovery from the culture supernatants of the cells after grown in A and A+P_i media.

Phosphate transport assay

X. citri, *Xac::pstS* and *Xac::pstSc* were grown on T-salt medium supplemented with 4 mM KH₂PO₄ and 0,2% Glucose until reach the O.D._{600nm} = 1.0. Samples were washed and resuspended on 10 mL of T-salt + 0,2% Glucose, 200 μM of chloramphenicol, and 5 mL submitted to phosphate label to evaluate the transporter under excess of P_i. The rest of culture was kept under shaking until reach the starvation during at least 1 hour. The sample was mixed with final concentration of 3 μM of KH₂PO₄ plus 1 μCi/μL of phosphorus labeled (³³P). Samples 500 μL taken at time points were filtered on cellulose membrane (pore size 0.22 μM) and washed with 5 mL of PBS 1X to remove the excess of ³³P. After, 5 mL of scintillation reagent was added on each filter and the measurement occurred on scintillator (Beckman LS6500).

Statistical analysis

The statistical analysis applied to functional studies were performed using unpaired t-bicaudal test with p<0,05.

3. Results

Proteome analysis of *X.citri* and other methodological interventions performed with *E. coli*, *Pseudomonas* sp. and other bacterial strains highlighted possible connections between pathogenic process and phosphate starvation (Pegos et al, 2014). *X. citri* conserves some molecular machineries elementary to infection including xanthan gum as a complex polysaccharide to causes citrus canker. In order to study *pstS* on infectious and disease evolution under phosphate starvation or inside of vegetal issue was constructed a mutant bacteria (*X. citri:pstS*). The complementary strain *X. citri::pstS* that receives promotor with phobox cloned into *pKx33* in frame with *pstS* from *X. citri* (pKX33pstS) (figure S1).

Influence of the *pstS* deletion in the *X. citri* growth

To verify the role of PstS protein during growth of *X. citri* in culture medium with different phosphate availability, cells of wild type, mutant *Xac::pstS* and complementary strain *Xac::pstSc* were grown in A and A+P_i media for 72 hours. The three strains had similar behavior in both media showing decreasing of the cells viability in A medium after 48 hours when compared to the A+P_i medium. These data indicated that the low concentration of phosphate did not affect the cell viability but reveal that there is no significant effect of the *pstS* deletion (Figure 1A to C).

Low concentration of phosphate stimulates the production of xanthan gum and adhesion

Although the strains showed similar behavior in the growth curves, we noticed that colonies of *Xac::pstS* presented smaller size and attenuated color when compared to the wild type and complementary strains (Figure 2A to C). This phenotype was previously observed in colonies of a *X. citri* mutant deleted for *ssuA2* gene (Araújo et al., 2014), and related to the fact that the mutant had the xanthan gum production reduced in 3 fold when compared to the wild type. In order to check if *Xac::pstS* had similar behavior we evaluated the xanthan gum production using the protocol developed by Voijnov and collaborators (1998). Curiously, we showed that there is no influence of the *pstS* deletion in the gum production but an increasing of the polysaccharide in lower levels of phosphate (A medium), which is consistent with the colonies phenotype observed in the rich medium LB (Figure 2). Since gum xanthan is an elementar constituent of extracellular matrix, responsible for biofilm formation, we performed adhesion assays on polypropylene surfaces in the same A and A+P_i medium. Corroborating the previous results obtained for xanthan gum production, the low phosphate availability (A medium) stimulates the bacterial adhesion in comparison with the adhesion on high phosphate availability (A+P_i) (Figure 2E). Moreover, the *pstS* deletion did not show any effect on that experiment, in presence of absence of phosphate.

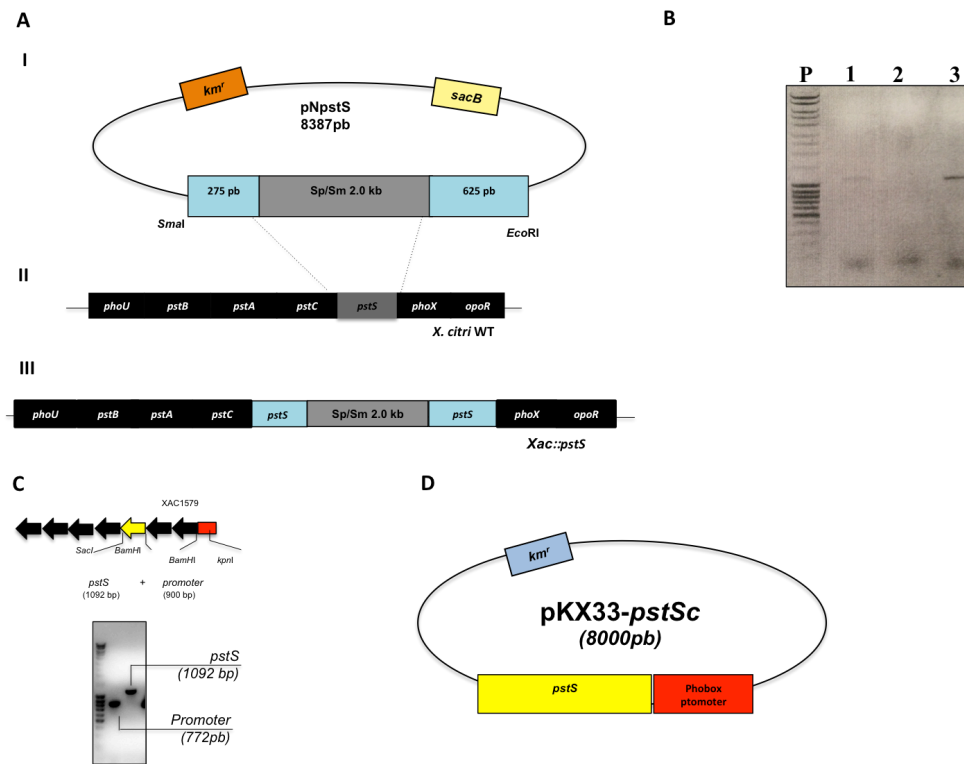


Figure S1 Construction of the *X. citri* *pstS*-deleted mutant (*Xac::pstS*) and complementary strain (*Xac::pstSc*) (A) Chromosomal deletion of the *pstS* gene was obtained after electroporation of the suicide pNpstS plasmid into the *X. citri* 306 strain (I) The first step in the construction of the *X. citri* mutant was the insertion of a 2-kb fragment encoding resistance to spectinomycin and streptomycin into the *KpnI* site of the *pstS* gene originating within the pNpstS (8152 bp) vector (II) After transformation of wild-type *X. citri* with pNpstS a double recombination event generated the *Xac::pstS* mutant strain (III) which was screened by selection of cells resistant to both spectinomycin and sucrose (B) PCR amplification of *pstS* genes of selected *X. citri* mutant colonies using primers *FpstS* and *RpstS* attesting recombination effect. Samples: P molecular weight markers; sample 1 was PCR control by full amplification of the *pstS* (1092 bp) from wild-type chromosome; sample 2 *pstS* gene amplification from *Xac::pstS*; sample 3 *pstS* amplification from *Xac::pstSc* strain. The construction of the complementary strain *Xac::pstSc* was performed in two steps (C) PCR amplification of the fragments corresponding to the full *pstS* gene (1092 bp) and promoter region of the *pstSCAB* operon (772 bp); (D) Cloning of both genes into the high-copy number vector pKX33. We confirmed all the constructions by PCR and DNA sequencing.

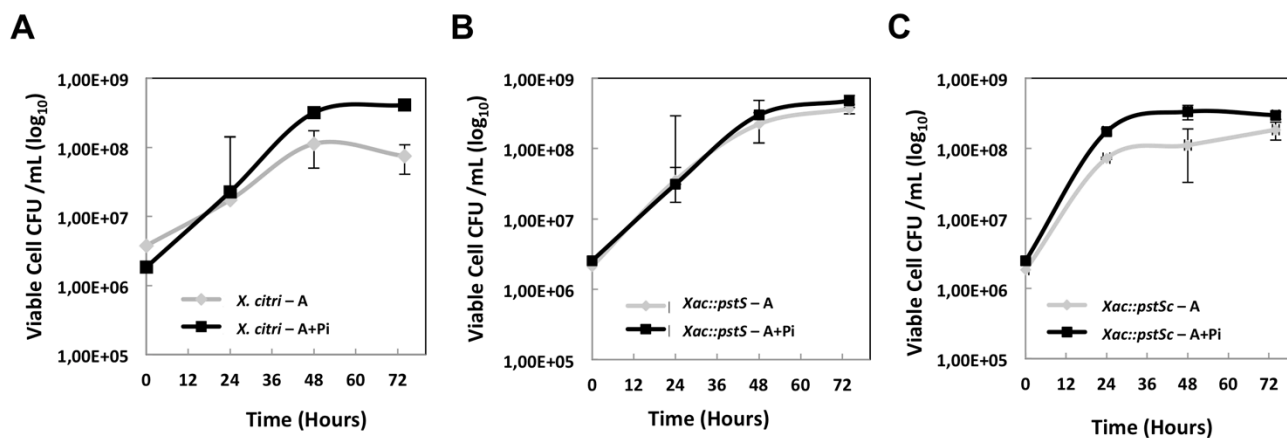


Figure 1 Influence of the *pstS* deletion in cells of *X citri* Growth curves of the strains were performed in A and A+P_i media *X citri* wild type (A) *Xac::pstS* mutant (B) and *Xac::pstSc* complementary strains (C) No statistical significance was observed (p<005) among the strains. Three biological independent samples were used (n=3).

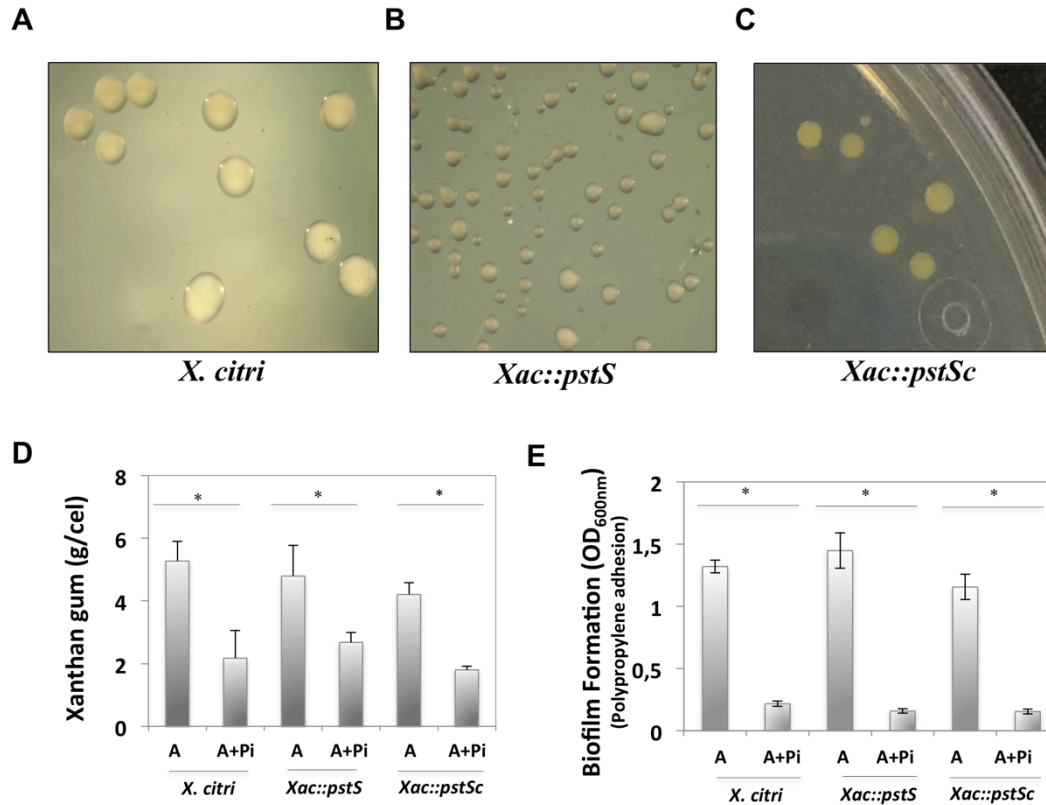


Figure 2 Influence of *pstS* deletion in the phenotype of the colonies production of xanthan gum and adhesion of *X. citri* in biotic and abiotic surfaces of *X. citri*, *Xac::pstS* and *Xac::pstSc* under cultivation on A and A+P_i media (n=3). Phenotype of the colonies of *X. citri* (A) *Xac::pstS* mutant (B) and *Xac::pstSc* complementary strains (C) grown in LB medium showing differences in the size and color of the mutant strain (D). Analysis of the xanthan gum production by the three strains in high and low levels of phosphate (A+P_i and A respectively) *pstS* deletion did not affect the production of the polysaccharide but the strains showed increasing of the gum in low levels of phosphate (E) Analysis of the adhesion of the cells on polypropylene surface bars show the adhesion of the each strain in A or A+P_i media. As already concluded in D phosphate levels are more important for adhesion than the presence of PstS protein. The asterisks represent statistical *t*-test with $p < 0.05$.

Effect of the *pstS* mutation during in vivo infection and adhesion

The next set of experiment was carried out in order to verify the influence of the PstS during infection of *X. citri* in *C. sinensis* leaves and development of the citrus canker. Cell suspensions of 10^6 cell/mL were infiltrate on orange tree leaves according Yan and coworkers (2012) and monitored by 12 days post infiltration (DPI). The phenotype of the canker was similarly evidenced in the wild type, mutant and complementary strains (Figure 3A). Indeed, all strains were capable to cause characteristic soaked lesions such as chlorosis and tumefaction. Again, it was not evidenced significant differences between mutant and wild type strains (Figure 3B).

In addition, the viable cells were recovered from leaves on a time course measurement and counted after spreading on LB medium. The plot of viable cells in different days revealed that despite the phenotype, the deletion of *pstS* leaded to a retard in the growth, which only started after 8 days of infection until levels compared to the wild type and complementary strains (Figure 3C). The results suggest that Pst absence mainly affected the initial steps of growth without compromise the number of cells at the end of the growth, which might explain the similar phenotypes observed in the leaves (Figure 3C). In addition, we analysed the capability of the strains to colonize the surface of sweet-orange leaves, observing the adherence and biofilm formation. The bacterial were cultivated on rich medium and 10^4 cell/mL were dropped off on the abaxial surface of two independent leaves, which were detached from the trees and kept at 30°C during 24 and 48 hours, respectively. After each period, the leave was gently washed and stained with violet crystal 2%. The qualitative measurement showed that similarly what was observed in the growth curve, adhesion of *Xac::pstS* strain was reduced in the first 24 hours, when compared with the two other strains, as evidenced by the lower number of stained cells in the border of the inoculation, but was comparable in the samples incubated for 48 hours (Figure 3D, I to IV). Altogether, these data reveal that PstS has an important role during the first hours of infection, affecting the growth and adherence.

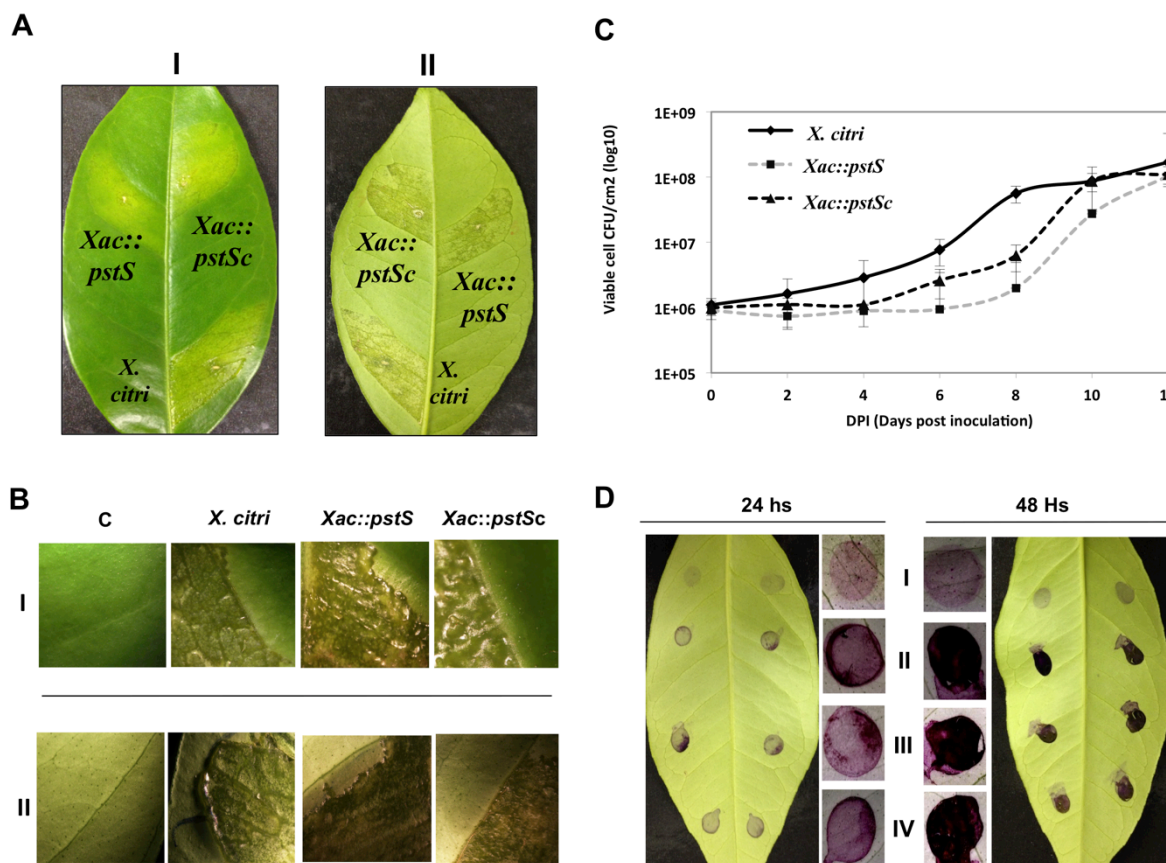


Figure 3 Role of PstS during infection of *X citri* in *Citrus sinensis* leaves (A) Phenotype of the canker symptoms in *C sinensis* leaves after inoculation of 10^6 UFC/mL I and II front and abaxial view of the leaves infected with *X citri*, *Xac::pstS* mutant, and *Xac::pstSc* complementary strain. (B) Detail of the canker symptoms (increase of 50 X) in front and abaxial sides. (C) Growth curve of the strains recovered from the inoculated leaves at different timepoints. The error bar represents the standard deviation of three distinct experiments (n=3). (D) Bacterial adhesion by *X citri* strains on abaxial surfaces of *C sinensis* leaves showed for 24 h and 48 h. Cells were cultivated in LB medium and samples of 10^4 UFC/mL were dropped into the leaves I LB (control); II *X citri* wild type; III *Xac::pstS* and IV *Xac::pstSc*. Detail of the drops is shown for each condition in the small figures. The figure represents the results of 4 independent experiments (n=4).

***pstS* deletion induces the constitutive expression of the *X. citri* ABC transporter Pst**

To check if the deletion of *pstS* gene affected the uptake and transport of phosphate in *X. citri*, we first cultivated the strains for 48 hours in T-salt medium supplemented with 4 mM phosphate, after washing of the cells they were resuspended in P_i-free medium and of radioactive ³³P and. The incubation on shaker of the free phosphate samples occurred for 2 h to completely deplete the intracellular phosphate levels. Addition of chloramphenicol at final concentration of 200 µg/mL was used to avoid protein synthesis during phosphate consumption. Samples were taken up to 1.40 minutes in presence and depletion of phosphate (Figure 4A and B, respectively). In presence of phosphate no transport was detected in the sample of *X. citri* wild type indicating that Pst system was not induced corroborating the expected results about repression of the system under high phosphate availability. Differently, we observed transport of approximately 3 ng of phosphate in the *Xac::pstS* mutant suggesting that *pstS* deletion induced a constitutive expression of the system. Intriguingly, the complementary strain showed exactly the same behavior of the mutant (Figure 4A) not restoring the wild type phenotype. On the other hand, all strains transported around 20 ng of the ion in medium with depletion of phosphate, which suggested that in this condition, the system is up regulated (Figure 4B), as evidenced in other microorganisms (Gebhard, et al 2006).

4. Discussion

Phosphate specific transport (Pst) and the Pho regulon have been extensively studied in many microorganisms due their importance for bacterial physiology and, mainly, the relationship with virulence (Lamarque et al, 2008). In this work, we studied the role of the *pstS* deletion in the physiology of *X. citri* under excess and scarcity of phosphate. Despite the proven importance of PstS in different microorganisms (O' May et al, 2008; Moura et al, 2008), nothing was described of *X. citri* PstS. Recently, based on

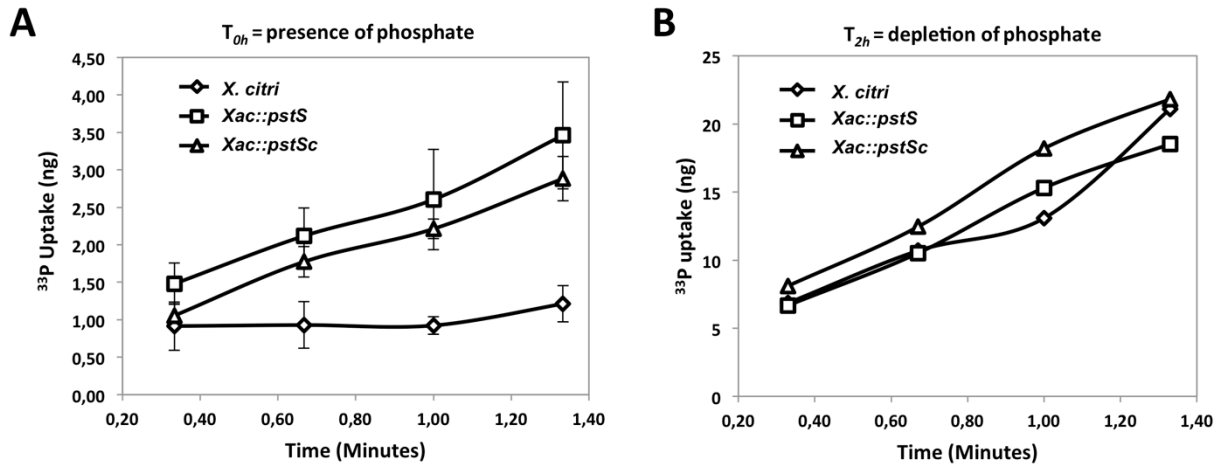


Figure 4 Uptake and transport of ^{33}P Phosphate by *X citri*, *Xac::pstS*, *Xac::pstSc* Cells were grown on T-salt supplemented with 4 mM of $\text{KH}_2\text{P}_i\text{O}_4$ until $\text{OD}_{600\text{nm}} = 10$. The cultures were washed and resuspended on T-salt supplemented with 0.5% of glucose and used for measurement of uptake rate and transport. Plots were made from data collected immediately after washing and inoculation (T_{0h}) (A) where there was phosphate and after two hours of incubation at 28°C (T_{2h}) (B) in depletion of phosphate.

proteomics analysis, our group showed that *X. citri* conserves the phosphate ABC transporter PstSCAB and the two-component system PhoR/PhoB and that both systems are highly induced during phosphate starvation (Pegos et al., 2014). Moreover, we showed that *X. citri* has another gene encoding a phosphate-binding protein (*phoX*, XAC1578) located in the operon *oprOphoX*. PhoX and PstS conserve 70% of residues of amino acids and share 50% of the residues PstS from *E. coli* including those that interacts directly with phosphate (Pegos et al., submitted). Both PstS and PhoX were up regulated in phosphate deficiency (fold-change of 49,1 fold and 33,5 fold to PhoX and PstS, respectively) revealing their importance during growth of the cells in that condition.

In this work, we built a *X. citri* mutant strain deleted for *pstS* gene and analysed its behavior using different approaches. Essentially, the results showed that the deletion did not affect the growth, production of xanthan gum and biofilm formation, suggesting that the PhoX might have a compensatory function in absence of PstS. However, *in vivo* assays showed an increasing in the *lag* phase of *Xac::pstS* when compared to the wild type strain, suggesting that both genes, in different operons, have distinct levels of activation, as evidenced in the proteomics analysis. Interestingly, the mutant strain showed active ^{33}P uptake in presence of phosphate, when the system should be repressed, indicating that the deletion induced a constitutive activation of Pst system (Figure 4A). In this sense, since that the phosphate still is being transported to the cell by PhoX, the physical lack of PstS protein seems to induce the system activation.

Although *pstS* mutant revealed similar behavior when compared to the wild type in the assays discussed above, our results revealed that the phosphate depletion induced and increasing of the production of gum and biofilm formation/adherence, evidencing that in stressing conditions, the bacterium might activates its mechanisms of virulence. The correlation between stress and phosphate starvation is well characterized in *E. coli* (Lamarche et al, 2008). Production of xanthan gum by the bacterium has largely been associated with the mature biofilm formation, but also with the protection against reactive oxygen species (ROS) produced by the host, storage of nutrients and retention of water to help with the process of host

colonization (Rigano et al, 2011 ;Li et al, 2011). Indeed, increased production of exopolysaccharide under low availability of phosphate has been shown for *Agrobacterium tumefaciens* and *Sinorhizobium. meliloti* (Rüberg et al, 1999; Danhorn et al, 2004), two phytopathogenic bacteria.

Altogether, in this work we showed that PstS protein is not necessary for growth, production of xanthan gum and biofilm formation, probably due the compensatory effect of the PhoX protein. However, the lack of PstS induced a constitutivity of the operon suggesting that as similarly evidenced for other bacteria, PstS has an additional regulatory role.

4. Acknowledgement

This work was supported by the Coordenação de Aperfeiçoamento Pessoal de Nível Superior - CAPES, Brazil, Fundação de Amparo à Pesquisa do Estado de São Paulo (FAPESP) and Laboratório Nacional de Biociências, LNBio, Campinas, Brazil. We also would like to thank Prof Celso Benedetti (Laboratório Nacional de Biociências, LNBio, Brazil) that helped with suggestions and in vivo assays.

5. Conflict of interests

The authors declare no conflict of interests.

6. References

- Araújo FB, Bolanos-Garcia VM, Pereira CT, Sanches M, Oshiro EE, Ferreira RCC, Chigardze DY, Barbosa JAG, Ferreira LCS, Benedetti, CE, Blundell TL, Balan A (2013). Structural and physiological analysis of the alkanesulphonate-binding protein (SsuA) of the citrus pathogen *Xanthomonas citri*. Plos One: 8: 1-14.
- Baldini RL, Tahara ST, Rosato YB (1999). A rolling-circle miniplasmid of *Xanthomonas campestris* pv. *glycines*: The nucleotide sequence and its use as a cloning vector. Plasmid 42:126-133.
- da Silva ACR, Ferro JA, Reinach FC, Farah CS, Furlan LR, Quaggio RB, Monteiro-Vitorello CB, Van Sluys MA, Almeida Jr NF, Alves LMC, do Amaral AM, Bertolini MC, Camargo LEA, Camarotte G, Cannavan

- F, Cardozo J, Chambergo F, Ciapina LP, Cicarelli RMB, Coutinho LL, Cursino-Santos JR, Dorry H, Faria JB, Ferreira AJS, Ferreira RCC, Ferro MIT, Formighieri EF, Franco MC, Greggio CC, Gruber A, Katsuyama AM, Kishi LT, Leite Jr RP, Lemos EGM, Lemos MVF, Locali EC, Machado MA, Madeira AMBN, Martinez-Rossi NM, Martins EC, Meidanis J, Menck CFM, Miyaki CY, Moon DH, Moreira LM, Novo MTM, Okura VK, Oliveira MC, Oliveira VR, Pereira JrHA, Rossi A, Sena JAD, Silva C de Souza RF, Spinola LAF, Takita MA, TamuraRE, Teixeira EC, Tezza RID, Trindade dos Santos M, Truffi D, Tsai SM, White FF, Setubal JC, Kitajima JP (2002). Comparison of the genomes of two *Xanthomonas* pathogens with differing host specificities *Nature* 417: 459-63
- Danhorn T, Hentzer M, Givskov M, Parsek MR, Fuqua C (2004). Phosphorus limitation enhances biofilm formation of the plant pathogen *Agrobacterium tumefaciens* through the PhoR-PHoB regulatory system. *Journal of Bacteriology* 186: 4492-4501.
- Gebhard S, Tran SL, Cook GM (2006). The Phn system of *Mycobacterium smegmatis*: a second high-affinity ABC transporter for phosphate. *Microbiology* 152:3453-3465.
- Gudesblat GE, Torres PS, Vojnov A (2009). *Xanthomonas campestris* overcomes Arabidopsis stomatal innate immunity through a DS cell-to-cell signal regulated virulence factor. *Plant Physiology* 149:1017-1027.
- Guo Y, Zhang Y, Li JL, Wang (2012) Diffusible signal factor-mediated quorum sensing plays a central role in coordinating gene expression of *Xanthomonas citri* subsp. *citri*. *MPMI* 25: 165-179.
- Hoffer S, Tommassen J (2001). The phosphate-binding protein of *Escherichia coli* is not essential for Pi-regulated expression of the Pho regulon. *Journal of bacteriology* 183:5768-5771.
- Kadosh BI, Zilka A, Yerushalmi G, Banin E (2013). The effect of *pstS* and *phoB* on Quorum sensing and swarming motility in *Pseudomonas aeruginosa*. *Plos One* 8: 1- 7.
- Lamarche MG, Wanner BL, Crépin S, Josée Harel (2008). The phosphate regulon and bacterial virulence: a regulatory network connecting phosphate hoemostasis and pathogenesis. *FEMS Microbiol Review* 32: 461-473.
- Levinthal C, Signer ER, Fetherolf K. (1962) Reactivation and Hybridization of reduced alkaline phosphatase. *Biochemistry* 48: 1230-1237.
- Li J, Wang N (2013). Foliar application of biofilm formation-inhibiting compounds enhances control of citrus canker caused by *Xanthomonas citri* subsp. *citri*. *Bacteriology* 104:134-142.
- Li J, Wang N (2011). Genome-Wide Mutagenesis of *Xanthomonas axonopodis* pv. *citri* reveals novel genetic determinants and regulation mechanisms of biofilm formation. *PLoS One* 6:1-16;
- O' May GA, Jacobsen DM, Longwell M, Stoodley P, Mobley HLT, Shirtliff ME (2009). The high-affinity phosphate transporter Pst in *Proteus mirabilis* HI4320 and its importance in biofilm formation. *Microbiology* 155:1523-1535.
- Oshiro EE, Nepomuceno RSL, Faria JB, Ferreira LCS, Ferreira RCC (2006). Site-directed replacement of the phytopathogen *Xanthomonas axonopodis* pv. *citri*. *Journal of Microbiological Methods* 65:171-179.
- Pegos VR, Nascimento JF, Sobreira TJ, Pauletti BA, Paes-leme A, Balan A. (2014) Phosphate regulated proteins of *Xanthomonas citri* subsp. *citri*: A proteomic approach. *Journal of proteomic* 108: 78-88.
- Rigano LA, Siciliano F, Ramón E, Sendín L, Filippone P, Torres PS, Questa J, Dow JM, Castagnaro AP, Vojnov AA, Marano MR (2011). Biofilme formation, epiphytic fitness and canker development in *Xanthomonas axonopodis* pv. *citri*. *Molecular plant-microbe interactions* 20:1222-1230.
- Rüberg A, Pühler A, Becker A (1999). Biosynthesis of the exopolysaccharide galactoglucan in *Sinorhizobium meliloti* is subject to a complex control by the phosphate-dependent regulator PhoB and the proteins ExpG and MucR. *Microbiology* 145:603-611.

- Vojnov AA, Zorreguieta A, Dow JM, Daniels MJ, Dankert M (1998) Evidence for a role for the *gumB* and *gumC* gene products in the formation of xanthan from its pentasaccharide repeating unit by *Xanthomonas campestris*. *Microbiology* 144: 1487-1493.
- Wanner B. (1996) Phosphorus assimilation and control of the phosphate regulon. *Escherichia coli* and *Salmonella thymurium* cellular and molecular biology 51: New York ASM Press, 47-54.
- Wanner BL (1993). Gene regulation by phosphate in Enteric bacteria. *Journal of Cellular Biochemistry* 51:47-54.
- Yan Q, Wang N. (2012) High-throughput screening and analysis of genes of *Xanthomonas citri* subsp. *citri* involved in citrus canker symptom development. *The American phytopathological society* 25: 60-84.
- Yuan ZC, Zaheer R, Finan Tm (2006). Regulation and properties of PstSCAB, a high affinity, high-velocity phosphate transport system of *Sinorhizobium meliloti*. *Journal of bacteriology* 3: 1089-1102.

Manuscrito III

Effects of phosphate and *pstS* deletion in the overall metabolism of *Xanthomonas axonopodis* pv. *citri*

(In preparation)

Vanessa Rodrigues Pegos, Rafael Renatino Canevarolo, Gabriela Meirelles, Ana Zeri,
Andrea Balan

Effects of phosphate and *pstS* deletion in the overall metabolism of *Xanthomonas axonopodis* pv. *citri*

Vanessa Rodrigues Pegos^{1,2}; Rafael Renatino Canevarolo^{2,3}; Adriana Paes Leme¹; Gabriela Meirelles¹; Ana Carolina de Matos Zeri¹, Andrea Balan^{4*}.

- 1- Laboratório Nacional de Biociências (LNBio), Centro de Pesquisas em Energia e Materiais (CNPEM), Campinas, São Paulo, Brazil.
- 2- Universidade Estadual de Campinas (UNICAMP) Instituto de Biologia (IB), Campinas, São Paulo, Brazil.
- 3- Boldrini Children Hospital, Molecular Biology Laboratory, Campinas, São Paulo, Brazil.
- 4- Departamento de Microbiologia, Instituto de Ciências Biomédicas (ICB2), Universidade de São Paulo (USP), São Paulo, São Paulo, Brazil.

*Correspondent Author: abalan@usp.br

Address for correspondence:

Laboratório de Biologia Estrutural Aplicada – LBEA

Departamento de Microbiologia, Instituto de Ciências Biomédicas II – ICBII

Universidade de São Paulo

Avenida Professor Lineu Prestes, 1374, 1º. Andar, Sala 166; Cidade Universitária – São Paulo, SP, Brazil, CEP 05508-000.

Key-words: Phosphate-Binding Protein, Phosphate regulon, Pst system, *Xanthomonas citri*.

1. Introduction

Xanthomonas genus is characterized of a high number of species that cause diseases in a wide range of hosts such as rice, orange, grapefruit and others (Ryan et al, 2011). *Xanthomonas axonopodis* pv. *citri* (*X. citri*) is the causative agent of citrus canker, disease that is easily identified in orange trees through the symptoms such as water-soaked lesions, chlorosis and loss of leaves and fruits. The bacterium is economically relevant since the prejudices caused in the citriculture affect the economies in many countries, mainly Brazil. Understanding the metabolism and physiology of this bacterium is an important step for the development of control strategies.

One essential element for growth and metabolism of any organism is phosphate. In prokaryotic organisms, sensing and uptake of this ion is regulated by the Pho regulon (phosphate regulon) that comprises more than 31 genes and widely studied in *E. coli* (van Bogelen et al, 1996) and *B. subtilis* (Botella et al, 2011). One of the mechanisms of uptake and transport of phosphate is the ATP-Binding Cassete (ABC) transporter, known as Pst system (*phosphate specific transport system*) that is constituted by a periplasmic-binding protein responsible for affinity and specificity, two permeases that forms the pore for ion passage through the membrane and two ATPases that give energy for the transport (Davidson et al., 2008). In a recent work, we showed that besides the Pst system (PstSBCA), *X. citri* presents the two-component system PhoR-PhoB, an anchored membrane protein PhoU and an additional periplasmic-binding protein for phosphate uptake, PhoX. In common, all genes encoding these proteins present the “phobox” consensus sequence (Baek et al, 2006) in the promoter region suggesting that they belong to the Pho regulon (Pegos et al, 2014). Moreover, PstS and PhoX, the two phosphate binding proteins share the same phylogenetic origin and conserve more than 60% of their amino acid sequence residues. The three-dimensional structure of PhoX was solved bound to phosphate and its structural comparison with a *X. citri* PstS model revealed conservation of 100% of the residues interacting with the ion (Pegos et al, in prep). The level of both proteins was highly

increased (49% and 64%, respectively) in low concentration of phosphate in the cultive medium indicating that they are regulated by phosphate level and needed in depletion of the ion (Pegos et al, 2014).

The importance of PstS also has been shown in other physiological processes in *E. coli* and *Proteus* sp. such as defense against oxidative and acid stress, decreasing of fimbriae production, decreasing of the cells in biofilm and reduction of the adherence and colonization (Ferreira et al, 2008; Crépin et al, 2011; O'May et al, 2009). More important, a regulatory role for PstS has been attributed in the Pho regulon, since the absence of the protein in mutants of *Proteus mirabilis* drastically affected the biofilme and viability (O'May et al, 2009). The deletion of *pstS* gene in *X. citri* had no significant effects on the in vitro growth, production of gum and phenotype of the canker, probably due the compensatory effect of the PhoX, which production is highly increased in absence of PstS (Pegos et al., in prep).

In this work, we analysed the effect of the *pstS* mutation in a systemic view that connected proteomics and metabolomics analysis of the cells grown in excess and depletion of phosphate. We observed two distinct answers that depend on the (i) phosphate level and (ii) PstS presence. The results evidenced that even with the compensatory effect of PhoX, *X. citri* has a different profile of expressed proteins and production of metabolites, which is only dependent of PstS absence. Moreover, the phosphate depletion induced the up regulation of proteins such as secretion systems type II, quorum-sensing proteins, degradative enzymes and membrane proteins. This is the first work that demonstrate the physiological effect of phosphate depletion in the bacterium, as well as the systematic role of PstS.

2. Methods

Bacterial strains and culture conditions

Xanthomonas citri strains used in this work were *Xanthomonas axonopodis* pv. *citri* 306 (da Silva et al, 2002) and its mutant *Xac::pstS* as previously built (Pegos et al., in prep). Cells were stocked on -80°C and

first cultivated in LB medium at 28°C and 200 rpm for 24 hours in presence of appropriated antibiotic for selection. After gentle harvesting by centrifugation on 6000 g and two washes with 1 mL of TBS 1X to remove excess of medium, the optical density of the samples was measured at 600 nm and used as a parameter for the number of cells to be inoculated. For proteomics analysis of the mutant strain, cells were grown and inoculated exactly as performed in Pegos and coworkers (2014a), using minimum medium A (Levinthal et al, 1967) or A supplemented with 10 mM of Na₂HPO₄ (A+Pi).

Proteomic by MS/MS

Cultures of *Xac::pstS* were grown, washed and treated exactly as described by Pegos and coworkers (2014a). All mass spectrometric raw files associated with this study are available for downloading via FTP from the PeptideAtlas data repository (<ftp.peptideatlas.org>) and the original full data are shown in Table S1 (Supplementary material). Processing of data was performed by Mascot using *Xanthomonas axonopodis* pv. *citri* 306 as a database. Scaffold Q+ (version 3.6, Proteome Software Inc. Portland or USA) was used for estimates the peptide and protein probabilities according Keller and collaborators (2002). Table S2 (Supplementary material) shows the list of all identified proteins after statistical analysis. Spectral count from 3 distinct samples was counting and normalized according Pegos and collaborators (2014a). When the peptides were identified on A and A+P_i media the fold change refers A/A+P_i considering the normalized spectral counts average from each one, and when peptides were exclusive of culture condition just the spectral count average was reported (Table S3, Supplementary material).

Metabolomic analysis of *X. citri* and *Xac::pstS* by ¹H-NMR

The intracellular metabolome of *X. citri* and its *pstS* mutant was obtained after growing of the cultures during 48 hours in A and A+P_i media. Cells were recovered by centrifugation at 6x10³g and the equivalent to

wet weight 0.45 grams in 125 μ L was used for extraction of the metabolites using the standardized protocol described by Pegos and collaborators (2014b) based on chloroform/methanol extraction followed by ultracentrifugation for removal of the xanthan gum. The spectra of samples were acquired using a Varian Inova NMR spectrometer (Agilent Technologies Inc.) equipped with a triple resonance probe and operating at a ^1H resonance frequency of 600 MHz and constant temperature of 25°C. Each sample was submitted to 256 measurements and the shim spectrum was at least 0.7. The identification of metabolites, leads quantification and profiling was performed using the Chenomx NMR suite 7.6 software (Chenomx Inc.), considering TSP (0.5 mM) as reference molecule. The raw data from metabolomic analysis and the data after statistical treatment are shown in Table S4 and Table S5, respectively (Supplementary material). In all experiments at least 3 biological samples were used.

Table S2. List of all proteins identified by LS MS/MS in *Xac*::*pstS* proteome in A and A+P_i media. To compare with the previously obtained data from *X. citri* proteome (Pegos et al, 2014), proteins exclusively identified in the mutant are shown with one asterisk (*).

KEGG ID	Pathway Protein Function	Gene name	A Medium	A+P _i Medium
Carbohydrate metabolism				
XAC0030	cellulase	<i>egl</i>	x	x
XAC0168	5-keto-4-deoxyuronate isomerase	<i>kduI</i>	-	x
XAC0224	pyruvate dehydrogenase	<i>poxB</i>	x	x
XAC0472	ribulose-phosphate 3-epimerase	<i>rpe</i>	x	x
XAC0532*	acetyl-CoA carboxylase biotin carboxyl carrier protein subunit	<i>bccP</i>	x	-
XAC0604	trehalase	<i>treA</i>	x	x
XAC0680	6-phosphogluconate dehydrogenase-like protein	<i>gndA</i>	x	x
XAC0902	transaldolase B	<i>talB</i>	x	x
XAC1006	malate dehydrogenase	<i>mdh</i>	x	x
XAC1534	dihydrolipoamide succinyltransferase	<i>sucB</i>	x	x
XAC1584	3-hydroxybutyryl-CoA dehydratase	<i>crt</i>	x	x
XAC1785	3-methyl-2-oxobutanoate hydroxymethyltransferase	<i>panB</i>	-	x
XAC2077*	succinate dehydrogenase flavoprotein subunit	<i>sdhA</i>	x	-
XAC2078*	succinate dehydrogenase iron-sulfur subunit	<i>sdhB</i>	x	-
XAC2385	extragenic supressor protein SuhB	<i>suhB</i>	-	-
XAC2874	phosphoglycerate mutase	<i>gpmA</i>	x	x
XAC3344	fructose-bisphosphate aldolase	-	-	x
XAC3352	glyceraldehyde-3-phosphate dehydrogenase	<i>gapA</i>	x	x
XAC3388	type II citrate synthase	<i>gltA</i>	x	x
XAC3470	malic enzyme	<i>maeB</i>	x	x
XAC3659	dihydrolipoamide dehydrogenase	<i>lpdA</i>	x	x
XAC3661	dihydrolipoamide acetyltransferase	<i>phdB</i>	x	x
XAC4132	6-phytase; K01093 4-phytase / acid phosphatase	<i>appA</i>	x	-
XAC4150	nodulation protein	<i>nodL</i>	-	x
Energy metabolism				
XAC0204*	glutamine synthetase	<i>glnA</i>	x	x
XAC0348	transferase	-	x	x
XAC0724	cytochrome c4	<i>cycA</i>	x	x
XAC1258	cytochrome o ubiquinol oxidase subunit II	<i>cyoA</i>	x	x
XAC1462	carbonic anhydrase	<i>cynT</i>	x	-
XAC1604*	carbonic anhydrase	<i>yadF</i>	x	x
XAC3442	inorganic pyrophosphatase	<i>ppa</i>	x	x
XAC3649	F0F1 ATP synthase subunit beta	<i>atpD</i>	x	x

XAC3650*	uncG; F0F1 ATP synthase subunit gamma	<i>atpG</i>	x	-
XAC3651	F0F1 ATP synthase subunit alpha	<i>atpA</i>	x	x
XAC3652*	F0F1 ATP synthase subunit delta	<i>atpH</i>	x	-
XAC3653*	uncF; F0F1 ATP synthase subunit B	<i>atpF</i>	x	-
XAC3654*	F0F1 ATP synthase subunit C	<i>atpE</i>	x	-
Lipid Metabolism				
XAC0384*	3-oxoacyl-[acyl-carrier protein] reductase	-	x	-
XAC0433*	3-oxoacyl-[ACP] reductase	-	x	-
XAC0833	acyl-CoA thioesterase I	<i>tesA</i>	x	-
XAC1024*	non-hemolytic phospholipase C		x	-
XAC1127*	3-ketoacyl-(acyl-carrier-protein) reductase	<i>fabG</i>	x	-
XAC1128	acyl carrier protein	<i>acpP</i>	x	x
XAC1129	3-oxoacyl-(acyl carrier protein) synthase II	<i>fabF</i>	x	-
XAC1463	phospholipase	-	x	-
XAC2780*	lipoprotein	<i>rlpB</i>	x	x
XAC2885	phospholipase A1	-	x	x
Nucleotide metabolism				
XAC1158	adenylosuccinate synthetase	<i>purA</i>	x	x
XAC2015	nucleoside diphosphate kinase	<i>ndk</i>	x	x
XAC2360	dihydroorotase	<i>pyrC</i>	x	x
XAC2740*	deoxycytidine triphosphate deaminase	<i>dcd</i>	x	x
XAC3345	pyruvate kinase	<i>pykA</i>	x	-
XAC3437	adenylate kinase	<i>adk</i>	x	x
Amino acid metabolism				
XAC0484*	S-adenosylmethionine decarboxylase	<i>speD</i>	x	-
XAC0743	serine hydroxymethyltransferase	<i>glyA</i>	x	x
XAC0813	Methionine adenosyltransferase	<i>metK</i>	x	x
XAC0927	branched-chain amino acid aminotransferase	<i>ilvE</i>	x	x
XAC1336	5'-methylthioadenosine phosphorylase	<i>deoD</i>	-	x
XAC1533	dihydrolipoamide dehydrogenase	<i>ldp</i>	x	x
XAC1637	histidine ammonia-lyase	<i>hutH</i>	x	x
XAC2547	dihydrodipicolinate synthetase	<i>dapA</i>	x	x
XAC2932	protease	<i>pfpI</i>	x	-
XAC3309	aminopeptidase	-	x	x
XAC3341	cysteine synthase	<i>cysK</i>	x	x
XAC3556*	aminopeptidase AI	<i>pepA</i>	x	x
XAC3602*	cystathionine gamma-lyase-like protein	<i>metB</i>	x	x
XAC3628*	cystein synthase	<i>cysM</i>	-	x
XAC3924*	spermidine synthase	<i>speE</i>	x	x
XAC3987	leucine aminopeptidase	-	x	-
XAC4009	arginase	<i>argI</i>	-	x
XAC4187	2-hydroxyhepta-2,4-diene-1,7-dioate isomerase	-	x	x
Glycan biosynthesis and Metabolism				
XAC0662	Membrane bound lytic transglycolase (CDD)	<i>mltB</i>	x	-

XAC1466*	peptidoglycan-associated outer membrane lipoprotein	<i>pcp</i>	x	-
XAC1728*	lipoprotein nlpD	<i>nlpD</i>	x	-
XAC2585	GumB protein	<i>gumB</i>	x	x
XAC3225	transglycosylase	<i>mltB</i>	x	x
Cofactors and vitamin metabolism				
XAC0158	L-fucose dehydrogenase	-	x	x
XAC0750	6,7-dimethyl-8-ribityllumazine synthase	<i>ribH</i>	x	-
XAC2035	non-heme chloroperoxidase;	<i>cpoF</i>	x	x
XAC4040*	delta-aminolevulinic acid dehydratase	<i>hemB</i>	x	x
XAC4109	coproporphyrinogen III oxidase	<i>hemF</i>	x	-
XAC4302*	GTP cyclohydrolase I	<i>folE</i>	x	-
Terpenoid backbone biosynthesis				
XAC1348*	acetoacetyl-CoA thiolase	<i>atoB</i>	x	x
XAC3583*	dTDP-4-dehydrorhamnose 3,5-epimerase	<i>rmlC</i>	x	x
Xenobiotics Biodegradation and Metabolism				
XAC0125*	aromatic amino acid aminotransferase	<i>tyrB</i>	-	x
XAC2736*	carboxymethylenebutenolidase	-	x	-
XAC3162	beta lactamase	<i>bla</i>	x	x
XAC4342	toluene tolerance protein	<i>yrbC</i>	x	x
RNA polymerase and Transcription				
XAC0996*	DNA-directed RNA polymerase subunit alpha	<i>rpoA</i>	x	x
XAC1643	poly(hydroxyalcanoate) granule associated protein	<i>phaF</i>	x	x
XAC2358	DnaK supressor	<i>dksA</i>	x	x
Translation and Ribosome				
XAC0957	elongation factor Tu	<i>tuf</i>	x	x
XAC0951	50S ribosomal protein L25	<i>rplY</i>	-	x
XAC0962	50S ribosomal protein L1	<i>rplA</i>	-	x
XAC0970	elongation factor Tu	<i>tuf</i>	x	x
XAC0978	30S ribosomal protein S3	<i>rpsC</i>	-	x
XAC0987	50S ribosomal protein L6	<i>rplF</i>	-	x
XAC1418	ribosome recycling factor	<i>frr</i>	x	-
XAC2380	elongation factor P	<i>efp</i>	x	-
XAC3392*	translation initiation inhibitor	<i>yjgF</i>	x	-
XAC4229	starvation sensing protein	<i>rspA</i>	x	x
DNA Replication				
XAC0027*	plasmid stable protein K	-	x	-

XAC0120	TldD protein	<i>tldD</i>	x	x
XAC0121	TldD protein		x	x
XAC2905	single-stranded DNA-binding protein	<i>hupB</i>	x	x
XAC3058*	histone H1	-	x	-
XAC3123	DNA-binding-like protein	-	x	-
XAC3356*	endonuclease	-	x	-
XAC3979	histone H1-like protein	<i>bpH1</i>	x	-

Folding and Sort degradation

XAC0023*	carboxyl-terminal protease	<i>ctp</i>	x	x
XAC0541*	co-chaperonin GroES	<i>groES</i>	x	-
XAC0542	Chaperonina 60 kDa	<i>groEL</i>	x	x
XAC0637	ATP-dependent protease peptidase subunit;	<i>hslV</i>	x	x
XAC0865	peptidyl-prolyl cis-trans isomerase	<i>surA</i>	x	-
XAC1585	peptidyl-prolyl cis-trans isomerase	<i>ppiB</i>	x	-
XAC1078*	ATP-dependent Clp protease proteolytic subunit	<i>clpP</i>	x	x
XAC1085	peptidyl-prolyl cis-trans isomerase	<i>ppiD</i>	x	-
XAC1456	peptidyl-dipeptidase	<i>dcp</i>	x	-
XAC1550	FKBP-type peptidyl-prolyl cis-trans isomerase	<i>fkpA</i>	x	-
XAC3550	disulfide isomerase	<i>dsbC</i>	-	-

Membrane Transport

XAC0008*	TonB protein	<i>tonB</i>	-	x
XAC0009	biopolymer transport ExbB protein	<i>exbB</i>	x	x
XAC0011*	biopolymer transport ExbD2 protein	<i>exbD2</i>	x	-
XAC0019	outer membrane protein	<i>ompP1</i>	x	x
XAC0074	TonB-dependent receptor	<i>cirA</i>	x	-
XAC0176	ferrityoverdine receptor	<i>fpvA</i>	x	x
XAC0221	preprotein translocase subunit SecB	<i>secB</i>	x	-
XAC0291	Oar protein	<i>oar</i>	-	x
XAC0473*	membrane protein	-	x	-
XAC0693	TonB-dependent receptor	<i>fecA</i>	x	-
XAC0716	TonB-dependent receptor	<i>fyuA</i>	x	x
XAC0823	outer membrane hemin receptor	<i>phuR</i>	-	x
XAC0829	NitT/TauT family transport system substrate-binding protein	<i>nit/ tau</i>	-	x
XAC0849	sulfonate-binding protein	<i>ssuA</i>	-	x
XAC0852	TonB-dependent receptor	<i>tonB</i>	-	x
XAC0866	LPS-assembly protein	<i>ostA</i>	x	x
XAC0947	outer membrane lipoprotein LolB	<i>lolB</i>	x	-
XAC1012	outer membrane protein	<i>mopB</i>	x	x
XAC1017	Sulfate binding protein	<i>sbp</i>	x	x
XAC1023	TonB-dependent receptor	<i>fecA</i>	x	-
XAC1113	outer membrane protein Slp	<i>slp</i>	x	x
XAC1143*	TonB-dependent receptor	<i>fyuA</i>	x	x
XAC1149	bacterioferritin	-	x	-

XAC1156*	integral membrane proteinase subunit	<i>hflC</i>	x	x
XAC1276	TonB-dependent receptor	<i>fyuA</i>	x	-
XAC1347	outer membrane protein	-	x	x
XAC1413	outer membrane antigen	<i>oma</i>	x	x
XAC1435	iron receptor complex outer membrane receptor protein	<i>fhuA</i>	-	x
XAC1479	OmpA family protein	-	x	x
XAC1578	phosphate-binding protein	<i>phox</i>	x	-
XAC2151	YapH protein	<i>yapH</i>	x	x
XAC2185	ferrichrome-iron receptor	<i>fhuA</i>	-	x
XAC2531	TonB-dependent receptor	<i>btuB</i>	-	x
XAC2600	TonB-dependent receptor	<i>btuB</i>	x	-
XAC2620	virB9	<i>virB9</i>	-	x
XAC2672	Oar protein	<i>oar</i>	x	x
XAC2742	TonB-dependent receptor	<i>btuB</i>	x	x
XAC2743	Oar protein	<i>oar</i>	x	x
XAC2772	outer membrane protein	<i>bp26</i>	x	x
XAC2773*	outer membrane protein	<i>bp26</i>	-	x
XAC2830	TonB-dependent receptor	<i>fhuA</i>	x	x
XAC2884	accessory protein	<i>plaS</i>	-	x
XAC3050	TonB-dependent receptor	<i>btuB</i>	x	x
XAC3141	outer membrane protein P6	<i>ompP6</i>	x	x
XAC3142	translocation protein TolB;	<i>tolB</i>	x	x
XAC3158	TonB-dependent receptor	<i>fhuA</i>	x	-
XAC3166	ferric enterobactin receptor	<i>bfeA</i>	x	x
XAC3168	ferric enterobactin receptor	<i>bfeA</i>	x	x
XAC3176	citrate-dependent iron transporter	<i>fecA</i>	-	x
XAC3201	TonB-dependent receptor	<i>fyuA</i>	-	x
XAC3207	ferric enterobactin receptor	<i>bfeA</i>	x	x
XAC3218	competence lipoprotein	<i>comL</i>	x	x
XAC3300	esterase-lipase	<i>estA</i>	x	x
XAC3308	large-conductance mechanosensitive channel	<i>mscL</i>	x	-
XAC3311	TonB-dependent receptor	<i>iroN</i>	x	-
XAC3334	TonB-dependent receptor	<i>fecA</i>	x	x
XAC3354	outer membrane protein W	<i>ompW</i>	x	x
XAC3355	outer membrane protein 21	<i>omp21</i>	-	x
XAC3358	Molybdate-binding protein	<i>modA</i>	x	-
XAC3370	ferric iron uptake outer membrane protein	<i>fhuE</i>	x	x
XAC3444	TonB-dependent receptor	<i>btuB</i>	x	x
XAC3463	TolC	<i>tolC</i>	x	x
XAC3472	polyphosphate-selective porin O	<i>oprO</i>	x	x
XAC3475*	molybdate-binding protein	<i>modA</i>	x	-
XAC3498	ferric iron uptake outer membrane protein	<i>fhuE</i>	x	x
XAC3534	general secretion pathway protein D	<i>xpsD</i>	x	-
XAC3613	TonB-dependent receptor	<i>btuB</i>	-	x
XAC3664	outer membrane protein	<i>ompW</i>	x	x
XAC4048	TonB-dependent receptor	<i>iroN</i>	x	x
XAC4162	cation efflux system protein	<i>czcC</i>	x	-

XAC4273	OmpA-related protein	-	X	X
XAC4274	OmpA-related protein	-	X	X
XAC4344	lipoprotein	<i>vacJ</i>	X	X
XAC4368	TonB-dependent receptor	<i>fecA</i>	X	-
Two-component system				
XAC0834*	two-component system regulatory protein	<i>colR</i>	X	-
XAC4023	two-component system regulatory protein	<i>phoP</i>	X	X
XAC4369*	phosphatase	<i>phoC</i>	X	-
Cell Motility and Attachment				
XAC0108*	AtsE protein	<i>atsE</i>	X	-
XAC2017	type IV pilus assembly protein pilF	<i>pilF</i>	X	X
XAC3241*	type IV pilus assembly protein PilA	<i>fimA</i>	X	-
Cell cycle				
XAC1155	Integral membrane protease	<i>hflK</i>	X	-
XAC1224*	cell division topological specificity factor MinE	<i>minE</i>	X	-
XAC1321	periplasmic protease	<i>mucD</i>	X	X
Heat shock, osmotic and oxidative stress				
XAC0209	superoxide dismutase like protein	<i>yojM</i>	X	X
XAC0210	superoxide dismutase	<i>sodC2</i>	X	X
XAC0493	bacterioferritin	<i>bfr</i>	X	X
XAC0723	disulfide oxidoreductase	<i>dsbA</i>	X	X
XAC0907	alkyl hydroperoxide reductase subunit C	<i>ahpC</i>	X	X
XAC1005*	peptidyl-prolyl cis-trans isomerase	<i>ppiB</i>	X	-
XAC1211*	catalase	<i>katE</i>	X	X
XAC1438*	Bacterioferritin	-	X	-
XAC1521	heat shock protein GrpE	<i>grpE</i>	X	-
XAC2386	superoxidase dismutase	<i>sodM</i>	X	X
XAC2454*	stringent starvation protein A	<i>sspA</i>	X	X
XAC2783	thioredoxin	<i>trx</i>	X	X
XAC2915*	osmotically inducible protein	<i>osmC</i>	X	-
Hypothetical/No classification				
XAC0006	conserved hypothetical protein		X	X
XAC0139*	conserved hypothetical protein		X	-
XAC0177*	conserved hypothetical protein		X	-
XAC0223	conserved hypothetical protein		X	X
XAC0272	conserved hypothetical protein		X	X
XAC0292	conserved hypothetical protein		X	X
XAC0338	conserved hypothetical protein		X	-
XAC0450*	conserved hypothetical protein		X	-
XAC0555	conserved hypothetical protein		X	X
XAC0603	conserved hypothetical protein		X	X

XAC0665	conserved hypothetical protein	X	X
XAC0677	conserved hypothetical protein	X	X
XAC0683*	conserved hypothetical protein	X	-
XAC0765	conserved hypothetical protein	X	X
XAC0836	conserved hypothetical protein	X	-
XAC0838	conserved hypothetical protein	X	X
XAC1045*	conserved hypothetical protein	X	-
XAC1230	conserved hypothetical protein	X	X
XAC1236*	conserved hypothetical protein	X	X
XAC1238	conserved hypothetical protein	X	-
XAC1244	conserved hypothetical protein	X	X
XAC1262	conserved hypothetical protein	X	-
XAC1278*	conserved hypothetical protein	X	-
XAC1302*	conserved hypothetical protein	X	X
XAC1344	conserved hypothetical protein	X	X
XAC1346*	conserved hypothetical protein	X	-
XAC1364*	conserved hypothetical protein	X	-
XAC1371*	conserved hypothetical protein	X	-
XAC1397	conserved hypothetical protein	X	X
XAC1554	conserved hypothetical protein	X	X
XAC1761	conserved hypothetical protein	X	X
XAC2020	conserved hypothetical protein	X	X
XAC2083	conserved hypothetical protein	X	X
XAC2155*	conserved hypothetical protein	X	-
XAC2312	conserved hypothetical protein	X	-
XAC2319*	conserved hypothetical protein	X	-
XAC2491*	conserved hypothetical protein	X	-
XAC2525*	conserved hypothetical protein	X	-
XAC2946	conserved hypothetical protein	-	X
XAC2958	conserved hypothetical protein	X	-
XAC2968	conserved hypothetical protein	-	X
XAC3032	conserved hypothetical protein	X	-
XAC3037	conserved hypothetical protein	X	-
XAC3108*	conserved hypothetical protein	X	-
XAC3140	conserved hypothetical protein	X	-
XAC3439*	conserved hypothetical protein	X	-
XAC3525	conserved hypothetical protein	X	X
XAC3657	conserved hypothetical protein	X	X
XAC3703*	conserved hypothetical protein	X	-
XAC3725	conserved hypothetical protein	X	X
XAC3726	conserved hypothetical protein	X	X
XAC3746*	conserved hypothetical protein	X	-
XAC3802	conserved hypothetical protein	X	X
XAC3844	conserved hypothetical protein	X	X
XAC3904*	conserved hypothetical protein	X	-
XAC3966	conserved hypothetical protein	X	-
XAC3972	conserved hypothetical protein	X	X
XAC3981*	conserved hypothetical protein	X	-

XAC4007*	conserved hypothetical protein	x	-
XAC4042*	conserved hypothetical protein	x	-
XAC4131	conserved hypothetical protein	x	-
XAC4178	conserved hypothetical protein	x	x
XAC4204*	conserved hypothetical protein	x	-
XAC4219	conserved hypothetical protein	x	-

Table S5. List of metabolites and statistics identified in *X. citri* and *Xac::pstS* in A and A+Pi media.

Metabolites are grouped in two blocks according the levels identified in the metabolome as shown in the heat map based on Euclidean distances. Metabolites and values mark as blue and black bold refer respectively, to differences in A+Pi and A.

Metabolites	<i>Xac::pstS</i>				<i>X. citri</i>			
	A medium		A+Pi medium		A medium		A+Pi medium	
	Average	SD	Average	SD	Average	SD	Average	SD
Valine	100,95		88,05	9,77	84,50	12,90	69,45	46,25
Cytidine	32,95		21,95	10,37	22,20	7,43	19,20	17,97
Glutamine	1222,40	202,42	875,00	163,83	999,40	149,09	712,75	455,62
Trehalose	24249,15	3779,36	24562,45	3728,23	16695,60	3076,80	24876,10	14282,26
2-Aminobutyrate	11,25	2,39	10,20	1,38	7,70	2,62	8,10	4,30
Adenine	11,70	8,12	17,75	6,50	7,50	2,15	9,25	4,90
Asparagine	67,25	37,08	64,05	34,51	49,70	13,78	26,80	21,78
2-Amino adipate	627,75	99,14	119,55	21,19	95,80	14,17	0,00	14,90
Methanol	208,75	69,69	44,75	4,59	39,00	5,97	40,60	30,16
Pyridoxine	11,75	1,91	6,40	2,23	5,60	1,14	6,40	2,21
Glycine	320,70	62,53	169,70	24,12	189,30	60,13	168,20	129,30
Dihydroxyacetone	24,20	5,42	11,80	3,06	12,70	1,80	5,10	12,63
Phenylalanine	11,45	1,42	9,05	1,38	5,80	1,98	5,90	2,93
Ethanol	40,70	31,75	28,85	2,69	51,00	17,31	20,25	17,16
Xanthosine	5,75	2,82	1,85	1,33	3,10	0,85	2,60	1,19
UDP-galactose	19,00	12,93	11,80	1,93	15,80	3,15	9,05	5,46
UDP-glucose	14,45	17,66	6,60	3,88	9,50	1,95	8,30	4,46
Uracil	64,25	14,83	30,35	6,04	55,20	18,91	31,65	13,28
Formate	4671,25	1998,81	1085,35	312,37	3343,30	725,78	1572,15	583,12
Dimethylamine	17,70	3,55	5,10	1,01	11,90	1,72	3,30	2,00
Uridine	150,35	37,56	38,20	17,09	100,20	41,52	29,80	21,53
Guanosine	82,65	20,61	21,70	10,10	48,70	19,65	23,15	13,63
Thymidine	24,70	7,22	0,00	0,00	9,30	4,91	1,80	1,54
Acetate	1005,75	301,67	314,10	108,48	423,10	165,21	286,60	153,75
Ornithine	212,70	35,35	42,10	13,08	77,90	48,79	41,65	28,99
Lysine	385,10	62,70	122,95	14,19	182,20	54,54	79,15	59,06
Tyrosine	21,20	1,50	9,25	1,20	14,70	4,32	6,70	3,69
Glutamate	7782,60	1189,20	1225,10	188,93	6671,30	1310,96	696,00	334,90
Aspartate	481,75	29,71	86,00	24,09	260,00	114,34	42,80	29,92
Glutathione	277,60	50,46	41,25	16,86	292,20	141,58	15,50	10,62
Niacinamide	16,55	2,51	5,20	2,49	21,80	9,20	5,55	3,46
Glucose	19490,75	3401,31	6085,75	1551,78	19945,5	2577,92	6627,80	5623,04

Block 2

					0			
Choline	22,55	3,58	11,90	2,35	20,60	4,19	8,90	5,55
Fumarate	4,85	1,68	3,85	0,39	3,80	2,81	6,05	2,47
Oxypurinol	3,70	65,41	52,90	45,95	0,00	0,00	35,20	279,83
Succinate	90,70	8,95	151,75	33,08	152,30	34,02	311,10	178,85
Propionate	8,35	2,63	5,85	0,95	7,70	3,37	4,50	3,15
3-Hydroxyisobutyrate	5,55	1,00	4,90	1,11	8,00	1,95	4,65	2,53
O-Phosphocholine	9,40	3,61	9,15	2,48	13,00	3,46	9,20	5,68
ATP	10,70	1,84	17,50	8,12	21,90	4,32	12,50	3,37
Methylhistidine	3,30	0,85	7,35	0,51	7,10	1,46	4,75	2,35
Leucine	37,25	3,50	47,00	6,16	27,80	6,56	33,35	18,51
Lactate	75,95	28,15	115,15	20,26	69,20	21,28	74,00	45,19
Pyruvate	36,30	10,51	57,20	7,91	34,90	6,57	37,15	26,57
Betaine	81,90	13,27	219,95	30,54	47,20	5,48	117,50	67,40
3-Hydroxybutyrate	32,85	7,05	89,75	15,97	18,10	2,07	37,15	24,51
Methylsuccinate	3,45	1,18	13,05	1,52	3,80	1,57	4,75	3,01
Histidine	39,90	5,36	127,75	15,78	14,70	4,53	83,00	49,25
AMP	0,00	0,00	89,70	35,67	0,00	0,00	74,30	30,70
Malate	83,40	34,89	136,75	24,69	84,10	26,04	149,85	65,24
NADP+	0,00	0,00	20,40	3,10	0,00	0,00	20,95	11,94
4-Hydroxybutyrate	0,00	0,00	147,75	21,02	62,20	17,94	162,95	82,59
NAD+	32,15	9,64	167,45	26,09	82,60	13,30	130,85	83,37
dTTP	47,05	7,37	116,85	20,97	41,30	4,98	106,65	69,99
Alanine	308,65	57,38	607,20	127,65	213,60	52,02	623,10	403,04
Ethanolamine	117,30	33,09	354,75	39,87	90,80	22,74	209,85	178,38
Isoleucine	20,00	2,86	35,10	4,49	17,90	4,26	26,75	17,43

Construction of the interactome maps of *X. citri* and *Xac::pstS*

The interactome maps of the strains were built based on the proteome data from *X. citri* wild type (Pegos et al, 2014a) and mutant strain (Table S1, Supplementary material) and metabolome data (Table S4, Supplementary material). The dataset was integrated in networks using the Integrate Interactome System Platform (IIS) (Carazolle et al, 2014), developed at the Brazilian Biosciences National Laboratory (LNBio), Brazil. Once *X. citri* does not present enough information related to the metabolic processes and protein-protein interactions on databases of system biology, the interaction map was built based on orthologues of the identified proteins. In this case, we performed a stringent blast available in the annotation module of IIS, which used *X. citri* as an input to search orthologues in the *E. coli* proteins. As criteria for choice of the proteins we applied the fold change in the data obtained from A and A+Pi media. The network of interaction highlights the pathways and processes activated on *X. citri*. The following parameters were used for network construction: first neighbor deleted first node, expression cutoff of 2 and -2, *Escherichia coli* K12 as organism. The enriched biological processes from KEGG pathway database were calculated in each network using hypergeometric distribution. Cytoscape v.2.8.3 platform (Shannon et al, 2003) was used to visualize the interactions. The final map was built using all 57 identified metabolites and 36% of proteins from proteome dataset.

Statistical Analysis

The statistical analysis applied to proteome data was performed using unpaired t-test with $p < 0,05$ on scaffold software based on normalized spectral counts values. For analysis of the proteome and metabolome from wild type and mutant strains, we also used the principal component analysis (PCA) on Metaboloanalyst online server (Xia et al, 2012).

3. Results and Discussion

The effect of phosphate in the proteome of *Xac::pstS*

The importance of phosphate for *X. citri* proteome was previously characterized in excess and limitation of the ion (Pegos et al, 2014a). PstS and PhoX, which origin arises from gene duplication, are both responsible for phosphate uptake in depletion of the ion. The deletion of *pstS* gene in *Xac::pstS* mutant strain had no effect on in vitro growth, production of xanthan gum, phenotype of the citrus canker in *Citrus sinensis* leaves, and in the phosphate transport, strongly suggesting that PhoX was capable to compensate the effects of the PstS absence in depletion of phosphate. In contrast, the transport in A+Pi medium (excess of phosphate) was not affected indicating that *pstS* deletion induced a constitutive expression of the system and that PstS might have a regulatory function (Pegos et al., in prep), as suggested by other authors (Spira et al, 2010).

In order to verify if *pstS* deletion affected the proteome of *X. citri* and the bacterium physiology, in this work we performed proteomic analysis of *Xac::pstS* in the same conditions described before: excess (A+Pi medium) and depletion (A medium) of phosphate. Proteins identified in the proteome of *Xac::pstS* were categorized based on their functions following the pathway available on KEGG database (Figure 1). In total we identified 280 in A and A+Pi media (Table S2, Supplementary material).

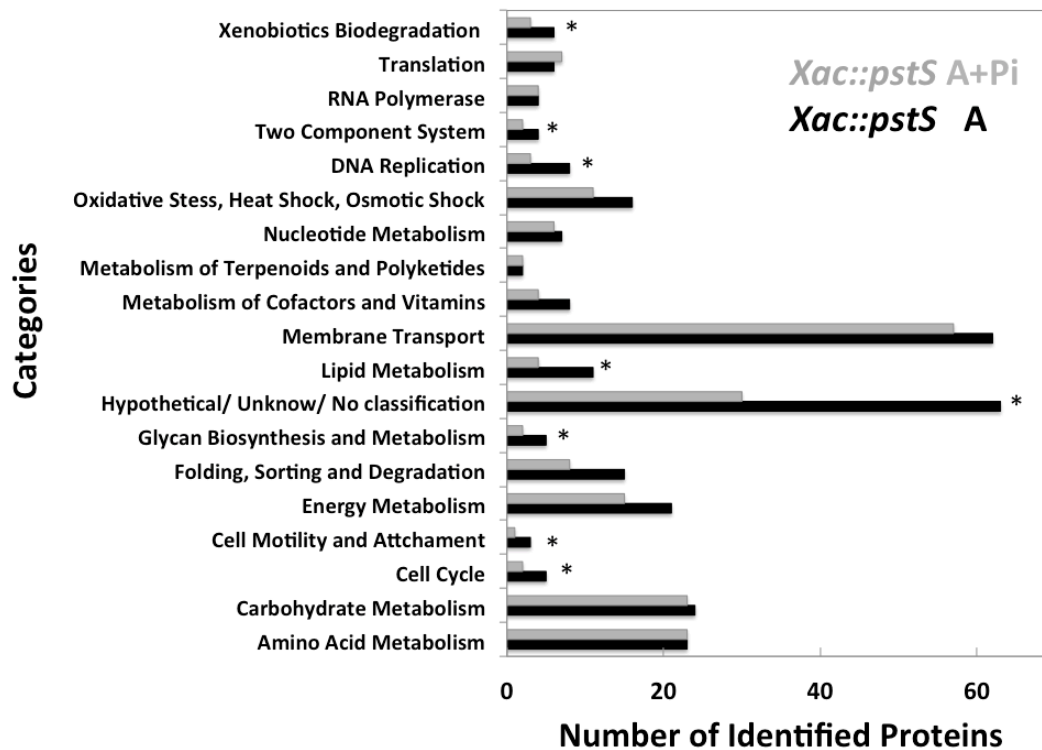


Figure 1. Proteins identified in *Xac::pstS* proteome classified in categories according the KEGG server.

This dataset correspond to 280 proteins of primary metabolism identified considering stringent peptide parameters on Mascot and Scaffold Q+ softwares. The FRD (False Rate Discovery) of this dataset was 0.1%.

Asterisks (*) are used to evidence the significant changes in proteomes of A and A+P_i.

The first analysis obtained from this experiment was that starvation phosphate conditions established in A medium significantly increased the number of proteins identified in xenobiotics degradation, two-component system, DNA replication, lipid metabolism, glycan biosynthesis and metabolism, cell motility and attachment, cell cycle and hypothetical proteins (Figure 1, marked with asterisk). In comparison with the wild type results in the same media, the phosphate depletion did not induced significant differences in the number of proteins identified in the categories (Pegos et al, 2014a), which is evident in the mutant strain suggesting that this is an effect of the PstS absence. Still, *Xac::pstS* proteome has 77 proteins not identified in the proteome of the wild type strain, suggesting that these might be related to the PstS effect on the cell. Interestingly, we also observed that 104 were exclusively found in A medium and 30 exclusively from A+Pi medium, evidencing the influence of the phosphate in the mutant bacterium metabolism. The Table 1 shows a list of all exclusive proteins identified after the *t*-test analysis where 74 and 14 were significantly altered. Again this result evidences that the phosphate depletion in *Xac::pstS* has a enhanced effect. As expected, PstS was not identified in this proteome but PhoX showed a spectral count of 67 only in A medium (Table 1). This data helps to understand why the *Xac::pstS* strain presented similar behavior when compared to the wild type strain in experiments that evaluated the in vitro growth, production of gum, and transport of phosphate. PhoX is capable to bind phosphate and showed quite similar structure to PstS (Pegos et al, in prep).

Moreover, other proteins exclusively identified in A medium were the two alkaline phosphatases (XAC1792 and XAC2759) (Table 1, bold) that are members of the Pho regulon (Wanner et al, 1993). The alkaline phosphatase PhoA (XAC2759) is considered a biological marker of Pho regulon activation (Torriani, 1990). Additionally we identified a periplasmic acid phosphatase AppA (XAC4132) that is responsible for the cleavage of phosphor organic compounds (Wanner et al, 1996). Other proteins belonging to the central metabolism for energy production were identified with expressive spectra. Specifically we detach two

Table 1. List of proteins of *Xac::pstS* proteome exclusively identified in media A and A+Pi that showed statistical significance after *t*-test ($p < 0.05$). Proteins in bold belong to the *X. citri* Pho regulon and those showed with asterisk were only identified in the *Xac::pstS* proteome but not in the wild type (Pegos et al., 2014).

KEGG ID	Protein Function	Gene name	Quantitative Value (normalized total spectra count)
<i>A medium</i>			
XAC0007	Conserved hypothetical protein	-	50,25
XAC0008*	Hypothetical protein	-	3,65
XAC0011*	Biopolymer Transport ExbD2 Protein	<i>exbD2</i>	4,95
XAC0074	TonB-dependent receptor	<i>cirA</i>	39,48
XAC0108	AtsE	<i>atsE</i>	2,46
XAC0139*	Conserved hypothetical protein	-	3,64
XAC0292	Conserved hypothetical protein	-	11,10
XAC0484*	S-adenosyl methionine decarboxylase proenzyme	<i>speD</i>	3,98
XAC0662	Membrane-bound lytic transglycosylase	<i>mltB</i>	9,57
XAC0682	Conserved hypothetical protein	-	21,60
XAC0693	TonB-dependent receptor	<i>fecA</i>	18,98
XAC0750	6,7-dimethyl-8-ribityllumazine synthase	<i>ribH</i>	3,10
XAC0833	Acyl-Coa thioesterase I	<i>tesA</i>	9,20
XAC0836	Conserved hypothetical protein	-	9,92
XAC1005*	Peptidyl-prolyl cis-trans isomerase	<i>ppiB</i>	3,36
XAC1024*	Non-hemolytic phospholipase C	-	11,22
XAC1045*	Conserved hypothetical protein	-	1,81
XAC1127*	3-oxoacyl-[ACP] reductase	<i>fabG</i>	4,77
XAC1149	Bacterioferritin	-	6,21
XAC1224*	Cell division topological specificity factor	<i>minE</i>	2,13
XAC1262	Carbonic anhydrase	<i>cynt</i>	10,38
XAC1276	Tonb-dependent receptor	<i>fyuA</i>	14,30
XAC1278*	Conserved hypothetical protein	-	3,65
XAC1346*	Conserved hypothetical protein	-	3,00
XAC1364*	Conserved hypothetical protein	-	9,28
XAC1371*	Conserved hypothetical protein	-	6,76

XAC1410	(3r)-hydroxymyristoyl ACP dehydrase	<i>fabZ</i>	5,85
XAC1438*	Bacterioferritin	<i>brf</i>	7,35
XAC1456*	Peptidyl-dipeptidase	<i>dcp</i>	3,93
XAC1516	Outer membrane protein	<i>smpA</i>	8,63
XAC1521*	Heat Shock Protein GrpE	<i>grpE</i>	1,81
XAC1550	FKBP-type peptidyl-prolyl cis-trans isomerase	<i>fkpA</i>	1,48
XAC1578	Phosphate binding protein	<i>phoX</i>	67,16
XAC1585	Peptidyl-prolyl cis-trans isomerase	<i>fpkA</i>	43,06
XAC1728*	Lipoprotein	<i>nlpD</i>	5,90
XAC1792	Alkaline phosphatase	<i>phoX</i>	4,20
XAC2077*	Succinate dehydrogenase flavoprotein subunit	<i>sdhA</i>	4,07
XAC2078*	Succinate dehydrogenase iron-sulfur protein	<i>sdhB</i>	2,79
XAC2135	Hypothetical protein	-	3,40
XAC2155*	Conserved hypothetical protein	-	4,95
XAC2319	Conserved hypothetical protein	-	5,18
XAC2525	Conserved hypothetical protein	-	8,90
XAC2526	Lipopolysaccharide synthesis enzyme	<i>kdtB</i>	3,94
XAC2736*	Carboxymethylenebutenolidase	-	6,28
XAC2759	Alkaline phosphatase	<i>phoA</i>	4,56
XAC2915*	Osmotically inducible protein	<i>osmC</i>	11,95
XAC2932	Protease	<i>pfpI</i>	36,23
XAC3032	Conserved hypothetical protein	-	2,22
XAC3037	Hydrolase	-	8,82
XAC3123	DNA-binding related protein	-	12,89
XAC3140	Conserved hypothetical protein	-	6,11
XAC3158	TonB-dependent receptor	<i>fhuA</i>	32,18
XAC3241*	Fimbrillin – type IV	<i>fimA</i>	2,77
XAC3308	Large-conductance mechanosensitive channel	<i>mscL</i>	4,30
XAC3358	Molybdate-binding periplasmic protein; permease	<i>modA</i>	11,10
XAC3392*	Translation initiation inhibitor	<i>yjgF</i>	10,45
XAC3439*	Conserved hypothetical protein	-	4,32
XAC3534	General secretion pathway protein D	<i>xpdS</i>	12,94
XAC3652*	ATP synthase delta chain	<i>uncH</i>	4,25
XAC3653	ATP synthase B chain	<i>atpB</i>	1,81
XAC3654*	ATP synthase C chain	<i>uncE</i>	3,39
XAC3703*	Conserved hypothetical protein	-	2,15
XAC3746*	Conserved hypothetical protein	-	8,76
XAC3966	Conserved hypothetical protein	-	38,82
XAC3981	Conserved hypothetical protein	-	12,27
XAC4007*	Conserved hypothetical protein	<i>csbD</i>	2,41
XAC4042*	Conserved hypothetical protein	-	2,12
XAC4131	Conserved hypothetical protein	-	29,20
XAC4132	Acid phosphatase	<i>appA</i>	3,12
XAC4162	Cation efflux system protein	<i>czcC</i>	16,48

XAC4219	Conserved hypothetical protein	-	6,44
XAC4368	TonB-dependent receptor	<i>fecA</i>	50,45
XAC4369*	Phosphatase precursor	<i>phoC</i>	2,49

A+Pi
Medium

XAC0291	Oar protein	<i>oar</i>	36,67
XAC0823	Outer membrane hemin receptor	<i>phuR</i>	89,57
XAC0829	ABC transporter substrate binding protein	<i>tauA</i>	25,15
XAC1336	Purine nucleoside phosphorylase	<i>deoD</i>	2,60
XAC1435	Iron receptor	<i>fhuA</i>	7,01
XAC2185	Ferrichrome-iron receptor	<i>fhuA</i>	4,78
XAC2946	Conserved hypothetical protein	-	16,22
XAC2968	Conserved hypothetical protein	-	15,40
XAC3169	BfeA gene product	<i>bfeA</i>	6,26
XAC3176	Citrate-dependent iron transporter	<i>fecA</i>	1,75
XAC3201	TonB-dependent receptor	<i>fyuA</i>	5,27
XAC3613	TonB-dependent receptor	<i>btuB</i>	13,78
XAC3628	Cysteine synthase	<i>cysM</i>	3,08
XAC4150	Nodulation protein	<i>nodL</i>	3,19

succinate dehydrogenases (XAC2077 and XAC2078) from Krebs' cycle, and the chains B (XAC3656), D (XAC3652) and C (XAC3654) of the ATP synthase (Table 1).

It is interesting to notice that the *Xac::pstS* during depletion of phosphate expressed a set of proteins related to adhesion and biofilm formation, which have been demonstrated to be induced in stress conditions (Lamarche et al, 2007). AtsE (XAC0108) is required for bacterial cell attach and starting of the colonization process. A medium stimulated the expression of peptidylprolyl-*cis-trans* isomerases XAC1005, XAC1550 and XAC1585. The biological role of these proteins is control the folding, but recently they were associated to the diffusible signal factor (DSF) synthesis, an elementary small molecule involved in quorum-sensing (Zhao et al, 2011). Considering that quorum sensing occurs on mature biofilm, the hypothesis that phosphate could interfere directly in this process was reinforced by the high levels of expression detected for ExbD2 (XAC0011), a protein responsible for biopolymer transport according to genome annotation information. In *X. citri*, the canker symptoms are completely eliminated when the gene XAC0010, which belongs to the same operon of *exbD2*, is deleted (Yan et al, 2012).

On the other hand, the high phosphate availability on A+Pi medium leads a small number of exclusive proteins being the most part belonging to the processes associated to the membranes, such as transporters (TauA/XAC0829, PhuR/XAC0823, PhuA/XAC1435), TonB receptors (FyuA/XAC3201 and BtuB/XAC3613), OmpA related protein (Oar/XAC0291) (Table 1). Another interesting protein was CysM (XAC3628), a cysteine synthase involved in the sulfur metabolism of *X. citri* that was previously characterized by Moutran and collaborators (*submitted*).

The effect of phosphate in *Xac::pstS* strain

In order to characterize the behavior of proteins that were identified in both media, we calculated the fold change based on spectral counts normalized average from A and A+Pi. Proteins were considered up or down regulated by phosphate when expression levels were increased more than 1.5-fold or decreased more than

0.67-fold according to Crabbé and collaborators (2012). The complete list of data is shown in Table S3 (Supplementary material). The results show a large number of proteins that suffered up regulation by phosphate levels in the mutant strain, when compared to the down-regulated proteins (Table 2). Again, we observed that from the up-regulated proteins a large amount represents the membrane proteins or related (11 from 45) to and that the fold change for these proteins is general is higher than 4.0. We detach two up-regulated members of the Pho regulon, the phosphoglycerate mutase (XAC2874, fold change 10.4) and adenylate kinase (XAC3437, fold change 7.3) (Table 2, in bold). The adenylate kinase is involved in the intracellular phosphate metabolism for cAMP synthesis, a molecule involved on signaling, starvation and bacterial motility (Botsford et al, 1992). On the other hand, the phosphoglycerate mutase is responsible to the conversion of 3-phosphoglycerate into 2-phosphoglycerate during the glycolysis pathway. Moreover, we identified the up-regulation of PilF protein (XAC2017) that is involved in adhesion, transformation, biofilm, motility and other biological processes linked with bacterial pathogenesis (Craig et al, 2004). Similarly, we reported on Table 1 the presence of two other adhesins, AtsE and filbrillin, exclusively identified on A medium, evidencing that the deletion has affected the proteins involved with the processes for colonization. The deletion of *pstS* also affected degradative enzymes such as the periplasmic protease MucD (XAC1321, fold change 8,4) and a cellulase (XAC0030, fold change 2,3). Other important enzymes are related to the protection against reactive oxygen. In general, they are induced when the bacterium prepares itself to resist to the host defense mechanisms. SodM (XAC2386, fold change 2.4) is an important virulence factor since it is considered as *Pathogen-Associated Molecular Patterns* (PAMP) and its sequence is recognized by host receptors after the secretion of extracellular environment (Watt et al, 2006; Austua-Monge et al, 2010).

Table 2. Up and down regulated proteins identified in the *Xac::pstS* proteome in response to phosphate. Fold change values were calculated based on the spectra count of A and A+Pi ($p < 0.05$). Proteins with asterisk (*) are exclusively identified in the proteome of the mutant strain. The two proteins in bold are members of the Pho regulon.

KEGG ID	Protein	Gene name	Fold change
Up-regulated			
XAC1418	ribosome recycling factor	<i>frt</i>	27,7
XAC1643	poly(hydroxyalcanoate) granule associated protein	<i>phaF</i>	14,5
XAC3058	histone H1	-	13,2
XAC2874	phosphoglycerate mutase	<i>gpm</i>	10,4
XAC0542	60 kDa chaperonin	<i>groEL</i>	8,9
XAC3388	citrate synthase	<i>gltA</i>	8,8
XAC1321*	periplasmic protease	<i>mucD</i>	8,4
XAC3437	adenylate kinase	<i>adk</i>	7,3
XAC2672	Oar protein	<i>oar</i>	6,6
XAC1113	outer membrane protein Slp	<i>slp</i>	6,4
XAC3987	leucine aminopeptidase	-	6,3
XAC2454*	stringent starvation protein A	<i>sspA</i>	6,0
XAC3715	conserved hypothetical protein	-	6,0
XAC3664*	outer membrane protein	<i>ompW</i>	5,5
XAC3335	TonB-dependent receptor	<i>fecA</i>	5,4
XAC4178	conserved hypothetical protein	-	5,4
XAC3556*	aminopeptidase A/I	<i>pepA</i>	4,6
XAC1554	conserved hypothetical protein	-	4,6
XAC1413	outer membrane antigen	<i>oma</i>	4,5
XAC3726	conserved hypothetical protein	-	4,5
XAC0716	TonB-dependent receptor	-	4,4
XAC0677	conserved hypothetical protein	-	4,1
XAC3661	dihydrolipoamide acetyltransferase	<i>phdB</i>	3,6
XAC2017	fimbrial biogenesis protein pilF	<i>pilF</i>	3,4
XAC3844	conserved hypothetical protein	-	3,4
XAC1479	OmpA family protein	<i>ompA</i>	3,2
XAC1761	conserved hypothetical protein	-	3,2
XAC1230	conserved hypothetical protein	-	3,1
XAC0006	conserved hypothetical protein	-	3,1
XAC4342	toluene tolerance protein	<i>yrbC</i>	2,9

XAC2020	conserved hypothetical protein	-	2,8
XAC2780*	lipoprotein	<i>rlpB</i>	2,5
XAC2386	superoxidase dismutase	<i>sodM</i>	2,4
XAC1078*	ATP-dependent Clp protease proteolytic subunit	<i>clpP</i>	2,3
XAC4048	TonB-dependent receptor	<i>iroN</i>	2,3
XAC0030	cellulase	<i>egl</i>	2,3
XAC3354	outer membrane protein W	<i>ompW</i>	2,1
XAC0493	bacterioferritin	<i>bfr</i>	2,1
XAC2783*	thioredoxin	<i>trx</i>	2,0
XAC1244	conserved hypothetical protein	-	1,9
XAC4023	two-component system regulatory protein	<i>phoP</i>	1,9
XAC1211*	catalase	<i>katE</i>	1,8
XAC3218	competence lipoprotein	<i>comL</i>	1,8
XAC1534	dihydrolipoamide S-succinyltransferase	<i>sucB</i>	1,6
XAC0907	alkyl hydroperoxide reductase subunit C	<i>ahpC</i>	1,6

Down-regulated

XAC3341	cysteine synthase	<i>cysK</i>	0,1
XAC0176	ferripyoverdine receptor	<i>fpvA</i>	0,1
XAC3355	outer membrane protein	<i>omp21</i>	0,1
XAC0604	trehalase, periplasmic	<i>treA</i>	0,1
XAC3498	outer membrane receptor for ferric iron uptake	<i>fhuE</i>	0,1
XAC2905	single-stranded DNA binding protein	<i>ssb</i>	0,2
XAC0473	membrane protein	-	0,2
XAC0957	elongation factor Tu	<i>tufB</i>	0,2
XAC2742	TonB-dependent receptor	<i>btuB</i>	0,2
XAC0348	transferase	-	0,2
XAC2743	Oar protein	<i>oar</i>	0,3
XAC1344	conserved hypothetical protein	-	0,3
XAC1017	ABC transporter sulfate binding protein	<i>sbp</i>	0,4
XAC2035	non-heme chloroperoxidase	<i>cpoF</i>	0,4
XAC3141	outer membrane protein P6 precursor	<i>ompP6</i>	0,4
XAC3207	ferric enterobactin receptor	<i>bfeA</i>	0,4
XAC3050	TonB-dependent receptor	<i>btuB</i>	0,4
XAC3166	ferric enterobactin receptor	<i>bfeA</i>	0,5
XAC0223	conserved hypothetical protein	-	0,6
XAC3924*	spermidine synthase	<i>speE</i>	0,6
XAC1128	acyl carrier protein	<i>acpP</i>	0,6

In addition the catalase KatE (XAC1211) and Thioredoxin (XAC2783) identified are involved on neutralization of hydrogen peroxides and redox balance (Tondo et al, 2010).

On the other hand, the low phosphate availability culture condition leads mutant *X. citri* reduced the abundance of elongation factor TU (XAC0957) that is involved in protein synthesis; the sulfate binding protein Sbp (XAC1017) from the cognate ABC transporter and cysteine synthase (XAC3341) that are member of same pathway involved in sulfur acquisition and cysteine synthesis in *X. citri* (Moutran et al, submitted). Other proteins were single-strand DNA binding protein (XAC2905) and spermidine synthase (XAC3924), which are involved in prokaryotic recombination process and polyamine synthesis, respectively. Still, we observed down-regulation for the trehalase protease TreA, an enzyme related to osmoprotection of the bacterium under stress (Ruhel et al, 2012).

Altogether, the identification of proteins that suffered regulation by phosphate level suggest the low phosphate availability on *Xac::pstS* mutant evokes a possible activation of processes such as adaptive response, protection against ROS production, DNA recombination, and transport through the membrane that are needed for the establishment of the pathogenesis.

Response to phosphate depletion in the mutant strain compared to the wild type

Since the proteomes of wild type and mutant strains were performed exactly the same way, we compared the effect of *pstS* deletion in the phosphate response, based on the most significant up and down regulated proteins from both proteomes (Table 3). Proteins from *Xac::pstS* and *X. citri* proteomes were classified according

Table 3. Comparison of the response to phosphate in *X. citri* (Pegos et al., 2014) and *Xac::pstS* strains based on up and down regulated proteins. Values of fold change higher than 1.6 and lower than 0.6 indicate up and down regulation, respectively.

KEGG ID	Protein	Gene Name	<i>Xac::pstS</i> (This work)	<i>X. citri</i> (Pegos et al 2014)
<i>Pho Regulon Members</i>				
XAC1577	Phosphate-binding Protein	<i>pstS</i>	-	33,5
XAC1578	Phosphate-binding Protein	<i>phoX</i>	67,16	49,2
XAC1792	Alkaline phosphatase	<i>phoX</i>	4,20	2,5
XAC2759	Alkaline phosphatase	<i>phoA</i>	4,56	19,8
XAC3442	Inorganic pyrophosphatase	<i>ppa</i>	4,67	1,7
XAC4132	Acid phosphatase	<i>appA</i>	3,12	1,3
<i>Metabolism of Energy</i>				
XAC0957	Elongation factor Tu	<i>tuf</i>	0,15	0,33
XAC2077	Succinate dehydrogenase/fumarate reductase chain A	<i>sdhA</i>	4,73	-
XAC2078	Succinate dehydrogenase/fumarate reductase chain B	<i>sdhB</i>	2,79	-
XAC3651	ATP synthase FOF1 subun. alfa	<i>atpA</i>	-	3,2
XAC3652	ATP synthase FOF1 subun. delta	<i>atpH</i>	4,25	-
XAC3653	ATP synthase FOF1 subun. B	<i>atpB</i>	1,8	4,0
XAC3654	ATP synthase FOF1 subun. C	<i>atpE</i>	3,39	-
XAC2874	phosphoglyceromutase	<i>gpmA</i>	10,41	0,7
XAC2077	Succinate dehydrogenase flavoprotein	<i>sdhA</i>	4,07	-
XAC2078	Succinate dehydrogenase flavoprotein	<i>sdhB</i>	2,79	-
<i>Purine Metabolism / DNA replication</i>				
XAC2905	Single-stranded DNA binding protein	<i>ssb</i>	0,15	1,28
XAC3437	Adenylate kinase	<i>adk</i>	7,26	-
<i>Two-component systems</i>				
XAC0204	glutamine synthetase	<i>glnA</i>	1,45	-
XAC0834	two-component system regulatory protein	<i>colR</i>	2,61	-
XAC4023	two-component system regulatory protein	<i>phoP</i>	1,88	1,10
XAC4369	phosphatase	<i>phoC</i>	2,49	-
<i>Attachment and Adhesion</i>				
XAC0108	AtsE	<i>atsE</i>	2,46	-
XAC2017	Fimbrial Biogenesis Protein PilF	<i>pilF</i>	3,4	2,1

XAC2151	YapH Protein	<i>yapH</i>	0,89	6,4
XAC3241	Fimbrillin	<i>fimA</i>	2,77	-
<i>Quorum sensing</i>				
XAC0865	Peptidyl-Prolyl Cis-Trans Isomerase	<i>surA</i>	1,57	1,3
XAC1005	Peptidyl-Prolyl Cis-Trans Isomerase	<i>ppiB</i>	3,36	-
XAC1550	FKBP-Type Peptidyl-Prolyl Cis-Trans Isomerase	<i>fkpA</i>	1,48	0,3
XAC1585	Peptidyl-Prolyl Cis-Trans Isomerase	<i>fpkA</i>	43,06	1,1
<i>Oxidative Response</i>				
XAC2386	Superoxidase Dismutase	<i>sodM</i>	2,4	2,4
XAC2783	Thioredoxin	<i>trx</i>	2.01	2,2
<i>Degradative enzymes</i>				
XAC0030	Cellulase	<i>egl</i>	2,3	0,6
XAC0604	Trehalase, Periplasmic	<i>treA</i>	0,1	0,8
XAC1456	Peptidyl-Dipeptidase	<i>dcp</i>	3,93	0,8
XAC1321	Periplasmic protease	<i>mucD</i>	8,36	0,84
XAC4369	Phosphatase Precursor	<i>phoC</i>	2,49	-
<i>Secretion System</i>				
XAC2620	VirB9	<i>virB9</i>	2,30	3,2
XAC2619	VirB10	<i>virB10</i>	-	3,9
XAC3534	General Secretion Pathway Protein D	<i>xpsD</i>	12,94	4,4
<i>Amino acid metabolism</i>				
XAC0120	TldD	<i>tldD</i>	0,82	0.50
XAC0743	Serine Hydroxymethyltransferase	<i>glyA</i>	0.80	0.50
XAC1211	catalase	<i>katE</i>	1,80	2,01
XAC1204	Alanyl Dipeptidyl Peptidase	-	-	2,00
XAC2959	Phosphoribosylformylglycinamide Cyclo-Ligase	<i>purM</i>	-	0.40
XAC3225	Transglycosylase	<i>mltB</i>	-	0.2
XAC3309	Aminopeptidase	-	-	0.3
XAC3341	Cysteine Synthase	<i>cysK</i>	0,1	0,4
XAC3352	Glyceraldehyde-3-Phosphate Dehydrogenase	<i>gapA</i>	-	0.2
XAC3388	Type II Citrate Synthase	<i>gltA</i>	6,48	3,3
XAC3847	N-Acyl-L-Amino Acid Amidohydrolase	<i>ama</i>	-	0.2
XAC4009	Arginase	<i>argI</i>	-	0.4
<i>Transport Proteins Scavenging</i>				
XAC0008	TonB-dependent receptor	-	0.93	-
XAC0011	Biopolymer Transport ExbD2 Protein	<i>exbD2</i>	4,94	2,1
XAC0473	Membrane protein	-	0,28	-

XAC0823	Outer hemin	<i>phuR</i>	0,01	0,2
XAC1143	TonB-dependent receptor	<i>fyuA</i>	1,12	-
XAC1155	Integral membrane protease subunit	<i>hflK</i>	1,26	0,36
XAC1156	Integral membrane protease subunit	<i>hflC</i>	0,45	-
XAC1466	Peptideglycan associated outer membrane	<i>pcp</i>	1,15	-
XAC1728	Lipoprotein NlpD	<i>nlpD</i>	5,9	2,02
XAC2773	Outer membrane protein	<i>bp26</i>	0,76	-
XAC3334	TonB-dependent receptor	<i>fecA</i>	-	7,6
XAC3613	TonB-dependent receptor	<i>cirA</i>	-	0.1
XAC3201	TonB-dependent receptor	<i>fyuA</i>	0,18	0,45
XAC0829	Substrate-binding protein	<i>tauT/nitT</i>	0,04	0,4
XAC1017	Sulfate-binding protein	<i>sbp</i>	0,36	0,95
XAC3358	Molybdate-binding Protein	<i>modA</i>	11.10	12,4

their biological role and relevance for pathogenesis. First analysis was related to the identified Pho regulon members PhoX, PstS, alkaline and acid phosphatases and the pyrophosphatase that in the proteome of the wild type strain had the expression increased during depletion of phosphate (Table 3). Activation of the Pho regulon was confirmed by the high level of alkaline phosphatase PhoA (fold change = 19.8), but also by the up regulation of *pstS* and *phoX* genes. As expected, PstS was not identified in the mutant strain but PhoX had an additional increasing in the fold change from 49.2 in the wild type to 67.16. This result strongly suggested that PhoX has a compensatory effect in the mutant. In fact, these data are in accordance with the previous functional analysis that tested the effect of PstS absence in in vitro growth and adhesion. In that assays, the *Xac::pstS* showed quite similar behavior when compared to the wild type (Pegos et al, in prep.). Another interesting effect of the *pstS* deletion was observed regarding to the alkaline phosphatases. In the proteome of the wild type, the fold change of these enzymes was increased in depletion of phosphate specially PhoA that had an increasing of 19-fold. In *Xac::pstS* proteome, however, although the enzymes showed an increased in the fold change, it was much lower than in the wild type (Table 3). These data corroborate the hypothesis that in absence of PstS the operon is constitutively regulated (Pegos et al, in prep.).

Still, significant differences were observed in the proteomes related to the succinate dehydrogenases and proteins from the complex ATP synthase. We identified 4 exclusive succinate dehydrogenases in the proteome's mutant and increasing of the fold change of proteins involved in synthesis of ATP indicating that although PhoX production is highly induced in the mutant strain, the PstS absence might affect the metabolism of energy. Significant differences also were identified in proteins from two-component systems, membrane proteins or involved with transport, categories where we identified exclusive proteins in the mutant strain. Although *Xac::pstS* did not show difference in the adhesion assays carried out in polypropylene surfaces when compared to the wild type, the proteome of this strain revealed the presence of two exclusive proteins, AtsE and fimbriin, and increasing of the PilF fold change. Related to the process of

colonization, we also observed an increasing in the fold change of the peptidyl-prolyl cis-trans isomerase involved in quorum sensing and proteins involved with the degradation of polymers.

We showed that *pstS* deletion affected positively the expression of proteins related to important pathways and metabolisms in the cell. However, the proteome of the mutant strain also evidenced similar fold change for SodM and TrX suggesting that the oxidative response mediated by these proteins were not affect by *pstS* deletion, but might be an effect of phosphate starvation. In addition, a large number of proteins involved in amino acid metabolism were not identified in the proteome from mutant strain or did not show significant differences in the fold change values (Table 3).

Metabolome of *X. citri* – influence of phosphate and *pstS* deletion

To associate the protein profile of *X. citri* and its *pstS* mutant with the phosphate levels we carried out a metabolomic analysis of both strains in A and A+P_i media. Three distinct cultures of wild type and mutant strains grown in the both media had the set of metabolites analysed by NMR. The raw data and profile of NMR are shown in Table S4 (Supplementary material). After the identification and quantification of metabolites using Chenomix software 57 metabolites were selected from the extracts of the two strains (Table S5, Supplementary material) even some peaks on the spectrum not allowed profiling and quantification of the metabolites (Figure S1). An exploratory analysis of the metabolites identified on wild type and mutant cultivated on A and A+P_i media was performed using the principal component analysis (PCA) and presented in Figure 2A. The 2D-PCA based on z-score values showed the distributions of the metabolites in two well-defined groups that represent (i) presence (A+P_i, cyan and green circles) or (ii) absence of phosphate (red and blue circles), independently of the mutation. Two mainly groups separating A and A+P_i media were observed showed that the phosphate concentration is the mainly biological

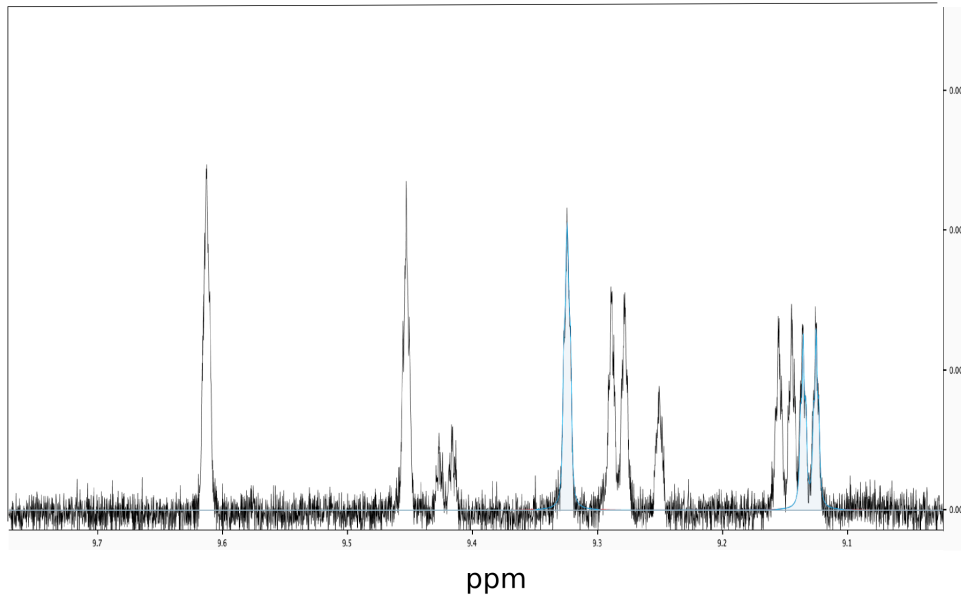
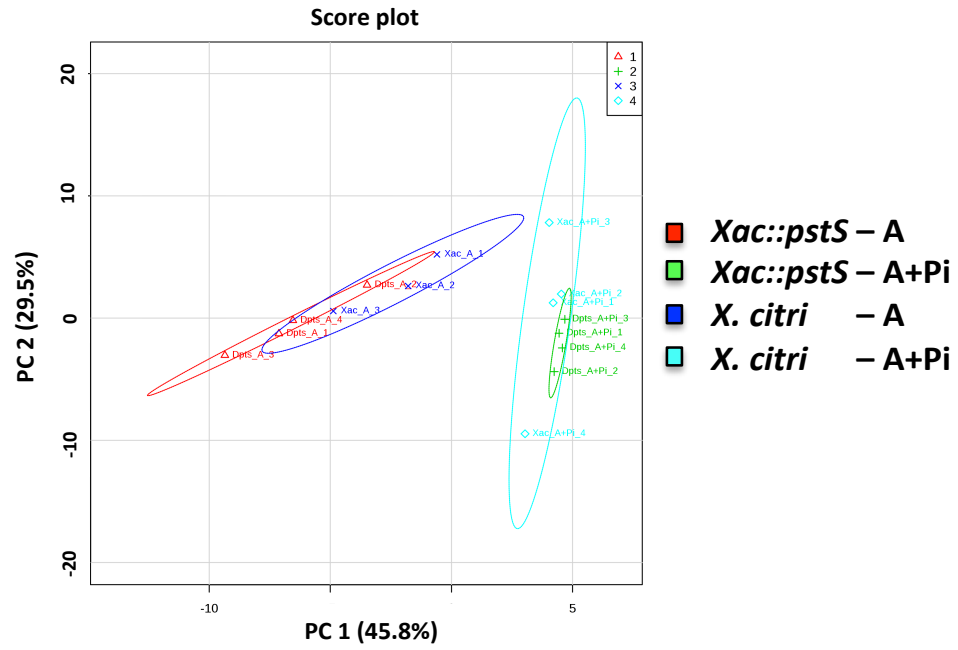


Figure S1. Resonance Magnetic Nuclear spectrum from metabolomics analysis from *X. citri*. In blue, NADH signal on the spectra under quantification and identification, in black peaks without profiling. Some metabolites were not available on ChEMIX database.

A



B

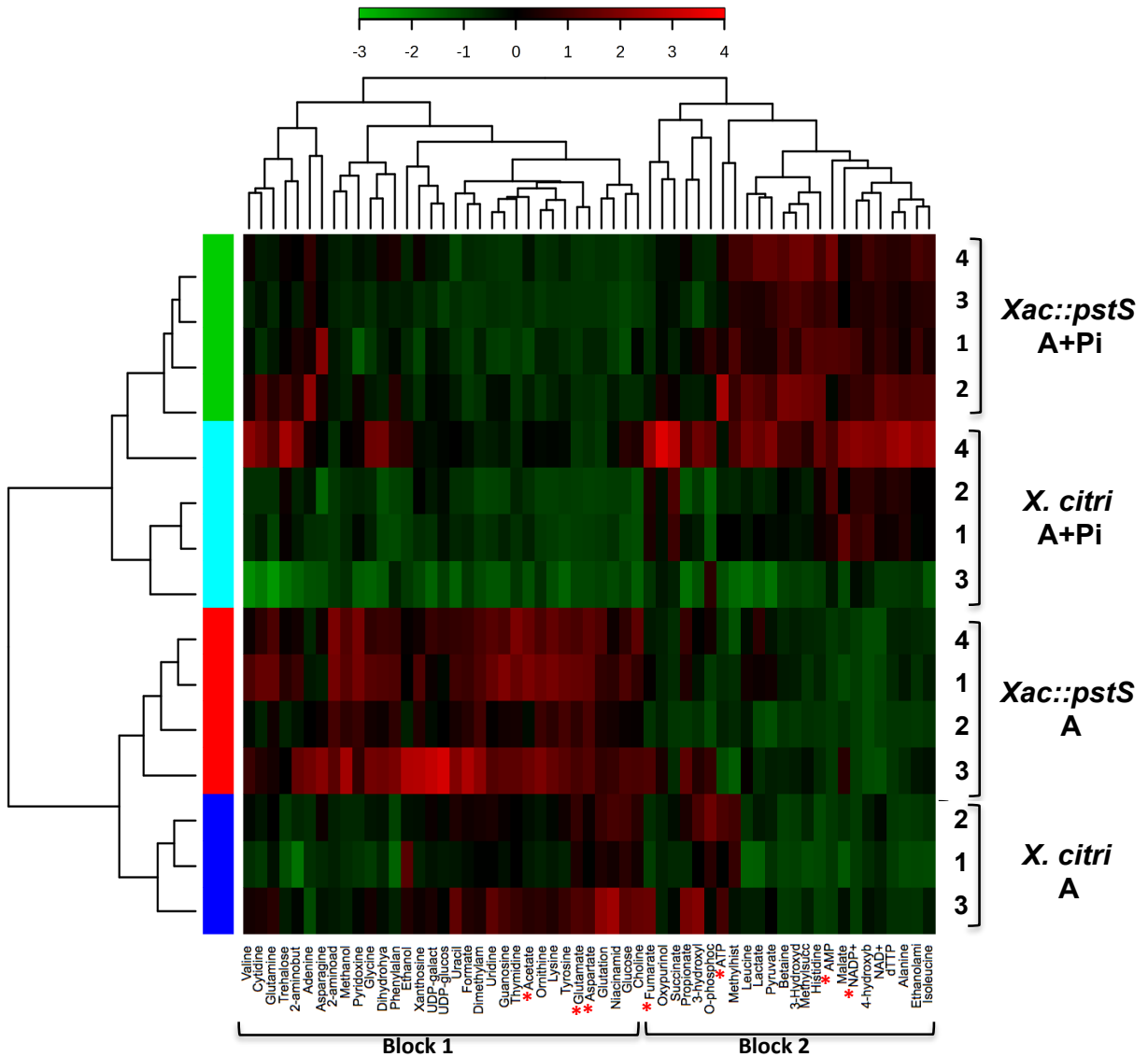


Figure 2. Distribution of metabolites identified in the metabolome of *Xac::pstS* and *X. citri* in A and A+Pi media. A) 2D-PCA analysis of the metabolomes defining two groups of metabolites depending on the phosphate concentration. B) Heat map of the metabolomes of wild type and mutant strains. The plot is shown in a cladogram that separates A and A+Pi results. Red and green colors correspond to high and low levels of metabolites identified. The list of each metabolite is shown on the bottom of the figure separated in two blocks (1 and 2). Metabolites of each block are presented in Table S5 from supplementary material with their values. Red asterisks (*) show the most significant differences observed in the dataset. At least four samples of each experiment were used for the analysis as shown by the numbers.

interference. Also, the ellipse size of the each metabolome dataset from each strain showed homogeneity due the size of the ellipse and all samples belonging to the same cluster. On the other hand, it is possible to see the influence of PstS absence on each group. PstS absence drastically affected the diversity and amount of metabolites in presence of phosphate (green circle). Spectra of metabolites identified in the wild type strain in absence of phosphate is similar to the one observed in presence, what is not observed in the mutant strain. *Xac::pstS* spectra in presence of phosphate is largely reduced than in absence (circles cyan and blue, respectively). The heat map based on Euclidean distance is also shown and revealed a clear difference in the metabolites profile dependent of the phosphate levels (Figure 2B, Blocks 1 and 2). Metabolites belonging to each block and their values are shown in Table S5 (Supplementary material). In general, wild type and mutant strain showed similar behavior repressing or producing in lower levels the metabolites from Block 1 in presence of phosphate and metabolites from block 2 in absence (red and green colors represent high and low level of metabolite, respectively). In block 1 we found among others, amino acids, glucose, nitrogenate bases and trehalose. Interestingly, this disaccharide is the most abundant metabolite found in both metabolomes and its presence is maintained even in A and A+Pi (Table S5, Supplementary material). However, when we compare the effect of *pstS* deletion, we noticed that even if both cells apparently respond to the phosphate level similarly switching the blocks of metabolites, the response in the mutant strain is much more expressive in number of metabolites than the wild type (Figure 2B, red scores). These changes in the *Xac::pstS* metabolome, even in A or A+Pi, show that PhoX is not capable to complement all the functions of PstS and reinforce the hypothesis that PstS might has an additional role in regulation of members from Pho regulon, affecting the full cellular metabolism in general. On the mutant strain the *pstS* deletion resulted on metabolic changes, where nucleotides and amino acids were used under low phosphate availability. In the mutant strain, we observed an increasing of cetonic species, glutamate, acetate, aspartate, glutatione, betaine, 3-hydroxybutyrate and ethanolamine in presence of phosphate. On the other hand, fumarate and succinate had their levels decreased when compared to the wild type (Table S5 blue bold, Supplementary material). As

evidenced by the heat map, in the depletion of phosphate it is observed an increasing of metabolites from block 1 such as aspartate, acetate, guanosine, amino acids UDP-glucose and 2-aminoadipate (Table S5 black bold, Supplementary material). The most significant changes are detached with a red asterisk in Table S5 (Supplementary material).

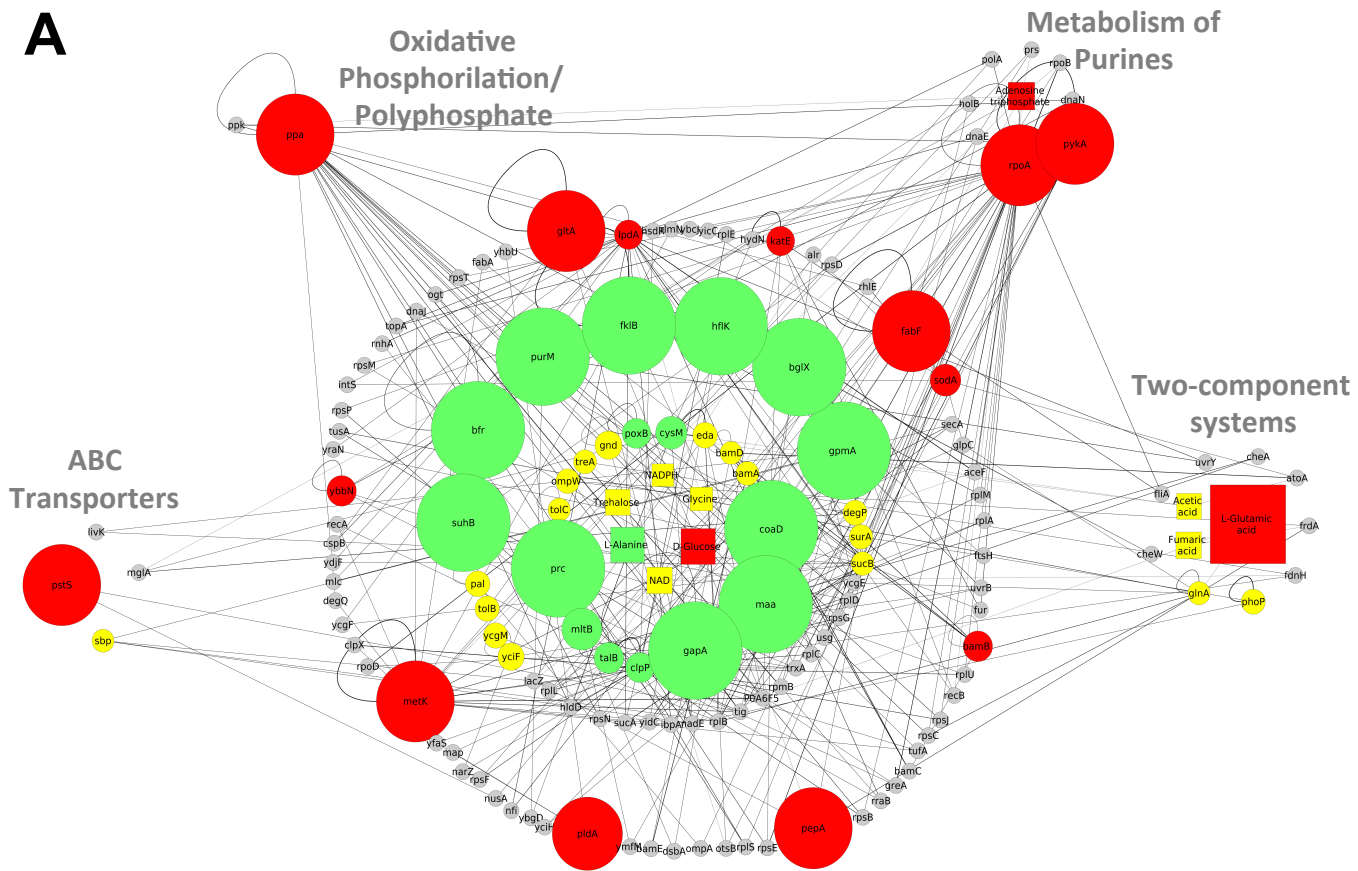
Phosphate dependent interactome map of *X. citri* and *Xac::pstS*

Interested on to have a overview of the effect of the phosphate and the *pstS* deletion, we performed analysis of system biology using as input the dataset from proteomics and metabolomics of *X. citri* and *Xac::pstS*. Analyses were performed using A and A+Pi media. Since *X. citri* has no information of metabolic pathways/interactome in the databanks, we used *E. coli* as a model. The results are presented as interactome maps that correlate proteins in their putative metabolisms and pathways (Figure 3). Proteins are shown as circles and metabolites as squares and colors code are shown in the legend. Through this maps we can analyse the effect of *pstS* deletion more clearly. In the *X. citri* wild type we observe that differences in the phosphate levels leads to a down regulation of many proteins and 4 categories or processes are evidenced: ABC transporters, oxydative phosphorilation, metabolism of purines and two-componet systems (Figure 3A). This panorama, however, is completely altered when PstS is absent, once we had up regulation of proteins and 8 processes/categories are evidenced. The same four identified in the wild type strains, but also induction of metabolism of pyruvate, cycle of citrate, chaperones, biofilm regulators and pentose phosphate pathway (Figure 3B). These deep changes reinforce the hypothesis that PstS has another role in the cell besides its function as a periplasmic binding protein. In all experiments we performed here in this work, and in previous one (Pegos et al, in prep) we showed that PhoX is able to transport phosphate but not to keep the bacterium metabolism.

Conclusions

The relevance of phosphate for *X. citri* physiology evidencing that in depletion of the ion, the bacterium reduces its metabolism down-regulation a set of proteins, but induces the ABC transport system for phosphate uptake, two component systems and others. In addition, we showed that the deletion of *pstS* drastically affects the bacterium physiology, which up-regulates metabolites and proteins as a phosphate response. *X. citri* presents PhoX, a duplication of PstS that is capable to complement the phosphate transport and the effects of *pstS* deletion for in vitro growth. However, this protein is not able to complement the general effect that *pstS* deletion has in the bacterium physiology, suggesting that PstS has also a regulatory function in the cell.

A



B

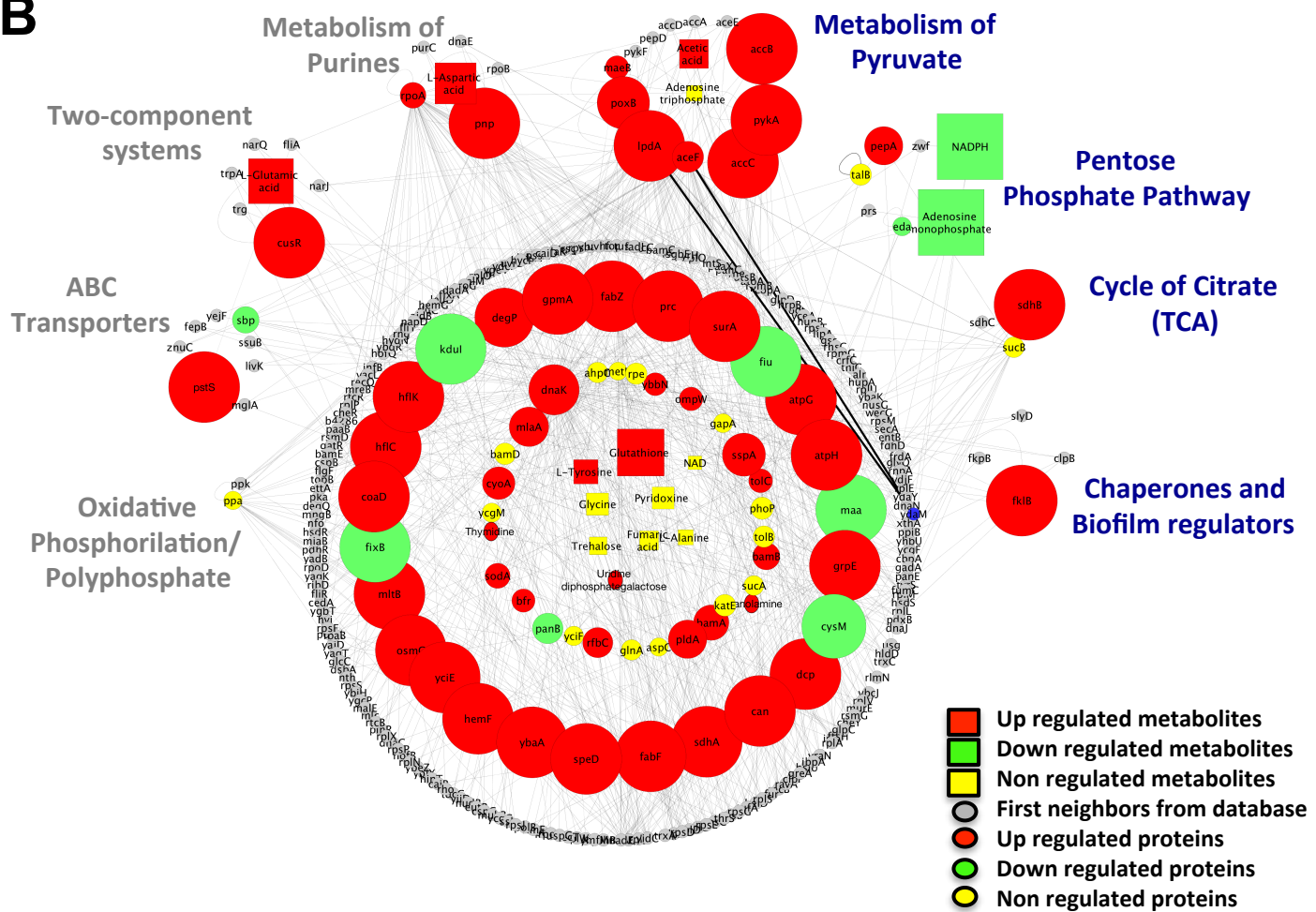


Figure 3. Interactome maps of *X. citri* and its mutant *Xac::pstS* in response to phosphate levels. The maps were built based on dataset from proteomics and metabolomics analyses performed in A and A+Pi media. Based on *X. citri* proteins, orthologues of *E. coli* were used for building of the pathways and maps. The full list of proteins, orthologues and scores is present in Table S4 (Supplementary material). Four categories or processes that were enriched in the interactome of the *X. citri* are described in gray. The additional proteins and processes in the mutant are detached in dark blue.

4. Acknowledgements

This work was supported by the Coordenação de Aperfeiçoamento Pessoal de Nível Superior - CAPES, Brazil, the Fundação de Amparo à Pesquisa do Estado de São Paulo (FAPESP) and Laboratório Nacional de Biociências, LNBio, Campinas, Brazil.

5. Conflict of interests

The authors declare no conflict of interests.

6. References

- Araújo FB, Bolanos-Garcia VM, Pereira CT, Sanches M, Oshiro EE, Ferreira RCC, Chigardze DY, Barbosa JAG, Ferreira LCS, Benedetti, CE, Blundell TL, Balan A (2013). Structural and physiological analysis of the alkanesulphonate-binding protein (SsuA) of the citrus pathogen *Xanthomonas citri*. Plos One: 8: 1-14.
- Astua-Monge G, Freitas-Astua, Bacocina F, Roncoletta J, et al. (2005) Expression profiling of virulence and pathogenicity genes of *Xanthomonas axonopodis* pv. *citri*. Journal of Bacteriology 187:1201-1205.
- Baek, JH, Lee SY (2006). Novel members in the Pho regulon of *Escherichia coli*. FEMS Microbiol Lett, 264: 104-109.
- Botella E, Hubner S, Hokamp K, Hansen A, Bisicchia P, Noone D, Powell L, Salzber LI, Devine KM (2011). Cell envelope gene expression in phosphate-limited *Bacillus subtilis* cell. Microbiology 157:2470-2484.
- Botsford JL (1992). Cyclic AMP in prokaryotes. Microbiology and Molecular Biology Reviews, 56:100-122.
- Carazzolle MF, Carvalho LM, Slepick HH, Vidal RO, Pereira GAG, Kobarg J, Meirelles GV (2014). Iss – Integrated interactome system: a web-based platform for the annotation, analysis and visualization of protein-metabolite-gene-drug interactions by integrating a variety of data sources and tools. Plos One 9: 1-13.
- Crabbé A, Leroy B, Wattiez R, Aertsen A, Leys N, Cornelis P, Houdt RV (2012). Differential proteomics and physiology of *Pseudomonas putida* KT2440 under filament-inducing conditions. BMC microbiology 12:1-9.
- Craig L, Pique ME, Tainer JA (2014). Type IV pilus structure and bacterial pathogenicity. Nature Reviews Microbiology 2:363-378.
- Crépin S, Chekabab SM, Bihan GL, Bertrand N, Dozois CM, Harel J (2011). The Pho regulon and the pathogenesis of *Escherichia coli*. Veterinary Microbiology 153:82-88.
- da Silva ACR, Ferro JA, Reinach FC, Farah CS, Furlan LR, et al. (2002). Comparison of the genomes of two *Xanthomonas* pathogens with differing host specificities. Nature, 417: 459-63.
- Ferreira GM, Spira B. (2008) The *pst* operon of enteropathogenic *Escherichia coli* enhances bacterial adherence to epithelial cells. Microbiology 154: 2025-2036.
- Keller A, Nesvizhskii AI, Kolker R, Aebersold R. (2002) Empirical statistical model to estimate the accuracy of peptide identifications made by MS/MS and database search. Anal Chem 20: 5383-5392.
- Lamarche MG, Wanner BL, Crépin S, Harel J (2007). The phosphate regulon and bacterial virulence: a regulatory network connecting phosphate homeostasis and pathogenesis. FEMS 32:461-473.
- Levinthal C, Signer ER, Fetherolf K. (1962) Reactivation and Hybridization of reduced alkaline phosphatase. Biochemistry 48: 1230-1237.

- O' May GA, Jacobsen DM, Longwell M, Stoodley P, Mobley HLT, Shirtliff ME (2009). The high-affinity phosphate transporter Pst in *Proteus mirabilis* HI4320 and its importance in biofilm formation. *Microbiology* 155:1523-1535.
- Pegos VR, Nascimento JF, Sobreira TJ, Pauletti BA, Paes-leme A, Balan A. (2014) Phosphate regulated proteins of *Xanthomonas citri* subsp. *citri*: A proteomic approach. *Journal of proteomic* 108: 78-88.
- Pegos, VR, Canevarolo RR, Sampaio AP, Balan A, Zeri ACM (2013) Xanthan gum removal for 1H-NMR analysis of the intracellular metabolome of the bacteria *Xanthomonas axonopodis* pv.*citri* 306. *Metabolites* 3: 1-15.
- Rigano LA, Siciliano F, Enrique R, Sendín L, et al. (2007) Biofilm formation, Epiphytic fitness, and canker development in *Xanthomonas axonopodis* pv.*citri*. *The American phytopathological society* 10: 1222-1230.
- Ruhal R, Kataria R, Choudhury B (2012). Trends in bacterial trehalose metabolism and significant nodes of metabolic pathway in the direction of trehalose accumulation. *Microbial biotechnology* 6: 493-502.
- Ryan RP, Vorhölter FJ, Potnis N, Jones JB, Sluys MAV, Bogdanove AJ, Dow M (2011). Pathogenomics of *Xanthomonas*: understanding bacterium – plant interactions. *Nature Microbiology* 9: 344-355.
- Shannon P, Markiel A, Ozier O, Baliga NS, Wang JT, et al. (2003) Cytoscape: a software environment for integrated models of biomolecular interaction networks. *Genome Res* 13: 2498–504.
- Spira B, Agüena M, Oliveira JVC, Yagil E (2010). Alternative promoters in the *pst* operon of *Escherichia coli*. *Mol Genet Genomics* 284:489-498.
- Tondo ML, Petrocelli S, Ottado J, Orellano EG (2010). The monofunctional catalase KatE of *Xanthomonas axonopodis* pv. *citri* is required for full virulence in citrus plant. *PLoS one* 5: 1-12.
- Torriani A (1990). From cell membranes to nucleotides: The Phosphate regulon in *Escherichia coli*. *Bioessays* 12:371-376.
- vanBogelen R, Olson ER, Wanner BL, Neidhart FC (1996). Global analysis of proteins synthesized during phosphorus restriction in *Escherichia coli*. *Journal of bacteriology* 178:4344-4366.
- Wanner B. (1996) Phosphorus assimilation and control of the phosphate regulon. *Escherichia coli* and *Salmonella thymurium* cellular and molecular biology 51: New York ASM Press, 47-54.
- Wanner BL (1993). Gene regulation by phosphate in enteric bacteria. *Journal of cellular biochemistry* 51: 47-54.
- Watt SA, Tellstrom V, Patschkowski T, Niehaus K (2006). Identification of the bacterial superoxide dismutase (SodM) as plant-inducible elicitor of an oxidative burst reaction in tobacco cell suspension culture. *Journal of Biotechnology* 12:78-86.
- Weljie A, Newton J, Mercier P, Carlson E, Slupsky CM (2006). Targeted Profiling: Quantitative Analysis of 1H NMR metabolomics Data. *Anal. Chem* 78:4430-4442;
- Xia J, Mandal R, Sinelnikov I, Broadhurst D, Wishart D. (2012) MetaboAnalyst 2.0 – a comprehensive server for metabolomics data analysis. *Nucl Acids Res* 40: 127-133.
- Yan Q, Wang N. (2012) High-throughput screening and analysis of genes of *Xanthomonas citri* subsp. *citri* involved in citrus canker symptom development. *The American phytopathological society* 25: 60-84.
- Zhao Y, Qian G, Yin F, Fan J, Zhai Z, Liu C, Hu B, Liu F (2011). Proteomic analysis of the regulatory function of DSF-dependent quorum sensing in *Xanthomonas oryzae* pv.*oryzae*. 50: 48-55.

Discussão

4. Discussão

A presente sessão abordará em tópicos a discussão dos resultados apresentados no capítulo 3. A motivação deste trabalho veio do interesse em responder qual o papel de transportadores ABC na fisiologia da *X. citri*. Um dos transportadores que se mostrou interessante pela importância atribuída em outros microrganismos e pela ausência de dados relacionados ao gênero *Xanthomonas*, foi o transportador de fosfato PstSBCA. Neste sentido, buscamos relatar análises funcionais e estruturais, tendo como base a proteína ligadora periplasmática PstS. Todos os demais resultados foram consequência deste interesse e os dados apresentados neste trabalho mostram um pouco deste transportador, bem como de outras proteínas supostamente pertencentes ao Pho regulon.

4.1. O efeito do fosfato na fisiologia de *X. citri*

As implicações na oscilação da concentração de fosfato no ambiente intra e extracelular tem sido estudados em procariotos desde a década de 60 do último século, no entanto, os dados de *X. citri* neste contexto são insipientes. Com o intuito de responder questões relacionadas as funcionalidades do sistema transportador do tipo ABC, especialmente a respeito de seus componentes periplasmáticos, os estudos de proteoma foram realizados com células cultivadas em meios com limitada e alta concentração de fosfato disponível. Os dados de proteômica revelaram que a carência de fosfato pode resultar em duas magnitudes de respostas: 1) a ativação de sistemas diretamente regulados pela disponibilidade de fosfato integrantes do regulon de fosfato tais como o sistema Pst (Phosphate specific transport) do qual o transportador ABC de fosfato é membro e também do sistema dois componentes (Two-component system) dependente do sistema PhoBR de sinalização celular; 2) a ativação de respostas secundárias em decorrência da carência de fosfato, que podem depender de sinalização da mensageiros secundários como ppGpp ou da ativação da resposta ao estresse comumente induzido pelo fosfato.

O proteoma da bactéria *X. citri* revelou a ativação funcional do sistema pst incluindo a regulação da proteína PhoX e da proteína PstS, designadas para mesma função biológica de internalizar

o fosfato contra um gradiente de concentração. O sistema *pst* em questão, assim como em outras bactérias, foi ativado somente na carência de fosfato com o aumento considerável da produção das proteínas PhoX, PstS e da enzima fosfatase alcalina (PhoA) comumente citada nos artigos como um marcador de ativação do regulon de fosfato em bactérias. O regulador transcricional PhoB é o principal regulador da transcrição dos genes do regulon de fosfato, e em virtude de sua elementariedade para fisiologia de *X. citri* dificuldades foram encontradas para produção de mutantes *phoB* em *X. citri*. Os dados de proteômica foram validados ou corroborados através de experimentos funcionais como captação de fosfato marcado, produção de goma e biofilme. A ativação do sistema foi comprovada pelos ensaios funcionais da enzima PhoA que apresentou atividade elevada na presença de fosfato clivando o substrato *p*-nitrofenol. Além disso, a carência de fosfato resultou na captação de fosfato marcado em *X. citri* em elevadas taxas quando cultivada no meio com baixa disponibilidade de fosfato (Meio A). O suporte de análises de bioinformática auxiliaram na predição na região promotora dos genes do sistema *pst*, dois componentes e do gene *phoA* comprovando que uma região não necessariamente cercana, mas próxima quando se discute sistema de regulação em nível transcricional fora encontrado em regiões intergênicas no genoma de *X. citri*. Como abordado na introdução deste trabalho, estes sistemas são regulados pelo ativador transcricional PhoB, que em situações de restrição de fosfato, estimula uma resposta adaptativa regulando a expressão de diversos genes bacterianos. Através do sistema dois componentes a bactéria monitora a disponibilidade de fosfato extracelular para que possa então alterar a expressão de seus genes e garantir a adaptação e sobrevivência nessa situação de carência nutricional. Nessas condições, o sistema *pst* por ser regulado por PhoB, tornou-se ativo e capaz de realizar a captação de fosfato marcado em taxas bem maiores que em situações anteriores demonstrando que o sistema ABC de fosfato é ativo em condições de carência (manuscrito 2, sessão 3.2) para estocagem de fosfato pela bactéria bem como crescimento nessas condições de cultivo.

Com relação aos efeitos secundários ou globais da restrição de fosfato, os dados de proteoma também permitiram a identificação de proteínas relacionadas ao sistema de secreção do tipo II e tipo IV, adesinas, proteínas envolvidas na síntese e na exportação de goma. Esses achados sustentaram a hipótese de que a carência de fosfato poderia facilitar a formação de goma e por sua vez biofilme. Alguns trabalhos neste sentido apontaram a influência do fosfato na adesão bacteriana e a dificuldade de constituir biofilme maduro. Conforme a tabela 1 apresentada na revisão de literatura de Crépin e colaboradores (2011), o efeito do fosfato pode aumentar ou diminuir esses efeitos sendo considerado particular para cada gênero ou linhagem bacteriana. A carência de fosfato e sua consequência biológica independente do regulon de fosfato foi apresentada no manuscrito 2 (item 3.2). Foi possível observar

que a carência de fosfato estimula a produção de goma xantana bem como a adesão das bactérias em superfície abiótica, neste caso, polipropileno. A produção de polissacarídeos foi mostrada em alguns organismos de solo, mas muitos destes organismos apresentam regulação dos genes responsáveis por codificar enzimas para a síntese de tais moléculas são reguladas diretamente por PhoB assim como o sistema *pst*, como no caso de *A. vinelandii*. No caso de *X. citri* o operon *gum* não possui até 1000 pares de bases a montante a região consenso *phobox*. Certamente a produção de goma e conseqüentemente a formação de biofilme são conseqüências secundárias a carência de fosfato não sendo regulada diretamente por PhoB. Das 197 proteínas identificadas no proteoma de *X. citri* algumas proteínas envolvidas na resposta ao estresse oxidativo tais como SodM e catalase tiveram sua produção aumentada assim como tioredoxina, adesinas (YapH) e algumas chaperonas como GroEL (artigo 2, material suplementar e Tabela 2). Nestas condições, nossos dados evidenciaram a maior produção de goma xantana e formação de biofilme. O biofilme além de ser um ambiente favorável para a diversidade genética é também um ambiente de proteção bacteriana o que justificaria a regulação dessas proteínas concomitante ao favorecimento de sua formação. As implicações a respeito da carência de fosfato são, portanto, o estímulo à adesão, sistemas de secreção de enzimas de degradação e proteínas efetoras que rapidamente podem modular a expressão da célula hospedeira, sugerindo colonização e proteção bacteriana. *E. coli* é o organismo no qual o metabolismo de fosfato e o regulon Pho é melhor entendido. O desbalanço intracelular do íon, seja pela por depleção ambiental ou por linhagens mutantes, resultou na regulação pela pequena molécula derivada de guanosina trifosfato denominada de ppGpp que por sua vez participa da regulação de alguns genes, dentre eles o RpoS de resposta ao estresse (Lamarche et al, 2008). Inclusive, em *X. citri* a síntese desse hormônio é dependente das enzimas PpiK e PpiX que possuem atividade de quinase e fosfatase, respectivamente. A transcrição dessas enzimas em *X. citri* são reguladas por PhoB em virtude de seus genes pertencerem ao óperon do sistema dois componentes sugerindo que na carência de fosfato além do sistema dois componentes, as enzimas PpK e PpX poderiam apresentar sua síntese aumentada. No entanto, essas proteínas não foram identificadas nos dados de proteoma. Isso poderia ocorrer primeiro em virtude da complexidade da amostra aplicada a fragmentação e ionização no espectrômetro como também os parâmetros estridentes estabelecidos durante o estudo para evitar taxas de falso positivo e manter esses dados perante aos vieses e a estatísticas confiáveis. Ainda considerando o efeito secundário e global da restrição ao fosfato, embora não houvesse severas influências quanto ao crescimento celular que é dependente de fosfato, o perfil proteômico das proteínas fora alterado consideravelmente. As respostas moleculares deflagradas não são exclusividade de *X. citri*. Em estudos realizados por

vanBogelen e colaboradores (1996) através de proteômica revelaram que mais de 400 proteínas tiveram sua síntese influenciada pela restrição ao fosfato. Em virtude da profusão dos efeitos secundários do fosfato, é plausível que os estímulos de produção de goma assim como a adesão em superfícies abióticas ocorram em *X. citri* acompanhado da regulação de proteínas relacionadas a sistema de secreção e resposta ao estresse oxidativo.

Interessantemente, os dados de proteoma também permitiram a identificação de outras proteínas periplasmáticas pertencentes a sistemas do tipo ABC para transporte de molibdato, alcano sulfonatos, nitrato e sulfato. Pela primeira vez, foi observada a identificação dessas proteínas neste tipo de ensaio, atestando a indução de sistemas de alta afinidade para captação de micronutrientes em *X. citri* que até então têm apenas sido explorados através de bioinformática em projetos do nosso grupo.

4.2. O efeito da deleção do gene *pstS* e do fosfato na fisiologia de *X. citri*

Nesta tese nós mostramos que *X. citri* apresenta o sistema de transporte tipo ABC para fosfato constituído de uma proteína periplasmática ligadora, PstS, duas permeases PstB e PstC e duas ATPases PstA. Adicionalmente, *X. citri* tem uma duplicação que constitui outra proteína periplasmática ligadora de fosfato denominada PhoX. PstS e PhoX são codificadas a partir de diferentes óperons os quais apresentam uma região para interação com o regulador PhoB, denominada de *phobox*. No mesmo operon de *phoX*, encontramos o gene *oprO*, o qual codifica uma porina de membrana externa específica para fosfato. Em nossas análises de proteômica, tanto PstS como PhoX são altamente induzidas na carência de fosfato sugerindo a atividade do sistema ABC e papel de captadoras das proteínas, como demonstrado em outras bactérias. Além disso houve indução da porina OprO e da fosfatase alcalina PhoA, proteína usada como marcador de ativação do regulon Pho. Estes dados em conjunto com análises de bioinformática que evidenciaram vários outros genes relacionados ao regulon Pho, todos com *phobox* na região promotora do operon, corroboram a idéia de que também em *X. citri*, a resposta à carência de fosfato é similar ao que é observado em *E. coli*. Ainda importante, é a presença do sistema dois-componentes PhoR-PhoB, sendo PhoB o regulador que se liga em *phobox*, altamente conservado. PhoX e PstS têm níveis de indução diferenciados, provavelmente em decorrência da localização de seus respectivos genes em óperons distintos. Agüena e colaboradores (2007) evidenciaram que no operon *pst* há regiões intergênicas espaçadoras entre os componentes

periplasmáticos e os componentes membranares que são regiões regulatórias formadoras de grampos para proteção do transcrito contra ataques de RNAses ou poderiam ser candidatos a promotores adicionais do operon regulados por PhoB. Esses espaçadores intergênicos estão presentes também no operon *pst* e entre o operon *oprOphoX*.

Para estudarmos a importância da PstS em *X. citri*, construímos uma linhagem mutante portadora de deleção no gene *pstS* e usamos esta linhagem para estudos em meios com alta e baixas concentrações de fosfato. Ainda avaliamos o comportamento da linhagem mutante durante a infecção de folhas de laranja doce (pêra) e o fenótipo do cancro. Todos os ensaios foram realizados conjuntamente com a linhagem selvagem e uma linhagem complementar que continha um plasmídeo para expressão do gene deletado *pstS*. As análises que avaliaram o crescimento das linhagens nos meios A e A+P_i, indicaram que a mutação *pstS* não afetou o crescimento da *X. citri*, mesmo durante a carência de fosfato. O mesmo ocorreu nos ensaios de produção de goma, formação de biofilme e fenótipo em folhas de *Citrus sinensis*, sugerindo que a PhoX poderia complementar a ausência de PstS. De fato, os ensaios de proteoma da linhagem mutante, evidenciaram a expressão ainda mais aumentada de PhoX em carência de fosfato (valores de fold change que na linhagem selvagem eram 49X passaram para 67X). PhoX, além dividir 70% de identidade com PstS em sua sequência de aminoácidos, teve sua estrutura resolvida ligada ao mesmo, e mostrou que todos os resíduos da interação são idênticos aos de proteínas de ortólogos, comprovando a sua função predita. Interessantemente, a deleção de *pstS* afetou a regulação do transportador, uma vez que os ensaios de captação de fosfato em meio A+P_i evidenciaram aumentados níveis de transporte quando comparados com a linhagem selvagem, o que indica a constitutividade do óperon. Nestas condições, o esperado era que tanto PstS como PhoX estivessem reprimidas como na linhagem selvagem. Este dado vai ao encontro do que tem sido observado em mutantes de *pstS* em *E. coli* (Wanner et al, 1996) que evidenciam a constitutividade do sistema. Ainda, mostram que apesar de PhoX complementar a ausência de PstS, ela não atua como a mesma, a qual deve ter um papel regulatório ainda não estabelecido. Outra observação importante foi que nos ensaios de crescimento das bactérias nas folhas, a linhagem mutante, embora tenha alcançado os mesmo nível de crescimento das linhagens selvagem e complementar, apresentou um retardo no seu crescimento durante a fase *lag*. Se PhoX complementa a captação de fosfato de forma que não observamos diferenças nos outros ensaios, na folha, a deleção de *pstS* se mostrou mais importante. Estes dados podem sugerir que os níveis de fosfato captados por PhoX não são suficientes, ou que a PstS é importante para a ativação de outros sistemas, em seu papel regulatório, e que a bactéria necessita de um tempo maior para a adaptação. Estes dados podem novamente, fortalecer a teoria de

que PstS tem um papel regulatório dentro do contexto funcional do regulon de fosfato. As análises de proteômica mostram que a linhagem mutante aumenta a expressão de enzimas degradativas, de formação de biofilme, ExbD, de sensor de quórum (PpiB) e demais peptidil-transferases identificadas que auxiliariam na colonização.

A deleção do gene *pstS* aumentou a expressão de proteínas envolvidas com a virulência, uma vez que foram reportadas alterações significativas nos valores de fold-change de proteínas do sistema de secreção do tipo II, enzimas degradativas, proteínas envolvidas na secreção de goma xantana, e de proteínas que podem participar do sensor de quórum (fold-change de 45X). Todas essas proteínas apresentaram maior abundância no meio A (baixa disponibilidade de fosfato) em relação ao meio A+P_i (elevada disponibilidade de fosfato). Essas alterações com relação ao “*fold change*” (leia-se abundância dos peptídeos identificados em cada condição) revelam que essas vias que já eram ativadas em excesso de fosfato e se tornaram mais abundantes na carência do íon, o que pode ser explicado não como um efeito da PstS, mas como uma resposta geral da célula em condições de estresse. De fato, os ensaios de goma e biofilme/aderência não mostram efeito da PstS, mas da carência do fosfato.

O interessante seria construirmos uma linhagem portadora de deleção em *phoX* e uma linhagem portadora de dupla deleção em ambos os genes.

4.3. PstS, PhoX, ortólogos e análise estrutural

No genoma de *X. citri* encontramos a anotação de duas proteínas periplasmáticas ligadoras de fosfato presentes no mesmo operon. Vale ressaltar que segundo nossas análises isso não é uma particularidade de *X. citri*, mas do gênero *Xanthomonas* sp. Além disso, diversos organismos de solo têm apresentado uma ou mais cópias extras das proteínas ligadoras de fosfato, como no caso de *Mycobacterium smegmatis* que apresenta dois transportadores do tipo ABC inteiros e dedicados exclusivamente à importação de fosfato em condição de carência nutricional ou restrição deste (Gebhard et al, 2006). Bactérias e cianobactérias apresentam proteínas ligadoras de fosfato em múltiplas cópias (Orchard et al, 2009) (sessão 3.2). Os estudos de filogenia realizados evidenciam a duplicação que deu origem à PhoX (XAC1576) e PstS (XAC1577). Os organismos em que encontramos diversas cópias de proteínas ligadoras de fosfato (Pbp) são bactérias de solo e de ambiente marinho, mas também enterobactérias como *Y. pestis*, que poderiam ter adquirido as cópias extras por transferência horizontal de genes. A árvore filogenética que caracteriza a origem destas proteínas em

diferentes organismos mostrou que o maior grupo é constituído basicamente por gama-proteobactérias, dentre elas *X. citri* e *E. coli*, as quais têm como ancestral comum a proteína periplasmática ligadora de fosfato da delta-proteobactéria *D. alkenivorans*. A explicação para que Pbp pertencentes ao sistema pst seja encontrada em diversas bactérias bem como cianobactérias poderia vir da baixa disponibilidade de fosfato nestes ambientes.

Desde 2009, alguns trabalhos têm reportado novos membros do regulon de fosfato através de ensaios funcionais como também mostrado a regulação transcricional, genômica e filogenia a relação de cópias extras de Pbp em diversos organismos correlacionando seus habitats de origem com a concentração de fosfato disponível (Orchard et al, 2009; Letelier et al, 2011; Tetu et al, 2009). No entanto, no caso de *X. citri* mesmo existindo a conservação de 60% dos resíduos o objetivo era além de mostrar o lado funcional, também levantar peculiaridades com relação às estruturas dessas proteínas de forma a correlacionarmos estrutura e função. Por conseguinte, cristais da proteína PhoX foram obtidos e difratados permitindo a resolução dessa molécula por cristalografia de raios-X. Como PstS apresenta 60% de identidade em relação à PhoX, havia uma homologia considerável para usar a estrutura desta proteína como modelo da PstS. Ressalta-se que nenhuma outra proteína ligadora de fosfato disponível nos bancos de estrutura apresentava identidade sequencial tão alta.

Curiosamente a estrutura da proteína PhoX apresentou uma peculiaridade estrutural com relação à outras Pbp, em relação ao bolsão de interação com o íon. Com base na superposição de estruturas (manuscrito 1 – sessão 3.2), os resíduos para coordenação do fosfato na estrutura da PhoX de *X. citri* e na PstS de *E. coli* são os mesmos. PhoX ainda apresenta uma extensa fita beta de conexão entre os domínios que em outras estruturas não se mostra tão longa. Esta observação resulta em uma mobilidade dos resíduos diferenciada de forma a influenciar a captação do íon e interações com o componente de membrana.

Com relação aos resíduos que realizam interação direta com o fosfato embora conservados, nem sempre a distância das ligações são exatamente as mesmas, em virtude da posição do ligante dentro da fenda de ligação. Assim como na PstS de *E. coli*, PhoX apresenta a formação de hélices dipolo para auxiliar no reconhecimento e seletividade do fosfato e também na discriminação entre outros oxianions. Os aminoácidos Arg159 e Asp80 estão presentes em duas hélices paralelas usando como referência espacial localização do fosfato na fenda e ambas situadas no lobo C-terminal. No caso do resíduo de aminoácido arginina ele é o único aminoácido positivo encontrado na fenda e que interage diretamente com o ligante, assim ele tem a função de atrair o fosfato para essa região mais facilmente, tornando-a positiva e portanto de carga oposta a do ligante. O sítio de ligação da PhoX conta ainda com a

presença de resíduos neutros e apolares tais como Phe35 que, aparentemente, limita a profundidade da fenda em que o fosfato se acomoda. A asparagina por sua vez assume um papel nessa estrutura e ortólogos de reconhecimento específico entre fosfato e outros oxianions como sulfato, arsenato e molibdato. Assim, os resíduos que participam para a distinção entre diferentes oxianions no sítio de ligação de PstS e PhoX de *E. coli* e *X. citri* são os mesmos, mas a arginina como um aminoácido de cadeia lateral positiva tem mais influência na estabilização do ligante nas periplasmáticas do fitopatógeno. É válido ressaltar que diferentemente de outras proteínas ligadoras de oxianions, o sítio de ligação do fosfato não possui espaço para moléculas de água não sendo hidratado. Geralmente este tipo de interação é observada em outras proteínas como por exemplo na proteína ligadora de molibdato – ModA (Santacruz et al, 2013).

Comparações estabelecidas entre PhoX e PstS de *X. citri* revelam ambas embora conservem os resíduos de interação direta e distâncias, os resíduos de aminoácidos ao redor do sítio de interação contribuem para um potencial eletrostático de superfície diferenciados (manuscrito 1 – sessão 3.2). As comparações estabelecidas revelam que PhoX é mais negativa e apresenta a distribuição de cargas ao redor dessa região contrária ao observado para PstS que é positiva. A mesma observação é aplicada às regiões RI, ou seja do domínio N-terminal, mas RII é que apresenta maiores divergência quando às cargas de superfície. Essas análises estruturais sugerem que embora o posicionamento do fosfato seja idêntico, a afinidade pelo mesmo bem como a interação com os componentes de membrana. Estes dados poderiam alterar a cinética de transporte. Contudo, como não temos o mutante de *X. citri* para *phoX*, este mecanismos se resume a uma hipótese neste momento.

4.4. Redes de interação das linhagens selvagem e mutante: o metabolismo de *X. citri* e de *Xac::pstS*

O perfil metabólito das bactérias selvagem e mutante em meio A e meio A+P_i. Foi analisado através da abordagem de ressonância magnética nuclear. Um total de 57 metabólitos foram identificados considerando as linhagens selvagem e mutante e os meios A e A+P_i. Ao invés de nos basearmos no efeito biológico e no test-t para averiguar o efeito da oscilação da concentração de fosfato no metabolismo, a análise dos componentes principais (PCA) foi utilizada. A compração entre o metabolismo na presença e na carência de fosfato bem como das linhagens selvagem e mutante, foi observado que a condição do meio foi mais portante que a mutação. As duas componentes principais de maior variância apresentaram-se bem distintas e bem concentradas agrupando meios e não linhagens

(manuscrito 3, sessão 3.2) ainda que essa é uma análise exploratória. Quando os dados foram expostos no heatmap utilizando a distância euclidiana, também ficou nítido que o meio permitia uma maior segregação dos metabólitos quanto sua concentração do que a mutação em si.

Os metabólitos que dependem de fosfato para modificarem seu estado de oxidação tais como os nucleotídeos NAD⁺, NADP⁺, ATP, AMP, entre outros, foram preferencialmente utilizados quando o fosfato estava presente. Em situações em que a disponibilidade de fosfato era baixa, foi observado que aminoácidos eram preferencialmente utilizados além do processo de fermentação acontecer. No entanto, embora o meio apresente maior variância, é possível observar que a concentração de alguns metabólitos oscila quando comparado entre as linhagens selvagem e mutante no heatmap (manuscrito 3, sessão 3.2). Dentre os metabólitos que podemos destacar neste contexto o lactato e o ATP que é utilizado em maiores quantidades em situação de carência para a bactéria selvagem, e em concentração de abundância de fosfato passa a ser utilizada em maiores concentrações pela linhagem mutante. Essas pequenas alterações na concentração de metabólitos podem indicar alterações e desvios das rotas metabólicas sugerindo que a bactéria mutante embora tenha a captação de fosfato ativa pelo efeito compensatório de PhoX, talvez não ocorra nos níveis desejados limitado por algumas particularidades das proteínas que poderiam limitar a eficiência do transporte. Algumas dessas particularidades foram abordadas no item 4.1 como também no manuscrito 1, sessão 3.2 da presente tese, no qual as regiões de interação com a membrana das proteínas PhoX e PstS apresentaria distribuição de cargas diferenciadas bem como regiões ao redor do sítio de ligação ao fosfato. Por conseguinte, as discretas alterações metabólicas entre as linhagens selvagem e mutante poderiam reforçar a hipótese de que embora haja o efeito compensatório de PhoX durante os ensaios de captação de fosfato e dos valores de fold change em meio A na proteômica: 1) uma proteína não é suficiente para atender a demanda de fosfato em *X. citri*; 2) há uma regulação em que a presença física da PstS é necessária e não somente o aporte de fosfato.

Os dados de metabolômica se analisados dessa forma isolada e pontual contribuíram pouco neste contexto e ficaria difícil deflagrar alterações metabólicas em conjunto com os dados de proteômica. Assim, os 57 metabólitos e as proteínas identificadas em cada condição e linhagem foram utilizados para a construção de uma rede de interação no programa IIS (Integrate Interactome System) considerando que vias metabólicas seriam alteradas pelo fosfato ou pela mutação.

As redes de interações foram construídas integrando os dados de metaboloma e de proteoma da bactéria selvagem e mutante oriundos dos meios A (baixa disponibilidade de fosfato) e meio A+P_i (elevada disponibilidade de fosfato). Em virtude do baixo número de interações de *X. citri* depositada

nos bancos públicos, uma rede baseada em ortólogos foi construída. Por conseguinte, identificou-se os ortólogos das proteínas de *X. citri* em *E. coli* para que tanto a rede quanto os processos de enriquecimento fossem viáveis. Nesta etapa grande, os valores dos alimentos são inestimáveis, e por isso, parte das proteínas identificadas no proteoma são perdidas, sendo um viés experimental. No entanto, essa foi a única maneira encontrada para integrar os dados. Esses dados são os mais recentes adquiridos e estão sob análise e discussão. Em um primeiro momento é possível observar que a carência de fosfato na bactéria *X. citri* apresentou enriquecimento das vias de sistemas dois componentes, metabolismo de purina, ciclo de Krebs, transportador do tipo ABC e fosforilação oxidativa. Com relação à linhagem mutante, às vias enriquecidas foram sistema dois componentes, metabolismo de purina, ciclo de Krebs, fosforilação oxidativa, transportadores ABC, metabolismo de piruvato e via da pentose. Mesmo a bactéria mutante apresentando algumas vias enriquecidas, a leitura global das redes embora óbvia para os especialistas em regulon de fosfato, sugere que todos os esforços são para alimentar vias metabólicas para produção de adenina e guanina, bem como no metabolismo de purina e pentose é para a produção de ATP. Embora as enzimas de degradação de fosfato (PpK e PpX) estão sob o controle do regulador PhoB, essas enzimas não tiveram sua abundância controlada pelo fosfato segundo os dados observados. No entanto, essas enzimas são responsáveis pela degradação dos estoques celulares de fosfato e interagem com proteínas envolvidas na fosforilação oxidativa provendo fosfato diretamente à produção de ATP e por essa razão integram essa via no KEGG. Curiosamente, no mapa do mutante, a via de piruvato tem como interação uma proteína anotada como YadM e que esta poderia participar da regulação do biofilme. Conforme mencionado anteriormente, as rotas bioquímicas e o papel do transportador ABC neste contexto ainda estão em análise, uma vez que os dados produzidos sugerem que a PstS tenha um papel regulatório que PhoX não pode desempenhar.

5. Conclusões

Os resultados obtidos na presente tese, baseados em uma gama de diferentes métodos, permitiram evidenciar em *X. citri* a presença de membros importantes do regulon Pho, os quais são ativados em condições de carência do íon, com relevância dada ao transportador ABC PstSCBA. Além do transportador mostramos que *X. citri* tem duas proteínas ligadoras periplasmáticas PstS e PhoX, originadas de uma duplicação gênica que leva à estruturas tridimensionais semelhantes e conservação dos resíduos no sítio de interação de fosfato. No entanto, as regiões de interação com as permeases sugerem que a velocidade de transporte do fosfato por essas proteínas possa ser diferenciada. Em condições de carência de fosfato, além da ativação do sistema ABC e do regulon Pho, a bactéria apresenta maior capacidade de adesão em tubos de polipropileno e produção de goma xantana, dois fatores importantes para o estímulo e produção de biofilme.

Visando evidenciar o papel da PstS na bactéria, construímos o mutante *Xac::pstS* e realizamos ensaios funcionais. Na ausência de PstS e de fosfato, PhoX tem sua expressão aumentada em cerca de 20X (49 para 67X) e aparentemente complementa a atividade da proteína PstS, uma vez que não há diferenças na produção de goma ou adesão. Por outro lado, a deleção de *pstS* leva a um crescimento mais lento da bactéria em folhas de *C. sinensis* e constitutividade do sistema de transporte em presença do fosfato.

As análises do metaboloma da *X. citri* e mutante em presença e ausência de fosfato mostraram dois efeitos diferenciados: (i) o do fosfato, que como em todos os organismos é essencial para a produção de ATP. Neste caso, *X. citri* reorganiza suas vias metabólicas priorizando o metabolismo de purina e fosforilação oxidativa (ii) outro é o efeito da mutação, que altera significativamente vias metabólicas envolvidas com sistemas de sensibilização, oxidação, via das pentoses e o transportador ABC, destacando que PstS realmente pode apresentar um papel regulatório.

Adicionalmente, é importante ressaltar que este é o primeiro trabalho a mostrar que membros do regulon Pho estão presentes em *X. citri*, que são ativados em carência de fosfato e que apesar de PhoX cumprir o papel de PstS para o transporte, PstS parece ter um papel relevante no transporte e regulação de várias proteínas. Os dados apresentados para *X. citri* podem ser usados como modelo para o estudo destes sistemas em outras bactérias do gênero ou em fitopatógenos.

Referências Bibliográficas

6. Referência Bibliográfica

- Aguena, Meire. Análise transcricional do operon *pst* de *Escherichia coli*. 2007. Tese (Doutorado em Microbiologia) – Instituto de ciências biomédicas II. Universidade de São Paulo, São Paulo.
- Araújo, F.,B., Bolanos-Garcia, V.M., Pereira, C.T., Sanches, M., Oshiro, E.E., Ferreira, R.,C.,C., Chigardze, D.,Y., Barbosa, J.A.G, Ferreira, L.C.S., Benedetti, C.E., Blundell, T.L., Balan, A. Structural and physiological analysis of the alkanesulphonate-binding protein (SsuA) of the citrus pathogen *Xanthomonas citri*. Plos One, v 8, 2013.
- Baek, J.H., Lee, S.Y. Novel members in the Pho regulon of *Escherichia coli*. FEMS Microbiol Lett, v 264, 2006.
- Balan, A., Santacruz, C.P., Moutran, A., Ferreira, R.C.C., Medrano, F.J., Pérez, C.A., Ramons, C.H.I., Ferreira, L.C.S. The molybdate-binding protein (ModA) of the plant pathogen *Xanthomonas axonopodis* pv. *citri*. Protein expression and purification, v 50, 2006.
- Berntsson, R.P.A, Smits, S.H.J, Schitt, L., Slotboom, D-J., Poolman, B. A structural classification of substrate-binding proteins. FESB Letters, v 584, 2010.
- Bertrand, N., Houle, S., LeBihan, G., Poirier, E., Dozois, C.M., Harel, J. Increased Pho regulon activation correlates with decreased virulence of an avian pathogenic *Escherichia coli* O78 strain. Infection and Immunity, v 78, 2010.
- Braibant, M., Gilot, P., Content, J. The ATP binding cassette (ABC) transport systems of *Mycobacterium tuberculosis*. FEMS Microbiology Reviews, v 24, 2000.
- Brunings, A, M., Gabriel, D., W. *Xanthomonas citri*; breaking the surface. Molecular Plant pathology, v 3, 2003.
- Büttner, D., Bonas U. Regulation and secretion of Xanthomonas virulence factors. FEMS Microbiol Review, v 34, 2010.
- Cassino, P., Rubio, V., Marina, A. The mechanism of signal transduction by two-component systems. Current Opinion in Structural Biology, v 20, 2010.
- Cernadas, R., C., Camillo, L., R., Bendetti, C., E. Transcriptional analysis of the sweet Orange interaction with the citrus canker pathogens *Xanthomonas axonopodis* pv. *citri* and *Xanthomonas axonopodis* pv. *aurantigolii*. Molecular plant pathology, v 9, 2008.

- Chung, W.J., Shu, H.Y., Lu, C.Y., Wu, C.Y., Tseng, Y.H., Tsai, S.F., Lin, C.H. Qualitative and comparative proteomic analysis of *Xanthomonas campestris* pv. *campestris* 17. *Proteomics*, v 7, 2007.
- Crépin S., Lamarche, M., Garneau P., Séguin, J., Proulx J., Dozois, C.M., Harel, J. Genome-wide transcriptional response of an avian pathogenic *Escherichia coli* (APEC) *pst* mutante. *BMC genomics*, v 9, 2008.
- Crépin, S., Chekabab, S.M., Bihan, L. G., Bertrand, N., Dozois, C., M., Harel, J. The Pho regulon and the pathogenesis of *Escherichia coli*. *Veterinary Microbiology*, v 153, 2011.
- da Silva, A.C.R., Ferro, J.A., Reinach, F.C., Farah, C.S., Furlan, L.R., Quaggio, R.B.,Monteiro-Vitorello, C.B., Van Sluys, M.A., Almeida Jr.,N.F., Alves, L.M.C., do Amaral,A.M., Bertolini, M.C., Camargo, L.E.A., Camarotte, G., Cannavan, F., Cardozo, J.,Chambergo, F., Ciapina, L.P., Cicarelli, R.M.B., Coutinho, L.L., Cursino-Santos, J.R., Dorry, H., Faria, J.B., Ferreira, A.J.S., Ferreira, R.C.C., Ferro, M.I.T., Formighieri, E.F.,Franco, M.C., Greggio, C.C., Gruber, A., Katsuyama, A.M., Kishi, L.T., Leite Jr.,R.P.,Lemos, E.G.M., Lemos, M.V.F., Locali, E.C., Machado, M.A., Madeira, A.M.B.N., Martinez-Rossi, N.M., Martins, E.C., Meidanis, J., Menck, C.F.M., Miyaki, C.Y., Moon, D.H.,Moreira, L.M., Novo, M.T.M., Okura, V.K., Oliveira, M.C., Oliveira, V.R., Pereira Jr.,H.A.,Rossi, A., Sena, J.A.D., Silva, C., de Souza, R.F., Spinola, L.A.F., Takita, M.A., Tamura,R.E., Teixeira, E.C., Tezza, R.I.D., Trindade dos Santos, M., Truffi, D., Tsai, S.M., White,F.F., Setubal, J.C.; Kitajima, J.P.. Comparison of the genomes of two *Xanthomonas* pathogens with differing host specificities. *Nature*, v 417, 2002.
- Das, A.K. Citrus Canker- A review. *J. App. Hort*, v 5, 2003.
- Davidson, A., L., Dassa, E., Orelle, C., Chen, J. Structure, Function, and evolution of bacterial ATP-binding cassette system. *Microbiology and Molecular biology reviews*, v 72, 2008.
- Edelhoch, H. Spectroscopy determination of tryptofan and tisorine in proteins. *Biochemistry*, v 6, 1967.
- Ehmann, M., Ehrle, R., Hofmann, E., Boos, W., Schlösser, A. The ABC maltose transporter. *Molecular Microbiology*, 29, 1998.
- Eliás, A.O., Abarca, M.J., Montes, R.A., Chasteen, T.G., Donoso, P.J.M., Vásquez C.C. Tellurite enters *Escherichia coli* mainly through the PitA phosphate transporter. *Microbiology Open*, v 1, 2012.
- Gardner, S.G., Johns, K.D., Tanner, R., McCleary, W.R. The PhoU protein from *Escherichia coli* interacts with PhoR, PstB and Metals to form a phosphate-signaling complex at membrane. *Journal of Bacteriology*, v 196, 2014.

- Gebhard, S., Ekanayaka, N., Cook, G.M. The low-affinity phosphate transporter PitA is dispensable for *in vitro* growth of *Mycobacterium smegmatis*. BMC microbiology, v 9, 2009.
- Gebhard, S., Tran, S.L., Cook, G. The Phn system of *Mycobacterium smegmatis*: a second high-affinity ABC-transporter for phosphate. Microbiology, v 152, 2009.
- Gilmour, R., Foster, E.J., Sheng, Q., McClain, J.R., Riley, A., Sun, P.M., Ng, W-L., Yan, D., Nicas, T.I., Henry, K., Winkler, M.E. New class of competitive Inhibitor of bacterial histidine kinases. Journal of bacteriology, v 187, 2005.
- Gottig, N., Garavaglia, B., S., Garofalo, C., G., Orellano, E., G., Ottado, J. A filamentous hemagglutinin-like protein of *Xanthomonas axonopodis* pv. *citri*, the phytopathogen responsible for citrus canker, is involved in bacterial virulence. PLoS one, v 4, 2009.
- Graham, J., Gottwald, T.R., Cubero, J., Achor, D. *Xanthomonas axonopodis* pv. *citri*: factors affecting successful eradication of citrus canker. Molecular plant pathology, v 5, 2004.
- Gudesblat, G.E., Torres, P.S., Vojnov, A.A. *Xanthomonas campestris* overcomes Arabidopsis stomatal innate immunity through a DSF cell-to-cell signal-regulated virulence factor. Plant Physiology, v 149, 2009.
- Guo, Y., Zhang, Y., Li, J.L., Wang, B. Diffusible signal factor-mediated quorum sensing plays a central role in coordinating gene expression of *Xanthomonas citri* subsp. *citri*. MPMI, v 25, 2012.
- Gupta, D.K., Chatterje, S., Datta, S., Veer, V., Walther, C. Role of phosphate fertilizers in heavy metal uptake and detoxification of toxic metals. Chemosphere, v 108, 2014.
- Gurlebeck, D., Thieme, F., Bonas, U. Type III effector proteins from the plant pathogen *Xanthomonas* and their role in the interaction with the host plant. Journal of Plant Physiology, v 16, 2003.
- Hajri, M., N., Jacques, M., A., Koebnik, R. Adhesion Mechanisms of plant-pathogenic *Xanthomonadaceae*. Bacterial Adhesion, Advances in Experimental, Spring Bioscience Press, Capitulo 5, 2011.
- Hall, J.A., Ganensen, A.K., Chen, J., Nikaido, H. Two modes of ligand binding maltoseprotein of *Escherichia coli*. Functional significance in active transport. J. Biol. Chem, v 272, 1997.
- Harris, R.M., Webb, D.C., Howitt, S.M., Cox, G.B. Characterization of PitA and PitB from *Escherichia coli*. Journal of bacteriology, v 183, 2001.
- Hoffer, S.M., Tommassen, J. The Phosphate-binding protein of *Escherichia coli* is not essential for Pi-regulated expression of the *pho* regulon. Journal of Bacteriology, v 183, 2001.

- Hollenstein, K., Dawson, R.J.P., Locher, K.P. Structure and mechanism of ABC transporter proteins. *Current Opinion in structural biology*, v 17, 2007.
- Hollenstein, K., Frei, D.C., Locher, K.P. Structural of an ABC transporter in complex with its binding protein. *Nature*, v 446, 2007.
- Hsieh, Y., J., Wanner, B., L. Global regulation by the seven-component Pi signalling system. *Current opinion in Microbiology*, v 13, 2010.
- Igarasho, M., Watanabe, T., Hashida, T., Umekita, M., Hatano, M., Yanagida, Y., Kino, H., Kimura, T., Kinoshita, N., Inoue, K., Sawa, R., Nishimura, Y., Utsumi, R., Nomoto, A. Wldiomycin, a novel Walk-histidine Kinase inhibitor from *Streptomyces* sp. MK844-mF10. *The jornal fo antibiotics*, v.66, 2013.
- Kaserer, A. O., West, A.H. Histidine kinases in Two-component Signaling Pathways. *Handbook of Cell Signalling*. Elsevier, 3 edição, 2010.
- Khill, P.P., Otero, C.D. Over 1000 genes are involved in the DNA damage response of *Escherichia coli*. *Molecular Microbiology*, v 44, 2002.
- Kim, J., Senadheera, D.B., Lévesque, C.M., Cvitkovitch, D.G. TcyR regulates L-cystine uptake via the TcyABC transporter in *Streptococcus mutans*. *FEMS Microbiol Letter*, v 328 , 2012.
- Kononova, S.V., Nesmwyanova, M.A, Phosphonates and their degradation by microorganisms. *Biokhimiya*, 2001.
- Lamarche MG, Wanner BL, Crépin S, Josée Harel (2008). The phosphate regulon and bacterial virulence: a regulatory network connecting phosphate hoemostasis and pathogenesis. *FEMS Microbiol Review* 32: 461-473.
- Lee, S.J., Park Y.S., Kim S.J., Lee, Bong-Jin, Suh, S.W. Crystal Structure of PhoU from *Pseudomonas aeruginosa*, a negative regulator of the Pho regulon. *Journal of Structural Biology*, v 188, 2014.
- Letelier, A., M., Olmedo, G., Eguiarte, L., E., Castilla-Martinez, L., Souza, V. Parallel Evolution and Horizontal Gene transfer of the *pst* operon in *Firmicutes* from Oligotrophic Environments. *International Journal of Evolutionary Biology*, v 2011 2011.
- Levinthal, C., Signer, E., Fetherolf, K. Reactivation and Hybridization of reduced alcaline phosphatase. *PNAS*, v 48, 1962.
- Lewis, V., G., Ween, M., P., McDevitt, C., A. The role of ATP-binding cassette transportes in bacterial pathogenicity. *Protoplasma*, 2012.

- Lorimier, R.M., Smith, J.J., Dwyer, M.A., Looger, L.L., Sali, K.M., Vola, P.A.A., Rizk, S.S., Sadigov, S., Conrad, D.W., Loew, L., Hellinga, H.W. Construction of fluorescent biosensor Family. *Protein Science*, v 11, 2002
- Lu, G., Davidson, A.L., Chen, J. ATP hydrolysis is required to reset the ATP-binding cassette dimer into the resting-state conformation. *PNAS*, v 192, 2005.
- Luecke H, Quioco FA (1990). High specificity of a phosphate transport protein determined by hydrogen bonds. *Nature* 347: 402-406.
- Makino, K., Amemura M., Kim., S., Nakata, A., Shinagawa, H. Role of the σ^{70} subunit of RNA polymerase in transcriptional activation by activator protein PhoB in *Escherichia coli*. *Genes & Development*, v 7, 1993.
- Marco Fava Neves. O retrato da citricultura Brasileira. Editora Fea: Ribeirão Preto, 2012.
- Marina, A., Waldburger, C., D., Hendrickson, W., A. Structure of the entire cytoplasmic portion of a sensor histidine-kinase protein. *The Embo Journal*, v, 24, 2005.
- Marina, A., Waldburger, C.D., Hendrickson, W.A. Structure of the entire cytoplasmic portion of a sensor histidine-kinase protein. *The EMBO journal*, v 24, 2005.
- Medrano, F., J., de Souza, C., S., Romero, A., Balan, A. Structure determination of a sugar-binding protein from the phytopathogenic bacterium *Xanthomonas citri*. *Acta Crystallogra F Struct Biol Commun*, v 70, 2014.
- Moerck, G.S., Coulton J.W. TonB-dependent iron acquisition: mechanisms of siderophore-mediated active transport. *Molecular Microbiology*, v 28, 1998.
- Monge, A.G., Astua, F.J., Bacocina, G., Roncoletta, J., carvalho S.A., Machado, M.A. Expression profile of virulence and pathogenicity genes of *Xanthomonas axonopodis* pv. *citri*. *Journal of bacteriology*, v 187, 2005.
- O'May, G.A., Jacobsen, S.M., Longwell, M., Stoodley, P., Mobley, H.L.T. Shirliff, M.E. The high-affinity phosphate transporter Pst in *Proteus mirabilis* HI4320 and its importance in biofilm formation. *Microbiology*, v 155, 2009.
- Oldham, M.L., Davidson, A.L., Chen, J. Structural insight into ABC transporter mechanism. *Current Opinion in Structural Biology*, v 18, 2008.
- Orchard, E.D., Webb, E.A., Dyhrman, S.T. Molecular analysis of the phosphorus starvation response in *Trichodesmium* ssp. *Environmental Microbiology*, v 11, 2009.

- Pegos, V.R., Medrano, F.J., Balan, A. Crystallization and preliminary X-ray diffraction analysis of the phosphate-binding protein PhoX from *Xanthomonas citri*. *Acta Crystallographica Section F*, v 70, 2014.
- Pegos, V.R., Nascimento, J.F., Sobreira, T.J.P., Pauletti, B.A., Paes-Leme, A., Balan, A. Phosphate regulated proteins in *Xanthomonas subsp.citri*: A proteomic approach. *Journal of proteomics*, v 108, 2014.
- Petronilli, V., Ames, G., F., L. Binding protein-independent histidine permease mutants. *The journal of biological chemistry*, v 266, 1991.
- Rees, D., C., Johnson, E., Lewinson, O. ABC transporter: The power to change. *Nat Rev Mol Cell Biol*, v 10, 2009.
- Rigano, L.A., Siciliano, F., Enrique, R., Sendín L., Filippone, P., Torres, P.S, Qüesta, J., Dow, J.M., Castagnaro, A.P., Vojnov, A.A., Marano, MR. Biofilm formation, Epiphytic fitness, and canker development in *Xanthomonas axonopodis* pv.*citri*. *Molecular plant-microbe interactions*, v 20, 2007.
- Rodríguez H., Rico, S., Díaz, M., Santamaría,R. Two componente system in *Streptomyces*: key regulators of antibiotic complex pathways. *Microbial Cell Factories*, v 12, 2013.
- Ryan, R.P., Vorhölter, F.J., Potnis, N., Jones, J.B., Sluys., M.A.V., Bogdanove, A.J., Dow, M. Pathogenomics of *Xanthomonas* understanding bacterium-plant interactions. *Nature*, v 9, 2011.
- SAMBROOK, J.; RUSSELL, D. **Molecular Cloning**: a laboratory manual. 3a edição: Cold Spring Harbor Press, 2001.
- Sampaio, A. P. Estudos estruturais e funcionais do sistema de captação de nitrato. Universidade de São Paulo, 2015.
- Santacruz-perez, C., Pegos, V., R., Honorato, R., V., Verli, H., Lindahl, E., Barbosa, J., A., R., G., Balan, A. A specific interdomain interaction preserves the structural and binding properties of the ModA protein from the phytopathogen *Xanthomonas citri* domain interaction and transport in ModA. *Archives of Biochemistry and Biophysics*. 2013.
- Shannon, P., Markiel, A., Ozier, O., Baliga, N.S., Wang, J.T. Cytoscape: a software environment for integrated models of biomolecular interaction networks. *Genome Res*, v 13, 2003.

- Souza, D., P., Andrade, M., O., Alvarez-martinez, C., E., Arantes, G., M., Farah, C., S., Salinas, R., K. A component of the Xanthomonadaceae type IV secretion combines a VirB7 motif with a N0 domain found in outer membrane transport proteins. *PLoS Pathogen*, v 7, 2011.
- Stall, R.E. Canker: a Threat to citrus in the gulf-coast states. *Plant Disease* , v 63, 1983.
- Stall, R.E., Marco, G. M., Canteros B.I. Importance of mesophyll in mature-leaf resistance to canker of citrus. *Phytopathology*, v 72, 1982.
- Tetu, S.G., Brahmsha, B., Johnson, D.A., Tai, V., Phillippy, K., Palenik, B., Paulsen, I.T. Microarray analysis of phosphate regulation in the marine cyanobacterium *Synechococcus* sp. WH8102. *ISME Journal*, v 3, 2009.
- Tomii, K., Kanehisa M. A comparative analysis of ABC transporters in Complete Microbial Genomes. *Genome Res*, v 8, 1998.
- Torriani, A. From cell Membrane to nucleotides: The phosphate regulon in *Escherichia coli*. *BioEssays*, v 12, 1990.
- Torriani, A. Influence of inorganic phosphate in the formation of phosphatases by *escherichia coli*. *Bioch. Biophys. Acta*, v 38, 1960.
- VanBogelen, R.A., Olson, E.R., Wanner, B.L., Neidhardt F. Global Analysis of proteins synthesized during phosphorus restriction in *Escherichia coli*. *Journal of Bacteriology*, v 178, 1996.
- Véscovi, E.G. Sciara, M.I., Castelli, M.E. Two component systems in the spatial program of bacteria. *Current Opinion in Microbiology*, v 13, 2010.
- Vojnov, A., Zorreguieta, A., Dow, J.M., Daniels, M.J., Dankert, M.A. Evidence for a role for the gumB and gumC gene products in the formation of xanthan from its pentasaccharide repeating unit by *X.campestris*. *Microbiology*, v144, 1998.
- Vyas, N.K., Vyas, M.N., Quijcho, F.A. Crystal structure of M.tuberculosis ABC phosphate transport receptor: Specificity and Charge compensation Dominated by Ion-dipole Interactions. *Structure*, v 11, 2013
- Wakimoto, S., Imaohji, H.N., Icimura, M., Morita, H., Hirakawa, K., Hayashi, T., Yasutomo, K., Kuwahara, T. PhoB regulates the survival of *Bacteroides fragilis* in peritoneal abscesses. *Plos One*, v 8, 2013.
- Wang, Z., Luecke, H., Yao, N., Quijcho, F.A. A low energy short hydrogen bond in very-high resolution structures protein receptor-phosphate complexes. *Nature*, v 4, 1997.

- Wanner B.L. Gene regulation by phosphate in enteric bacteria. *Journal of cellular biochemistry*, v 51, 1993.
- Wanner, B. Phosphorus assimilation and control of the phosphate regulon. *Escherichia coli* and *Salmonella thphimurium* cellular and molecular biology . New York ASM Press, 47-54, 1996.
- Wanner, B.L., Boline, J.A. Mapping and molecular cloning of the *phn* (*psiD*) locus for phosphonate utilization in *Escherichia coli*. *Journal of Bacteriology*, v 172, 1990.
- Watt, S.A., Tellstrom, V., Patschkowski, T., Niehaus, K. Identification of the bacterial superoxide dismutase (SodM) as plant-inducible elicitor of an oxidative burst reaction in tobacco cell suspension culture. *Journal of Biotechnonology*, v 12, 2006.
- Weljie, A., Newton, J., Mercier, P., Carlson, E., Slupsky, C.M. Targeted Profiling: Quantitative Analysis of 1H NMR metabolomics. *Data. Anal. Chem*, v 78, 2006.
- Wende, A., Furtwängler, K., Oesterhelt, D. Phosphate-dependent behaviour of the Archeon *Halobacterium salinarum* Strain R1. *Journal Bacteriology*, v 191, 2009.
- Yan, Q., Wang, N. High-Troughput screening and analysis of genes of *Xanthomonas citri* subsp. *citri* Involved in Citrus Canker Symptom development. *American phytopathological society*, v 2, 2012.
- Yan, Q., Wang, N. The ColR/ColS two-component system plays multiple roles in the pathogenicity of the citrus canker pathogen *Xanthomonas citri* subsp. *citri*. *Journal of bacteriology*, v 193, 2011.
- Yoshida, Y., Sugiyama, S., Oyamada, T., Yokoyamada, K., Makino, K. Novel members of the phosphate regulon in *Escherichia coli* O157:H7 identified using a whole-genome shotgun approach. *Gene*, v 502, 2012.
- Yuan, Z.C., Zaheer, R., Finan, T.M. Regulation and properties of PstSCAB, a high-affinity, High-velocity phosphate transport system of *Sinorhizobium meliloti*. *Journal of bacteriology*, v 188, 2006.
- Yuan, Z.C., Zaheer, R., Morton, R., Finan, T.M. Genome prediction of PhoB regulated promoters in *Sinorhizobium meliloti* and twelve proteobacteria. *Nucleic acids research*, v 34, 1993.
- Zhang, P., Khursigara, C.M., Hartnell, L.M., Subramaniam, S. Direct visualization of *Escherichia coli* chemotaxis receptor arrays using cryo-electron microscopy. *PNAS*, v 104, 2007.
- Zimaro, T., Thomas, L., Maronedze, C., Garavaglia, B.S., Gehring. C., Ottado. J., et al. Insights into *Xanthomonas axonopodis* pv. *citri* biofilm through proteomics. *BMC Microbiol*, v 13,2013.

Anexos

7. Anexo 1 - Resultados Complementares

Nesta sessão serão reportados dados relacionados às proteínas PhoU, PhoB e PhoR que não tiveram suas análises concluídas durante o período de doutoramento. PhoU, PhoR e PhoB são proteínas envolvidas na sinalização dependente de fosfato. In *E. coli*, PhoB, como ativador transcricional, regula diretamente mais de 31 genes e indiretamente mais de 400 genes (vanBogeleegen et al, 1996). PhoR e PhoB pertencem ao mesmo óperon e formam o sistema dois-componentes, onde PhoR, uma histidina-quinase, tem a função de ativador transcricional de PhoB (Wanner 1993). PhoU ainda não tem papel claramente designado mas sabe-se que pode estar envolvida em interações entre o sistema dois-componentes e o transportador ABC Pst (Gardner, et al 2014).

7.1. Metodologia

7.1.1. Clonagem molecular dos genes *phoU*, *phoB* e *phoR*

A clonagem molecular dos genes *phoU*, *phoR* e *phoB* foi realizada através da amplificação por PCR dos genes a partir do genoma de *X. citri*. A amplificação foi realizada com oligonucleotídeos apresentados na Tabela 2. As amplificações foram realizadas com *Taq* Hi-Fi ou enzima KOD (Toyobo global). As reações foram realizadas com volume final de 50 µL e seguiram o protocolo recomendado pelos fabricantes. O ciclo de amplificação consistiu de 95°C por três minutos como temperatura de desnaturação inicial, 25 ciclos de 95°C para desnaturação por 30 segundos, 55°C para anelamento dos primers por 50 segundos, 72°C para extensão do fragmento por 50 segundos. Os produtos das amplificações foram analisados em gel de agarose 0,8%. Após a confirmação dos fragmentos, estes foram ligados no vetor de clonagem pGEM ou ZeroBlunt. A reação de ligação seguiu protocolo padrão (Sambrook et al, 2001). Após a ligação, amostras de 3 µl foram usadas para transformação por choque térmico de células competentes de *E. coli* DH5α. A reação de ligação foi mantida em contato com as células competentes em gelo por aproximadamente trinta minutos. A seleção das células que incorporaram o plasmídeo foi realizada com o plaqueamento das mesmas em LB agar contendo ampicilina (100mg /mL) e X-gal (20 mg/ml). As colônias brancas foram selecionadas para confirmação da clonagem molecular através de PCR de colônia seguindo a recomendação do manual da enzima *Taq* recombinante (Invitrogen).

Tabela 1. Oligonucleotídeos utilizados para amplificação dos genes *phoU*, *phoB* e *phoR* de *X. citri* e PCR de colônia para confirmação dos insertos. A sequência dos primers disponibilizados a seguir referem-se à direção 5'-3'. Regiões sublinhadas referem-se aos sítios das enzimas de restrição inseridos nos primers objetivando a clonagem.

Gene	Primer Forward	Primer Reverso
<i>phoU</i>	5' CATATGAACCAGCACCTCA 3'	5' AAGCTTCATGGCCGCAGCAGA
<i>phoB</i>	5' CATATGGACGACGAAGAC 3'	5' CTCGAGTCAGGTCGCCGAAGAAAAACG 3'
<i>phoR</i>	5' CATATGTTGCGCACCTACCGCGC 3'	5' CTCGAGTCACGCCGAGCGTGACA 3'
pGEM	5' TAATACGACTCACTATAGGG 3'	5' ATTTAGGTGACACTATAGAA 3'
pET28a	5' TAATACGACTCACTATAGGG 3'	5' GCTAGTTATTGCTCAGCGGTG 3'

A subclonagem foi realizada primeiramente com a extração alcalina do DNA recombinante pGEM das células de *E. coli* DH5- α , confirmadas através de PCR de colônia ou análise de restrição. Posteriormente, o vetor pGEM contendo os genes alvo foi submetido à digestão com as enzimas de restrição *NdeI* e *XhoI*. A digestão com as enzimas de restrição foi idealizada para o volume de 50 μ L contendo 15 μ L do plasmídeo pGEM, 1 μ L da enzima *NdeI* e 1 μ L da enzima *XhoI*, 0,5 μ L de BSA e 30,5 μ L de água mili-Q estéril. Os fragmentos foram recuperados por meio do procedimento de extração em gel de agarose (Qiagen Gel Extraction) e ligados nos vetores de expressão pET28 ou pETMBP de acordo com o manual da enzima T4 DNA ligase da marca comercial Invitrogen®.

7.1.2. Extração e Expressão das Proteínas Recombinantes

A expressão dos genes de interesse para produção das proteínas PhoB, PhoR e PhoU foi realizada em células de *E. coli* Turner (DE3). As condições estabelecidas para a produção das mesmas foram: meio LB com canamicina (50 mg/mL), 200 r.p.m.; fase logarítmica de crescimento: D.O. 0.5 – 0.6 (A_{600}); 0.5 mM de indutor (IPTG – isopropil-beta-D-tiogalactopiranosídeo). Como controle do nível de expressão das proteínas, alíquotas do frasco de indução foram coletadas no tempo zero (indução prévia - T0) e após a indução de quatro horas (tempo quatro – T4). As células foram coletadas após centrifugação a 7000 r.p.m. por 25 minutos.

A extração das proteínas da fração solúvel iniciou-se pela ressuspensão das células em tampão Tris-HCl pH 8.0, 10 mM com 1% de Triton X-100 seguida de sonicação por 3 pulsos de 30 segundos com amplitude de 40% e intervalos de 1 minuto de descanso. As amostras foram submetidas à centrifugação por 20 minutos a 4°C na velocidade de 48 200 g, para separação de extratos solúveis e insolúveis.

A análise da expressão das proteínas foi realizada em SDS-PAGE 12% com espessura de 1,5 mm. Alíquotas do extrato solúvel, insolúvel, tempo zero (T0) e tempo quatro (T4) foram ressuspensas em tampão de amostra e aquecidas por 10 minutos a 100°C.

7.1.3. Purificação das proteínas recombinantes PhoU, PhoR e PhoB

A purificação das proteínas foi realizada pelo método de cromatografia de afinidade à níquel. Utilizou-se coluna Hi-trap™ HP de 5 mL (GE Healthcare®) em aparelho AKTA-FPLC (Amersham Biosciences) equipado com monitor UPC-900, bomba P-920, válvula INV-907, misturador M-925 e fracionador FRAC-900-901 (GE Healthcare®).

O procedimento de purificação foi padronizado para todas as proteínas utilizando como base o tampão Tris-Cl 10 mM pH 8,0, 500 mM NaCl e um gradiente de imidazol nas concentrações de 5 mM, 50 mM, 150 mM e 500 mM. A cromatografia de afinidade ao níquel foi realizada no aparelho AKTA purifier UPC-900, com os seguintes parâmetros: 2 volumes de coluna (2 cv) de tampão Tris-Cl 10 mM pH 8,0; 50 mL de injeção da amostra; 10 cv para lavagem da coluna sob pressão de 0.2 bar, com o fluxo de 1 mL por minuto. A maior concentração de proteína foi obtida com 150 mM de imidazol. Antes do início de cada experimento todos os tampões foram filtrados e deareados com o intuito de evitar bolhas de ar e retenção de micropartículas no interior do aparelho, e os extratos foram filtrados em filtros 0.45 µM (Millipore).

As frações de lavado e eluídas foram analisadas em gel SDS-PAGE a 12%. Para garantir a qualidade das amostras purificadas, após a análise em gel, as amostras mais puras oriundas da cromatografia de afinidade à metal foram concentradas em filtros Amicon (Millipore®) e submetidas à cromatografia de exclusão molecular realizada em coluna Superdex 16/60 200. As proteínas purificadas foram concentradas até o volume final de 1 mL em filtros Amicon (10.000 MWCO). A dosagem das proteínas purificadas foi realizada pelo método de Eldhoch (1967).

7.1.4. Ensaios de cristalização das proteínas PhoU, PhoR e PhoB e coleta de dados de cristalização

As proteínas PhoU, PhoR e PhoB foram submetidas aos ensaios de cristalização iniciais na concentração inicial de 10 mg/mL em tampão Tris-Cl 10 mM pH 8,0. Para cada proteína foram testadas aproximadamente 1000 condições de cristalização utilizando as soluções de cristalização dos

kits comerciais Crystal Screen 2 e Salt RX da empresa Hampton Research; Precipitant Synergy e Wizard I e II da Emeral Biosystem; PACT e JCSG+ da Quiagen.

O método de cristalização foi o método de gota pendurada por difusão de vapor com a proporção de 1:1 (solução de cristalização comercial: proteína 10 mg/mL), sendo o volume final da gota de 1 μ L e 50 μ L de solução de cristalização no reservatório de cristalização. Os ensaios iniciais de cristalização foram realizados no laboratório de cristalização de proteínas automatizado (Robolab, LNBio) e no Centro de Investigaciones Biológicas (Madrid). O refinamento das condições iniciais foram otimizados através do método de matriz esparsa variando a concentração de precipitante e do pH da condição de cristalização. Os cristais des proteínas tiveram seu padrão de difração coletados nas linhas de luz do laboratório Nacional de Luz Síncrotron localizado em Campinas (Brasil) e no síncrotron Paull-Scherrer (Suíça).

7.1.5. Medidas de espalhamento de Luz e proteólise com a protease 3C

As medidas de espalhamento de luz (Dynamic Light Scattering) foram realizadas em tampão Tris-Cl 10 mM pH 8.0, na concentração de 1 mg/mL no equipamento DynaPro com 100 acúmulos de coleta. Para as construções fusionadas à MBP a remoção da proteína de fusão foi realizada com a protease 3C utilizando-se a estequiometria 1:100, 1:200 e 1:400. A reação foi realizada em 10 mM de Tris-Cl pH 8.0, em um volume final de 500 μ L em 4°C durante 24 horas.

7.2. Resultados e Discussão

As proteínas PhoB e PhoR integram os sistema de sinalização bacteriana dois componentes como apresentado na introdução deste trabalho bem como no artigo de proteômica (artigo N° 2) apresentado na sessão 3.1 dos resultados. A proteína PhoU é expressa a partir do operon que contém os genes do sistema Pst. A identidade de sequências dos ortólogos de *E. coli* e as proteínas de *X. citri* são exibidos na tabela 3, a seguir.

Tabela 2. Ortólogos das proteínas do operon de fosfato de *E. coli* (K-12) encontrados no genoma de *X. citri*. Os dados foram adquiridos usando-se o banco de dados KEGG (<http://www.genome.jp/kegg/>).

Gene em <i>Eco</i>	Identificação gênica (<i>Eco</i>)	Descrição Funcional	Correspondente em <i>Xac306</i>	Identidade sequencial
<i>phoB</i>	16128384	Proteína ligadora de DNA em resposta ao componente PhoR; sistema dois componentes; Família Omp.	<i>Xac1042</i>	59%
<i>phoR</i>	16128385	Sensor histidina-quinase; sistema dois componentes com PhoB (EC:2.7.3.)	<i>Xac1041</i>	40%
<i>phoU</i>	16131592	Regulador negativo PhoR/PhoB	<i>Xac1573</i>	33%

O gene *phoU* o qual é integrante do operon *pst* codifica uma proteína com 28 kDa cuja função biológica não é totalmente entendida. A proteína PhoU aparentemente pode atuar como um regulador negativo do sistema de sinalização do fosfato, mas não intereferir diretamente no transporte. De acordo com Gardner (2014) e Lee (2014), a PhoU em *E.coli* comporta-se como um dímero em solução e interage diretamente com PhoR, a proteína sensorial do sistema dois-componentes. Além de interagir com o PhoR a proteína PhoU também interage diretamente com a proteína PstB, ATPase do sistema transportador de fosfato. Os estudos estruturais e duplo híbrido demonstraram nos últimos meses as regiões importantes para a dimerização de PhoU e sua interação direta com PhoR e PstB, no entanto, a mecânica do processo de sinalização e transporte ainda não foi elucidada (Gardner et al, 2014).

Por conseguinte, nossos esforços para entender o sistema de sinalização em *X. citri* foram iniciados com a clonagem do gene *phoU* em vetor pGEM e a subclonagem em vetor pET28a. Cada etapa da clonagem e da subclonagem foram conferidas através de análise de restrição e de sequenciamento de DNA (Figura 10). Posteriormente, os clones sem qualquer tipo de mutação foram transformados em *E. coli* Tuner (DE3) a qual possui uma mutação do componente de membrana LacZ e facilita a entrada uniforme do indutor IPTG (concentração do ensaio = 0,5 mM) nas células durante a indução,

melhorando o rendimento da proteína PhoU. A eluição da proteína PhoU ocorreu com 150 mM de Imidazol com 90% de pureza, após a lavagem e a concentração de PhoU, o rendimento obtido foi de 29 mg/mL para cada 500 mL de cultura induzidos (Figura 10B). PhoU apresentou-se estável durante a expressão e purificação e o extrato purificado apresentou coloração amarronzada indicativo de ligação ao ferro. Os ensaios de cristalização foram conduzidos no robô do laboratório de Biologia estrutural do Centro de Investigaciones Biológicas (CSIC-CIB) em Madrid. Pequenos cristais e em forma de agulha foram obtidos na condição de 10% PEG4000, 10% Isopropanol, 100 mM Citrato de Sódio pH 5.6 (Kit comercial JB1-4) e 10% PEG8000, 100 mM Fosfato de Potássio pH 6.2 e 200 mM de NaCl (Kit Comercial Wizard I e II). As tentativas de cristalização utilizando 10 mg/mL apresentaram intensa precipitação durante o refinamento das condições, dificultando o processo. A estratégia foi reduzir a concentração de proteína de 10 mg/mL para 6 mg/mL. Os melhores cristais foram obtidos através de refinamento manual com a proteína PhoU em 6 mg/mL na condição refinada de 12% PEG4000, 10% de Isopropanol e 100 mM Citrato de Sódio pH 5.6 (condição refinada do kit JB1-4). Durante o refinamento foi observado que havia uma forte influência da quantidade de precipitante, neste caso PEG400 para o refinamento, pois o pH entre 4.6 até 5.8 não foi limitante para a obtenção dos cristais, mas a concentração do precipitante sim. Ainda assim, os cristais não eram grandes e alguns em forma de placas.

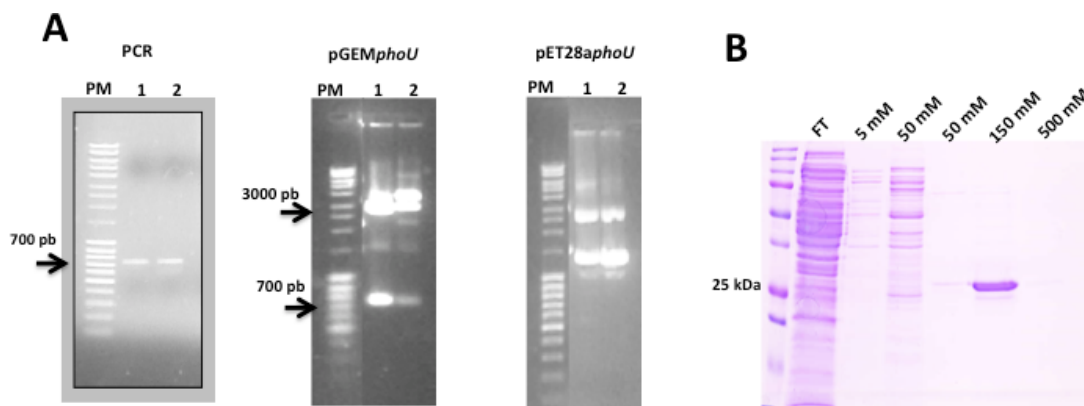


Figura 10. Clonagem do gene *phoU* e purificação da proteína recombinante PhoU. A) Clonagem do gene *phoU* ocorreu em três etapas: amplificação do fragmento de 700 pb através do PCR, clonagem no vetor pGEM (Novagen®). A confirmação da clonagem ocorreu através da análise de restrição e o clone 1 foi utilizado para a subclonagem no vetor pET28a. A confirmação dos clones 1 e 2 do vetor pET28 foram confirmados por análise de sequenciamento e de restrição. B) Expressão do gene *phoU* em células Tuner (DE3). Após a expressão, o lisado de bactérias foi submetido a purificação de afinidade a níquel em gradiente de imidazol. A proteína PhoU foi eluída com 150 mM de Imidazol com mais de 90% de pureza.

A proteína ligadora de maltose, MBP foi utilizada como estratégia para o domínio C-terminal da proteína PhoB e da proteína PhoR em sua porção citoplasmática com o intuito de melhorar o rendimento na fração solúvel. O domínio C-terminal (resíduos 140 a 225) com base na estrutura de PhoB de ortólogos é o domínio de interação com o DNA e sua produção seria interessante para ensaios estruturais, como também ensaios de mobilidade eletroforética ou gel-shift. A clonagem de *phoB* foi realizada através da amplificação pelo método de PCR, no qual o fragmento foi amplificado em elevadas concentrações com a enzima KOD, DNA polimerase de alta fidelidade com o intuito de evitar mutações eventuais que poderiam ocorrer com Taq recombinante. Os transformantes obtidos tiveram a confirmação da clonagem através da análise de restrição e sequenciamento. Os fragmentos obtidos da digestão do vetor *ZeroBluntphoU* foram ligados no vetor pETMBP digeridos previamente com as mesmas enzimas e confirmada a clonagem por sequenciamento. O domínio C-terminal da proteína PhoB foi purificada após o procedimento de indução através da IMAC, sendo a fração mais limpa das proteínas eluídas na concentração de 500 mM de Imidazol. Após a concentração foram obtidas amostras de 18 mg/mL para cada 500 mL de cultura (figura 11).

A proteína PhoB fusionada a proteína MBP foi submetida à cristalização de proteínas no laboratório de cristalização do Centro de Investigações Biológicas (CSIC-CIB) em Madrid, sob supervisão do Dr. Javier Medrano, mas nenhum cristal foi obtido e novas estratégias estão em andamento para obter o domínio C-terminal da proteína PhoB sem a cauda de MBP, a clonagem da construção completa, como também a clonagem da região N-terminal (resíduos 1 a 144).

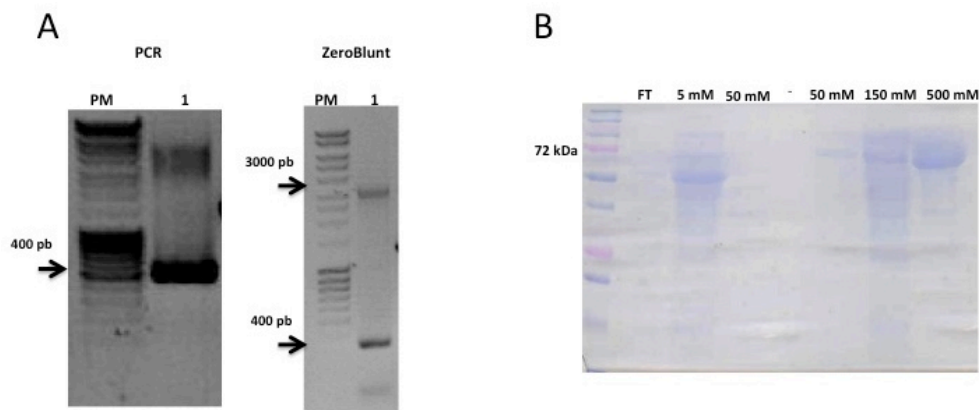


Figura 11. Clonagem e purificação do domínio C-terminal *phoB* de *X. citri*. A) Clonagem através da amplificação do domínio C-terminal de 400 pb em alto rendimento. Os fragmentos foram clonados no vetor de clonagem ZeroBlunt. B) o Domínio C-terminal da proteína PhoB foi clonado no vetor de expressão pETMBP para expressão em células Tuner (DE3) com 72 kDa.

Com relação à proteína PhoR, nossa estratégia de clonagem remeteu-se aos passos futuros de expressão e purificação considerando relevantes porções da região citosólica incluindo os domínios PAS e DhP. Conforme dito na introdução, o domínio PAS compreende os primeiros resíduos de aminoácidos logo após a membrana, ainda não compreendido totalmente no contexto da função biológica da PhoR e o domínio DhP é o domínio que sofre a autofosforilação, também conhecido como domínio HiskA. O gene *phoR* foi clonado nos vetores de expressão pET28a fusionado no N-terminal com cauda de 6 histidinas e vetor pETMBP fusionado à MBP no N-terminal (Figura 12A). Foram obtidos e confirmados por PCR de colônia dois clones do genes *phoR* no vetor de expressão pET28 e pETMBP.

A expressão do domínio citosólico com 40 kDa ocorreu em corpúsculos de inclusão sendo inviável a recuperação dessas proteínas. Neste contexto, a estratégia de produção da proteína PhoR fusionada à MBP foi assertiva e permitiu a expressão e a solubilização da proteína PhoR obtendo-se quantidades razoáveis para cada 500 mL de cultura (Figura 12B). A proteína PhoR fusionada à cauda MBP foi purificada através da cromatografia de afinidade a níquel, a eluição da proteína ocorreu na concentração de 500 mM de imidazol de forma pura e estável (Figura 12C). As amostras de 500 mM foram submetidas à digestão com a protease 3C para remoção da MBP e submetidas à filtração em gel (Figura 12D). No entanto, após a remoção da cauda MBP a proteína PhoR se comportou de forma instável em solução. Os picos obtidos na filtração em gel revelaram que após a clivagem houve a formação de agregados moleculares a eluição de PhoR, MBP e 3C em um único pico, o qual se referia ao volume morto da coluna. Para evitar esse problema, outras estratégias foram realizadas, mas nenhuma resultou na obtenção da proteína estável em solução após a remoção da MBP. Ressalta-se ainda que a digestão com a protease não foi completa observando fração de PhoR fusionada a proteína MBP na figura 12D (*).

Com o intuito de verificarmos se a proteína PhoR estava agregando desde a cromatografia de afinidade ao níquel ou durante sua extração, as amostras de PhoR não digeridas com a protease 3C foram submetidas à análise de DLS (Figura 13). Os resultados mostram que as amostras de PhoR apresentaram 17% de polidispersividade, correspondendo a 85% da amostra. Além disso, o DLS sugeriu que PhoRMBP (70 kDa) pode apresentar-se como dímeros em solução.

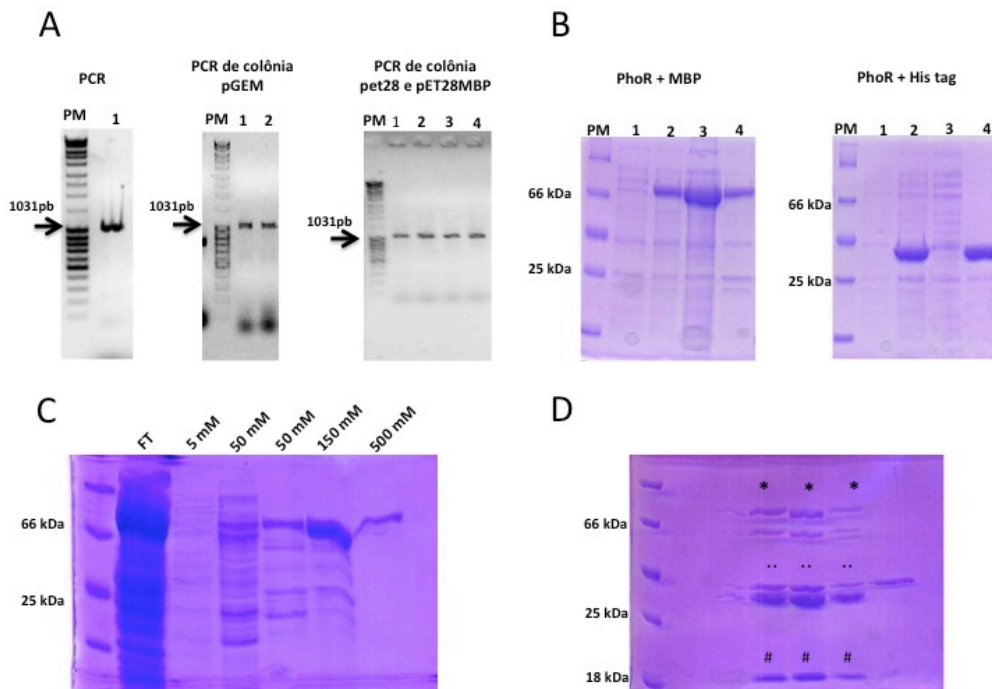


Figura 12. Clonagem, expressão e purificação da proteína PhoR de *X. citri*. A) Clonagem do fragmento de 1031 pares de bases referente ao gene *phoR* no vetor pGEM. O fragmento clonado no pGEM foi subclonado nos vetores de expressão pET28 e pETMBP. As amostras 1, 2, 3 e 4 foram confirmadas positivas para a clonagem do gene através do PCR de colônia e sequenciamento nos vetores pET28 e pETMBP, respectivamente. B) Expressão da proteína PhoR. Os vetores pET28phoR e pETMBPphoR foram transformados na linhagem de *E. coli* Turner (DE3) para expressão. Os géis de SDS-PAGE 12% PhoR+MBP (70 Kda) e PhoR+His tag (40 Kda) representam as seguintes amostras: PM – Marcador de peso molecular; 1 – Aliquota da cultura bacteriana prévia adição de IPTG denominada de tempo zero de indução; 2 – Aliquota de cultura bacteriana após 4 horas de indução; 3 – Fração Solúvel após lise bacteriana; 4- Fração insolúvel após lise bacteriana. A fusão da proteína MBP na região N-terminal da proteína PhoR resultou na produção da proteína PhoR na fração solúvel, o que não foi possível sem a cauda MBP. Somente a cauda de histidina fusionada no N-terminal da proteína PhoR foi produzida nos corpúsculos de inclusão bacterianos dificultando sua recuperação. C) Purificação da proteína PhoR+MBP. A eluição da proteína PhoR através de um gradiente de imidazol ocorreu na fração de 500 mM de Imidazol. A fração de 150 mM, concentração usualmente eluída grande parte das proteínas deste trabalho apresentou-se com muitos contaminantes, sugerindo adequação do volume de resina e volume de coluna utilizado para purificação em cada etapa. D) Remoção da MBP. A remoção da cauda MBP foi realizada por 18 horas utilizando a protease 3C. As amostras foram então, submetidas à filtração em gel na qual um único pico foi recuperado no volume morto da coluna. As amostras foram aplicadas no gel SDS-PAGE 12 % e revelaram que não houve a separação entre a proteína PhoR e MBP (...), assim como a ineficiência da digestão da proteína 3C (**) e a presença da protease 3C (#). Provavelmente a presença de todas essas proteínas em um mesmo pico sugerem agregação da amostra e instabilidade da proteína PhoR nas condições usadas para isolamento.

A estrutura da PhoR de *E. coli* que dimeriza em solução (Casino et al, 2010) e esse estado conformacional é elementar para sua função biológica de transferase e fosfatase. Portanto, mesmo fusionada à MBP a proteína PhoR exibiu maior estabilidade e estado dimérico de acordo com o peso molecular observado na medida de DLS, corroborando dados da literatura já descritos. Conforme exposto na tabela 4, a proteína PhoR de *X. citri* conserva 40% dos resíduos de amino ácidos da proteína PhoR de *E. coli*.

Proteína	Raio	%PD	PM	% Mass
PhoR	5.8	17%	206	85%

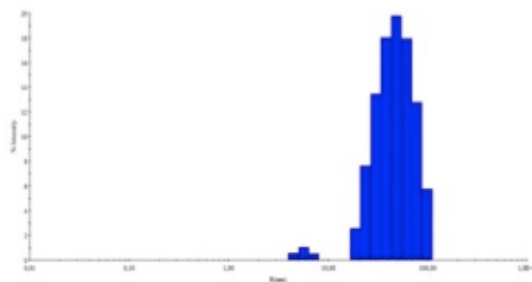


Figura 13. Análise de espalhamento dinâmico de luz, DLS (Dynamic Laser Scattering). Amostras da proteína PhoRMBP não digeridas com a protease 3C na concentração de 1 mg/mL foram submetidas à análise de DLS após a exclusão molecular (gel não mostrado na figura 23). O correspondente a 85% da amostra apresentou uma polidispersividade de 17% e um raio de 5.8. A massa molecular estimada para a amostra por meio dessa medida foi de aproximadamente 206 kDa referente a um dímero em solução.

8. Anexo 2 – Material Suplementar Manuscrito III

Table S1. List of all proteins identified by LS MS/MS in *X. citri::pstS* proteomics and comparison with previous data obtained for *X. citri* (Pegos et al., 2014). Cells were grown in A, A+P_i media.

KEGG ID	Pathway	<i>gene name</i>	A Medium	A+P _i Medium
	Protein			
Carbohydrate metabolism				
XAC0030	cellulase	<i>egl</i>	x	x
XAC0168	5-keto-4-deoxyuronate isomerase	<i>kdul</i>	-	x
XAC0224	pyruvate dehydrogenase	<i>poxB</i>	x	x
XAC0472	ribulose-phosphate 3-epimerase	<i>rpe</i>	x	x
XAC0532	acetyl-CoA carboxylase biotin carboxyl carrier protein subunit	<i>bccP</i>	x	-
XAC0604	trehalase	<i>treA</i>	x	x
XAC0680	6-phosphogluconate dehydrogenase-like protein	<i>gndA</i>	x	x
XAC0902	transaldolase B	<i>talB</i>	x	x
XAC0927	branched-chain amino acid aminotransferase	<i>ilvE</i>	x	x
XAC1006	malate dehydrogenase	<i>mdh</i>	x	x
XAC1024	non-hemolytic phospholipase C		x	-
XAC1348	acetoacetyl-CoA thiolase	<i>atoB</i>	x	x
XAC1533	dihydrolipoamide dehydrogenase	<i>ldp</i>	x	x
XAC1534	dihydrolipoamide succinyltransferase	<i>sucB</i>	x	x
XAC1584	3-hydroxybutyryl-CoA dehydratase	<i>crt</i>	x	x
XAC1785	3-methyl-2-oxobutanoate hydroxymethyltransferase	<i>panB</i>	-	x
XAC2077	succinate dehydrogenase flavoprotein subunit	<i>sdhA</i>	x	-
XAC2078	succinate dehydrogenase iron-sulfur subunit	<i>sdhB</i>	x	-
XAC2385	extragenic suppressor protein SuhB	<i>suhB</i>	-	-
XAC2874	phosphoglycerate mutase	<i>gpmA</i>	x	x
XAC3344	fructose-bisphosphate aldolase		-	x
XAC3345	pyruvate kinase	<i>pykA</i>	x	x
XAC3352	glyceraldehyde-3-phosphate dehydrogenase	<i>gapA</i>	x	x
XAC3388	type II citrate synthase	<i>gltA</i>	x	x
XAC3470	malic enzyme	<i>maeB</i>	x	x
XAC3659	dihydrolipoamide dehydrogenase	<i>lpdA</i>	x	x
XAC3661	dihydrolipoamide acetyltransferase	<i>phdB</i>	x	x
XAC4132	6-phytase; K01093 4-phytase / acid phosphatase	<i>appA</i>	x	-
XAC4150	nodulation protein	<i>nodL</i>	-	x
Energy metabolism				

XAC0204	glutamine synthetase	<i>glnA</i>	x	x
XAC0348	transferase		x	x
XAC0724	cytochrome c4	<i>cycA</i>	x	x
XAC0743	serine hydroxymethyltransferase	<i>glyA</i>	x	x
XAC1211	Catalase	<i>katE</i>	x	x
XAC1258	cytochrome o ubiquinol oxidase subunit II	<i>cyoA</i>	x	x
XAC1462	carbonic anhydrase	<i>cynT</i>	x	-
XAC1604	carbonic anhydrase	<i>yadF</i>	x	X
XAC1637	histidine ammonia-lyase	<i>hutH</i>	x	x
XAC2077	succinate dehydrogenase flavoprotein subunit	<i>sdhA</i>	x	-
XAC2078	succinate dehydrogenase iron-sulfur subunit	<i>sdhB</i>	x	-
XAC3341	cysteine synthase	<i>cysK</i>	x	x
XAC3442	inorganic pyrophosphatase	<i>ppa</i>	x	x
XAC3602	cystathionine gamma-lyase-like protein;	<i>metB</i>	x	x
XAC3628	cysteine synthase	<i>cysM</i>	-	x
XAC3649	F0F1 ATP synthase subunit beta	<i>atpD</i>	X	x
XAC3650	uncG; F0F1 ATP synthase subunit gamma	<i>atpG</i>	X	-
XAC3651	F0F1 ATP synthase subunit alpha	<i>atpA</i>	X	X
XAC3652	F0F1 ATP synthase subunit delta	<i>atpH</i>	x	-
XAC3653	uncF; F0F1 ATP synthase subunit B	<i>atpF</i>	x	-
XAC3654	F0F1 ATP synthase subunit C	<i>atpE</i>	x	-
XAC3924	spermidine synthase	<i>speE</i>	x	x
Lipid Metabolism				
XAC0384	3-oxoacyl-[acyl-carrier protein] reductase		x	-
XAC0433	3-oxoacyl-[ACP] reductase		x	-
XAC0833	acyl-CoA thioesterase I	<i>tesA</i>	x	-
XAC1024	non-hemolytic phospholipase C		x	-
XAC1127	3-ketoacyl-(acyl-carrier-protein) reductase	<i>fabG</i>	x	-
XAC1128	acyl carrier protein	<i>acpP</i>	x	X
XAC1129	3-oxoacyl-(acyl carrier protein) synthase II	<i>fabF</i>	x	-
XAC1348	acetoacetyl-CoA thiolase	<i>atoB</i>	x	x
XAC1463	phospholipase		x	-
XAC1472	glutaryl-CoA dehydrogenase	<i>gcdH</i>	-	-
XAC2780	lipoprotein	<i>rlpB</i>	X	x
XAC2885	phospholipase A1		X	x
Nucleotide metabolism				
XAC0996	DNA-directed RNA polymerase subunit alpha	<i>rpoA</i>	X	x
XAC1158	adenylosuccinate synthetase	<i>purA</i>	X	x
XAC2015	nucleoside diphosphate kinase	<i>ndk</i>	X	x
XAC2360	dihydroorotase	<i>pyrC</i>	X	x
XAC2740	deoxycytidine triphosphate deaminase	<i>dcd</i>	X	x
XAC3345	pyruvate kinase	<i>pykA</i>	X	-
XAC3437	adenylate kinase	<i>adk</i>	X	X
Amino acid metabolism				
XAC0804	adenosylhomocysteinase	<i>ahcY</i>	-	-
XAC0125	aromatic amino acid aminotransferase	<i>tyrB</i>	x	x
	indole-3-glycerol phosphate synthase	<i>trpC</i>	-	x

XAC0204	glutamine synthetase	<i>glnA</i>	x	X
XAC0336	5-methyltetrahydropteroyltrimethylglutamate-- homocysteine methyltransferase	<i>metE</i>	-	-
XAC0484	S-adenosylmethionine decarboxylase	<i>speD</i>	x	-
XAC0680	6-phosphogluconate dehydrogenase-like protein	<i>gndA</i>	x	X
XAC0743	serine hydroxymethyltransferase	<i>glyA</i>	x	X
XAC0813	Methionine adenosyltransferase	<i>metK</i>	x	X
XAC0815	methyltransferase		-	-
XAC0851	NADH-dependent FMN reductase	<i>sflA</i>	-	-
XAC0927	branched-chain amino acid aminotransferase	<i>ilvE</i>	x	x
XAC1158	adenylosuccinate synthetase	<i>purA</i>	x	x
XAC1204	alanyl dipeptidyl peptidase		-	-
XAC1336	5'-methylthioadenosine phosphorylase	<i>deoD</i>	-	x
XAC1348	acetoacetyl-CoA thiolase	<i>atoB</i>	x	x
XAC1472	glutaryl-CoA dehydrogenase	<i>gcdH</i>	-	-
XAC1533	dihydrolipoamide dehydrogenase	<i>ldp</i>	x	x
XAC1534	dihydrolipoamide succinyltransferase	<i>sucB</i>	x	x
XAC1635	urocanate hydratase	<i>hutU</i>	-	-
XAC1637	histidine ammonia-lyase	<i>hutH</i>	x	x
XAC2547	dihydrodipicolinate synthetase	<i>dapA</i>	x	x
XAC2932	protease	<i>pfpI</i>	x	-
XAC3309	aminopeptidase		x	x
XAC3318	alanyl aminopeptidase	<i>pepN</i>	-	-
XAC3341	cysteine synthase	<i>cysK</i>	x	x
XAC3556	aminopeptidase AI	<i>pepA</i>	x	x
XAC3602	cystathionine gamma-lyase-like protein	<i>metB</i>	x	x
XAC3628	cystein synthase	<i>cysM</i>		x
XAC3659	dihydrolipoamide dehydrogenase	<i>lpdA</i>	x	x
XAC3924	spermidine synthase	<i>speE</i>	x	x
XAC3987	leucine aminopeptidase		x	-
XAC4009	arginase	<i>argI</i>	-	x
XAC4187	2-hydroxyhepta-2,4-diene-1,7- dioateisomerase/5-carboxymethyl-2-oxo-hex- 3-ene-1,7-dioatedecarboxylase		x	x
XAC4369	phosphatase precursor	<i>phoC</i>	x	-

Glycan biosynthesis and Metabolism

XAC0662	Membrane bound lytic transglycolase (CDD)	<i>mltB</i>	x	-
XAC1466	peptidoglycan-associated outer membrane lipoprotein	<i>pcp</i>	x	-
XAC1728	lipoprotein nlpD	<i>nlpD</i>	x	-
XAC2585	GumB protein	<i>gumB</i>	x	x
XAC3225	transglycosylase	<i>mltB</i>	x	x

Cofactors and vitamin metabolism

XAC0158	L-fucose dehydrogenase		x	x
---------	------------------------	--	---	---

XAC0334	NADH-dependent FMN reductase	<i>sflA</i>	-	-
XAC0743	serine hydroxymethyltransferase	<i>glyA</i>	x	x
XAC0750	6,7-dimethyl-8-ribityllumazine synthase	<i>ribH</i>	x	-
XAC2035	non-heme chloroperoxidase;	<i>cpoF</i>	x	x
XAC4040	delta-aminolevulinic acid dehydratase	<i>hemB</i>	x	x
XAC4109	coproporphyrinogen III oxidase	<i>hemF</i>	x	-
XAC4302	GTP cyclohydrolase I	<i>folE</i>	x	-
XAC4369	phosphatase	<i>phoC</i>	x	-
Terpenoid backbone biosynthesis				
XAC1348	acetoacetyl-CoA thiolase	<i>atoB</i>	x	x
XAC3583	dTDP-4-dehydroorhamnose 3,5-epimerase	<i>rmlC</i>	x	x
Xenobiotics Biodegradation and Metabolism				
XAC0125	aromatic amino acid aminotransferase		<i>tyrB</i>	x
XAC0815	methyltransferase		-	-
XAC1472	glutaryl-CoA dehydrogenase	<i>gcdH</i>	-	-
XAC2077	succinate dehydrogenase flavoprotein subunit	<i>sdhA</i>	x	-
XAC2078	succinate dehydrogenase iron-sulfur subunit	<i>sdhB</i>	x	-
XAC2736	carboxymethylenebutenolidase		x	-
XAC3162	beta lactamase	<i>bla</i>	x	x
XAC4342	toluene tolerance protein	<i>yrbC</i>	x	x
RNA polymerase and Transcription				
XAC0996	DNA-directed RNA polymerase subunit alpha	<i>rpoA</i>	x	x
XAC1643	poly(hydroxyalcanoate) granule associated protein	<i>phaF</i>	x	x
XAC2358	DnaK supressor	<i>dksA</i>	x	x
XAC2454	stringent starvation protein A	<i>sspA</i>	x	x
Translation and Ribosome				
XAC0957	elongation factor Tu	<i>tuf</i>	x	x
XAC0951	50S ribosomal protein L25/general stress protein Ctc	<i>rplY</i>	-	x
XAC0962	50S ribosomal protein L1	<i>rplA</i>	-	x
XAC0970	elongation factor Tu	<i>tuf</i>	x	x
XAC0973	50S ribosomal protein L4;	<i>rplD</i>	-	-
XAC0978	30S ribosomal protein S3	<i>rpsC</i>	-	x
XAC0987	50S ribosomal protein L6	<i>rplF</i>	-	x
XAC1418	ribosome recycling factor	<i>frf</i>	x	-
XAC1421	elongation factor Ts	<i>tsf</i>	-	-
XAC2380	elongation factor P	<i>efp</i>	x	-
XAC3392	translation initiation inhibitor	<i>yjgF</i>	x	-
XAC4229	starvation sensing protein	<i>rspA</i>	x	x
DNA Replication				
XAC0027	plasmid stable protein K		x	-
XAC0120	TldD protein	<i>tldD</i>	x	x
XAC0121	TldD protein	<i>tldD</i>	x	x
XAC2905	single-stranded DNA-binding protein	<i>hupB</i>	x	x
XAC3058	histone H1		x	-

XAC3123	DNA-binding-like protein		X	-
XAC3356	endonuclease;		X	-
XAC3979	histone H1-like protein	<i>bpH1</i>	X	-
Folding and Sort degradation				
XAC0023	carboxyl-terminal protease	<i>ctp</i>	X	X
XAC0541	co-chaperonin GroES	<i>groES</i>	X	-
XAC0542	Chaperonina 60 kDa	<i>groEL</i>	X	X
XAC0637	ATP-dependent protease peptidase subunit;	<i>hslV</i>	X	X
XAC0865	peptidyl-prolyl cis-trans isomerase	<i>surA</i>	X	-
XAC0907	alkyl hydroperoxide reductase subunit C	<i>ahpC</i>	X	X
XAC1585	peptidyl-prolyl cis-trans isomerase	<i>ppiB</i>	X	-
XAC1078	ATP-dependent Clp protease proteolytic subunit	<i>clpP</i>	X	X
XAC1085	peptidyl-prolyl cis-trans isomerase	<i>ppiD</i>	X	-
XAC1321	periplasmic protease	<i>mucD</i>	X	X
XAC1456	peptidyl-dipeptidase	<i>dcp</i>	X	-
XAC1521	heat shock protein GrpE	<i>grpE</i>	X	-
XAC1550	FKBP-type peptidyl-prolyl cis-trans isomerase	<i>fkpA</i>	X	-
XAC2783	thioredoxin	<i>trx</i>	X	X
XAC3550	disulfide isomerase	<i>dsbC</i>	-	-
XAC3664	outer membrane protein	<i>ompW</i>	X	X
Membrane Transport				
XAC0008	TonB protein	<i>TonB</i>	-	X
XAC0009	biopolymer transport ExbB protein	<i>exbB</i>	X	X
XAC0011	biopolymer transport ExbD2 protein	<i>exbD2</i>	X	-
XAC0019	outer membrane protein	<i>ompP1</i>	X	X
XAC0074	TonB-dependent receptor	<i>cirA</i>	X	-
XAC0126	iron complex outer membrane receptor protein	<i>yncD</i>	-	-
XAC0176	ferripyoverdine receptor	<i>fpvA</i>	X	X
XAC0221	preprotein translocase subunit SecB	<i>secB</i>	X	-
XAC0291	Oar protein	<i>oar</i>	-	X
XAC0473	membrane protein		X	-
XAC0626	Outer membrane lipoprotein		-	-
XAC0693	TonB-dependent receptor	<i>fecA</i>	X	-
XAC0716	TonB-dependent receptor	<i>fyuA</i>	X	X
XAC0823	outer membrane hemin receptor	<i>phuR</i>	-	X
XAC0829	NitT/TauT family transport system substrate-binding protein	<i>Nit/Tau</i>	-	X
XAC0849	sulfonate-binding protein	<i>ssuA</i>	-	X
XAC0852	TonB-dependent receptor	<i>tonB</i>	-	X
XAC0866	LPS-assembly protein	<i>ostA</i>	X	X
XAC0947	outer membrane lipoprotein LolB	<i>lolB</i>	X	-
XAC1012	outer membrane protein	<i>mopB</i>	X	X
XAC1017	Sulfate binding protein	<i>sbp</i>	X	X
XAC1023	TonB-dependent receptor	<i>fecA</i>	X	-
XAC1113	outer membrane protein Slp	<i>slp</i>	X	X
XAC1143	TonB-dependent receptor	<i>fyuA</i>	X	X

XAC1149	bacterioferritin		X	-
XAC1155	integral membrane protease subunit	<i>hflK</i>	X	-
XAC1156	integral membrane proteinase subunit	<i>hflC</i>	X	X
XAC1276	TonB-dependent receptor	<i>fyuA</i>	X	-
XAC1347	outer membrane protein		X	X
XAC1413	outer membrane antigen	<i>oma</i>	X	X
XAC1435	iron receptor complex outer membrane receptor protein	<i>fhuA</i>	-	X
XAC1435	iron receptor	<i>fhuA</i>	-	X
XAC1466	peptidoglycan-associated outer membrane lipoprotein	<i>pcp</i>	X	-
XAC1479	OmpA family protein		X	X
XAC1578	phosphate-binding protein	<i>phox</i>	X	-
XAC1728	lipoprotein NlpD	<i>nlpD</i>	X	-
XAC1728	lipoprotein NlpD	<i>nlpD</i>	-	-
XAC2151	YapH protein	<i>yapH</i>	X	X
XAC2185	ferrichrome-iron receptor	<i>fhuA</i>	-	X
XAC2531	TonB-dependent receptor	<i>btuB</i>	-	X
XAC2600	TonB-dependent receptor	<i>btuB</i>	X	-
XAC2620	virB9	<i>virB9</i>	-	X
XAC2672	Oar protein	<i>oar</i>	X	X
XAC2742	TonB-dependent receptor	<i>btuB</i>	X	X
XAC2743	Oar protein	<i>oar</i>	X	X
XAC2772	outer membrane protein	<i>bp26</i>	X	X
XAC2773	outer membrane protein	<i>bp26</i>	-	X
XAC2780	lipoprotein	<i>rlpB</i>	X	X
XAC2830	TonB-dependent receptor	<i>fhuA</i>	X	X
XAC2884	accessory protein	<i>plaS</i>	-	X
XAC3050	TonB-dependent receptor	<i>btuB</i>	X	X
XAC3141	outer membrane protein P6	<i>ompP6</i>	X	X
XAC3142	translocation protein TolB;	<i>tolB</i>	X	X
XAC3158	TonB-dependent receptor	<i>fhuA</i>	X	-
XAC3166	ferric enterobactin receptor	<i>bfeA</i>	X	X
XAC3168	ferric enterobactin receptor	<i>bfeA</i>	X	X
XAC3176	citrate-dependent iron transporter	<i>fecA</i>	-	X
XAC3201	TonB-dependent receptor	<i>fyuA</i>	-	X
XAC3207	ferric enterobactin receptor	<i>bfeA</i>	X	X
XAC3218	competence lipoprotein	<i>comL</i>	X	X
XAC3300	esterase-lipase	<i>estA</i>	X	X
XAC3308	large-conductance mechanosensitive channel	<i>mscL</i>	X	-
XAC3311	TonB-dependent receptor	<i>iroN</i>	X	-
XAC3334	TonB-dependent receptor	<i>fecA</i>	X	X
XAC3354	outer membrane protein W	<i>ompW</i>	X	X
XAC3355	outer membrane protein 21	<i>omp21</i>	-	X
XAC3358	Molybdate-binding protein	<i>modA</i>	X	-
XAC3370	ferric iron uptake outer membrane protein	<i>fhuE</i>	X	X
XAC3444	TonB-dependent receptor	<i>btuB</i>	X	X

XAC3463	TolC	<i>tolC</i>	X	X
XAC3472	polyphosphate-selective porin O	<i>oprO</i>	X	X
XAC3475	molybdate transport system substrate-binding protein (hypothetical protein)		X	-
XAC3498	ferric iron uptake outer membrane protein	<i>fhuE</i>	X	X
XAC3534	general secretion pathway protein D	<i>xpsD</i>	X	-
XAC3605	outer membrane protein	<i>uptE</i>	-	-
XAC3613	TonB-dependent receptor	<i>btuB</i>	-	X
XAC3664	outer membrane protein	<i>ompW</i>	X	X
XAC4048	TonB-dependent receptor	<i>iroN</i>	X	X
XAC4162	cation efflux system protein	<i>czcC</i>	X	-
XAC4273	OmpA-related protein		X	X
XAC4274	OmpA-related protein		X	X
XAC4344	lipoprotein	<i>vacJ</i>	X	X
XAC4368	TonB-dependent receptor	<i>fecA</i>	X	-
Two-component system				
XAC0204	glutamine synthetase	<i>glnA</i>	X	X
XAC0834	two-component system regulatory protein	<i>colR</i>	X	-
XAC4023	two-component system regulatory protein	<i>phoP</i>	X	X
XAC4369	phosphatase	<i>phoC</i>	X	-
Cell Motility and Attachment				
XAC0108	AtsE protein	<i>atsE</i>	X	-
XAC2017	type IV pilus assembly protein pilF	<i>pilF</i>	X	X
XAC3241	type IV pilus assembly protein PilA	<i>fimA</i>	X	-
Cell cycle				
XAC1078	ATP-dependent Clp protease proteolytic subunit	<i>clpP</i>	X	X
XAC1155	Integral membrane protease	<i>hflK</i>	X	-
XAC1224	cell division topological specificity factor MinE	<i>minE</i>	X	-
XAC1321	periplasmic protease	<i>mucD</i>	X	X
XAC1728	lipoprotein	<i>nlpD</i>	X	-
Heat shock, osmotic and oxidative stress				
XAC0209	superoxide dismutase like protein	<i>yojM</i>	X	X
XAC0210	superoxide dismutase	<i>sodC2</i>	X	X
XAC0493	bacterioferritin	<i>bfr</i>	X	X
XAC0723	disulfide oxidoreductase	<i>dsbA</i>	X	X
XAC0907	alkyl hydroperoxide reductase subunit C	<i>ahpC</i>	X	X
XAC1005	peptidyl-prolyl cis-trans isomerase	<i>ppiB</i>	X	-
XAC1078	ATP-dependent Clp protease proteolytic subunit	<i>clpP</i>	X	X
XAC1211	catalase	<i>katE</i>	X	X
XAC1321	periplasmic protease	<i>mucD</i>	X	X
XAC1438	Bacterioferritin		X	-
XAC1456	peptidyl-dipeptidase		X	-
XAC1521	heat shock protein GrpE	<i>grpE</i>	X	-

XAC2386	superoxidase dismutase	<i>sodM</i>	X	X
XAC2454	stringent starvation protein A	<i>sspA</i>	X	X
XAC2783	thioredoxin	<i>trx</i>	X	X
XAC2915	osmotically inducible protein	<i>osmC</i>	X	-
XAC3550	disulfide isomerase	<i>dsbC</i>	-	-
Hypothetical/No classification				
XAC0006	conserved hypothetical protein		X	X
XAC0139	conserved hypothetical protein		X	-
XAC0177	conserved hypothetical protein		X	-
XAC0223	conserved hypothetical protein		X	X
XAC0272	conserved hypothetical protein		X	X
XAC0292	conserved hypothetical protein		X	X
XAC0338	conserved hypothetical protein		X	-
XAC0450	conserved hypothetical protein		X	-
XAC0555	conserved hypothetical protein		X	X
XAC0603	conserved hypothetical protein		X	X
XAC0623	conserved hypothetical protein		-	-
XAC0665	conserved hypothetical protein		X	X
XAC0677	conserved hypothetical protein		X	X
XAC0683	conserved hypothetical protein		X	-
XAC0765	conserved hypothetical protein		X	X
XAC0836	conserved hypothetical protein		X	-
XAC0838	conserved hypothetical protein		X	X
XAC1045	conserved hypothetical protein		X	-
XAC1230	conserved hypothetical protein		X	X
XAC1236	conserved hypothetical protein		X	X
XAC1238	conserved hypothetical protein		X	-
XAC1244	conserved hypothetical protein		X	X
XAC1262	conserved hypothetical protein		X	-
XAC1278	conserved hypothetical protein		X	-
XAC1302	conserved hypothetical protein		X	X
XAC1344	conserved hypothetical protein		X	X
XAC1346	conserved hypothetical protein		X	-
XAC1364	conserved hypothetical protein		X	-
XAC1371	conserved hypothetical protein		X	-
XAC1397	conserved hypothetical protein		X	X
XAC1554	conserved hypothetical protein		X	X
XAC1761	conserved hypothetical protein		X	X
XAC2020	conserved hypothetical protein		X	X
XAC2083	conserved hypothetical protein		X	X
XAC2155	conserved hypothetical protein		X	-
XAC2312	conserved hypothetical protein		X	-
XAC2319	conserved hypothetical protein		X	-
XAC2491	conserved hypothetical protein		X	-
XAC2525	conserved hypothetical protein		X	-
XAC2946	conserved hypothetical protein		-	X
XAC2958	conserved hypothetical protein		X	-

XAC2968	conserved hypothetical protein	-	X
XAC3007	conserved hypothetical protein	-	-
XAC3032	conserved hypothetical protein	X	-
XAC3037	hydrolase	X	-
XAC3108	conserved hypothetical protein	X	-
XAC3140	conserved hypothetical protein	X	-
XAC3439	conserved hypothetical protein	X	-
XAC3475	conserved hypothetical protein	X	-
XAC3525	conserved hypothetical protein	X	X
XAC3657	conserved hypothetical protein	X	X
XAC3703	conserved hypothetical protein	X	-
XAC3725	conserved hypothetical protein	X	X
XAC3726	conserved hypothetical protein	X	X
XAC3746	conserved hypothetical protein	X	-
XAC3802	conserved hypothetical protein	X	X
XAC3844	conserved hypothetical protein	X	X
XAC3904	conserved hypothetical protein	X	-
XAC3966	conserved hypothetical protein	X	-
XAC3972	conserved hypothetical protein	X	X
XAC3981	conserved hypothetical protein	X	-
XAC4004	peptidase	-	-
XAC4007	conserved hypothetical protein	X	-
XAC4042	conserved hypothetical protein	X	-
XAC4131	conserved hypothetical protein	X	-
XAC4178	conserved hypothetical protein	X	X
XAC4204	conserved hypothetical protein	X	-
XAC4219	conserved hypothetical protein	X	-
